Charge Transfer and Pair Production in Relativistic Heavy-Ion Collisions

Carl Ludwig Tim Brunne

Erster Gutachter: Prof. Dr. J. Eichler
Hahn-Meitner-Institut Berlin
Glienicker Strasse 100
D-14109 Berlin
E-Mail: eichler@hmi.de

Zweiter Gutachter: Prof. Dr. V. Linke
Fachbereich Physik
Freie Universität Berlin
Arnimallee 14
D-14195 Berlin
E-Mail: linke@physik.fu-berlin.de

Tag der Disputation: 2. Juli 2001

Adresse des Autors: Tim Brunne
Hahn-Meitner-Institut Berlin
Glienicker Strasse 100
D-14109 Berlin
E-Mail: tim@brunne.de

ZUSAMMENFASSUNG

In dieser Arbeit werden Ladungsaustausch und Elektron-Positron Paarerzeugung in relativistischen Stößen schwerer Ionen theoretisch untersucht. Dabei werden periphere Stöße von Schwerionen betrachtet, auch als atomare Stöße bezeichnet, bei denen die Atomkerne unverändert bleiben. Bei solchen Stößen ist der minimale Kernabstand beim Stoß genügend groß, so daß die starke Wechselwirkung der Kerne untereinander nicht von Bedeutung ist. Der theoretische Zugang beruht auf einer semiklassischen Näherung. Die Bewegung der Atomkerne, welche als klassische Ladungsverteilungen angesehen werden, wird durch relativistische klassische Trajektorien beschrieben, die Dynamik der Elektronen dagegen durch die Quantentheorie. Wir betrachten Stoßsysteme mit Kernladungszahlen zwischen $Z = 66$ und $Z = 92$ bei Stoßenergien von etwa $1\,\mathrm{GeV/Nukleon}$ kinetischer Energie im Ruhesystem eines Stoßpartners. Für solche Systeme ist eine relativistische quantentheoretische Beschreibung der Elektronen- und Positronen-Dynamik notwendig und gegeben durch die Zwei-Zentren-Dirac-Gleichung. Experimentell können derartige Stöße untersucht werden seitdem entsprechende Schwerionen und Energien in Beschleunigeranlagen zur Verfügung stehen, wie z.B. in Berkeley seit Mitte der achtziger Jahre.

Die nicht-störungstheoretische Lösung der zeitabhängigen Zwei-Zentren-Dirac-Gleichung ist Hauptgegenstand der vorliegenden Arbeit. Nach einer Einführung in dieses Modell relativistischer atomarer Stöße wird in Kapitel 3 eine relativistische Vielkanal-Streutheorie der Zwei-Zentren-Dirac-Gleichung formuliert und untersucht. Für eine Klasse von Zwei-Zentren-Dirac-Gleichungen mit abgeschirmten Kernladungen werden die asymptotische Konvergenz und die relativistische Invarianz der Anregungs- und Ladungstransfer-Amplituden nachgewiesen.

Zur numerischen Lösung der Gleichung wird die Methode der gekoppelten Kanäle herangezogen (siehe Kapitel 4). Im Vergleich zu früheren numerischen Rechnungen dieser Art erlaubt der für diese Arbeit neu erstellte numerische Code (siehe Anhang A) erstmals die Lösung der gekoppelte-Kanäle-Gleichungen in einer Vielzahl unterschiedlicher Lorentz-Bezugssysteme. Dadurch kann unter anderem erstmals die Verletzung der Lorentz-Invarianz aufgrund des Lösungsansatzes studiert und die Genauigkeit der Ergebnisse beurteilt werden (siehe Kapitel 6). Es zeigt sich durchgehend, daß die Verwendung von sogenannten Coulomb-verzerrten Basisfunktionen die Bezugssystem-Abhängigkeit der numerischen Ergebnisse deutlich vermindert. Eine weitere Neuerung der hier vorgestellten Rechnungen stellt die benutzte gekoppelte-Kanäle-Basis dar. Unterschiedliche Ansätze früherer Arbeiten werden in Form einer bezüglich der Zentren symmetrischen Basis vereinheitlicht, welche gleichzeitig freie Teilchen beschreiben kann.

Es werden numerische Ergebnisse zum relativistischen Elektronentransfer präsentiert. Wir beginnen mit Rechnungen, die publizierte theoretische Resultate zu diesem Prozeß bestätigen. Darüber hinaus wird erstmalig die Ladungszahl- und Stoßenergie-Abhängigkeit des totalen Ladungstransfer-Wirkungsquerschnittes nicht-störungstheoretisch untersucht. Die berechneten Ergebnisse sind in qualitativer Übereinstimmung mit den experimentellen Daten für schwere Stoßsysteme. Sie unterscheiden sich aber deutlich von den entsprechenden parametrischen Abhängigkeiten, wie sie von Störungstheorien für höhere Stoßenergien vorrausgesagt werden.

Desweiteren betrachten wir gebunden-freie Paarerzeugung, d.h. den Prozeß, in dem ein Elektron in einem gebundenen Zustand und ein Positron in einem freien Zustand erzeugt werden. Der Schwerpunkt der Untersuchungen liegt hierbei auf einem qualitativen Verständnis der Verwendung einer bezüglich der Stoßpartner symmetrischen Basis von Positronen-Zuständen. In der Literatur wird bislang ausschließlich eine unsymmetrische Beschreibung verwendet, was numerisch einfacher zu behandeln ist. Darüber hinaus wurde auch für den Paarerzeugungsprozeß erstmals die Abhängigkeit der numerischen Ergebnisse vom Lorentz-Bezugssystem untersucht. Diese Abhängigkeit erwies sich als sehr ausgeprägt. Aufgrund dieser Tatsache ergibt sich ein vorerst uneinheitliches Bild bezüglich der Frage, ob eine symmetrischen Basis zur Beschreibung des Paarerzeugungs-Prozesses bei mittleren relativistischen Stoßenergien notwendig ist. Das ist allerdings der Fall für die numerischen Rechnungen im Collider-System, die nicht nur dadurch ausgezeichnet sind, daß eine Symmetrie der exakten Streutheorie erhalten ist, sondern auch dadurch, daß sie den experimentellen Befunden am nächsten kommen. Schließlich wird durch numerische Rechnungen die Vermutung bestätigt, daß die Abhängigkeit der berechneten Ladungstransfer-Wahrscheinlichkeiten vom Bezugssystem durch die Hinzunahme von Basisfunktionen für freie Teilchen abgeschwächt wird.

Summary

In this thesis, we investigate the processes of charge transfer and electron-positron pair creation in relativistic collisions of heavy ions. Peripheral collisions are considered, also referred to as atomic collisions, in which the atomic nuclei remain intact. In such collisions the closest approach of the nuclei is large enough such that the strong interaction between the nuclei is of no importance. Electromagnetic interactions of the particles prevail. The theoretical treatment is based on a semiclassical model. The movement of the atomic nuclei, that are regarded as classical charge distributions, is described by relativistic classical trajectories, whereas for electrons a description by quantum theory is required. We consider collision systems with nuclear charge numbers ranging between $Z = 66$ and $Z = 92$. Collision energies, given in terms of the total kinetic energy in a rest frame of either nucleus, are in the $1\,\mathrm{GeV}$/nucleon range. In such collision systems the motion of electrons and positrons is relativistic and a suitable description of their dynamics is given by the two-centre Dirac equation. The experimental investigation of these collision systems became feasible by the use of heavy-ion accelerators, beginning in the mid 1980's in Berkeley.

The nonperturbative solution of the time-dependent two-centre Dirac equation is the principal topic of this work. After introducing this model of relativistic atomic collisions, we formulate and investigate analytically a relativistic multi-channel scattering theory in chapter 3. In particular, asymptotic convergence and relativistic invariance are shown for a class of two-centre Dirac equations with screened nuclear charges.

For the numerical solution of the Dirac equation we use the coupled channel method (see chapter 4). Contrary to similar calculations reported in the literature,

the numerical code newly written for this work (see chapter A) allows for the solution of the coupled channel equations in various different Lorentz frames. Hence, the violation of Lorentz invariance, owing to the coupled channel approximation, can be investigated quantitatively for the first time, thereby allowing for the estimation of the accuracy of relativistic coupled channel calculations (see chapter 6). Generally, we find that the frame dependence of the numerical results is less pronounced if so-called phase-distorted basis functions are used. Another innovation of the present calculations is the type of coupled channel basis used. Different approaches of previously reported calculations are combined to a unified treatment, namely a basis which is symmetric with respect to the centres and which is capable of describing free particles at the same time.

We present numerical results for relativistic electron transfer, beginning with calculations which reproduce previously published theoretical data. For the first time, the parametric dependencies of the charge transfer process on the charge numbers of the nuclei and the collision energy are investigated using a nonperturbative method. The results are in qualitative agreement with experimental measurements for heavy collision systems. However, they are distinctly different from the parametric dependencies obtained by most perturbative calculations for higher collision energies.

Furthermore, we consider the process of bound-free pair production, in which a free positron and a bound electron are created. The emphasis of the theoretical studies is on a qualitative understanding of the importance of a symmetrical basis of positron states for the description of this process at intermediate relativistic collision energies. In the literature only asymmetrical approaches are used, which are computationally less demanding. Furthermore, we investigate the Lorentz frame dependence of the numerical calculations for the pair creation process, which has likewise not been considered before. Owing to the pronounced frame dependence found, the necessity of a symmetrical basis for the description of the pair creation process cannot be assessed unambiguously. However, a symmetrical basis is important in calculations in the collider frame, which not only preserve a symmetry of the exact scattering theory, but are closest to the experimental findings as well. Finally, we confirm the conjecture that the addition of free-particle states to a coupled channel basis of bound states reduces the frame dependence of numerical results for the charge transfer process.

CONTENTS

Introduction

1.1 Relativistic ion-atom collisions

The aim of this thesis is to contribute to the theory of relativistic atomic collisions. In relativistic as well as nonrelativistic ion-atom and ion-ion collisions nuclear interactions of the ionic nuclei are of no importance for physical processes. Electromagnetic interactions prevail. Principal physical phenomena occurring in such collisions are, e.g., electronic excitation, ionisation, nonradiative and radiative electron transfer. In relativistic collisions another process, the electromagnetic creation of electron-positron pairs, has been observed as well.

There are two principal features each of which can make an atomic collision relativistic in character. First, large nuclear charge numbers of the colliding ions render a relativistic description of bound states of inner atomic shells mandatory. Second, a relativistic theory for the exchange of an electron is required in collisions with a relative velocity of the collision partners that is comparable to the speed of light. Moreover, for such relativistic collision velocities the retardation of electromagnetic fields of moving charges, neglected in nonrelativistic theories, must be taken into account. In this work collision systems are considered, for which the nuclear charge numbers of the ions are very large and also the collision velocities are comparable to the speed of light, but not approaching the latter.

The acceleration of heavy-ions to relativistic velocities requires large-scale experimental facilities. Table 1.1 lists the main laboratories that are capable of providing beams of highly charged heavy-ions with particle velocities exceeding 75% of the speed of light. As common practice in the field of relativistic atomic collisions, beam energies are given in terms of a Lorentz factor γ corresponding to a Lorentz boost from the laboratory frame to a rest frame of the accelerated ions. Collision experiments with heavy and highly-charged ions are usually performed with solid or gas targets, at rest in the laboratory. Only recently, when the Relativistic Heavy Ion Collider (RHIC) in Brookhaven started operating in July 2000, experiments with counter-propagating colliding beams of heavy ions have become feasible, yielding much higher collision energies compared to fixed target experiments.

The main purpose of investigating high-energy collisions of heavy ions is the study of nuclear interactions and nuclear matter under extreme conditions. The search for new phenomena in nuclear and particle physics has led to the construction of more and more powerful heavy-ion accelerators. However, due to the availability of these experimental facilities also the experimental and theoretical investigation of electromagnetic, or atomic, processes in these high-energy collisions has been revived during the last two decades. It should be mentioned that not only the physics of relativistic atomic collisions has become experimentally accessible by the advent of these accelerator facilities, but also other branches of atomic physics, like spectroscopic and recombination experiments with highly-charged few-electron ions [Mok94]. For

TABLE 1.1. Heavy-ion accelerators, storage rings, and colliders that are able to provide heavy-ion beams with relativistic particle velocities. Some typical accelerated ions are listed as well as typical *beam energies*. The latter are given in terms of the corresponding Lorentz factor γ. Accelerators and storage rings allow for fixed target experiments and the *collision energy* is, hence, characterised by the Lorentz factor γ given in the table. For colliding beam machines the collision energy instead corresponds to a Lorentz factor $2\gamma^2 - 1$, where γ is the Lorentz factor of the counter-propagating beams given in the table.

Accelerators and storage rings		
Schwerionen-Synchrotron (SIS), GSI, Darmstadt, Germany	$C^{6+} \ldots U^{73+}$ ($\gamma \approx 3$)	
Experimentier-Speicherring (ESR), GSI, Darmstadt, Germany	U^{92+} ($\gamma = 1.6$)	
BEVALAC (shut down in 1993), LBNL, Berkeley, U.S.A.	La^{57+} ($\gamma = 2.4$)	U^{92+} ($\gamma = 2.0$)
Alternating Gradient Synchrotron (AGS), BNL, Brookhaven	Au^{79+} ($\gamma = 12.6$)	
Super Proton Synchrotron (SPS), CERN, Geneva, Switzerland	O^{8+}, S^{16+} ($\gamma = 215$)	Pb^{82+} ($\gamma = 170$)
Colliders		
Relativistic Heavy-Ion Collider (RHIC), BNL, Brookhaven, U.S.A.	Au^{79+} ($\gamma = 108$)	
Large Hadron Collider (LHC), CERN, Geneva, Switzerland (under construction)	Pb^{82+} ($\gamma \approx 3000$)	

example, fully stripped uranium ions U^{92+} have been produced first using the BEVALAC at Berkeley. Today, the electron beam ion trap is a competing source of highly charged ions, but for spectroscopic studies of highly charged few-electron systems heavy ion accelerators are still important.

In heavy-ion collisions without nuclear, or strong, interaction between the ionic nuclei, the nuclei remain intact in the course of a collision (except for Coulomb dissociation of the nuclei [BB88, VGS93, BRBW96, NW98]). Such processes are physically possible due to the short-range nature of the strong interaction. The colliding nuclei pass each other at a distance that does not allow for strong interaction, the colliding nuclei exhibit no overlap. Therefore, these collisions are often referred to as *peripheral* or distant heavy-ion collisions. In such collisions all physical processes are of electromagnetic origin.

Moreover, in peripheral collisions with relativistic beam energies the Coulomb deflection of projectile nuclei by target nuclei is typically less than a few mradians [EM95]. Therefore, the marginal Coulomb scattering of the nuclei in high-energy collisions is not important for a theoretical description. An undisturbed linear motion of the ionic nuclei, without momentum transfer between the nuclei during a collision,

is an assumption widely adopted in relativistic and even nonrelativistic theoretical approaches to ion-atom collisions [BM92, EM95].

The physics of atomic collisions has been an intensely studied branch of both experimental and theoretical physics at least since the early days of quantum physics. The first theoretical description of charge exchange in atomic collisions, discovered by Henderson in 1923, was given by Thomas (1927) using a classical model. Oppenheimer (1928), and Brinkmann and Kramers (1930) published the first quantum mechanical calculations. Today, even the literature on relativistic peripheral collisions of heavy ions has become very extensive, since the investigation of high-energy peripheral collisions of highly charged nuclei provides a unique physical system to study quantum electrodynamics in the presence of the strongest electromagnetic fields experimentally accessible to date [TEL87]. For general reviews we mainly refer to [BM92], for the nonrelativistic theory, and to [EIC90, EM95], regarding relativistic collisions.

1.2 Survey of experiments

In the following, we want to describe briefly some experiments investigating peripheral heavy-ion collisions, in order to sketch the experimental status of the field.

The experimental investigation of relativistic charge transfer has been carried out since the mid 1980's using the most powerful heavy-ion accelerator at that time, the BEVALAC at the Lawrence Berkeley Laboratory. Cross sections for electron capture by 82, 140, and 200 MeV/u Xe^{54+}, Xe^{53+}, and Xe^{52+} ions incident on thin solid targets from Be to Au have been measured and reported in [MAE+85].[1] In [AMX+87] single electron capture has been investigated also for higher projectile charge numbers and collision energies, e.g., U^{92+} ions with collision energy of 430 and 955 MeV/u, with targets up to Au. In these experiments total capture cross sections have been measured, not differentiating between the various final states of the projectile electron. Two different processes contribute to this total cross section, non-radiative electron capture (NRC) and capture of an electron with the simultaneous emission of a photon, referred to as radiative electron capture (REC). The theoretical understanding of the measured cross sections, based on the relativistic eikonal theory of electron capture [EIC85] and photoelectric cross sections, has been regarded satisfactory. Electron capture measurements in relativistic collisions of bare ions, U^{92+} and La^{57+}, in the 1 GeV/u energy range impinging on solid targets of Cu, Ag and Au have been reported in [BGF+97] as well. Again, the theoretical understanding was found to be satisfactory except for the heavy collision system U^{92+}+Au, where the measured cross section was found to be larger than theoretically predicted by perturbative theories. Using the ESR in Darmstadt, Stöhlker and collaborators have performed electron capture measurements with 223 MeV/u Helium-like U^{90+} impinging on gaseous targets of N_2, Ar, Kr and Xe. They investigated the distribution of final states of the captured electron by means of x-ray spectroscopy of radiation

---

[1]The collision energy is given here in terms of the kinetic energy of the projectile in the target frame divided by the projectile nuclear mass in atomic mass units (cf. appendix C).

emitted by decaying excited projectile states. Their results, which are not published yet, partly lack theoretical understanding, in particular for the high-Z targets [Stö].

A general feature of the capture of target electrons is the decrease of the total cross section with increasing projectile kinetic energy. Another atomic process has been experimentally confirmed in 1993 [BGF$^+$93], namely 'capture from the vacuum' or bound-electron free-positron pair creation. Regarding the detection of a down-charged projectile ion, this process is appearing like an ordinary electron capture process. But it can be distinguished from the latter by the presence of an emitted positron. An important difference of 'capture from the vacuum' as compared to capture of target electrons is the increase of the cross section with increasing collision energy. In collision experiments, performed closely before the final shutdown of the BEVALAC accelerator, $0.96\,\mathrm{GeV/u}$ bare uranium ions (U^{92+}) have been used to observe this process, incident on various solid targets from Mylar foils up to Au. Down-charged U^{91+} have been measured in coincidence with positrons created in the collision. Cross sections have been determined not only for bound-electron free-positron pair production, but also for the creation of free electron-positron pairs in peripheral collisions. It was found that both cross sections are of the same order of magnitude for the U^{91+}+Au collision system. After a series of measurements had been carried out, it was concluded in [BGF$^+$97] that unlike capture and ionisation, bound-free pair creation at collision energies around $1\,\mathrm{GeV/u}$ is not reproduced well by any of the existing theoretical approaches.

Gould emphasized in 1984 that the bound-free pair creation process is of importance for the construction of heavy-ion colliders, since it can occur also in peripheral collisions of bare nuclei and its cross section increases with collision energy. The latter fact has been verified experimentally [BGF$^+$94] after it had been theoretically predicted. This capture mechanism limits the lifetime of stored beams of colliding bare ions in heavy-ion colliders, since lower charge-state projectiles are lost from the beam circulating in a ring. Therefore, the experimental and theoretical investigation of bound-free pair creation was stimulated starting in the late 1980's, when the design of the RHIC and LHC colliders began.

Cross sections of capture and pair creation in peripheral collisions have been measured also at higher energies using the $10.8\,\mathrm{GeV/u}$ Au^{79+} beam of the Alternating Gradient Synchrotron at Brookhaven [CBD$^+$97, BCD$^+$98]. For this collision energy the perturbative theories well describe experimental data, i.e. the absolute value of the cross section for the Au^{79+}+Au collision as well as the Z_T^2-dependence of the total cross section on the target charge number Z_T.

Electron capture measurements with Pb^{82+} ions at $160\,\mathrm{GeV/u}$, available from the Super Proton Synchrotron at CERN, are reported in [KVD$^+$98, VKD$^+$00, KVD$^+$01]. In peripheral heavy-ion collisions at this energy, the highest used to date in atomic physics experiments, bound-free pair creation becomes the most important mechanism for electron capture. This has been confirmed experimentally.

Many related experiments have been done for similar collision systems and energies, investigating processes like ionisation, free electron-positron pair production, spectra and angular distributions of emitted electrons and positrons, etc.. Here we have sketched briefly the development of relativistic electron-capture experiments

during the last fifteen years, since this process is of principal interest in the present work.

1.3 General theoretical approach

Generally, ion-atom collisions are processes involving many particles which mutually interact and which are coupled to the electromagnetic radiation field. It is clear that such many-particle theories are prohibitively complicated for practical calculations. Therefore, suitable idealisations of the physical situation are necessary in order to allow for theoretical investigations. Here, we want to describe briefly the main theoretical background of this work.

The principal model which has been studied theoretically by many authors is the three-particle system comprising two nuclei and a single electron. In fact, this system can be realised in experiments in which, for example, protons or alpha-particles impinge on hydrogenic targets. However, the three-particle model has proved to be extremely useful for understanding other, more complicated collision experiments as well. Today, beams of hydrogenic and bare heavy-ions are available. For the description of collision experiments with such beams and atomic targets, the passive target electrons are usually neglected or enter a theoretical description only indirectly. Qualitatively, it is comprehended that electron motion is primarily governed by the strong electromagnetic field of the heavy and highly charged nuclei.

In a relativistic atomic collision to a good approximation the nuclear motion can be described by classical mechanics while the motion of the electron must be described by quantum theory. This approach is highly successful also in nonrelativistic collisions, although in some circumstances, which are not discussed in this thesis, quantum interference effects are not negligible [BM92]. Moreover, not only the quantum character of the nuclei is simplified, but it is assumed as well that the motion of the nuclei is not influenced by the much lighter electrons. Taking this point of view, a simplified model of an atomic collision is given by the equation of motion of a single quantum-mechanical electron subject to the field of classical point charges moving along prescribed trajectories. As indicated above the Coulomb deflection of the colliding nuclei can often be neglected successfully in theoretical descriptions, in particular of collisions of heavy-ions at high collision energies.

If the motion of electrons and nuclei is not relativistic, the electrons may be treated as spinless particles and the Schrödinger equation can be used. The retardation of the electromagnetic fields of the classical nuclei and magnetic fields are not taken into account. This model is Galilean invariant and referred to as the *impact parameter model*, *semiclassical approximation* or charge-transfer model. The relation between nonrelativistic quantum-mechanical three-particle scattering and the charge-transfer model is described in more detail for example in [BM92]. Recently a precise mathematical discussion has appeared as well [ITO95].

A refined description, necessary for high collision velocities, must take into consideration the magnetic field induced by a moving point nucleus and the retardation of a time-dependent electromagnetic field. In addition, the electronic spin can be

described by the Pauli–Schrödinger equation. Note, however, that such quantum theories are neither Galilean nor Lorentz invariant.

Since the present work is concerned with high-energy ion-atom collisions of heavy ions the dynamical equation for electrons must be the Dirac equation with an external electromagnetic field. The electromagnetic field originates from the moving nuclei and includes both electric and magnetic field components and retardation effects. This description allows for Lorentz invariance. In the rest frame of one of the point nuclei, which is denoted by A in the following, this time-dependent Dirac equation reads:

$$\mathrm{i}\hbar\frac{\partial}{\partial t}\Psi(t,\boldsymbol{x}) = \left[-\mathrm{i}\hbar\boldsymbol{\alpha}\cdot\boldsymbol{\nabla} + m_{\mathrm{e}}c^2\beta + \frac{-e^2 Z_{\mathrm{A}}}{|\boldsymbol{x}|} + \frac{-e^2 Z_{\mathrm{B}}}{|\boldsymbol{x}'|}\gamma\left(1 - \frac{v}{c}\alpha_3\right)\right]\Psi(t,\boldsymbol{x}), \quad (1.1)$$

with

$$\boldsymbol{x}' = \boldsymbol{x} + (\gamma - 1)(x^3 - tv)\boldsymbol{e}_3 - \boldsymbol{b}.$$

Gaussian units have been used for the electrical charge. The quantities Z_{A} and Z_{B} denote the charge numbers of the nuclei and m_{e} the electron mass. The $\boldsymbol{e}_3$-axis of the spatial coordinate system has been chosen in the direction of linear motion of nucleus B. The latter moves with velocity v, corresponding to a Lorentz factor γ. The impact parameter of the trajectory is $\boldsymbol{b}$, with $\boldsymbol{b} \perp \boldsymbol{e}_3$, and $\alpha_1, \alpha_2, \alpha_3$ and β denote Dirac matrices. Clearly, in equation (1.1) the Dirac particle is subject to a stationary Coulomb potential of nucleus A and the time-dependent Liénard–Wiechert potential of the moving nucleus B. The numerical solution of equation (1.1), and corresponding Lorentz-transformed equations, is a major topic of this work.

Charge transfer. In the literature equation (1.1) has been used as a model to describe charge transfer in relativistic atomic collisions. The Dirac equation(1.1) has solutions which represent bound states of nucleus A or of nucleus B, as $t \to -\infty$ or as $t \to +\infty$ (cf. chapter 3). Denote by $a_{\mathrm{fi}}(\boldsymbol{b})$ the impact-parameter-dependent amplitude for the transition from an incoming configuration i, say a bound state of nucleus A, to an outgoing configuration f, say a bound state of nucleus B. As shown, e.g., in [EM95] the total cross section σ_{fi} for the nonradiative charge-transfer process i→f is then obtained by integrating the probability $|a_{\mathrm{fi}}(\boldsymbol{b})|^2$ over the entire impact-parameter plane:

$$\sigma_{\mathrm{fi}} = \int |a_{\mathrm{fi}}(\boldsymbol{b})|^2 \,\mathrm{d}^2 b. \tag{1.2}$$

The calculation of the transition amplitudes $a_{\mathrm{fi}}(\boldsymbol{b})$ is accordingly the principal task for the theoretical determination of NRC cross sections. Many different perturbative approaches have been used for that in the literature (see [EM95]). In addition, two-centre coupled channel calculations have been performed, prior to this work, in order to obtain transition amplitudes nonperturbatively [TE88B, TE88A, TE89]. In these numerical calculations the two-centre Dirac equation has been solved numerically using the coupled channel ansatz. They are reproduced and extended in the present work.

We note that the Dirac equation allows for an unambiguous interpretation only in a multi-particle theory, i.e. the framework of quantum field theory, as multiply
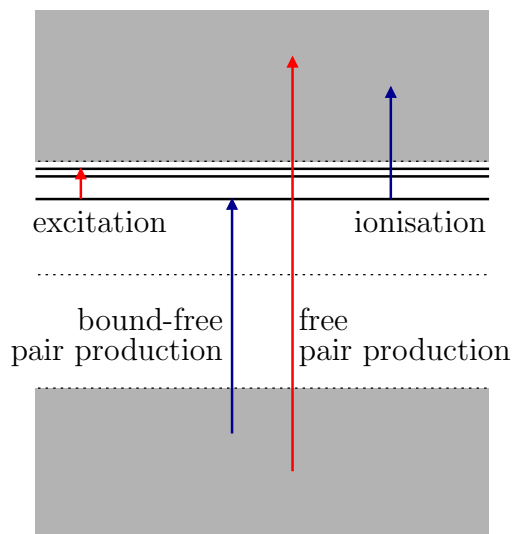
FIGURE 1.1. Furry picture of pair creation by an external perturbation.

discussed in the literature. Therefore, it is not surprising that multi-particle phenomena like pair creation have to be dealt with, as soon as a relativistic description of electron motion is sought.

Pair creation. The description of pair creation in peripheral heavy-ion collisions clearly requires a multi-particle theory. Frequently, pair creation is viewed as a transition from the negative energy continuum of a time-independent Dirac Hamiltonian to a state of positive energy. Consider the electron-positron field in the presence of a static external field, for example the Coulomb potential of nucleus A. The energy spectrum of the corresponding Dirac Hamiltonian is sketched in figure 1.1. Energy eigenvalues in the gap between the negative and positive energy continua correspond to bound states of the static external field, i.e. bound states of classical nucleus A. A time-dependent perturbation, as, e.g., the Liénard–Wiechert potential of nucleus B, leads to transitions between the eigenstates of the time-independent Dirac Hamiltonian of nucleus A,

$$H_{\mathrm{A}} = -\mathrm{i}\hbar\boldsymbol{\alpha} \cdot \boldsymbol{\nabla} + m_{\mathrm{e}}c^2\beta + \frac{-e^2 Z_{\mathrm{A}}}{|\boldsymbol{x}|}. \tag{1.3}$$

Transitions from the negative energy continuum to the positive energy continuum correspond to the creation of free electron-positron pairs, whereas transitions from states of negative energy to discrete eigenstates of nucleus A represent bound-free pair creation. Note that this theory also describes ionisation, but not charge transfer.

Assuming that the time-dependent perturbation vanishes as $t \to \pm\infty$ (which can be achieved technically by using the adiabatic switching formalism [THA92]) a proper multi-particle interpretation of the seemingly 'single-particle' transition amplitudes is obtained by second quantisation. Second quantisation is the construction of a multi-particle Fock space based on the spectral decomposition of the state-space of the classical 'single-particle' Dirac equation. For the spectral decomposition, and, therefore, the particle interpretation, reference to a time-independent

Hamilton operator is necessary. The relation between quantum field theory subject to external classical sources and the classical Dirac equation has been discussed in the literature for a long time, starting with the early works of Feynman, Dyson and others (e.g. [SCH58]). It is a mathematically well-established theory (e.g. [SM53, CAP69, SEI72, RUI77A, RUI77B, RUI77C]) discussed in many text books (e.g. [RS79, FGS91, THA92, SCH95]). We do not review this formalism in the present work but take the 'single-particle' point of view right from the beginning. For a few important remarks we refer to section 3.6.

As an alternative to the Furry picture, in which the particle interpretation refers to the Dirac Hamiltonian with a stationary external Coulomb potential (1.3), the external fields of nuclei A and B may be regarded both as perturbations of the free Dirac Hamiltonian,

$$H_0 = -\mathrm{i}\hbar\boldsymbol{\alpha} \cdot \boldsymbol{\nabla} + m_{\mathrm{e}}c^2\beta. \tag{1.4}$$

This point of view corresponds to the Feynman–Dyson approach to quantum electrodynamics, in which all particles are asymptotically free. This approach does not allow for particles bound to either classical nucleus A or B. Therefore, the description of the elementary bound-free pair creation process is not feasible in this picture.

In both approaches, the Furry picture and the Feynman–Dyson interaction picture, pair creation cross sections are calculated by the determination of transition amplitudes of the 'single-particle' theory. This has been done using many different approximations. Principally perturbation theory has been used, in combination with a variety of initial and final states (reviewed in [EM95, ION97]). Moreover, several attempts to solve the two-centre Dirac equation (1.1) numerically using a variety of different techniques have been published (e.g. [MGS91, TBM⁺92, WOU⁺92, RSG93, THGS95, MBS96, MGS98, IB99]). These numerical solutions are generally very demanding with respect to computing time and, therefore, their reliability is still more or less limited by this fact. However, for peripheral collisions at small impact parameters of heavy and highly charged nuclei these nonperturbative calculations are regarded to be more appropriate than perturbation theory, due to the very strong electromagnetic interaction in this case.

Finally, let us mention briefly another theoretical approach to describe ionisation and pair creation in peripheral collisions. It makes use of the equivalent-photon method developed by Fermi, von Weizsäcker and Williams [JAC99, EM95], replacing the Liénard–Wiechert potential of nucleus B by a pulse of linearly polarised electromagnetic radiation. This is a suitable approximation for high collision velocities and can be applied to describe many different electromagnetic processes in atoms and nuclei induced by passing charged projectiles [BB88]. The Fermi–Weizsäcker–Williams method has been the basis of the first calculations of electron-positron pair creation in the 1930's, published by Landau and Lifshitz, Bhabha, Racah, Nishina, Tomonaga and Kobayashi. However, we will not encounter this approach in this work again.

1.4 Aim and context

In view of the presumed necessity of a nonperturbative description of bound-free pair creation in peripheral collisions of highly charged nuclei, several different attempts to

Target frame:

Collider frame:

Projectile frame:
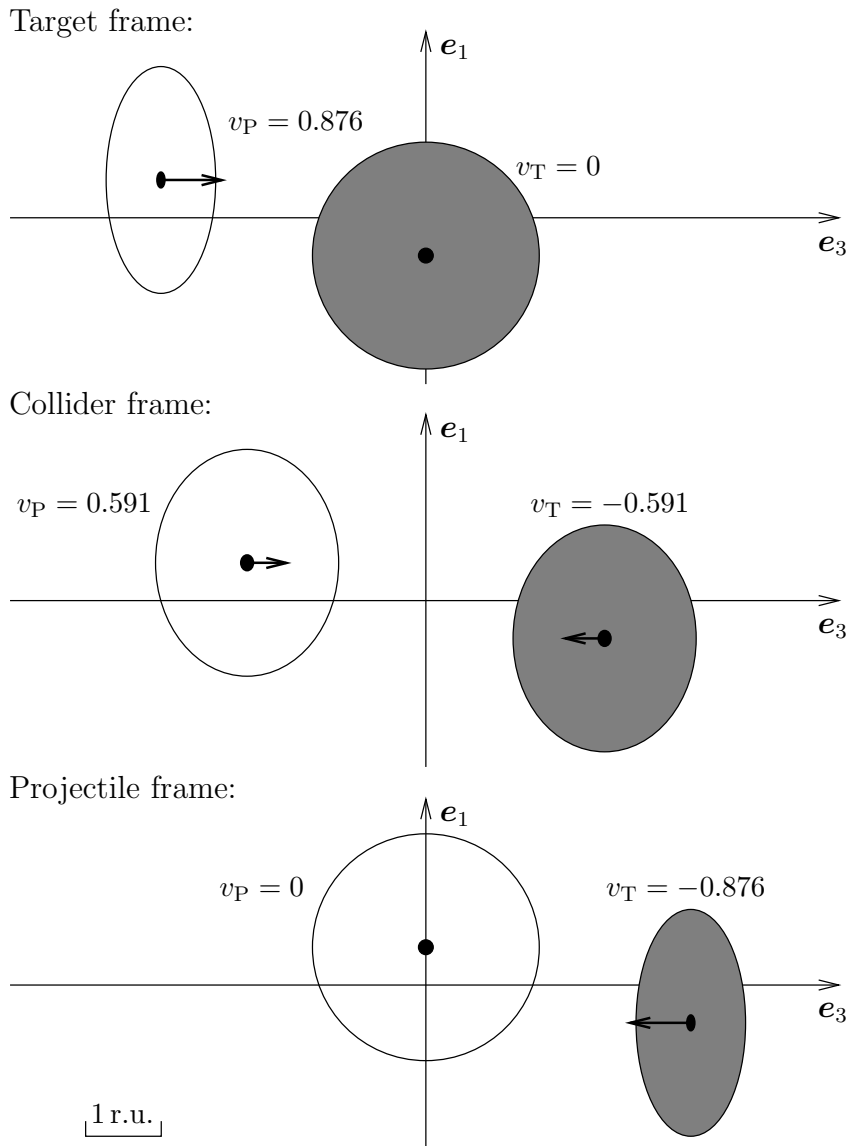
FIGURE 1.2. Three different frames of reference are depicted which have been studied numerically in this work. The Lorentz contraction of moving bound states is shown for a collision energy of $1\,\mathrm{GeV/u}$ in all three cases. One centimetre of the drawing corresponds to one relativistic unit of both length and velocity. In relativistic natural units $\hbar = c = m_\mathrm{e} = 1$ holds. The Lorentz-contracted circles have the size of the K-shell of uranium ($\approx 1.5\,\mathrm{r.u.}$). In all three cases, the impact parameter is $1\,\mathrm{r.u.}$ and the time is $4\,\mathrm{r.u.}$ before the closest approach of the nuclei.

solve the time-dependent Dirac equation (1.1) numerically have been published. Due to the more or less successful explanation of experimental data at collision energies above $10\,\mathrm{GeV/u}$, or equivalently $\gamma \geq 12$, the energy regime of interest for the present work is $1\,\mathrm{GeV/u}$. By contrast to higher energies, the cross sections of the first experiments observing bound-free pair creation at this intermediate relativistic collision energy have not been reproduced reliably by theoretical calculations [BGF$^+$97].

In particular, single-centre coupled channel calculations have been done to determine probabilities of bound-free pair creation at intermediate relativistic collision

energies. In such single-centre calculations the solution $\Psi(t, \boldsymbol{x})$ of equation (1.1) is approximated by a finite linear combination of eigenstates $\Phi_{A,k}(t, \boldsymbol{x})$ of the Coulomb–Dirac Hamiltonian (1.3),

$$\Psi(t, \boldsymbol{x}) = \sum_k c_{A,k}(t)\Phi_{A,k}(t, \boldsymbol{x}), \tag{1.5}$$

and the coefficients $c_{A,k}(t)$ are determined numerically. Some authors have found that a strong nonperturbative enhancement of pair creation is exhibited by these calculations [RMS+91, RSG93] others have argued later that this could not be reproduced if larger coupled channel bases are used [BRBW93, BRBW94].

A principle objection against single-centre expansions as in equation (1.5) is that it does not allow for the description of the charge transfer process. Moreover, the representation of the free-particle states is asymmetrical with respect to the nuclei. In [EIC95] a 'transfer-like' bound-free pair creation description by perturbative means has been proposed. In this approach, the electron bound state and the positron states are referred to different nuclei.

Apart from single-centre coupled channel calculations, also relativistic two-centre coupled channel calculations have been reported [TE88B, TE88A, TE90]. The latter make use of the two-centre expansion,

$$\Psi(t, \boldsymbol{x}) = \sum_k c_{A,k}(t)\Phi_{A,k}(t, \boldsymbol{x}) + \sum_k c_{B,k}(t)\Phi_{B,k}(t, \boldsymbol{x}), \tag{1.6}$$

using bound-state wave functions $\Phi_{A,k}(t, \boldsymbol{x})$ and $\Phi_{B,k}(t, \boldsymbol{x})$ of the nuclei A and B respectively. These calculations allowed for the determination of charge transfer amplitudes and have been carried out as well for the $1\,\mathrm{GeV/u}$ collision-energy range. Attempts to describe ionisation in such two-centre calculations as well, by using so-called pseudo-states, have been made [TE89]. Although this approach is very successful in nonrelativistic coupled channel calculations, the use of pseudo-states in relativistic calculations, however, gave rise to serious problems.

A two-centre coupled channel treatment of the Dirac equation (1.1) with a suitable description of free-particle states has not been attempted before this work. However, only such a coupled channel expansion allows for the investigation of two-centre effects in the process of bound-free pair creation. The question arose whether two-centre effects could be a reason for the remaining discrepancies between existing 'excitation-like' descriptions of bound-free pair creation and experimentally determined cross sections.

Another problem, which has not been paid much attention in the literature before this work, is the Lorentz frame dependence of numerical results obtained by means of relativistic coupled channel calculations. Since finite expansions of the form (1.5) and (1.6) respectively can only be approximations to exact solutions of the two-centre Dirac equation, Lorentz invariance is not guaranteed. Such a problem does not exist for nonrelativistic coupled channel calculations, since Galilean boosts do not transform the time axis. A quantitative study of the frame dependence of numerical results has been carried out in the present work. Previous numerical calculations only considered the frame of reference in which the initial electronic configuration before the collision is at rest (top subfigure of figure 1.2). Two other reference frames, which have been used for numerical calculations of the present work, are also shown

in figure 1.2. Note that this figure depicts the same collision system as viewed in different reference frames. In fact, the problem of frame dependence of numerical calculations has not been considered in the literature for any of the approaches to solve the time-dependent Dirac equation until now.

For the coupled channel calculations of this work a new computer code had to be written. Owing to the availability of this numerical code it became feasible to extend existing nonperturbative studies of the relativistic charge transfer process. In particular coupled channel calculations for the determination of parametric dependencies of the electron transfer cross section on the charge numbers Z_A and Z_B of the nuclei and the collision energy γ have not been done prior to this work. Such parametric dependencies had been theoretically derived by perturbative approaches only. However, the applicability of perturbation theories is doubtful for collisions of two heavy ions at intermediate relativistic collision energies.

1.5 Outline of this work

Chapter 2 gives a detailed exposition of the semiclassical approximation, i.e. the impact parameter model in which colliding nuclei are represented by classical charge distributions moving along prescribed trajectories. Particular emphasis is put onto the choice of the frame of reference with the aim of formulating a relativistically invariant theory. Symmetries of the two-centre Dirac equation are presented. In *chapter 3* a multi-channel scattering theory for the classical two-centre Dirac equation is formulated. Transition amplitudes are defined, and the asymptotic convergence and orthogonality of the Møller wave operators are proved, provided the charges of the nuclei are screened. A similar presentation of the scattering theory of the two-centre Dirac equation is not available in the literature. In particular we demonstrate the Lorentz invariance of the excitation and transfer amplitudes. The aspects regarding second quantisation are discussed, furthermore, Coulomb boundary conditions are explained. The latter have been used previously to deal with the problem of the long-range nature of the unscreened Coulomb potential in coupled channel and perturbative calculations.

The coupled channel method, employed in the present work for the approximate, but nonperturbative numerical solution of the two-centre Dirac equation, is presented in *chapter 4*. Properties of the fundamental solution of the coupled channel equations and its relation to transition amplitudes are discussed. In *chapter 5* we describe the specific two-centre coupled channel ansatz that was used for the numerical calculations of this work. The basis functions for asymptotically bound and asymptotically free particles are presented and motivation for their choice is given. Numerical results are shown that demonstrate the proper numerical implementation of the coupled channel ansatz. These results not only represent an important test of the software, but also, for the first time, reproduce some existing numerical data found in the literature.

In *chapter 6* we present the new numerical results of this thesis, together with their discussion and comparison with literature. Heavy-ion collision systems with

charge numbers ranging from $Z = 66$ to $Z = 92$ are considered at collision energies in the $1\,\mathrm{GeV/u}$ range. In the first sections of the chapter, we discuss coupled channel calculations that use a basis of bound state functions only. Such calculations allow for the theoretical investigation of the relativistic charge transfer process. The frame dependence of such numerical calculations is demonstrated and analysed in this work for the first time. Furthermore, parametric dependencies are studied nonperturbatively, which has likewise not been done before. In the last two sections of chapter 6 results from two-centre coupled channel calculations using bound-state and free-particle basis functions are presented. Such calculations have neither been published nor attempted before. We show results of calculations which have been performed to assess the importance of two-centre effects for the process of bound-free pair creation in peripheral collisions. The problem of frame dependence of the results is discussed, as well as the influence of the free-particle channels on the charge transfer process.

The technical details of the numerical calculations are not described in the main part of the thesis but in *appendix A*. In that appendix not only numerical methods are explained but also some aspects of the implementation of the calculations. In *appendix B* we state and prove some mathematical results referred to in the main chapters, but which are not easily found in literature. *Appendix C* states some conventions and definitions used in this work, in particular it comprises a table of notation and symbols. Finally, relativistic natural units (r.u.) for which $\hbar = c = m_\mathrm{e} = 1$ are used throughout this work, unless specified explicitly.

collide, collision. *It is sometimes asserted that these two words are 'properly' restricted to circumstances involving a violent impact between two moving objects. There is no basis for such a belief. [...]*

H. W. Fowler and R. W. Burchfield, *Modern English Usage*

Semiclassical Approximation

In collision experiments with heavy-ion accelerators the laboratory frame is frequently identical to the target frame of reference, in which the initial electronic state is at rest. In the literature, the two-centre Dirac equation has only been considered in the target, collider or projectile frames of reference, with the direction of relative motion chosen as the e_3-axis. However, with the aim of formulating a relativistically invariant theory, it is necessary to start with the most general inertial frame, in which the colliding nuclei move in arbitrary directions. Furthermore, this approach provides general insight into the theory. The scattering theory, presented in the next chapter, refers to this general approach.

On the other hand, for numerical calculations, as those presented later in this work, a specific frame of reference must be chosen. Again, in the literature only the target and collider frames have been used for numerical calculations. In this work numerical calculations are presented, which have been done in various different reference frames, thereby showing the influence of the choice of the reference frame on the numerical results.

2.1 Relativistic kinematics

We start by considering an arbitrary frame of reference, where the centres of force A and B move with constant velocities along straight line trajectories. These
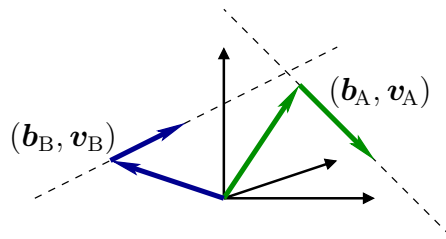
trajectories will be written in the following form,

$$\begin{aligned} \boldsymbol{R}_{\mathrm{A}}(t) &= \boldsymbol{b}_{\mathrm{A}} + t\boldsymbol{v}_{\mathrm{A}}, \\ \boldsymbol{R}_{\mathrm{B}}(t) &= \boldsymbol{b}_{\mathrm{B}} + t\boldsymbol{v}_{\mathrm{B}}, \end{aligned} \qquad (2.1)$$

with three-velocities $\boldsymbol{v}_{\mathrm{A}}$ and $\boldsymbol{v}_{\mathrm{B}}$ that satisfy $|\boldsymbol{v}_{\mathrm{A}}|, |\boldsymbol{v}_{\mathrm{B}}| < 1$, and arbitrary three-vectors $\boldsymbol{b}_{\mathrm{A}}$ and $\boldsymbol{b}_{\mathrm{B}}$. The world-line corresponding to the trajectory of centre A is given by the four-vector,

$$\mathfrak{X}_{\mathrm{A}}^{\mu}(s) = \Big(\gamma_{\mathrm{A}}s, \boldsymbol{b}_{\mathrm{A}} + \gamma_{\mathrm{A}}s\,\boldsymbol{v}_{\mathrm{A}}\Big),$$

Here, the proper time is denoted by s. The definition of $\mathfrak{X}_{\mathrm{B}}^{\mu}(s)$ is analogous. The Lorentz factors, corresponding to the velocities $\boldsymbol{v}_{\mathrm{A}}$ and $\boldsymbol{v}_{\mathrm{B}}$, are denoted by γ_{A} and γ_{B}

respectively:

$$\gamma_\Gamma = \frac{1}{\sqrt{1 - \boldsymbol{v}_\Gamma^2}},$$

with $\Gamma = \mathrm{A, B}$. The world-line representation $\mathfrak{X}_\Gamma^\mu(s)$ of the trajectories is useful for the computation of Lorentz transformed trajectories, since $\mathfrak{X}_\Gamma^\mu(s)$ transforms like a Lorentz four-vector.

2.1.1 Lorentz invariants. The relative motion of the centres A and B is described entirely by two Lorentz invariant quantities, namely the collision energy and the impact parameter. Their relation to the parameters of the trajectories is discussed next.

Since the modulus $|\boldsymbol{v}_\mathrm{B} - \boldsymbol{v}_\mathrm{A}|$ is not invariant with respect to Lorentz boosts, it is not suitable for a characterisation of the collision energy of the centres. One may, therefore, consider the modulus v of the relative velocity of A and B in a rest frame either of centre A or equivalently of centre B. This velocity v is a Lorentz invariant, as well as the corresponding Lorentz factor $\gamma = (1 - v^2)^{-1/2}$, which in terms of $\boldsymbol{v}_\mathrm{A}$ and $\boldsymbol{v}_\mathrm{B}$ is given by:

$$\gamma = \gamma_\mathrm{A} \gamma_\mathrm{B} (1 - \boldsymbol{v}_\mathrm{A} \cdot \boldsymbol{v}_\mathrm{B}). \tag{2.2}$$

As mentioned in the introduction, it is customary to indicate the collision energy, associated with the trajectories (2.1), by this Lorentz factor γ.

Moreover, as opposed to nonrelativistic kinematics, the distance of closest approach of the centres may be different in reference frames which are moving with respect to each other. Hence, the impact parameter b must be defined as the distance of closest approach of the centres in a rest frame of either centre A or centre B. In terms of the parameters $\boldsymbol{b}_\mathrm{A}, \boldsymbol{b}_\mathrm{B}, \boldsymbol{v}_\mathrm{A}$ and $\boldsymbol{v}_\mathrm{B}$ of the pair of trajectories (2.1), the Lorentz invariant impact parameter b is given by the relation:

$$b^2 = \boldsymbol{d}^2 - \frac{((\boldsymbol{d} \cdot (\boldsymbol{v}_\mathrm{B} - \boldsymbol{v}_\mathrm{A}))^2 - ((\boldsymbol{d} \cdot \boldsymbol{v}_\mathrm{A}) \, \boldsymbol{v}_\mathrm{B} - (\boldsymbol{d} \cdot \boldsymbol{v}_\mathrm{B}) \, \boldsymbol{v}_\mathrm{A})^2}{(\boldsymbol{v}_\mathrm{B} - \boldsymbol{v}_\mathrm{A})^2 - \boldsymbol{v}_\mathrm{A}^2 \boldsymbol{v}_\mathrm{B}^2 + (\boldsymbol{v}_\mathrm{A} \cdot \boldsymbol{v}_\mathrm{B})^2}. \tag{2.3}$$

Here, the abbreviation $\boldsymbol{d} = \boldsymbol{b}_\mathrm{B} - \boldsymbol{b}_\mathrm{A}$ was used. In the limit $|\boldsymbol{v}_\mathrm{A}|, |\boldsymbol{v}_\mathrm{B}| \ll 1$ the nonrelativistic expression for the impact parameter is recovered.

2.1.2 Lorentz scalars. In the following, some Lorentz scalars associated with the pair of trajectories (2.1) are defined for later reference. Let primed quantities refer to a rest frame of centre A, such that the transformed trajectory $\boldsymbol{R}_\mathrm{A}'(t')$ of A satisfies,

$$\boldsymbol{R}_\mathrm{A}'(t') = 0.$$

We define r_A' in the primed coordinate system as the radial distance from the spatial origin, i.e.:

$$r_\mathrm{A}'(t', \boldsymbol{x}') = |\boldsymbol{x}'|.$$

Transforming this quantity back to the unprimed reference frame one obtains,

$$r_\mathrm{A}(t, \boldsymbol{x}) = \left| (\boldsymbol{x} - \boldsymbol{b}_\mathrm{A}) + (\gamma_\mathrm{A} - 1)(\hat{\boldsymbol{v}}_\mathrm{A} \cdot (\boldsymbol{x} - \boldsymbol{b}_\mathrm{A})) \, \hat{\boldsymbol{v}}_\mathrm{A} - \gamma_\mathrm{A} t \boldsymbol{v}_\mathrm{A} \right|$$

$$= \sqrt{(\boldsymbol{x}_\perp - \boldsymbol{b}_{\mathrm{A}\perp})^2 + \gamma_\mathrm{A}^2 \left(\boldsymbol{x}_\parallel - \boldsymbol{b}_{\mathrm{A}\parallel} - t \boldsymbol{v}_\mathrm{A} \right)^2}, \tag{2.4}$$

which is a Lorentz scalar by definition. Here, the subscripts $\parallel$ and $\perp$ indicate components parallel and perpendicular to the velocity $\boldsymbol{v}_A$. The corresponding scalar with reference to centre B will be denoted by $r_B(t, \boldsymbol{x})$. The Lorentz scalars $r_\Gamma(t, \boldsymbol{x})$ are related to the trajectories $\boldsymbol{R}_\Gamma(t)$ by the following inequality:

$$|\boldsymbol{x} - \boldsymbol{R}_\Gamma(t)| \; \leq \; r_\Gamma(t, \boldsymbol{x}) \; \leq \; \gamma_\Gamma \, |\boldsymbol{x} - \boldsymbol{R}_\Gamma(t)| \,, \tag{2.5}$$

with $\Gamma = A, B$.

Moreover, consider the distance between centres A and B at time t' in the primed frame, the rest frame of centre A, and define,

$$d'_A(t', \boldsymbol{x}') = |\boldsymbol{R}'_B(t')|.$$

By substituting $t' = \gamma_A(t - \boldsymbol{v}_A \cdot (\boldsymbol{x} - \boldsymbol{b}_A))$ the Lorentz scalar $d_A(t, \boldsymbol{x})$ in the unprimed frame is obtained. A purely algebraic calculation shows that $d_A(t, \boldsymbol{x})$ is given by:

$$d_A(t, \boldsymbol{x})^2 = b^2 + \left\{ \frac{\gamma_B \boldsymbol{v}_B \cdot \boldsymbol{d}}{\gamma v} - \frac{\gamma_A \boldsymbol{v}_A \cdot \boldsymbol{d}}{\gamma^2 v} + v \gamma_A \Big(t - \boldsymbol{v}_A \cdot (\boldsymbol{x} - \boldsymbol{b}_A) \Big) \right\}^2 . \tag{2.6}$$

Here, the quantities b, v, γ and $\boldsymbol{d}$ are defined as above. Similarly, the scalar $d_B(t, \boldsymbol{x})$ is derived from the distance between the centres A and B in a rest frame of centre B. Contrary to nonrelativistic kinematics d_A and d_B differ.

2.2 Static charge distributions

With each of the centres A and B we may associate a spherically symmetric electric charge distribution $\rho_\Gamma(r)$ that is time-independent in the respective rest frame of each centre $\Gamma = A, B$. The two charge distributions model the moving nuclei in a peripheral heavy ion collision, and possibly a mean field of their bound electrons as well. These charge distributions $\rho_\Gamma(r)$ shall refer to the respective rest frames of their centres: the primes, usually employed to indicate this fact, are omitted here for simplicity of the notation.[1] A Lorentz boost of these static charge distributions to an arbitrary unprimed frame of reference yields a four-current, which is time-dependent.

In principle, the charge distributions do not have to be spherically symmetric in their respective rest frames. However, spherical symmetry considerably simplifies the following discussion. In this case, the relative orientation of the rest frame coordinates does not matter and the discussion is not complicated by the necessity for rotations in coordinate transformations. Furthermore, the most simple charge distribution, the point charge, occurring most often in the literature and applied in numerical calculations of this work, has spherical symmetry. For the presentation of the scattering theory in the next chapter, it is mandatory to consider more general spherical charge distributions than the point charge only.

The radially symmetric electrostatic potential $V_\Gamma(r)$ in the rest frame of centre Γ (again omitting primes) and the charge distribution $\rho_\Gamma(r)$ are related by the Poisson

---

[1]This convention allows us to refer unambiguously to the charge distributions $\rho_\Gamma(r)$, and also their spherically symmetric electrostatic potentials $V_\Gamma(r)$, in contexts in which primed coordinates do not denote rest frame coordinates of these entities.

equation, which is given in the spherically symmetric case by:

$$-\frac{1}{4\pi r}\,\frac{\partial^2}{\partial^2 r}\,rV_\Gamma(r) = \rho_\Gamma(r) \qquad \text{(for } r \neq 0\text{)}. \tag{2.7}$$

We use Gaussian units for the electrical charge everywhere in this thesis, because they are usually preferred in atomic physics (cf. appendix C).

The time-dependent electromagnetic field in the unprimed reference frame, originating from the moving charge distribution $\rho_\Gamma(r)$, time-independent only in a rest frame of centre Γ, is given by the following electromagnetic four-potential:

$$\left(A_\Gamma{}^0(t,\boldsymbol{x}), \boldsymbol{A}_\Gamma(t,\boldsymbol{x})\right) = \gamma_\Gamma\, V_\Gamma(r_\Gamma(t,\boldsymbol{x}))\,(1, \boldsymbol{v}_\Gamma)\,. \tag{2.8}$$

This four-potential satisfies the Lorenz gauge condition [JAC99]. It is obtained by a Lorentz boost of the electrostatic potential $V_\Gamma(r)$ from a rest frame of centre Γ to the unprimed reference frame. In the case of a moving point charge it is usually referred to as a Liénard–Wiechert potential [JAC99, EM95].

A particular class of radially symmetric charge distributions will be important in the subsequent presentation, especially serving as an example in chapter 3. Consider the static charge distribution,

$$\rho_\Gamma(r) = -\frac{eZ_\Gamma\,\mu_\Gamma^2\exp(-\mu_\Gamma r)}{4\pi r} + eZ_\Gamma \begin{cases} \frac{3}{4\pi}\varrho_\Gamma^{-3} & \text{if } r \leq \varrho_\Gamma, \\ 0 & \text{otherwise,} \end{cases} \tag{2.9}$$

leading to the following electrostatic potential, vanishing at spatial infinity:

$$V_\Gamma(r) = \frac{eZ_\Gamma\exp(-\mu_\Gamma r) - eZ_\Gamma}{r} + \frac{eZ_\Gamma}{r} \begin{cases} \frac{3}{2}\frac{r}{\varrho_\Gamma} - \frac{1}{2}\left(\frac{r}{\varrho_\Gamma}\right)^3 & \text{if } r \leq \varrho_\Gamma, \\ 1 & \text{otherwise.} \end{cases} \tag{2.10}$$

Here e denotes the unit charge. This electrostatic potential depends on three parameters, namely Z_Γ, ϱ_Γ and μ_Γ. In the limit $\rho_\Gamma \to 0$ we obtain the Yukawa potential. The case where only $\mu_\Gamma = 0$ corresponds to the potential of a homogeneously charged sphere. If both $\mu_\Gamma = 0$ and $\rho_\Gamma = 0$ the potential $V_\Gamma(r)$ is identical to the Coulomb potential of a point charge with charge number Z_Γ. Clearly, the charge distribution (2.9) is a sum of a homogeneously charged sphere, with radius $\rho_\Gamma \geq 0$ and total charge eZ_Γ, and an infinitely extended screening charge distribution, with inverse screening length $\mu_\Gamma \geq 0$ (also known as the Debye screening parameter [JAC99]) and total charge $-eZ_\Gamma$. The total charge q_Γ corresponding to the charge distribution (2.9) is given by:

$$q_\Gamma = 4\pi \int_0^\infty r^2 \rho_\Gamma(r)\,\mathrm{d}r = \begin{cases} eZ_\Gamma & \text{if } \mu_\Gamma = 0, \\ 0 & \text{if } \mu_\Gamma > 0. \end{cases}$$

In particular Z_Γ is not the charge number of the total charge in the case of the Yukawa potential, but represents its field strength near the origin.

Such a potential is not unphysical, it is used as a simple model for an atomic potential, describing the finite nuclear size and the screening of the nuclear charge by the electrons of an atom. The nuclear radius then determines ϱ_Γ and the screening length μ_Γ is obtained by a rough fit to the Thomas–Fermi atomic potential [JAC99, 13.5]. In some situations the idealisation of the atomic nucleus as a point charge

is an over-simplification: a proper finite nuclear radius is essential, for example, in quantum electrodynamical calculations [MPS98].

2.3 Two-centre Dirac equation

We shall now introduce the Dirac equation for particles that are subject to the external electromagnetic field of the two linearly moving classical charge distributions presented in the previous section. This Dirac equation reads:

$$[H_0 + W_A(t, \boldsymbol{x}) + W_B(t, \boldsymbol{x}) - \mathrm{i}\partial_t]\,\Psi(t, \boldsymbol{x}) = 0. \tag{2.11}$$

Here, the following abbreviations have been used, which will be used throughout this thesis:

$$H_0 = -\mathrm{i}\boldsymbol{\alpha} \cdot \nabla + \beta, \tag{2.12}$$

$$W_A(t, \boldsymbol{x}) = -eV_A(r_A(t, \boldsymbol{x}))\,\gamma_A(1 - \boldsymbol{v}_A \cdot \boldsymbol{\alpha}), \tag{2.13}$$

$$W_B(t, \boldsymbol{x}) = -eV_B(r_B(t, \boldsymbol{x}))\,\gamma_B(1 - \boldsymbol{v}_B \cdot \boldsymbol{\alpha}). \tag{2.14}$$

Here $\boldsymbol{\alpha} = \alpha_1, \alpha_2, \alpha_3$ and β denote Dirac matrices. For the numerical calculations of this thesis the standard Dirac–Pauli representation has been used (cf. appendix C). However, all subsequent analytical considerations hold for an arbitrary, unitarily equivalent representation of the Dirac matrices, if not indicated otherwise.

In this thesis, equation (2.11) is referred to as the *two-centre Dirac equation*. The uppercase Greek letter Ψ usually denotes solutions of this two-centre Dirac equation. Note that the external electromagnetic field is minimally coupled to the Dirac field. We denote the unitary time-evolution operator of the two-centre Dirac equation by $U(t, s)$. It satisfies:

$$U(t, t) = 1, \quad U(t, s_0) = U(t, s)U(s, s_0), \quad U(t, s)^{-1} = U(t, s)^* = U(s, t), \tag{2.15}$$

and

$$[H_0 + W_A(t, \boldsymbol{x}) + W_B(t, \boldsymbol{x}) - \mathrm{i}\partial_t]\,U(t, s) = 0. \tag{2.16}$$

2.3.1 Note on the unitary time-evolution. If the external fields $W_A(t, \boldsymbol{x})$ and $W_B(t, \boldsymbol{x})$ are bounded functions, then it is well-known that the time-evolution operator is given by a Dyson series [RS75, THA92]. However, the Coulomb and Yukawa potentials (and their corresponding Liénard-Wiechert potentials) are not bounded. Therefore, the existence of a unitary time-evolution is a more complicated mathematical problem, since the self-adjointness of the time-dependent Hamilton operator $H(t)$ is not sufficient. The existence has been proved for the Dirac equation with moving point charges by Kato and Yajima using the technique of local pseudo-Lorentz transformations [KY91].

2.4 Symmetry

In this section, symmetries of the two-centre Dirac equation are discussed. Recall that a symmetry is a transformation of a solution $\Psi_1(t, \boldsymbol{x})$ of the time-dependent

Dirac equation into another time-dependent wave function $\Psi_2(t, \boldsymbol{x})$, such that both, Ψ_1 and Ψ_2, solve the same two-centre Dirac equation,

$$[H_0 + W_{\mathrm{A}}(t, \boldsymbol{x}) + W_{\mathrm{B}}(t, \boldsymbol{x}) - \mathrm{i}\partial_t]\,\Psi_i(t, \boldsymbol{x}) \qquad \text{for } i = 1, 2.$$

Such transformations must commute with the external field operator $W(t, \boldsymbol{x})$ and, therefore, they reflect the symmetries of the external field. In common text book presentations of invariance properties of the Dirac equation, the transformation of wave functions is always accompanied by a transformation of the external field. Occasionally, this form invariance of the Dirac equation, namely that a transformed Dirac spinor solves the transformed Dirac equation, is also called a symmetry of the Dirac equation [SCH95]. We shall stress that this is not meant by symmetry here. Instead the symmetries, described below, establish conserved quantities and the corresponding symmetry operators commute with the unitary time evolution $U(t, s)$ of the two-centre Dirac equation.

In order to facilitate the discussion of the symmetries of the two-centre Dirac equation it is useful to chose a particular frame of reference. In this section unprimed
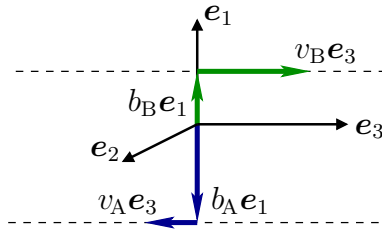
coordinates $(t, \boldsymbol{x})$ exclusively refer to a reference frame for which the trajectories $\boldsymbol{R}_{\mathrm{A}}(t)$ and $\boldsymbol{R}_{\mathrm{B}}(t)$ are given by:

$$\begin{aligned}
\boldsymbol{R}_{\mathrm{A}}(t) &= b_{\mathrm{A}}\boldsymbol{e}_1 + t v_{\mathrm{A}}\boldsymbol{e}_3, \\
\boldsymbol{R}_{\mathrm{B}}(t) &= b_{\mathrm{B}}\boldsymbol{e}_1 + t v_{\mathrm{B}}\boldsymbol{e}_3.
\end{aligned} \tag{2.17}$$

In such frames of reference the trajectories are invariant under a reflection at the $\boldsymbol{e}_1$-$\boldsymbol{e}_3$-plane. Another symmetry transformation is time-reversal in combination with a reflection in the $\boldsymbol{e}_1$-$\boldsymbol{e}_2$-plane. In order to construct operators representing these transformations on Dirac four-spinors, recall that an active rotation by some angle φ around an axis, which is given in terms of the unit three-vector $\boldsymbol{n}$, is generally represented by the following spinor transformation matrix [THA92, eq. (2.172)]:

$$\exp\left(-\frac{\mathrm{i}\varphi}{2}\,\boldsymbol{n} \cdot \gamma_5\boldsymbol{\alpha}\right).$$

Here the matrix γ_5 is defined as $\gamma_5 = \mathrm{i}\gamma_0\gamma_1\gamma_2\gamma_3$, in agreement with the phase conventions in [BD66, THA92, SCH95]. In the particular case of a rotation by an angle π around one of the coordinate axes the previous expression simplifies to:

$$\exp\left(-\frac{\pi\mathrm{i}}{2}\,\boldsymbol{e}_i \cdot \gamma_5\gamma^0\boldsymbol{\gamma}\right) = \exp\left(-\frac{\pi\mathrm{i}}{2}\,\gamma^i\gamma_5\gamma^0\right) = -\mathrm{i}\gamma^i\gamma_5\gamma^0.$$

A reflection at the plane that is perpendicular to $\boldsymbol{e}_i$ and passes through the origin can be obtained by a space inversion $\mathcal{P}$ (cf. section C.2 of the appendix) followed by

a rotation by π around $\boldsymbol{e}_i$. Therefore, the reflection of a Dirac wave function $\Psi(t, \boldsymbol{x})$ at the $\boldsymbol{e}_1$-$\boldsymbol{e}_3$-plane is accomplished by an operator $\mathcal{P}_2$ defined as follows:

$$(\mathcal{P}_2 \Psi)(t, \boldsymbol{x}) = \gamma^2 \gamma^5 \Psi(t, \boldsymbol{x} - 2x^2 \boldsymbol{e}_2). \tag{2.18}$$

Correspondingly the operators $\mathcal{P}_1$ and $\mathcal{P}_3$ may be defined by substituting all indices 2 with 1 and 3 respectively.

The operator $\mathcal{T}_3$ implementing the other transformation described above, namely a time reversal followed by a reflection at the $\boldsymbol{e}_1$-$\boldsymbol{e}_2$-plane, may be defined as,

$$\mathcal{T}_3 = \mathcal{P}_3 \mathcal{T}.$$

Here $\mathcal{T}$ denotes the time-reversal operator (cf. appendix C.2). In the following, C shall denote the unitary 4×4 matrix which satisfies $\gamma^{\mu T} = -C^{-1} \gamma^\mu C$ and $C^T = -C$, and which is employed in the standard definition of the time-reversal operator $\mathcal{T}$ for Dirac spinor-fields. With reference to C the operator $\mathcal{T}_3$ is then given explicitly by:

$$(\mathcal{T}_3 \Psi)(t, \boldsymbol{x}) = \gamma^3 C \Psi^*(-t, \boldsymbol{x} - 2x^3 \boldsymbol{e}_3), \tag{2.19}$$

The operators $\mathcal{T}_i$, where $i = 1, 2$, may again be defined similarly by $\mathcal{T}_i = \mathcal{P}_i \mathcal{T}$.

In the definitions (2.18) and (2.19) the phases have been chosen such that the operators $\mathcal{P}_i$ and $\mathcal{T}_i$ are involutions:

$$(\mathcal{P}_i{}^2 \Psi)(t, \boldsymbol{x}) = \gamma^i \gamma^5 \gamma^i \gamma^5 \Psi(t, \boldsymbol{x}) = \Psi(t, \boldsymbol{x}),$$

$$(\mathcal{T}_i{}^2 \Psi)(t, \boldsymbol{x}) = \gamma^i C K \gamma^i C K \Psi(t, \boldsymbol{x}) = \gamma^i C \gamma^{i*} C^* \Psi(t, \boldsymbol{x}) = \gamma^i \gamma^{i\dagger} \Psi(t, \boldsymbol{x}) = \Psi(t, \boldsymbol{x})$$

Here $i = 1, 2, 3$ and K denotes the operator of complex conjugation. Consequently, the eigenvalues of both $\mathcal{P}_i$ and $\mathcal{T}_i$ are ± 1. Note, however, that $\mathcal{P}_1 \mathcal{P}_2 \mathcal{P}_3 = i\mathcal{P}$. The following commutation and anti-commutation properties of the operators $\mathcal{P}_i$ and $\mathcal{T}_i$ are easily verified:[2]

$$[\mathcal{P}_i, \mathcal{T}_j] = 0. \; \{\mathcal{T}_i, \mathcal{T}_j\} = \{\mathcal{P}_i, \mathcal{P}_j\} = 2\delta_{ij}, \tag{2.20}$$

$$\tag{2.21}$$

2.4.1 Commutation properties. Next, it must be demonstrated that both of the commuting operators $\mathcal{P}_2$ and $\mathcal{T}_3$ implement a symmetry of the two-centre Dirac equation (2.11). Due to the particular choice of the Lorentz frame in this section, the scalars $r_A(t, \boldsymbol{x})$ and $r_B(t, \boldsymbol{x})$ satisfy the following identities:

$$r_\Gamma(t, \boldsymbol{x}) = r_\Gamma(t, \boldsymbol{x} - 2x^2 \boldsymbol{e}_2) = r_\Gamma(-t, \boldsymbol{x} - 2x^3 \boldsymbol{e}_3),$$

with $\Gamma = A, B$. Using this, we are able to verify that the external field operators W_A and W_B commute with both $\mathcal{P}_2$ and $\mathcal{T}_3$:

$$[\mathcal{P}_2, W_\Gamma] = [\mathcal{T}_3, W_\Gamma] = 0. \tag{2.22}$$

---

[2]For the standard Dirac-Pauli representation a valid choice for C is the real matrix $i\gamma^2\gamma^0$ (see section C.2 and [BD66, ch. 5]). Hence, the spinor transformation matrices of $\mathcal{P}_2$ and $\mathcal{T}_3$ take the form:

$$\gamma^2 \gamma^5 = i\gamma^2 \gamma^0 \gamma^1 \gamma^2 \gamma^3 = \begin{pmatrix} \sigma_2 & 0 \\ 0 & -\sigma_2 \end{pmatrix},$$

$$\gamma^3 C = i\gamma^3 \gamma^2 \gamma^0 = \begin{pmatrix} \sigma_1 & 0 \\ 0 & -\sigma_1 \end{pmatrix}.$$

First, it will be checked that the commutator of W_Γ and $\mathcal{P}_2$ vanishes:

$$
\begin{aligned}
(\mathcal{P}_2 W_\Gamma \mathcal{P}_2 \Psi)(t, \boldsymbol{x}) &= \gamma^2 \gamma^5 \, (W_\Gamma \mathcal{P}_2 \Psi)(t, \boldsymbol{x} - 2x^2 \boldsymbol{e}_2) \\
&= \gamma^2 \gamma^5 \, W_\Gamma(t, \boldsymbol{x} - 2x^2 \boldsymbol{e}_2) \, (\mathcal{P}_2 \Psi)(t, \boldsymbol{x} - 2x^2 \boldsymbol{e}_2) \\
&= -\gamma_\Gamma e \, V_\Gamma(r_\Gamma(t, \boldsymbol{x} - 2x^2 \boldsymbol{e}_2)) \, \gamma^2 \gamma^5 \, (1 - v_\Gamma \gamma^0 \gamma^3) \, \gamma^2 \gamma^5 \, \Psi(t, \boldsymbol{x}) \\
&= W_\Gamma(t, \boldsymbol{x}) \, \Psi(t, \boldsymbol{x}) = (W_\Gamma \Psi)(t, \boldsymbol{x}).
\end{aligned}
$$

Repeatedly using relation (C.9) of the appendix, the calculation for $\mathcal{T}_3$ is carried out similarly:

$$
\begin{aligned}
(\mathcal{T}_3 W_\Gamma \mathcal{T}_3 \Psi)(t, \boldsymbol{x}) &= \gamma^3 C \, (W_\Gamma \mathcal{T}_3 \Psi)^*(-t, \boldsymbol{x} - 2x^3 \boldsymbol{e}_3) \\
&= \gamma^3 C \, W_\Gamma^*(-t, \boldsymbol{x} - 2x^3 \boldsymbol{e}_3) \, (\mathcal{T}_3 \Psi)^*(-t, \boldsymbol{x} - 2x^3 \boldsymbol{e}_3) \\
&= \gamma^3 C \, W_\Gamma^*(-t, \boldsymbol{x} - 2x^3 \boldsymbol{e}_3) \, \gamma^{3*} C^* \, \Psi(t, \boldsymbol{x}) \\
&= -\gamma_\Gamma e \, V_\Gamma^*(r_\Gamma(-t, \boldsymbol{x} - 2x^3 \boldsymbol{e}_3)) \, \gamma^3 C (1 - v_\Gamma \gamma^{0*} \gamma^{3*}) C^* \gamma^3 \, \Psi(t, \boldsymbol{x}) \\
&= -\gamma_\Gamma e \, V_\Gamma(r_\Gamma(t, \boldsymbol{x})) \, \gamma^3 C C^* (1 - v_\Gamma \gamma^0 \gamma^3) \gamma^3 \, \Psi(t, \boldsymbol{x}) \\
&= W_\Gamma(t, \boldsymbol{x}) \, \Psi(t, \boldsymbol{x}) = (W_\Gamma \Psi)(t, \boldsymbol{x}).
\end{aligned}
$$

It remains to establish the commutation properties of $\mathcal{P}_2$ and $\mathcal{T}_3$ with H_0 and $\mathrm{i}D_0$. Up to a complex phase, the operators $\mathcal{P}_i$ and $\mathcal{T}_i$ are products of space-inversions, time-reversals and spatial rotations. Hence, the commutation relations can be deduced from well-known properties of the free Dirac equation. More precisely the following relations hold for $i = 1, 2, 3$ (for the notation cf. appendix C):

$$
[\mathcal{P}_i, H_0] = [\mathcal{T}_i, H_0] = 0, \tag{2.23}
$$

$$
[\mathcal{P}_i, \mathrm{i}D_0] = [\mathcal{T}_i, \mathrm{i}D_0] = 0 \tag{2.24}
$$

As an example the second part of (2.23) will be verified:

$$
\begin{aligned}
(\mathcal{T}_k H_0 \mathcal{T}_k \Psi)(t, \boldsymbol{x}) &= \gamma^k C \left(\gamma^0 \left(-\mathrm{i}\gamma^i D_i + 1 \right) \mathcal{T}_k \Psi \right)^* (-t, \boldsymbol{x} - 2x^k \boldsymbol{e}_k) \\
&= \gamma^k C \gamma^{0*} \left(\mathrm{i}\gamma^{i*} \partial_i - 2\mathrm{i}\gamma^{k*} \partial_k + 1 \right) (\mathcal{T}_k \Psi)^* (-t, \boldsymbol{x} - 2x^k \boldsymbol{e}_k) \\
&= \gamma^k C \gamma^{0*} \left(\mathrm{i}\gamma^{i*} \partial_i - 2\mathrm{i}\gamma^{k*} \partial_k + 1 \right) \gamma^{k*} C^* \Psi(t, \boldsymbol{x} - 2x^k \boldsymbol{e}_k) \\
&= -\gamma^k C C^* \gamma^0 \left(\mathrm{i}\gamma^{i*} \partial_i - 2\mathrm{i}\gamma^{k*} \partial_k - 1 \right) \gamma^k \Psi(t, \boldsymbol{x}) \\
&= \gamma^0 \left(\mathrm{i}\gamma^{i*} \partial_i + 1 \right) \Psi(t, \boldsymbol{x}) = (H_0 \Psi)(t, \boldsymbol{x}).
\end{aligned}
$$

Note that in the previous calculation there shall not be a summation over the repeated index $k = 1, 2, 3$.

2.4.2 Unitary time-evolution. Since $\mathcal{P}_2$ commutes with the time-dependent Hamiltonian of the two-centre Dirac equation and with the time-derivative, it is verified that $\mathcal{P}_2 U(t, s) \mathcal{P}_2$ is also a unitary time-evolution of the two-centre Dirac equation and, therefore, identical with $U(t, s)$. Hence, the operators $\mathcal{P}_2$ and $U(t, s)$ commute:

$$
U(t, s) \, \mathcal{P}_2 = \mathcal{P}_2 \, U(t, s).
$$

We conclude that solutions $\Psi(t, \boldsymbol{x})$ of the two-centre Dirac equation may be constructed such that they are eigenfunctions of both $\mathcal{P}_2$ and $\mathcal{T}_3$. In other words $\mathcal{P}_2$ and $\mathcal{T}_3$ represent conserved quantities of the time-dependent two-centre Dirac equation in any frame of reference where the trajectories are given by (2.17). In other

coordinate systems the symmetry operators corresponding to these conserved quantities may be obtained by a Poincaré-transformation of $\mathcal{P}_2$ and $\mathcal{T}_3$ respectively. It can be shown that $\mathcal{P}_2$ and $\mathcal{T}_3$ commute with Lorentz boosts in $\boldsymbol{e}_3$-direction and also with spatial translations in $\boldsymbol{e}_1$-direction. Hence, the definitions (2.18) and (2.19) are unambiguous.

The physical importance of these symmetries is that they lead to corresponding symmetries of the transition amplitudes, which are defined in the next chapter.

2.5 Homonuclear collisions

In the following a two-centre Dirac equation (2.11) is considered for which the radial electrostatic potentials V_A and V_B are equal. This situation corresponds to a homonuclear collision system. In order to discuss the additional symmetry, parity, present only in those homonuclear collisions, it is useful to chose a coordinate system, in which both centres move with equal but opposite velocities and have the same dis-

tance to the origin at time $t = 0$. Hence, the trajectories shall be given by equations (2.1) with,
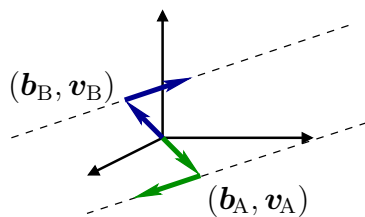
$$\boldsymbol{v}_B = -\boldsymbol{v}_A,$$
$$\boldsymbol{b}_B = -\boldsymbol{b}_A.$$

Then the following relation holds:

$$r_B(t, \boldsymbol{x}) = r_A(t, -\boldsymbol{x}). \tag{2.25}$$

It can be shown similarly to the previous section that the parity operator $\mathcal{P}$ (cf. equation (C.5) of appendix C) transforms the external field operators W_A and W_B into each other:

$$\mathcal{P}W_A\mathcal{P} = W_B,$$
$$\mathcal{P}W_B\mathcal{P} = W_A.$$

Therefore, in the reference frame considered here, the parity operator $\mathcal{P}$ commutes with the time-dependent Hamiltonian $H(t) = H_0 + W_A(t) + W_B(t)$ of the two-centre Dirac equation. Parity is a constant of motion.

Multi-Channel Scattering Theory

The two-centre Dirac equation has been introduced as a model, for describing charge transfer, ionisation and pair creation in peripheral collisions of highly charged heavy-ions. Intuition suggests that the two-centre Dirac equation should have solutions which correspond to particles asymptotically bound to the electrostatic potential V_Γ of centre A or centre B, or move away from both centres, as time t tends to $+\infty$ or $-\infty$. This corresponds to three different scattering channels or three different types of scattering states: those, which are essentially subject to either one of the external fields $W_A(t, \boldsymbol{x})$ or $W_B(t, \boldsymbol{x})$, and those, which are not significantly influenced by any external field, as t tends to $\pm\infty$.

The scattering theory of the two-centre Dirac equation is presented here essentially for two reasons. First, it seems that a formal discussion of this scattering theory is not available; although several authors have discussed the scattering theory of the similar two-centre Schrödinger equation from a conceptional and mathematical point of view [YAJ80, HAG82, WÜL88, GRA90]. Second, a precise definition of the transition amplitude is given. This is a necessary prerequisite in order to prove the relativistic invariance of the scattering theory. Boost invariance is not a trivial property in the present case, as it is for the scattering theory of the two-centre Schrödinger equation: Lorentz boosts transform the time axes, with respect to which the (necessarily) time-dependent scattering theory is formulated.

3.1 Scattering channels

First, let us introduce some notation. The three different scattering channels mentioned above correspond to three different Dirac equations, describing Dirac particles, which are bound to either of the external fields $W_\Gamma(t, \boldsymbol{x})$ or move freely. The Hamilton operators of these scattering-channel Dirac equations are:

$$
\begin{aligned}
H_A(t) &= H_0 + W_A(t, \boldsymbol{x}) \\
H_B(t) &= H_0 + W_B(t, \boldsymbol{x}) \\
H_C &= H_0.
\end{aligned}
\tag{3.1}
$$

As opposed to conventional quantum-mechanical multi-particle scattering theory [SAN72, SAN74, THI94], these scattering channel Hamiltonians have an explicit time-dependence. The time-dependence of the Hamiltonian operators $H_A(t)$ and $H_B(t)$ cannot be removed simultaneously by a Poincaré transformation, if the centres are moving with different velocities. The unitary time-evolution operators of the scattering-channel Dirac equations are respectively denoted by,

$$
U_A(t, s), \quad U_B(t, s) \quad \text{and} \quad U_C(t, s) = \exp(-\mathrm{i}(t - s)H_0).
$$

Solutions of the scattering-channel Dirac equations are denoted by the uppercase Greek letter Φ, with a lower index indicating the respective scattering channel, for

example:

$$[H_0 + W_A(t, \boldsymbol{x}) - \mathrm{i}\partial_t]\, \Phi_{A,k}(t, \boldsymbol{x}) = 0.$$

The second index k is used to differentiate between different solutions of the same Dirac equation symbolically. These wave functions $\Phi_{\Gamma,k}(t, \boldsymbol{x})$, where $\Gamma = A, B, C$ will be referred to as *asymptotic configurations*, following [BH63, THA92]. In other literature, they are also called in- and out-states [NEW82, WEI95].

3.1.1 Scattering states. A principal problem of scattering theory, as presenting itself in present context, is to find solutions $\Psi^+_{\Gamma,k}(t, \boldsymbol{x})$ and $\Psi^-_{\Gamma,k}(t, \boldsymbol{x})$ of the two-centre Dirac equation, which asymptotically approach the asymptotic configuration $\Phi_{\Gamma,k}(t, \boldsymbol{x})$:

$$\lim_{t \to -\infty} \| \Phi_{\Gamma,k}(t) - \Psi^+_{\Gamma,k}(t) \| = 0$$
$$\lim_{t \to +\infty} \| \Phi_{\Gamma,k}(t) - \Psi^-_{\Gamma,k}(t) \| = 0.$$

Here $\|.\|$ denotes the Hilbert-space norm of a wave function (cf. appendix C). The wave functions $\Psi^+_{\Gamma,k}(t, \boldsymbol{x})$ and $\Psi^-_{\Gamma,k}(t, \boldsymbol{x})$ are usually referred to as the *incoming* and the *outgoing scattering states* respectively. The seemingly paradoxical notation, in which Ψ^+ corresponds to the limit $t \to -\infty$ and vice versa, originates in the time-independent formulation of scattering theory. Although the latter cannot be applied in the present situation, this notation, common to many presentations of quantum scattering theory [BD66, SAN72, RS79, NEW82, HAG82, GRA90], is employed here as well. The question, whether scattering states $\Psi^+_{\Gamma,k}(t)$ and $\Psi^-_{\Gamma,k}(t)$ exist, for an arbitrary solution $\Phi_{\Gamma,k}(t, \boldsymbol{x})$ of the Dirac equation of the scattering channel Γ, is known as the problem of *asymptotic convergence*. For certain classes of electrostatic potentials $V_\Gamma(r)$ asymptotic convergence is proved in section 3.3 below.

In the case of the scattering channels A and B, only such asymptotic configurations that correspond to *bound states* of the respective potential are admitted. Wave functions corresponding to continuum eigenfunctions of the electrostatic potentials in their respective rest frames are moving away from their centres as time increases. Therefore, they are attributed to scattering channel C. Taking this convention into account, it will be shown that scattering states corresponding to different scattering channels are orthogonal to each other (see section 3.4 below):

$$\left(\Psi^+_{\Gamma,k}(t), \Psi^+_{\Delta,l}(t) \right) = \left(\Psi^-_{\Gamma,k}(t), \Psi^-_{\Delta,l}(t) \right) = 0, \qquad \text{if } \Gamma \neq \Delta.$$

This property is known as *asymptotic orthogonality*.

3.1.2 Wave operators. For the two-centre Dirac equation, asymptotic convergence is equivalent to the existence of the following strong operator limits:

$$\Omega^\pm_A(s) = \operatorname*{s\text{-}lim}_{t \to \mp\infty} \Omega_A(t, s) = \operatorname*{s\text{-}lim}_{t \to \mp\infty} U(t, s)^{-1}\, U_A(t, s)\, P_A(s).$$
$$\Omega^\pm_B(s) = \operatorname*{s\text{-}lim}_{t \to \mp\infty} \Omega_B(t, s) = \operatorname*{s\text{-}lim}_{t \to \mp\infty} U(t, s)^{-1}\, U_B(t, s)\, P_B(s), \qquad (3.2)$$
$$\Omega^\pm_C(s) = \operatorname*{s\text{-}lim}_{t \to \mp\infty} \Omega_C(t, s) = \operatorname*{s\text{-}lim}_{t \to \mp\infty} U(t, s)^{-1} \exp(-\mathrm{i}(t - s)H_0).$$

The Møller operators $\Omega^\pm_\Gamma(s)$ are time-dependent in the present situation, which has its origin in the time-dependence of the scattering-channel Hamiltonians (3.1). In

conventional multi-channel scattering theory the Møller wave operators are not time-dependent. But the same time-dependence occurs for the scattering theory of the two-centre Schrödinger equation (see e.g. [HAG82]).

In equations (3.2) the projection operators $P_A(s)$ and $P_B(s)$ have been introduced, in order to project onto the subspace of asymptotic configurations $\Phi_\Gamma(t, \boldsymbol{x})$ that correspond to bound states of the external fields $W_A(t, \boldsymbol{x})$ and $W_B(t, \boldsymbol{x})$ respectively. The projection operators are included into the definition of the wave operators $\Omega_A^\pm(s)$ and $\Omega_B^\pm(s)$, in order to obtain orthogonality of their ranges, which are then orthogonal proper subspaces of the state space $L^2(\mathbb{R}^3)^4$ of the classical Dirac equation.

For later reference, explicit representations of these time-dependent projection operators, $P_A(s)$ and $P_B(s)$, are given in the following. Let (Λ_A, a_A) denote the Poincaré transformation from the unprimed reference frame to a primed rest frame of centre A in which centre A is located at the spatial origin, i.e. $\boldsymbol{R}'_A(t') = 0$. In the primed frame, the Hamiltonian H'_A of scattering channel A does not depend on the time t':

$$H'_A = H'_0 - eV_A(|\boldsymbol{x}'|).$$

Throughout this chapter, the potential V_A is assumed to be of such a form that H'_A has bound states. In the primed frame, choose a complete set of orthonormal bound state eigenfunctions, denoted by $\phi_{A,k}(\boldsymbol{x}')$, with eigenenergies $\epsilon_{A,k}$. Then the projector P'_A onto the subspace of the bound states of the potential V_A in the primed frame is time-independent and given by:

$$(P'_A \phi)(\boldsymbol{x}') = \sum_k (\phi_{A,k}, \phi)' \, \phi_{A,k}(\boldsymbol{x}').$$

In the unprimed frame, the asymptotic configuration $\Phi_{A,k}(t, \boldsymbol{x})$, corresponding to the bound state $\phi_{A,k}(\boldsymbol{x}')$ in the primed frame, is obtained by a Poincaré transformation:

$$\Phi_{A,k}(t, \boldsymbol{x}) = S(\Lambda_A)^{-1} \exp(-\mathrm{i}t'\epsilon_{A,k})\phi_{A,k}(\boldsymbol{x}'), \tag{3.3}$$

Here $S(\Lambda_A)$ is the spinor-representation matrix of the Lorentz transformation Λ_A and the primed coordinates are given by $(t', \boldsymbol{x}') = \Lambda_A(t, \boldsymbol{x}) + (a^0, \boldsymbol{a})$. The time-dependent projector $P_A(s)$ in the unprimed reference frame, projecting onto the bound states of the external field $W_A(t, \boldsymbol{x})$, is thus given by:

$$(P_A(s)\psi) = \sum_k (\Phi_{A,k}(s), \psi) \, \Phi_{A,k}(s, \boldsymbol{x}). \tag{3.4}$$

An explicit representation of $P_B(s)$ is given analogously.

3.2 Transition amplitudes

The two-centre Dirac equation is used by many authors as a model in order to describe atomic processes in collisions of heavy and highly charged ions, like excitation, ionisation, charge transfer and pair creation [EM95]. For example, an electron initially bound to either of the colliding nuclei is represented in this model by an incoming scattering state, $\Psi_A^+(t, \boldsymbol{x})$ or $\Psi_B^+(t, \boldsymbol{x})$. Electron states after the collision are represented by outgoing scattering states $\Psi_\Gamma^-(t, \boldsymbol{x})$.
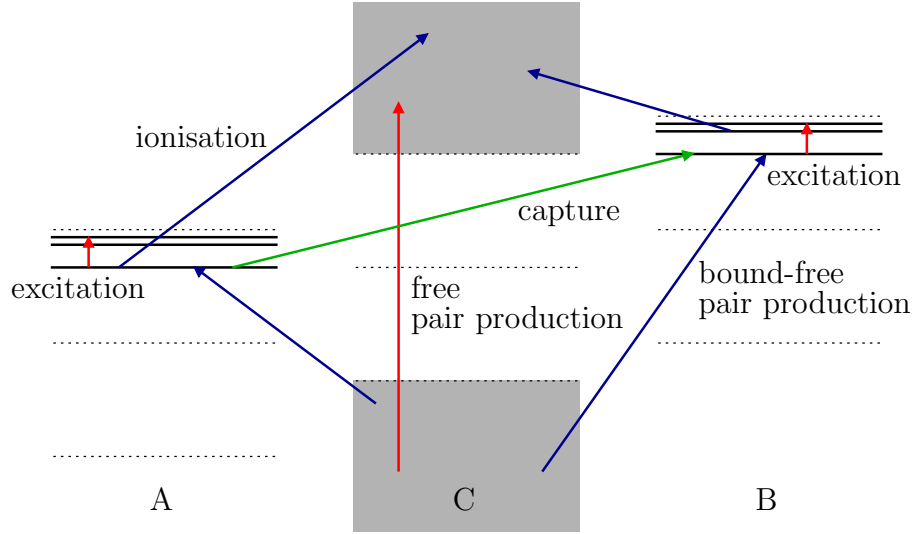
FIGURE 3.1. This figure illustrates the scattering theory of the two-centre Dirac equation. Transitions within the same scattering channel, i.e. excitation and free pair production, are depicted by red arrows. Blue arrows correspond to processes of ionisation and bound-free pair production. Finally, charge transfer is shown as a green arrow. The three different energy spectra represent the three scattering channels A, B and C.

The probability amplitude $a_{\Delta l, \Gamma k}$ for a state of incoming configuration $\Phi_{\Gamma, k}(s)$ to have the outgoing configuration $\Phi_{\Delta, l}(s)$ is given by,

$$a_{\Delta l, \Gamma k} = \left(\Psi^-_{\Delta, l}(s), \Psi^+_{\Gamma, k}(s) \right). \tag{3.5}$$

Due to the unitarity of the time-evolution of the two-centre Dirac equation, the definition of the transition amplitude is independent of the time s. The various atomic processes are depicted in figure 3.1. There are other equivalent expressions for the transition amplitude, some of them listed below. In particular, the post and prior forms frequently appear in the literature.

$$
\begin{aligned}
a_{\Delta l, \Gamma k} &= \left(\Omega^-_\Delta(s) \Phi_{\Delta, l}(s), \Omega^+_\Gamma(s) \Phi_{\Gamma, k}(s) \right) \\
&= \lim_{\substack{t_1 \to -\infty \\ t_2 \to \infty}} \left(U(s, t_2) U_\Delta(t_2, s) \Phi_{\Delta, l}(s), U(s, t_1) U(t_1, s) \Phi_{\Gamma, k}(s) \right) \\
&= \lim_{\substack{t_1 \to -\infty \\ t_2 \to \infty}} \left(\Phi_{\Delta, l}(t_2), U(t_2, t_1) \Phi_{\Gamma, k}(t_1) \right) \\
&= \lim_{t \to \infty} \left(\Phi_{\Delta, l}(t), \Psi^+_{\Gamma, k}(t) \right) \quad \text{(post form)} \\
&= \lim_{t \to -\infty} \left(\Psi^-_{\Delta, l}(t), \Phi_{\Gamma, k}(t) \right) \quad \text{(prior form).}
\end{aligned}
$$

For the discussion of asymptotic completeness we refer to section 3.6 below.

3.3 Asymptotic convergence

In this section, we will prove the existence of the operator-limits (3.2), defining the Møller wave operators $\Omega^\pm_\Gamma(s)$, under the assumption that the external fields $W_A(t, \boldsymbol{x})$

and $W_{\mathrm{B}}(t, \boldsymbol{x})$ are short-ranged. Asymptotic convergence is essential for an unambiguous definition of the transition amplitude $a_{\Delta l, \Gamma k}$ in equation (3.5). The case of particular interest, in which moving point charges are the source of external fields, is not covered in this section. This principal model of the literature has long-range external fields (cf. sections 3.6 and 3.7 below).

The material presented in the following has not appeared in literature, but some aspects resemble a discussion of the nonrelativistic charge-transfer model in [YAJ80]. Furthermore, the first subsection recalls standard mathematical results. For detailed explanations of the notation the reader is referred to appendix C.

3.3.1 Cook's method. The proofs of convergence given below are based on a method which was introduced by Cook [COO57]. Cook's method has become a standard tool for convergence proofs of wave operators, see e.g. [KAT80, DOL64, DV66, RS79, YAJ80, WÜL88]. In this subsection Cook's reasoning, as applicable in the present context, will be reviewed shortly (see in particular [KAT80, subsec. X.3.3] and [RS79, sec. XI.3]).

The convergence of the limit,

$$\Omega_{\Gamma}^{-}(s) = \underset{t \to \infty}{\text{s-lim}} \; \Omega_{\Gamma}(t, s)$$

with respect to the strong operator topology (cf. [RS80]) is equivalent to,

$$\left\| \left(\Omega_{\Gamma}(t_1, s) - \Omega_{\Gamma}(t_0, s) \right) \phi \right\| \to 0,$$

as $t_0, t_1 \to \infty$ for all $\phi(\boldsymbol{x})$, elements of the Hilbert space $L^2(\mathbb{R}^3)^4$. This equivalence holds due to the completeness of $L^2(\mathbb{R}^3)^4$ (Cauchy criterion). The convergence on a dense subspace already implies convergence on the complete state space in the present situation (see e.g. [KAT80, p. 151]). The estimate,

$$\left\| \Omega_{\Gamma}(t_1, s)\phi - \Omega_{\Gamma}(t_0, s)\phi \right\| = \left\| \int_{t_0}^{t_1} \left[\tfrac{\mathrm{d}}{\mathrm{d}t} \, \Omega_{\Gamma}(t, s)\phi \right] \mathrm{d}t \right\| \leq \int_{t_0}^{t_1} \left\| \tfrac{\mathrm{d}}{\mathrm{d}t} \, \Omega_{\Gamma}(t, s)\phi \right\| \mathrm{d}t,$$

leads to the following conclusion: A sufficient condition for the existence of the wave operator $\Omega_{\Gamma}^{-}(s)$ is the finiteness of the following time-integral,

$$\int_{t_0}^{\infty} \left\| \tfrac{\mathrm{d}}{\mathrm{d}t} \, \Omega_{\Gamma}(t, s)\phi \right\| \mathrm{d}t \; < \; \infty, \tag{3.6}$$

for some (arbitrary but finite) time t_0 and all $\phi(\boldsymbol{x})$ of a subspace of wave functions that is dense in the state space $L^2(\mathbb{R}^3)^4$.

Obviously, a sufficient condition for the convergence as $t \to -\infty$, i.e. the existence of the wave operator $\Omega_{\Gamma}^{+}(s)$, is established in a similar manner.

3.3.2 Asymptotically bound particles. In this subsection, we prove the existence of the strong operator limit $\Omega_{\mathrm{A}}^{-}(s)$. The other three wave operators $\Omega_{\mathrm{A}}^{+}(s)$ and $\Omega_{\mathrm{B}}^{\pm}(s)$ are treated analogously. The Cook integral (3.6) for $\Omega_{\mathrm{A}}^{-}(s)$ reads:

$$\int_{t_0}^{\infty} \left\| \tfrac{\mathrm{d}}{\mathrm{d}t} \, \Omega_{\mathrm{A}}(t, s)\phi \right\| \mathrm{d}t \; = \; \int_{t_0}^{\infty} \left\| W_{\mathrm{B}}(t) U_{\mathrm{A}}(t, s) P_{\mathrm{A}}(s)\phi \right\| \mathrm{d}t. \tag{3.7}$$

Recalling the definition (2.14) of $W_\mathrm{B}(t, \boldsymbol{x})$, the integrand on the right hand side of equation (3.7) is estimated as follows:

$$
\begin{aligned}
&\|W_\mathrm{B}(t) U_\mathrm{A}(t, s) P_\mathrm{A}(s)\phi\| \\
&= \left\| W_\mathrm{B}(t) \sum_k c_k \Phi_{\mathrm{A},k}(t) \right\| \\
&\leq \sum_k |c_k(s)|\, \|W_\mathrm{B}(t)\Phi_{\mathrm{A},k}(t)\| \\
&= \sum_k |c_k(s)|\, \|\gamma_\mathrm{B}(1 - \boldsymbol{v}_\mathrm{B}\cdot\boldsymbol{\alpha})\, V_\mathrm{B}(r_\mathrm{B}(t,\boldsymbol{x}))\, \Phi_{\mathrm{A},k}(t,\boldsymbol{x})\|_{L^2(\mathbb{R}^3, \mathrm{d}^3 x)^4} \\
&\leq \sum_k \gamma_\mathrm{B}|c_k(s)|\, \|(1 - \boldsymbol{v}_\mathrm{B}\cdot\boldsymbol{\alpha})\|_2\, \|V_\mathrm{B}(r_\mathrm{B}(t,\boldsymbol{x}))\Phi_{\mathrm{A},k}(t,\boldsymbol{x})\|_{L^2(\mathbb{R}^3, \mathrm{d}^3 x)^4}\,,
\end{aligned}
$$
(3.8)

with $c_k(s) = (\Phi_{\mathrm{A},k}(s), \phi)$ and $\|.\|_2$ denotes the matrix norm with respect to the scalar product in $\mathbb{C}^4$ (see appendix C or [GV96]). The following inequality may be proved for the straight line trajectories $\boldsymbol{R}_\mathrm{A}(t)$ and $\boldsymbol{R}_\mathrm{B}(t)$, as in equation (2.1), and arbitrary $\boldsymbol{x} \in \mathbb{R}^3$ and $t \in \mathbb{R}$:

$$
\frac{1}{1 + |\boldsymbol{x} - \boldsymbol{R}_\mathrm{A}(t)|^2} \frac{1}{1 + |\boldsymbol{x} - \boldsymbol{R}_\mathrm{B}(t)|^2} \leq \frac{2}{1 + |\boldsymbol{R}_\mathrm{A}(t) - \boldsymbol{R}_\mathrm{B}(t)|^2}.
$$

In conjunction with inequality (2.5) and the Hölder inequality [FOR84, RS80] the estimate of the integrand of the Cook integral (3.7) may be continued as follows:

$$
\begin{aligned}
&\|W_\mathrm{B}(t)\Phi_{\mathrm{A},k}(t)\| \\
&\leq \frac{2\gamma_\mathrm{B}\, \|(1 - \boldsymbol{v}_\mathrm{B}\cdot\boldsymbol{\alpha})\|_2}{1 + |\boldsymbol{R}_\mathrm{A}(t) - \boldsymbol{R}_\mathrm{B}(t)|^2} \times \\
&\qquad \left\| \left(1 + r_\mathrm{B}(t,\boldsymbol{x})^2\right) V_\mathrm{B}(r_\mathrm{B}(t,\boldsymbol{x})) \left(1 + r_\mathrm{A}(t,\boldsymbol{x})^2\right) \Phi_{\mathrm{A},k}(t,\boldsymbol{x}) \right\|_{L^2(\mathbb{R}^3, \mathrm{d}^3 x)^4} \\
&\leq \frac{2\gamma_\mathrm{B}\, \|(1 - \boldsymbol{v}_\mathrm{B}\cdot\boldsymbol{\alpha})\|_2}{1 + |\boldsymbol{R}_\mathrm{A}(t) - \boldsymbol{R}_\mathrm{B}(t)|^2} \left\| \left(1 + r_\mathrm{B}(t,\boldsymbol{x})^2\right) V_\mathrm{B}(r_\mathrm{B}(t,\boldsymbol{x})) \right\|_{L^p(\mathbb{R}^3, \mathrm{d}^3 x)} \times \\
&\qquad \sum_{i=1}^{4} \left\| \left(1 + r_\mathrm{A}(t,\boldsymbol{x})^2\right) \Phi_{\mathrm{A},k;i}(t,\boldsymbol{x}) \right\|_{L^q(\mathbb{R}^3, \mathrm{d}^3 x)}
\end{aligned}
$$

Here, the positive real numbers p and q have to be chosen such that $\frac{1}{p} + \frac{1}{q} = \frac{1}{2}$. The index i denotes the spinor index of the Dirac four-spinor $\Phi_{\mathrm{A},k}(t,\boldsymbol{x})$.

It remains to show that the norms,

$$
\left\| \left(1 + r_\mathrm{A}(t,\boldsymbol{x})^2\right) \Phi_{\mathrm{A},k;i}(t,\boldsymbol{x}) \right\|_{L^p(\mathbb{R}^3, \mathrm{d}^3 x)} \quad \text{and}
$$
$$
\left\| \left(1 + r_\mathrm{B}(t,\boldsymbol{x})^2\right) V_\mathrm{B}(r_\mathrm{B}(t,\boldsymbol{x})) \right\|_{L^q(\mathbb{R}^3, \mathrm{d}^3 x)}\,,
$$

are finite and moreover time-independent. This is true for arbitrary p and q, if the radial electrostatic potentials V_Γ are of the form (2.10) with $\mu_\Gamma > 0$ and $\rho_\Gamma > 0$. Furthermore, it can be verified that suitable p and q can be determined also in the case the Yukawa potentials, $\varrho_\Gamma = 0$, if $e^2 Z_\mathrm{B} < \frac{\sqrt{3}}{2}$ holds. The sum in equation (3.8) is finite if $\mu_\Gamma > 0$. In the cases mentioned, the estimate,

$$
\int_{t_0}^{\infty} \left\| \tfrac{\mathrm{d}}{\mathrm{d}t} \Omega_\mathrm{A}(t,s)\phi \right\| \mathrm{d}t \leq \int_{t_0}^{\infty} \frac{\text{const.}}{1 + |(\boldsymbol{b}_\mathrm{A} - \boldsymbol{b}_\mathrm{B}) + t(\boldsymbol{v}_\mathrm{A} - \boldsymbol{v}_\mathrm{B})|^2}\, \mathrm{d}t < \infty,
$$

holds and, thereby, shows that the Cook integral (3.6) for $\Omega_\mathrm{A}^-(s)$ is finite.

3.3.3 Asymptotically free particles. In order to show the existence of of $\Omega_{\mathrm{C}}^-(s)$ we consider the Cook integral (3.6) for scattering channel C:

$$
\int_{t_0}^{\infty} \left\| \tfrac{\mathrm{d}}{\mathrm{d}t} \, \Omega_{\mathrm{C}}(t,s)\phi \right\| \mathrm{d}t \;=\; \int_{t_0}^{\infty} \left\| [W_{\mathrm{A}}(t) + W_{\mathrm{B}}(t)] \, \mathrm{e}^{-\mathrm{i}(t-s)H_0} \, \phi \right\| \mathrm{d}t
$$

$$
\leq \; \sum_{\Gamma=\mathrm{A},\mathrm{B}} \int_{t_0}^{\infty} \left\| W_{\Gamma}(t) \, \mathrm{e}^{-\mathrm{i}(t-s)H_0} \, \phi \right\| \mathrm{d}t.
$$

Here $\phi(\boldsymbol{x})$ shall be a regular free Dirac wave packet,

$$
\phi(\boldsymbol{x}) = (2\pi)^{-3/2} \int \mathrm{e}^{\mathrm{i}\boldsymbol{x}\cdot\boldsymbol{p}} \, \hat{\phi}(\boldsymbol{p}) \, \mathrm{d}^3 p,
$$

with $\hat{\phi}(\boldsymbol{p}) \in C_0^\infty(\mathbb{R}^3)^4$ (cf. section B.1). It is sufficient to consider regular wave packets because they are dense in the state space $L^2(\mathbb{R}^3)^4$. The estimate is continued as follows:

$$
\left\| W_{\Gamma}(t) \, \mathrm{e}^{-\mathrm{i}(t-s)H_0} \, \phi \right\|
$$

$$
= \; \left\| \gamma_{\Gamma}(1 - \boldsymbol{v}_{\Gamma}\cdot\boldsymbol{\alpha}) V_{\Gamma}(r_{\Gamma}(t,\boldsymbol{x})) \, \mathrm{e}^{-\mathrm{i}(t-s)H_0} \, \phi(\boldsymbol{x}) \right\|_{L^2(\mathbb{R}^3,\mathrm{d}^3x)^4}
$$

$$
\leq \; \gamma_{\Gamma} \left\| 1 - \boldsymbol{v}_{\Gamma}\cdot\boldsymbol{\alpha} \right\|_2 \left\| V_{\Gamma}(r_{\Gamma}(t,\boldsymbol{x})) \, \mathrm{e}^{-\mathrm{i}(t-s)H_0} \, \phi(\boldsymbol{x}) \right\|_{L^2(\mathbb{R}^3,\mathrm{d}^3x)^4}
$$

$$
\leq \; 2\gamma_{\Gamma} \left\| 1 - \boldsymbol{v}_{\Gamma}\cdot\boldsymbol{\alpha} \right\|_2 \sup_{\boldsymbol{x}\in\mathbb{R}^3} \left\| \mathrm{e}^{-\mathrm{i}(t-s)H_0} \, \phi(\boldsymbol{x}) \right\|_2 \left\| V_{\Gamma}(r_{\Gamma}(t,\boldsymbol{x})) \right\|_{L^2(\mathbb{R}^3,\mathrm{d}^3x)}
$$

$$
\leq \; \frac{\mathrm{const.}}{(1+|t-s|^{3/2})} \int_0^\infty |r\,V_{\Gamma}(r)|^2 \, \mathrm{d}r
$$

For the last step, a propagation estimate for regular free wave packets has been used, which is reviewed in section B.1. Provided that the integral over $rV_{\Gamma}(r)$ is finite, the Cook integral for a regular wave packet ϕ is finite as well:

$$
\int_{t_0}^{\infty} \left\| \tfrac{\mathrm{d}}{\mathrm{d}t} \, \Omega_{\mathrm{C}}(t,s)\phi \right\| \mathrm{d}t \leq \int_{t_0}^{\infty} \frac{\mathrm{const.}'}{(1+|t-s|)^{3/2}} \, \mathrm{d}t < \infty.
$$

The integrability of $rV_{\Gamma}(r)$ holds in particular for potentials $V_{\Gamma}(r)$ as in equation (2.10), if $\mu_{\Gamma} > 0$.

3.4 Asymptotic orthogonality

In this section, we demonstrate the asymptotic orthogonality of the wave operators. The calculations are simple and given here for the sake of completeness. Asymptotic orthogonality means that the ranges of the wave operators are mutually orthogonal subspaces of the state space, i.e. $\operatorname{Ran}\Omega_{\Gamma}^\pm(s) \perp \operatorname{Ran}\Omega_{\Delta}^\pm(s)$ if $\Gamma \neq \Delta$. By definition this relation means that for any pair of states ϕ_1 and ϕ_2 the following scalar product vanishes,

$$
\left(\Omega_{\Delta}^\pm(s)\phi_2, \Omega_{\Gamma}^\pm(s)\phi_1 \right) = 0, \qquad \text{if } \Gamma \neq \Delta,
$$

which is equivalent to,

$$
\lim_{t\to\mp\infty} \left(U_{\Delta}(t,s)P_{\Delta}(s)\phi_2, U_{\Gamma}(t,s)P_{\Gamma}(s)\phi_1 \right) = 0.
$$

Here the projector $P_{\mathrm{C}}(s)$ is trivially defined as the unit operator. It is sufficient to consider the following two cases:

$$\mathrm{Ran}\,\Omega_{\mathrm{A}}^{-}(s) \perp \mathrm{Ran}\,\Omega_{\mathrm{B}}^{-}(s), \tag{3.9}$$

$$\mathrm{Ran}\,\Omega_{\mathrm{A}}^{-}(s) \perp \mathrm{Ran}\,\Omega_{\mathrm{C}}^{-}(s). \tag{3.10}$$

3.4.1 Orthogonality of channels A and B. Recalling the form (3.4) of the projection operators $P_{\mathrm{A}}(s)$ and $P_{\mathrm{B}}(s)$, it must be shown for any pair of asymptotic configurations $\Phi_{\mathrm{A},k}(t,\boldsymbol{x})$ and $\Phi_{\mathrm{B},l}(t,\boldsymbol{x})$ of the form (3.3) that

$$\lim_{t\to\infty}\left(\Phi_{\mathrm{A},k}(t),\Phi_{\mathrm{B},l}(t)\right) = 0, \tag{3.11}$$

in order to verify relation (3.9). We estimate the scalar product (3.11) as follows:

$$
\begin{aligned}
&\left|\left(\Phi_{\mathrm{A},k}(t),\Phi_{\mathrm{B},l}(t)\right)\right| \\
&\leq \int \left|\phi_{\mathrm{A},k}(\boldsymbol{x}')^{\dagger} S(\Lambda_{\mathrm{A}})^{\dagger^{-1}} S(\Lambda_{\mathrm{B}})^{-1}\phi_{\mathrm{B},l}(\boldsymbol{x}'')\right|\,\mathrm{d}^3x \\
&\leq \|S(\Lambda_{\mathrm{A}})^{\dagger^{-1}}S(\Lambda_{\mathrm{B}})^{-1}\|_2 \int \|\phi_{\mathrm{A},k}(\boldsymbol{x}')\|_2\,\|\phi_{\mathrm{B},l}(\boldsymbol{x}'')\|_2\,\mathrm{d}^3x \\
&\leq \frac{2\,\|S(\Lambda_{\mathrm{A}})^{\dagger^{-1}}S(\Lambda_{\mathrm{B}})^{-1}\|_2}{1+|(\boldsymbol{b}_{\mathrm{B}}-\boldsymbol{b}_{\mathrm{A}})+t(\boldsymbol{v}_{\mathrm{B}}-\boldsymbol{v}_{\mathrm{A}})|^2}\times \\
&\qquad\times \int \left\|(1+r_{\mathrm{A}}(t,\boldsymbol{x})^2)\,\phi_{\mathrm{A},k}(\boldsymbol{x}')\right\|_2 \left\|(1+r_{\mathrm{B}}(t,\boldsymbol{x})^2)\,\phi_{\mathrm{B},l}(\boldsymbol{x}'')\right\|_2\,\mathrm{d}^3x \\
&\leq \frac{\mathrm{const.}}{1+|(\boldsymbol{b}_{\mathrm{B}}-\boldsymbol{b}_{\mathrm{A}})+t(\boldsymbol{v}_{\mathrm{B}}-\boldsymbol{v}_{\mathrm{A}})|^2}\times \\
&\qquad\times \left\{\int (1+\boldsymbol{x}'^2)\,\|\phi_{\mathrm{A},k}(\boldsymbol{x}')\|_2^2\,\mathrm{d}^3x'\right\}^{\frac{1}{2}}\left\{\int (1+\boldsymbol{x}''^2)\,\|\phi_{\mathrm{B},l}(\boldsymbol{x}'')\|_2^2\,\mathrm{d}^3x''\right\}^{\frac{1}{2}}
\end{aligned}
$$

Here, the Cauchy–Schwarz and Hölder inequalities have been used. Doubly primed coordinates $\boldsymbol{x}''$ refer to the rest frame coordinates of centre B. The two integrals of the last expression are independent of the time t and finite, provided the eigenfunctions $\phi_{\mathrm{A},k}(\boldsymbol{x}')$ and $\phi_{\mathrm{B},l}(\boldsymbol{x}'')$ are decreasing sufficiently fast towards spatial infinity. In particular, if the potentials V_{A} and V_{B} are of the form (2.10) the eigenfunctions have the necessary fall-off property and equation (3.11) directly follows from the estimate above.

3.4.2 Orthogonality of the channels A and C. Equation (3.10), which expresses the asymptotic orthogonality of the outgoing channels A and C, is equivalent to,

$$\lim_{t\to\infty}\left(U_{\mathrm{A}}(t,s)P_{\mathrm{A}}(s)\phi_2,\,\mathrm{e}^{-\mathrm{i}(t-s)H_0}\,\phi_1\right) = 0,$$

for any pair of states $\phi_1(\boldsymbol{x})$ and $\phi_2(\boldsymbol{x})$. However, it is again sufficient to assume that $\phi_1(\boldsymbol{x})$ is a regular wave packet (cf. section B.1). Therefore, it remains to show that,

$$\lim_{t\to\infty}\left(\Phi_{\mathrm{A},k}(t),\,\mathrm{e}^{-\mathrm{i}(t-s)H_0}\,\phi\right) = 0,$$

for any regular wave packet $\phi(\boldsymbol{x})$ and asymptotic configuration $\Phi_{\mathrm{A},k}(t)$ of scattering channel A as in equation (3.3). The following sequence of estimates,

$$
\begin{aligned}
&\left|\left(\Phi_{\mathrm{A},k}(t), \mathrm{e}^{-\mathrm{i}(t-s)H_0}\,\phi\right)\right| \\
&\leq\ \int \left|\Phi_{\mathrm{A},k}(t,\boldsymbol{x})^{\dagger}\left(\mathrm{e}^{-\mathrm{i}(t-s)H_0}\,\phi\right)(\boldsymbol{x})\right| \mathrm{d}^3 x \\
&\leq\ \|S(\Lambda_{\mathrm{A}})^{-1}\|_2 \int \|\phi_{\mathrm{A},k}(\boldsymbol{x}')\|_2 \left\|\left(\mathrm{e}^{-\mathrm{i}(t-s)H_0}\,\phi\right)(\boldsymbol{x})\right\|_2 \mathrm{d}^3 x \\
&\leq\ \|S(\Lambda_{\mathrm{A}})^{-1}\|_2 \frac{\text{const.}}{(1+|t-s|)^{3/2}} \int \|\phi_{\mathrm{A},k}(\boldsymbol{x}')\|_2 \,\mathrm{d}^3 x',
\end{aligned}
$$

yields the desired convergence to zero as $t \to \infty$, if the remaining spatial integral is finite. Note that this remaining spatial integral does not depend on time t. It is finite if the bound state eigenfunctions $\phi_{\mathrm{A},k}$ are L^1-integrable, which is true in particular for the class of electrostatic potentials $V_{\Gamma}(r)$ as in equation (2.10). The estimate again makes use of estimate (B.2) for regular wave packets, described in the appendix B.

3.5 Relativistic invariance

The existence proofs in section 3.3 refer to some particular, although arbitrarily chosen, Lorentz frame. In different, relatively moving Lorentz frames, the limits appearing in the definition of wave operators and scattering states have to be taken with respect to different time axes. It is, therefore, necessary to prove that the transition amplitudes are nevertheless Lorentz invariant quantities.

Consider an arbitrary asymptotic configuration $\Phi_{\Gamma,k}(t,\boldsymbol{x})$ and the corresponding outgoing scattering state $\Psi_{\Gamma,k}^{-}(t,\boldsymbol{x})$ of the two-centre Dirac equation. Given a Poincaré transformation, $(t', \boldsymbol{x}') = \Lambda(t, \boldsymbol{x}) + (a^0, \boldsymbol{a})$, to an arbitrary primed coordinate system, the transformed wave functions in the primed coordinates are:

$$
\begin{aligned}
\Phi'_{\Gamma,k}(t',\boldsymbol{x}') &= S(\Lambda)\,\Phi_{\Gamma,k}(\Lambda^{-1}(t'-a^0, \boldsymbol{x}'-\boldsymbol{a})), \\
\Psi_{\Gamma,k}^{-}{}'(t',\boldsymbol{x}') &= S(\Lambda)\,\Psi_{\Gamma,k}^{-}(\Lambda^{-1}(t'-a^0, \boldsymbol{x}'-\boldsymbol{a})).
\end{aligned}
$$

The question arises whether the transformed wave function $\Psi_{\Gamma,k}^{-}{}'(t',\boldsymbol{x}')$ is identical to the (unique) outgoing scattering state that corresponds to the asymptotic configuration $\Phi'_{\Gamma,k}(t',\boldsymbol{x}')$ in the primed frame of reference. In other words, it has to be checked whether the following holds:

$$
\lim_{t'\to\infty} \|\Psi_{\Gamma,k}^{-}{}'(t',\boldsymbol{x}') - \Phi'_{\Gamma,k}(t',\boldsymbol{x}')\|_{L^2(\mathbb{R}^3,\mathrm{d}^3 x')^4} = 0. \tag{3.12}
$$

Of course, the analogous convergence as $t' \to -\infty$ is similarly conjectured for the Poincaré-transformed incoming scattering state $\Psi_{\Gamma,k}^{+}{}'(t',\boldsymbol{x}')$.

If these conjectures can be verified, then, in the primed frame, the transition amplitude $a'_{\Delta l,\Gamma k}$ is given in terms of the Poincaré-transformed scattering states of the unprimed frame, according to:

$$
a'_{\Delta l,\Gamma k} = \left(\Psi_{\Delta,l}^{-}{}'(t'), \Psi_{\Gamma,k}^{+}{}'(t')\right).
$$

The relativistic invariance of the transition amplitude is then simply a consequence of the Poincaré invariance of the scalar product between two wave functions that solve

the same Dirac equation (cf. section B.2):

$$a'_{\Delta l, \Gamma k} = \left(\Psi_{\Delta,l}^{-}{}'(t'), \Psi_{\Gamma,k}^{+}{}'(t') \right)' = \left(\Psi_{\Delta,l}^{-}(t), \Psi_{\Gamma,k}^{+}(t) \right) = a_{\Delta l, \Gamma k}.$$

Note that in this equation the two scalar products refer to different spatial integrations or hypersurfaces in Minkowski space.

Equation (3.12) is most easily verified, if the Poincaré transformation is only a product of spatial rotations and space-time translations, which do not mix time and spatial coordinates. For a verification of equation (3.12) only Lorentz boosts need to be considered.

3.5.1 Boost invariance of the excitation and capture amplitudes. In this subsection, it is demonstrated that (3.12) holds for $\Gamma = A$. The case $\Gamma = B$ and the limits $t \to -\infty$ are treated similarly. In the course of the following calculations, several assumptions about the radially symmetric potentials V_A and V_B are necessary. These assumptions hold in particular, if both electrostatic potentials $V_\Gamma(r)$ are of the form (2.10) with $\varrho_\Gamma > 0$ and $\mu_\Gamma > 0$.

Without loss of generality, it may be assumed that the unprimed Lorentz frame is a rest frame of centre A, where centre A is located at the origin. This is sufficient because the Poincaré transformation between two arbitrary Lorentz frames can be decomposed into a product of a boost into a rest frame of centre A, spatial rotations, space-time translations, and the inverse of another boost into a rest frame of centre A. Hence, the primed coordinates, for which the convergence (3.12) must be proved, are connected to the unprimed coordinates by a pure boost. In this section the velocity of this boost is denoted by $\boldsymbol{v}$. Again, without loss of generality, the parameter $\boldsymbol{b}_B$ of the trajectory $\boldsymbol{R}_B(t) = \boldsymbol{b}_B + t\boldsymbol{v}_B$ of centre B in the unprimed coordinates can be taken to be perpendicular to the boost velocity $\boldsymbol{v}$. Hence, $\boldsymbol{b}_B = \boldsymbol{b}'_B$ holds. Assuming this case, the following estimates hold for the Lorentz scalars $r_\Gamma(t, \boldsymbol{x})$ and $r'_\Gamma(t', \boldsymbol{x}')$ in the primed and unprimed frames respectively:

$$\begin{aligned}
\frac{1}{1 + r_A(t, \boldsymbol{x})^2} \frac{1}{1 + r_B(t, \boldsymbol{x})^2} &\leq \frac{2}{1 + |\boldsymbol{b}_B + t\boldsymbol{v}_B|^2}, \\
\frac{1}{1 + r'_A(t', \boldsymbol{x}')^2} \frac{1}{1 + r'_B(t', \boldsymbol{x}')^2} &\leq \frac{2}{1 + |\boldsymbol{b}_B + t'(\boldsymbol{v} + \boldsymbol{v}'_B)|^2},
\end{aligned} \tag{3.13}$$

where $\boldsymbol{v}'_B$ is the velocity of centre B in the primed coordinates.

The asymptotic condition $\Phi_A(t, \boldsymbol{x})$ (for the sake of simplicity omitting the second index in this subsection) may be chosen as,

$$\Phi_A(t, \boldsymbol{x}) = \exp(-it\epsilon_A)\phi_A(\boldsymbol{x}),$$

where $\phi_A(\boldsymbol{x})$ is a normalised bound state eigenfunction of the electrostatic potential V_A. The statement, that $\Psi_A^-(t, \boldsymbol{x})$ is the outgoing scattering state which corresponds to the asymptotic condition $\Phi_A(t, \boldsymbol{x})$, is equivalent to the following convergence property:

$$\lim_{t \to \infty} \left(\Psi_A^-(t), \Phi_A(t) \right) = 1. \tag{3.14}$$

Similarly, the asymptotic convergence of the two transformed Dirac wave functions $\Psi_A^{-'}(t', \boldsymbol{x}')$ and $\Phi_A'(t', \boldsymbol{x}')$ in the primed frame is equivalent to:

$$\lim_{t' \to \infty} \left(\Psi_A^{-'}(t'), \Phi_A'(t') \right)' = 1. \tag{3.15}$$

In order to prove that (3.15) follows from (3.14), the difference of both scalar products is considered for some finite times $t = \zeta$ and $t' = \gamma\zeta$. Here γ denotes the Lorentz factor corresponding to the boost velocity $\boldsymbol{v}$. The limit of this difference of scalar products is shown to vanish as ζ tends to $+\infty$. Using the Gaussian integral theorem in Minkowski space, the difference of the scalar products is transformed into a four-dimensional integral:

$$
\begin{aligned}
\left(\Psi_A^-(\zeta), \Phi_A(\zeta) \right) - \left(\Psi_A^{-'}(\gamma\zeta), \Phi_A'(\gamma\zeta) \right)' &= \int_{D(\zeta)} \partial_\mu \left(\overline{\Psi_A^-}(y)\, \gamma^\mu\, \Phi_A(y) \right) \mathrm{d}^4 y \\
&= \int_{D(\zeta)} \Psi_A^-(y)^\dagger\, W_B(y)\, \Phi_A(y)\, \mathrm{d}^4 y.
\end{aligned}
\tag{3.16}
$$

For the second step, we have used that $\Psi_A^-(t, \boldsymbol{x})$ solves the two-centre Dirac equation, whereas $\Phi_A(t, \boldsymbol{x})$ solves the Dirac equation of scattering channel A. The four-volume of integration $D(\zeta)$ is given by:

$$D(\zeta) = \left\{ y \in \mathbb{R}^4 : 0 \le y^0 - \zeta \le \boldsymbol{v} \cdot \boldsymbol{y} \quad \text{or} \quad 0 \ge y^0 - \zeta \ge \boldsymbol{v} \cdot \boldsymbol{y} \right\}.$$

It is the volume of space-time bounded by the two spacelike hypersurfaces, which are determined by $t = \zeta$ and $t' = \gamma\zeta$. (See section B.2 for a similar calculation.)

According to the inequalities (3.13), the following estimate holds for sufficiently large parameter ζ:

$$\sup_{y \in D(\zeta)} \frac{1}{1 + r_A(y)^2} \frac{1}{1 + r_B(y)^2} \le \frac{1}{C_1 \zeta^2} \tag{3.17}$$

Here the constant $C_1 > 0$ depends on $\boldsymbol{b}_B$, $\boldsymbol{v}_B$ and $\boldsymbol{v}$ only.

Since the time-dependence of the scattering state $\Psi_A^-(t, \boldsymbol{x})$ is not known explicitly, the integral (3.16) must be estimated in order to demonstrate that it converges to zero as $\zeta \to \infty$. The following estimate is based on the assumption that the solution $\Psi_A^-(t, \boldsymbol{x})$ of the two-centre Dirac equation is bounded in space-time by some constant C_2:

$$\left\| \| \Psi_A^-(y) \|_2 \right\|_{L^\infty(\mathbb{R}^4)} \le C_2 \tag{3.18}$$

This cannot be expected to be true in general. In fact, it is false if the external fields $W_\Gamma(t, \boldsymbol{x})$ correspond to linearly moving Yukawa potentials. But a suitable assumption on the electrostatic fields $V_\Gamma(r)$ should be sufficient in order to obtain this property. Although a proof is not given here, (3.18) is expected to hold in particular if the radial potentials $V_\Gamma(r)$ are of the form (2.10), with $\varrho_\Gamma > 0$ and $\mu_\Gamma > 0$. The latter condition provides that the potentials $V_\Gamma(r)$, their eigenfunctions, and the multiplication operators $W_\Gamma(t, \boldsymbol{x})$ are bounded.

The estimate of the integral (3.16) is done as follows:

$$\left| \int_{D(\zeta)} \Psi_A^-(y)^\dagger \, W_B(y) \, \Phi_A(y) \, \mathrm{d}^4 y \right|$$

$$\leq \int_{D(\zeta)} \|\Psi_A^-(y)\|_2 \, \gamma_B \, \|1 - \boldsymbol{v}_B \cdot \boldsymbol{\alpha}\|_2 \, |V_B(r_B(y))| \, \|\Phi_A(y)\|_2 \, \mathrm{d}^4 y$$

$$\leq \frac{\gamma_B \|1 - \boldsymbol{v}_B \cdot \boldsymbol{\alpha}\|_2}{C_1 \zeta^2}$$
$$\int_{D(\zeta)} \|\Psi_A^-(y)\|_2 \, (1 + r_B(y)^2) \, |V_B(r_B(y))| \, (1 + r_A(y)^2) \, \|\Phi_A(y)\|_2 \, \mathrm{d}^4 y$$

$$\leq \frac{C_2 C_3 \gamma_B \|1 - \boldsymbol{v}_B \cdot \boldsymbol{\alpha}\|_2}{C_1 \zeta^2} \int_{D(\zeta)} (1 + \boldsymbol{y}^2) \, \|\phi_A(\boldsymbol{y})\|_2 \, \mathrm{d}^4 y$$

$$\leq \frac{C_2 C_3 \gamma_B \|1 - \boldsymbol{v}_B \cdot \boldsymbol{\alpha}\|_2 \, |\boldsymbol{v}|}{C_1 \zeta^2} \int_{\mathbb{R}^3} |\boldsymbol{y}| (1 + \boldsymbol{y}^2) \|\phi_A(\boldsymbol{y})\|_2 \, \mathrm{d}^3 y.$$

The remaining integral is finite, in particular, if the bound state eigenfunction $\phi_A(\boldsymbol{x})$ is exponentially decreasing towards spatial infinity. Furthermore, it has been used that the term $|(1 + r^2) V_B(r)|$ is bounded by a constant C_3. Both requirements are satisfied for the class of potentials $V_\Gamma(r)$ of equation (2.10) with $\mu_\Gamma > 0$ and $\varrho_\Gamma > 0$. Therefore, the integral (3.16) vanishes as ζ approaches infinity.

3.6 Remarks

3.6.1 Two-centre Dirac equation with moving point charges. In section 3.3, asymptotic convergence has *not* been shown for the two-centre Dirac equation with moving unscreened point charges. The proofs cannot be extended to include Coulomb potentials, because the inverse screening lengths μ_A and μ_B must not vanish. This means that the radial potentials $V_\Gamma(r)$ have to be short-ranged.

Furthermore, it seems hardly possible that asymptotic convergence can be proved for long-range electrostatic potentials $V_\Gamma(r)$, like the Coulomb potential, without a modification of the dynamics of the scattering channels. The reason for this conviction is as follows: For the nonrelativistic and relativistic quantum mechanical scattering by a *single* Coulomb potential, the corresponding fact has been demonstrated by Dollard in [DOL64, DV66] (reviewed in [THA92]). Also, the scattering theory of the *two-centre* Schrödinger equation with long-range potentials has been investigated by Wüller in [WÜL88]. There, it was found that modified dynamics for the scattering channels of the two-centre Schrödinger equation are necessary, in order to prove the existence and asymptotic completeness of the Møller wave operators if long-range forces are present. The modified dynamics of each of the three different scattering channels closely resembles the distorted free-time-evolution that was given by Dollard for the nonrelativistic case.

Wüller, in his analysis [WÜL88], made use of geometrical methods of scattering theory, which have been developed by Enß and have also been applied to the discussion of the Dirac equation [THA92]. Therefore, a proper discussion of the scattering theory for the Dirac equation with moving point charges may be feasible by using similar methods as in [WÜL88]. Such a mathematical investigation does not exist in

the literature, but it is required, in particular, for a proof of relativistic invariance in the long-range case. See, however, the next section for the discussion of Coulomb boundary conditions.

3.6.2 Asymptotic completeness. Note that *asymptotic completeness* of the scattering theory of the two-centre Dirac equation is neither proved in this thesis nor has it been considered in the literature. It is conjectured that it can be shown similarly to the complicated, corresponding proofs that have been published for the nonrelativistic charge-transfer model [YAJ80, HAG82, WÜL88, GRA90].

Asymptotic completeness is defined as the existence of complete sets of orthonormal incoming scattering states $\Psi^+_{\Gamma,k}(t, \boldsymbol{x})$ and outgoing scattering states $\Psi^-_{\Gamma,k}(t, \boldsymbol{x})$. It means that *any* solution $\Psi(t, \boldsymbol{x})$ of the two-centre Dirac equation can be written rigorously as linear combination of either incoming or outgoing scattering states:

$$\Psi(t, \boldsymbol{x}) = \sum_{\Gamma,k} a^+_{\Gamma,k}\, \Psi^+_{\Gamma,k}(t, \boldsymbol{x}) = \sum_{\Gamma,k} a^-_{\Gamma,k}\, \Psi^-_{\Gamma,k}(t, \boldsymbol{x}).$$

As the scattering states $\Psi^\pm_{\Gamma,k}(t, \boldsymbol{x})$ are asymptotically equal to asymptotic configurations $\Phi_{\Gamma,k}(t, \boldsymbol{x})$ as $t \to \mp\infty$, formally the linear expansions above turn into linear combinations of asymptotic configurations $\Phi_{\Gamma,k}(t, \boldsymbol{x})$ in the limit $t \to \mp\infty$ (cf. chapter 4).

If the solution $\Psi(t, \boldsymbol{x})$ is itself a scattering state, the coefficients of linear expansion are identical to the transition amplitudes $a_{\Delta l, \Gamma k}$ defined in section 3.2:

$$\Psi^+_{\Gamma,k}(t, \boldsymbol{x}) = \sum_{\Delta,l} a_{\Delta l, \Gamma k}\, \Psi^-_{\Delta,l}(t, \boldsymbol{x}),$$

$$\Psi^-_{\Gamma,k}(t, \boldsymbol{x}) = \sum_{\Delta,l} a^*_{\Gamma k, \Delta l}\, \Psi^+_{\Delta,l}(t, \boldsymbol{x}).$$

Therefore, the 'conservation of probability',

$$\|\Psi^\pm_{\Gamma,k}(t)\| = \sum_{\Delta,l} |a_{\Delta l, \Gamma k}|^2 = 1, \tag{3.19}$$

is a consequence of asymptotic completeness. Suppose that an initial configuration (Γ, k) is a bound state of either centre A or centre B. In general, the sum over transition probabilities $|a_{\Delta l, \Gamma k}|^2$ to final configurations (Δ, l) which are not asymptotic configurations of channel C with negative energy is strictly less then one. This means that the naive interpretation of the initial configuration as a one-particle state is not entirely correct, since the total probability of finding an initial bound state (Γ, k) in a final configuration of positive energy is not one, as it must be for a single-particle theory. This reflects that the Dirac theory can only be interpreted as a multi-particle theory.

3.6.3 Problem of second quantisation. A multi-particle theory requires a multi-particle state space, namely the Fock space of quantum field theory. The Fock space formalism of pair creation in external fields makes use of the fact that the *time-dependent* external fields vanish everywhere in space as time t tends to $\pm\infty$. This property is necessary, it allows for the construction of the Fock space (the 'second quantisation') based on a spectral decomposition of the state

space of the classical Dirac field with respect to the time-independent Hamiltonian at $t = \pm\infty$ [THA92, SCH95].[1] This time-independent Hamiltonian is identical to the Hamiltonian the interaction picture of quantum field theory refers to (see e.g. [RS75, FGS91, SCH95]). In common presentations of quantum field theory this is frequently the free Hamiltonian $H_0 = -\mathrm{i}\boldsymbol{\alpha}\cdot\nabla + \beta$ (e.g. [FGS91, SCH95, WEI95]) or the free Hamiltonian plus a stationary Coulomb field, referred to as the Furry picture of quantum field theory [MPS98].

Clearly, for the two-centre Dirac equation there is no such limit of the time-dependent Dirac Hamiltonian as $t \to \pm\infty$. Therefore, the usual Fock space construction is not possible, although, as we have seen above, a multi-particle interpretation of the transition amplitudes is inevitable. The problem of second quantisation of the scattering theory presented in this chapter remains unsolved. For the present work we take the pragmatic point of view that transition amplitudes between an asymptotic configuration of negative energy and an asymptotic configuration of positive energy have to be interpreted as probability amplitudes of single pair production or annihilation processes, as depicted in figure 3.1. Furthermore, in numerical calculations of this work these amplitudes are so small that the 'one-particle' interpretations of other transition amplitudes, namely those between asymptotic configurations of positive energy as depicted in 3.1, are reasonable, because numerical uncertainties are much larger than the 'error due to a loss of probability' as a consequence of transitions to negative energy configurations of scattering channel C.

Finally, we take a look at the role of quantum field theory in other approaches to pair creation in peripheral heavy-ion collisions. Note, that the scattering channels A and B of the two-centre Dirac equation can be removed by an adiabatic switching formalism, namely by replacing the external fields $W_\Gamma(t, \boldsymbol{x})$, for example, by fields $\mathrm{e}^{-\varepsilon^2 t^2} W_\Gamma(t, \boldsymbol{x})$ that vanish as time t tends to infinity. For a Dirac field with such an external potential all particles are asymptotically free. The scattering channels A and B are removed by the exponential damping factor and the scattering theory can be formulated with respect to the free particle Fock space (Feynman–Dyson QED). Although not mentioned explicitly, this point of view is taken implicitly, e.g., in [BS89, WBS90]. A second possibility, allowing for an asymmetrical description of bound-free pair production, is given by exponentially damping only the external field of one of the centres, say $W_\mathrm{B}(t, \boldsymbol{x})$. Then, in a rest frame of centre A, the total two-centre Hamiltonian also becomes stationary as time t tends to $\pm\infty$. This allows for a proper Fock space theory as well and corresponds to the single-centre approaches to pair creation making use of the Furry picture. It is clearly asymmetrical, since one of the nuclei only acts as a perturbation.

It is well-known that in quantum field theories, subject to asymptotically vanishing time-dependent external field, transition amplitudes of the multi-particle theory are directly related to transition amplitudes of the scattering theory of the classical Dirac field (e.g. [FGS91, SCH95]) and it is, therefore, sufficient to consider the latter. In conclusion, we have argued in this subsection that the scattering theory of the

---

[1]Strictly speaking even stronger assumptions on the time-dependent external fields are necessary for a second quantised field theory: The scattering matrix of the classical Dirac field must be implementable in Fock space. A sufficient condition for the implementability is known as the Shale–Stinesping criterion. (See e.g. [RUI77A, RUI77B, RUI77C, THA92, SCH95].)

two-centre Dirac equation, which allows for bound states of both centres, represents a more complicated case, for which a proper multi-particle theory is not known.

3.7 Coulomb boundary conditions

In this section, the case of long-range forces is considered. This means that the electrostatic potential of a charge distribution ρ_Γ in its rest frame is Coulomb-like at large distances from the corresponding centre. It has been argued in the previous section 3.6 that scattering theory as described in section 3.1 is not applicable in this case, because the potential is not decreasing sufficiently fast towards spatial infinity to obtain asymptotic convergence. A workaround for that is the modification of the wave equations for the scattering channels.

Modified Dirac equations for the scattering channels A and B have been proposed in [EIC87], and reviewed in [TE90] and [EM95, ch. 5], where they have been termed asymptotic equations. In these wave equations the residual interaction of centre B with bound states of centre A is added to the corresponding channel Hamiltonian of centre A, and vice versa, leading to *modified scattering-channel Hamiltonians.*

A relativistically moving point charge not only induces a long-range electric-field, but also a long-range magnetic field. The magnetic field only vanishes in the rest frame of the point source. Therefore, the asymptotic influence of centre B on bound states of centre A is best considered in the rest frame of centre B. A state bound to centre A means here that it is localised in the vicinity of centre A for *all* times. Such a bound state is subject to the long-range Coulomb potential of centre B also at arbitrarily large times. This is expressed by the fact that asymptotic convergence is not achieved, if this large-time influence of centre B is neglected. It has, therefore, been proposed by Eichler [EIC87, TE90, EM95] to include the following residual interaction into the Hamiltonian of scattering channel A:

$$W_{\mathrm{B}}^{\infty\prime\prime}(t'', \boldsymbol{x}'') = \frac{-e^2 \tilde{Z}_{\mathrm{B}}}{d_{\mathrm{B}}''(t'', \boldsymbol{x}'')}. \tag{3.20}$$

Here, doubly primed coordinates denote rest frame coordinates of centre B and the distance between the centres A and B as determined in the rest frame of centre B is given by the Lorentz scalar $d_{\mathrm{B}}''(t'', \boldsymbol{x}'')$ (cf. section 2.1). The charge number $\tilde{Z}_{\mathrm{B}}$ has been introduced to indicate the strength of the Coulomb-like tail of the electrostatic potential of centre B. It is distinguished from the charge number Z_{B}, since the latter has been used as well for the Yukawa potential, in order to indicate its field strength near the origin. Clearly, $Z_{\mathrm{B}} = \tilde{Z}_{\mathrm{B}}$ for the Coulomb potential.

In fact, in the doubly primed frame the external field $W_{\mathrm{B}}^{\infty\prime\prime}(t'', \boldsymbol{x}'')$ does not depend on spatial coordinates $\boldsymbol{x}''$. In the rest frame of centre B, it corresponds to the Coulomb potential at the position of the moving centre A, of a point charge $e\tilde{Z}_{\mathrm{B}}$ located at the origin. A Poincaré transformation from the doubly primed coordinates back to an unprimed coordinate system yields the residual external field of centre B on bound states of centre A,

$$W_{\mathrm{B}}^{\infty}(t, \boldsymbol{x}) = \frac{-e^2 \tilde{Z}_{\mathrm{B}}}{d_{\mathrm{B}}(t, \boldsymbol{x})} \gamma_{\mathrm{B}}(1 - \boldsymbol{v}_{\mathrm{B}} \cdot \boldsymbol{\alpha}), \tag{3.21}$$

where $\boldsymbol{v}_{\mathrm{B}}$ is the velocity of centre B in the unprimed frame. Similarly, the residual external field of centre A on bound states of centre B is given in terms of the parameter $\tilde{Z}_{\mathrm{A}}$ and the Lorentz scalar $d_{\mathrm{A}}(t, \boldsymbol{x})$. These residual fields have non-vanishing magnetic-field components, to which bound states are exposed at arbitrarily large times.

The modified Hamiltonians of the scattering channels A and B are therefore:

$$
\begin{aligned}
H_{\mathrm{A}}^{\infty}(t) &= H_0 + W_{\mathrm{A}}(t, \boldsymbol{x}) + W_{\mathrm{B}}^{\infty}(t, \boldsymbol{x}), \\
H_{\mathrm{B}}^{\infty}(t) &= H_0 + W_{\mathrm{B}}(t, \boldsymbol{x}) + W_{\mathrm{A}}^{\infty}(t, \boldsymbol{x}).
\end{aligned}
\tag{3.22}
$$

These Hamilton operators are time-dependent in any Lorentz frame. For the rest frames of centre A and B they have been described in the works of Eichler and co-workers. It was recognised first in [EIC87] that the corresponding scattering-channel Dirac equations have *bound-state* solutions, because the residual fields $W_{\Gamma}^{\infty}(t, \boldsymbol{x})$ can be removed by a gauge transformation.

A gauge function suitable to remove the external field $W_{\mathrm{B}}^{\infty}(t, \boldsymbol{x})$ is given by:

$$
g_{\mathrm{B}}(t, \boldsymbol{x}) = \frac{e^2 \tilde{Z}_{\mathrm{B}}}{v} \log\left[d_{\mathrm{B}}(t, \boldsymbol{x}) - \frac{\gamma_{\mathrm{A}} \boldsymbol{v}_{\mathrm{A}} \cdot \boldsymbol{d}}{\gamma v} + \frac{\gamma_{\mathrm{B}} \boldsymbol{v}_{\mathrm{B}} \cdot \boldsymbol{d}}{\gamma^2 v} + v \gamma_{\mathrm{B}}\left(t - \boldsymbol{v}_{\mathrm{B}} \cdot (\boldsymbol{x} - \boldsymbol{b}_{\mathrm{B}}) \right) \right].
\tag{3.23}
$$

The abbreviations v, γ and $\boldsymbol{d}$ have been introduced in section 2.1, where $d_{\mathrm{B}}(t, \boldsymbol{x})$ has been defined as well. Similarly a gauge function $g_{\mathrm{A}}(t, \boldsymbol{x})$ removing $W_{\mathrm{A}}^{\infty}(t, \boldsymbol{x})$ is obtained, by interchanging in equation (3.23) the indices A and B and reversing the sign of $\boldsymbol{d}$, which was defined as $\boldsymbol{d} = \boldsymbol{b}_{\mathrm{B}} - \boldsymbol{b}_{\mathrm{A}}$. These gauge functions satisfy:

$$
\{\partial_t + \boldsymbol{\alpha} \cdot \nabla\} g_{\Gamma}(t, \boldsymbol{x}) = -W_{\Gamma}^{\infty}(t, \boldsymbol{x}).
$$

The gauge functions $g_{\Gamma}(t, \boldsymbol{x})$ are determined only up to constant and, therefore, other, equivalent gauge functions exist. Given a solution $\Phi_{\mathrm{A}}(t, \boldsymbol{x})$ of the unperturbed scattering channel Dirac equation,

$$
[H_0 + W_{\mathrm{A}}(t, \boldsymbol{x}) - \mathrm{i}\partial_t] \Phi_{\mathrm{A}}(t, \boldsymbol{x}) = 0,
$$

the gauge transformed wave function $\Phi_{\mathrm{A}}^{\infty}(t, \boldsymbol{x})$, given by,

$$
\Phi_{\mathrm{A}}^{\infty}(t, \boldsymbol{x}) = \exp(\mathrm{i}g_{\mathrm{B}}(t, \boldsymbol{x})) \, \Phi_{\mathrm{A}}(t, \boldsymbol{x}),
$$

then solves the Coulomb-distorted channel Dirac equation,

$$
[H_0 + W_{\mathrm{A}}(t, \boldsymbol{x}) + W_{\mathrm{B}}^{\infty}(t, \boldsymbol{x}) - \mathrm{i}\partial_t] \Phi_{\mathrm{A}}^{\infty}(t, \boldsymbol{x}) = 0.
$$

By virtue of this connection, Dirac equations of the scattering channels A and B, with Hamilton operators according to equation (3.22), have solutions which *permanently* remain localised in the vicinity of their respective centre. Therefore, they are appropriate for the description of bound states, if Coulomb forces are present. Following Eichler and Dewangan the wave function $\Phi_{\mathrm{A}}^{\infty}(t, \boldsymbol{x})$ is said to satisfy *Coulomb boundary conditions* [EM95].

Recently, it has been asserted in [WSE99] that the asymptotic equations, as presented in this section, are 'not formally correct' (see in particular appendix A of [WSE99]). Another residual interaction has been proposed by Segev in the article quoted. The present author does not agree with Segev for the following reason: The Hamilton operator of the asymptotic equation, as proposed by Segev, is time-dependent in a nontrivial way in *any* Lorentz frame. This means that there are no

solutions of Segev's asymptotic equations, which remain localised at a single centre for all times. Clearly, the asymptotic equations of Segev are not suitable to describe bound states. Contrary to the argument in [WSE99], the earlier proposal of Eichler [Eic87] seems to be the only appropriate choice for the Coulomb-modified Dirac equations of the scattering channels A and B, corresponding to asymptotically bound particles of the two-centre Dirac equation with unscreened nuclear charges.

CHAPTER 4

Coupled Channel Approximation

In this chapter, we give an introduction to the coupled channel method, used in this work to solve the two-centre Dirac equation numerically. Although this method has been widely used for many years, also for the solution of the two-centre Schrödinger equation, a brief account of this ansatz is necessary to explain its principal ideas and present notational conventions. Here, particular emphasis is given to the fundamental solution of the coupled channel equations and its properties. In this respect the following sections differ from standard presentations of the numerical method [BM92, EM95].

4.1 Coupled channel equations for the semiclassical approximation

The principal idea of the coupled channel ansatz is to construct an approximate solution $\tilde{\Psi}(t, \boldsymbol{x})$ of the Dirac equation (2.11) as a finite time-dependent linear combination of asymptotic configurations $\Phi_{\Gamma,i}(t, \boldsymbol{x})$:

$$\tilde{\Psi}(t, \boldsymbol{x}) = \sum_{\Gamma,i} c_{\Gamma,i}(t)\, \Phi_{\Gamma,i}(t, \boldsymbol{x}). \tag{4.1}$$

The states $\Phi_{\Gamma,i}$ included in this finite sum are usually referred to as the *basis functions* of the coupled channel expansion [BM92, EM95]. Note that generally an exact solution of the two-centre Dirac equation cannot be written as *finite* sum of asymptotic configurations. However, in the case of the two-centre Dirac equation an infinite series expansion is suitable to represent an arbitrary solution. The accuracy and usefulness of this ansatz depends on the physical situation under consideration and the corresponding choice of basis functions. More general expansions are possible in which the basis functions are equal to the asymptotic configurations $\Phi_{\Gamma,i}$ only asymptotically (i.e. for large times).

The determination of the complex expansion coefficients $c_{\Gamma,i}(t)$ is guided by the following reasoning. Assume that a solution $\Psi(t, \boldsymbol{x})$ of a Dirac equation with a time-dependent Hamilton operator $H(t)$,

$$[H(t) - \mathrm{i}\partial_t]\, \Psi(t, \boldsymbol{x}) = 0,$$

may be approximated by a wave function of the type given in equation (4.1), then $\tilde{\Psi}(t, \boldsymbol{x})$ approximately solves that Dirac equation:

$$[H(t) - \mathrm{i}\partial_t] \sum_{\Gamma,i} c_{\Gamma,i}(t)\, \Phi_{\Gamma,i}(t, \boldsymbol{x}) \approx 0. \tag{4.2}$$

Multiplying this equation from the left by the adjoint of some basis function $\Phi_{\Delta,j}^{\dagger}$ and integrating over x yields a set of *approximate* equations for the coefficients $c_{\Gamma,i}(t)$. By turning the approximate equality into an exact equality a *prescription* for the determination of the coefficients $c_{\Gamma,i}(t)$ is obtained. Therefore, given the time-dependent

Dirac-Hamiltonian $H(t)$, according to this prescription the expansion coefficients $c_{\Gamma,i}(t)$ have to be determined by solving the following set of differential equations:

$$\sum_{\Gamma,i} c_{\Gamma,i}(t) \Big(\Phi_{\Delta,j}(t), [H(t) - \mathrm{i}\partial_t] \, \Phi_{\Gamma,i}(t) \Big) - \mathrm{i} \sum_{\Gamma,i} (\partial_t \, c_{\Gamma,i}(t)) \Big(\Phi_{\Delta,j}(t), \Phi_{\Gamma,i}(t) \Big) = 0. \quad (4.3)$$

These equations will be referred to as the *coupled channel equations*. In the non-relativistic impact parameter model, based, e.g., on the Schrödinger equation, the coupled channel equations may also be derived from a variational principle [BM92]. Note that in the literature on atomic physics the term coupled channel equations sometimes also refers to other (integro-differential) equations which are more or less related to the present set of equations (4.3) [BM92, FRI90].

The important, distinctive property of the coupled channel equations is that the norm $\|\tilde{\Psi}(t)\|$ of an approximate solution $\tilde{\Psi}(t, \boldsymbol{x})$ is independent of the time t. Following [BM92] it is verified as follows. As a consequence of equation (4.3) we have,

$$\int \tilde{\Psi}(t, \boldsymbol{x})^{\dagger} \Big([H(t) - \mathrm{i}\partial_t] \, \tilde{\Psi}(t, \boldsymbol{x}) \Big) \, \mathrm{d}^3 x = 0,$$

although $\tilde{\Psi}(t, \boldsymbol{x})$ is not an exact solution of the Dirac equation in general. Due to the hermitian property of the Hamiltonian $H(t)$ the time-independence of the norm $\|\tilde{\Psi}(t)\|$ is obtained by taking the time derivative of the norm squared:

$$\partial_t \|\tilde{\Psi}(t)\|^2 = \Big(\partial_t \tilde{\Psi}(t), \tilde{\Psi}(t) \Big) + \Big(\tilde{\Psi}(t), \partial_t \tilde{\Psi}(t) \Big)$$
$$= \Big(-\mathrm{i}H(t)\tilde{\Psi}(t), \tilde{\Psi}(t) \Big) + \Big(\tilde{\Psi}(t), -\mathrm{i}H(t)\tilde{\Psi}(t) \Big) = 0. \quad (4.4)$$

In the same way it is proved that the scalar product between two arbitrary approximate solutions $\tilde{\Psi}^{(1)}(t)$ and $\tilde{\Psi}^{(2)}(t)$, which are different linear combination of the same basis functions, is conserved:

$$\partial_t \Big(\tilde{\Psi}^{(1)}(t), \tilde{\Psi}^{(2)}(t) \Big) = 0 \quad (4.5)$$

This property, which will be used below, is in fact equivalent to (4.4) due to the polarisation identity of the scalar product [RS80, KAT80].

To conclude this section, we note that the coupled channel ansatz (4.1) can be formulated in various relativistic frames of reference. Then the coupled channel equations (4.3) stated in two different reference frames differ if the Lorentz frames are moving with respect to each other. This constitutes a peculiarity of the relativistic theory of coupled channel equations. Nonrelativistic inertial frames all have the same time axis and the coupled equations are the same in all nonrelativistic inertial frames. By contrast, in the relativistic theory the time axis is transformed by a Lorentz boost. The influence of the choice of the relativistic frame of reference on transition amplitudes computed by means of the coupled channel method is investigated systematically in this thesis, numerical results are presented in chapter 6.

4.2 Fundamental solution and asymptotic unitarity

In this section, the general mathematical properties of solutions $c_{\Gamma,i}(t)$ of the coupled channel equations (4.3) are discussed. In order to simplify the notation in the subsequent presentation, the double indices (Γ, i) of the basis functions are mapped one

to one and onto the integers from 1 to n, where n is the number of basis functions occurring in the expansion (4.1). Given such a mapping for some particular set of basis functions $\Phi_{\Gamma,i}$, the basis functions may be labelled more simply by a single integer i. Defining the overlap matrix $N(t)$ of the basis functions $\Phi_i(t, \boldsymbol{x})$ as,

$$N_{ij}(t) = (\Phi_i(t), \Phi_j(t)), \tag{4.6}$$

and the interaction matrix $V(t)$ as,

$$V_{ij}(t) = (\Phi_i(t), [H(t) - \mathrm{i}\partial_t] \Phi_j(t)), \tag{4.7}$$

the coupled channel equations (4.3) may be rewritten in the equivalent matrix form [BM92, EM95]:

$$\partial_t c(t) = -\mathrm{i}N(t)^{-1}V(t)c(t). \tag{4.8}$$

Here, $c(t)$ denotes a vector of expansion coefficients, $c(t) = (c_1(t), \dots, c_n(t))$. Equation (4.8) is a homogeneous linear ordinary differential equation. It is assumed in the following that every initial value problem of equation (4.8) has a unique solution defined for all times t. It is known from the theory of ordinary differential equations that, under this assumption, a system of n linear independent solutions exists such that every solution of (4.8) is a linear combination of these linear independent solutions [CL55, WAL93].

We introduce the fundamental solution of equation (4.8) and discuss its properties: Let $F(t, t_{\mathrm{i}})$ denote the matrix of column-vectors $c^{(i)}(t, t_{\mathrm{i}})$ which are solutions of (4.8) and meet the initial condition $c_j^{(i)}(t_{\mathrm{i}}, t_{\mathrm{i}}) = \delta_{ij}$ at time t_{i}:

$$F(t_{\mathrm{i}}, t_{\mathrm{i}}) = \left(c^{(1)}(t_{\mathrm{i}}, t_{\mathrm{i}}), c^{(2)}(t_{\mathrm{i}}, t_{\mathrm{i}}), \dots, c^{(n)}(t_{\mathrm{i}}, t_{\mathrm{i}})\right) = 1. \tag{4.9}$$

Throughout this work, multiples of the unit matrix are represented simply by complex numbers, therefore, the numeral 1 in the previous equation stands for the unit matrix. Such a system of solutions is commonly known as a fundamental system of solutions [WAL93]. It exists for any initial time t_{i} (see above). The two-parameter matrix-valued function $F(t, t_{\mathrm{i}})$ will be referred to as *the* fundamental solution of the coupled channel equations for the initial time t_{i}. The properties of this fundamental solution have not yet been explicitly discussed in the literature on coupled channel calculations.

As a consequence of the unique solvability of the initial value problem, the fundamental solution F has the following additional properties:

$$F(t_2, t_1)F(t_1, t_0) = F(t_2, t_0), \tag{4.10}$$

$$F(t_1, t_0)^{-1} = F(t_0, t_1), \tag{4.11}$$

satisfied for arbitrary times t_0, t_1 and t_2.

Note that F is generally not a unitary matrix (i.e. a unitary time evolution), because the matrix $-\mathrm{i}N(t)^{-1}V(t)$ of the coefficients of the linear differential equation (4.8) is not anti-hermitian. However, this coefficient matrix may be anti-hermitian in particular cases, e.g. in single-centre coupled channel equations. In such cases $F(t, t_{\mathrm{i}})$ is unitary for all arguments t and t_{i} [CL55, WAL93]. However, the matrix $F(t_2, t_1)$ is *asymptotically* unitary, if the overlap matrix $N(t)$ converges to the unit matrix as $t \to \pm\infty$, i.e. if the basis functions are asymptotically orthogonal.

Asymptotic unitarity is useful later in this work in order to check and assess the accuracy of a numerically evaluated fundamental solution $F(t_\mathrm{f}, t_\mathrm{i})$.

It can be verified that the time-independence of the scalar product (4.5) is equivalent to the following relation between the fundamental solution F and the overlap matrix $N(t)$:

$$F(t_1, t_0)^\dagger N(t_1) F(t_1, t_0) = N(t_0). \tag{4.12}$$

Given the asymptotic orthonormality of the basis functions, the asymptotic unitarity of the fundamental solution F is obtained by taking the limits $t_1 \to \infty$ and $t_0 \to -\infty$:

$$\lim_{t_1 \to \infty} \lim_{t_0 \to -\infty} F(t_1, t_0)^\dagger F(t_1, t_0) = 1. \tag{4.13}$$

This means in particular that the norms at $t = \pm\infty$ of some arbitrary solution $c(t)$ of the coupled channel equations are equal,

$$\lim_{t \to -\infty} \|c(t)\|_2 = \lim_{t \to \infty} \|c(t)\|_2, \tag{4.14}$$

if $N(t) \to 1$ as t approaches $\pm\infty$.

Note that the existence of the limits $\lim_{t \to \pm\infty} c(t)$ themselves is not implied by (4.14). Their existence can be deduced from the asymptotic convergence of the fundamental solution,

$$\lim_{t_1 \to \infty} \lim_{t_0 \to -\infty} F(t_1, t_0) = F(\infty, -\infty), \tag{4.15}$$

which is likewise not implied by (4.13) and, in principle, requires a separate mathematical discussion. The limit $F(\infty, -\infty)$ takes the role of the 'coupled channel scattering matrix' (see section 4.3 below) and satisfies:

$$F(\infty, -\infty)^\dagger = F(\infty, -\infty)^{-1} = F(-\infty, \infty). \tag{4.16}$$

4.2.1 Unitarity criterion. In this subsection a numerically useful method is developed in order to assess the deviation of the fundamental solution $F(t, t_\mathrm{i})$ from unitarity. The unitarity of a fundamental solution $F(t, t_\mathrm{i})$ is equivalent to the property,

$$\|F(t, t_\mathrm{i})u\|_2 = 1, \tag{4.17}$$

for all times t and unit vectors u. The unit vector u describes an initial condition at some initial time t_i of a solution $c(t) = F(t, t_\mathrm{i})u$ of the coupled channel equations. It has been mentioned in the previous section that the fundamental solution is generally not unitary, which means that,

$$\|F(t, t_\mathrm{i})u\|_2 \neq 1.$$

As a measure of the deviation of F from unitarity, one may compute the range of the vector norm $\|F(t, t_\mathrm{i})u\|_2$ substituting all unit vectors u. It turns out that the upper limit,

$$\max_{\|u\|_2=1} \|F(t, t_\mathrm{i})u\|_2,$$

and the lower limit,

$$\min_{\|u\|_2=1} \|F(t, t_\mathrm{i})u\|_2,$$

of this range, may be computed easily, because they are related to the so-called singular values of the the matrix $F(t, t_i)$. The singular values of a matrix F are defined as the positive square roots of the eigenvalues of the matrix $F^\dagger F$ [WIL65, KAT80, RS80, DH93]. Due to the positivity of $F^\dagger F$, the singular values of F are positive numbers and they will be denoted, in descending order, by $\sigma_1, \ldots, \sigma_n$. We may then compute:

$$\min_{\|u\|_2=1} \|F a_i\|_2 = \left(\min_{v \in \mathbb{C}^n} \frac{\|Fv\|_2^2}{\|v\|_2^2} \right)^{\frac{1}{2}} = \left(\min_{v \in \mathbb{C}^n} \frac{v^\dagger F^\dagger F v}{v^\dagger v} \right)^{\frac{1}{2}} = \sigma_n. \tag{4.18}$$

The last step is obtained by writing the vector $v \in \mathbb{C}^n$ as a linear combination of orthonormal eigenvectors of the hermitian matrix $F^\dagger F$. In the same way the relation,

$$\max_{\|u\|_2=1} \|F u\|_2 = \sigma_1, \tag{4.19}$$

is obtained. We conclude that,

$$\sigma_n(t, t_i) \le \|F(t, t_i) u\|_2 \le \sigma_1(t, t_i), \tag{4.20}$$

for any unit vector u. In particular, a fundamental solution matrix $F(t, t_i)$ is unitary if and only if $\sigma_1(t, t_i) = \sigma_n(t, t_i) = 1$. Therefore, the determination of the singular values is an appropriate method to assess the unitarity of $F(t, t_i)$ in numerical calculations. It is also an efficient method because stable iterative methods for the evaluation of singular values of square matrices exist (see [GV96, DH93, ABB$^+$99]).

4.3 Approximate transition amplitudes

The coupled channel method is used to compute approximate transition amplitudes numerically. In order to deduce the relation between the analytically defined transition amplitude and the fundamental solution matrix, recall the post form of the transition amplitude, presented in section 3.2:

$$a_{\Delta l, \Gamma k} = \lim_{t \to \infty} \left(\Phi_{\Delta, l}(t), \Psi_{\Gamma, k}^+(t) \right). \tag{4.21}$$

Consider an approximate solution $\tilde{\Psi}_{\Gamma, k}^+(t, \boldsymbol{x})$ of the two-centre Dirac equation, which is obtained by means of the coupled channel method and approaches the asymptotic configuration $\Phi_{\Gamma, k}(t, \boldsymbol{x})$ as $t \to -\infty$,

$$\lim_{t \to -\infty} \left\| \tilde{\Psi}_{\Gamma, k}^+(t) - \Phi_{\Gamma, k}(t) \right\| = 0.$$

The approximate transition amplitude $\tilde{a}_{\Delta l, \Gamma k}$ is defined similarly to equation (4.21) by,

$$\tilde{a}_{\Delta l, \Gamma k} = \lim_{t \to \infty} \left(\Phi_{\Delta, l}(t), \tilde{\Psi}_{\Gamma, k}^+(t) \right). \tag{4.22}$$

Assuming asymptotic orthogonality of the basis functions $\Phi_{\Gamma,k}(t,\boldsymbol{x})$ of the coupled channel expansion, the short calculation,

$$
\begin{aligned}
\tilde{a}_{\Delta l,\Gamma k} &= \lim_{t\to\infty}\left(\Phi_{\Delta,l}(t),\sum_{\Theta,m}c_{\Theta,m}(t)\,\Phi_{\Theta,m}(t)\right) \qquad (\text{where } \lim_{t\to-\infty}c_{\Theta,m}(t)=\delta_{\Theta m,\Gamma k}) \\
&= \sum_{\Theta,m}\lim_{t\to\infty}c_{\Theta,m}(t)\,\lim_{t\to\infty}\left(\Phi_{\Delta,l}(t),\Phi_{\Theta,m}(t)\right) \\
&= \lim_{t\to\infty}c_{\Delta,l}(t),
\end{aligned}
$$

shows that the approximate transition amplitudes are identical to the elements of the matrix $F(\infty,-\infty)$ defined in equation (4.15),

$$
F(\infty,-\infty)_{\Delta l,\Gamma k}=\tilde{a}_{\Delta l,\Gamma k}.
$$

As a consequence of the unitarity of $F(\infty,-\infty)$ the finite sum over all approximate transition probabilities is one, for any initial configuration (Γ,k), i.e.

$$
\sum_{\Delta,l}|\tilde{a}_{\Delta l,\Gamma k}|^2=1.
$$

This property is not a consequence of the conservation of probability (3.19), which was discussed in the context of the exact scattering theory of the two-centre Dirac equation. But it is a feature of the coupled channel equations. In general the corresponding finite sum over the *exact* transition probabilities $|a_{\Delta l,\Gamma k}|^2$ will be smaller than one.

   As demonstrated by numerical calculations presented in chapter 6, the approximate transition amplitude $\tilde{a}_{\Delta l,\Gamma k}$ is not invariant under Lorentz boosts. This fact also reflects the breaking of the Lorentz invariance due to the coupled channel approximation.

   Certainly, the matrix of transition amplitudes $F(\infty,-\infty)$ must be approximated in numerical calculations by a fundamental solution matrix $F(t_{\mathrm{f}},t_{\mathrm{i}})$ with finite initial and final times t_{i} and t_{f}.

# Implementation of the Coupled Channel Approximation

In this chapter, the capabilities of the numerical code for coupled channel calculations, which has been written for the present work, are described.

In addition, some numerical results are presented. This serves two different purposes: On one hand, the examples illustrate the principal features of the two-centre coupled channel method. On the other hand, these exemplary calculations also demonstrate the proper functioning and the correctness of the numerical software.

The entire computer code used for the numerical computations presented in this work has been newly written, except for some publicly available source code packages employed for standard tasks, like linear algebra calculations and inter-process communication in distributed computations. The general functionality, structure and algorithmic details of the program are not described in this chapter, but in appendix A.

5.1 Reference frames

The program does not permit to solve the coupled channel equations (4.8) in an arbitrarily chosen frame of reference, but it is the first which is capable of performing numerical computations in various different relativistic frames of reference. The coupled channel equations can be solved in such Lorentz frames, in which the centres move along the e_3-axis and the centres are located on the e_1-axis at time $t = 0$.
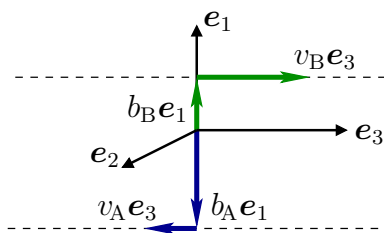
Hence, it is assumed in the following that the parameters $\boldsymbol{b}_\Gamma$ and $\boldsymbol{v}_\Gamma$ of the straight line trajectories (2.1) are given by,

$$\boldsymbol{b}_\Gamma = b_\Gamma \boldsymbol{e}_1,$$

$$\boldsymbol{v}_\Gamma = v_\Gamma \boldsymbol{e}_3,$$

where b_Γ and v_Γ are not necessarily positive.

Note, however, that the overlap and interaction matrix elements, as defined in equations (4.6) and (4.7), are invariant under spatial rotations and translations, and, therefore, the coupled channel equations in Lorentz frames connected by such Poincaré transformations are *identical*. Hence, it is true that the program allows

for the solution of the coupled channel equations in all Lorentz frames, in which the centres move on *parallel* straight-line trajectories and in which the distance of closest approach of both centres is reached at time $t = 0$. The particular orientation of the coordinate axes as defined above is not important.

In this chapter, primed and doubly primed coordinates are always understood as defined below:

$$t' = \gamma_A(t - v_A x^3), \quad \boldsymbol{x}' = (\boldsymbol{x} - x^3 \boldsymbol{e}_3) + \gamma_A(x^3 - tv_A)\boldsymbol{e}_3 - b_A \boldsymbol{e}_1,$$
$$t'' = \gamma_B(t - v_B x^3), \quad \boldsymbol{x}'' = (\boldsymbol{x} - x^3 \boldsymbol{e}_3) + \gamma_B(x^3 - tv_B)\boldsymbol{e}_3 - b_B \boldsymbol{e}_1. \tag{5.1}$$

Clearly, they are rest frame coordinates of centre A and B respectively. The particular orientation of these coordinate systems later determines the angular momentum quantisation axis of coupled channel basis functions. The rapidity of centre Γ, a useful quantity denoted by χ_Γ in the following, is related to velocity v_Γ by:

$$v_\Gamma = \tanh \chi_\Gamma.$$

Although numerical calculations presented in this work have been carried out for an external field originating from moving point charges, the extension of the program to arbitrary spherically symmetric charge distributions is straightforward. Thus the more general case will be considered here, in which the external field matrix $W_\Gamma(t, \boldsymbol{x})$ is of the form:

$$W_\Gamma(t, \boldsymbol{x}) = -e\, V_\Gamma(r_\Gamma(t, \boldsymbol{x}))\, S(2\chi_\Gamma).$$

However, V_Γ is always assumed to be an attractive electrostatic potential for negatively charged electrons, such that electron bound states exist. For the matrix part $S(2\chi_\Gamma)$ of the previous equation the abbreviation,

$$S(\chi) = \exp\left(-\frac{\chi}{2}\alpha_3\right) = \left(\cosh\frac{\chi}{2}\right) - \left(\sinh\frac{\chi}{2}\right)\alpha_3,$$

has been introduced for the boost representation matrix $S(\chi)$. It satisfies:

$$S(2\chi_\Gamma) = S(\chi_\Gamma)^2 = \gamma_\Gamma(1 - v_\Gamma \alpha_3).$$

The hermitian matrix $S(\chi)$ is a real matrix in case of the standard Pauli–Dirac representation of the γ-matrices, used in the numerical code (see appendix C). For the present choice of reference frames, the residual external fields $W_\Gamma^\infty(t, \boldsymbol{x})$, defined in section 3.7, may be written as follows:

$$W_\Gamma^\infty(t, \boldsymbol{x}) = \frac{-e^2 \tilde{Z}_\Gamma}{d_\Gamma(t, \boldsymbol{x})}\, S(2\chi_\Gamma).$$

It is worth mentioning again the expressions for the Lorentz scalars $r_\Gamma(t, \boldsymbol{x})$ and $d_\Gamma(t, \boldsymbol{x})$, which are defined in equations (2.4) and (2.6) and are particularly simple in the present context:

$$r_\Gamma(t, \boldsymbol{x}) = \sqrt{(x^1 - b_\Gamma)^2 + (x^2)^2 + \gamma_\Gamma^2(x^3 - tv_\Gamma)^2}, \tag{5.2}$$

$$d_\Gamma(t, \boldsymbol{x}) = \sqrt{(b_A - b_B)^2 + v^2\gamma_\Gamma^2(t - v_\Gamma x^3)^2}, \tag{5.3}$$

Here the velocity v is given by,

$$v = \tanh|\chi_A - \chi_B|, \tag{5.4}$$

and is the relative velocity of the centres in a rest frame of either centre (cf. section 2.1). Hence, the collision energy is given by the Lorentz factor $\gamma = \cosh(\chi_A - \chi_B)$.

5.2 Spherical symmetry

The spherical symmetry of the electrostatic potential $V_A(|\boldsymbol{x}'|)$ in the primed coordinates has the following well-known implications [Ros61, BD66, Sak67, Tha92, EM95]. The t'-independent Hamiltonian in the primed Lorentz frame,

$$H_A' = -i\boldsymbol{\alpha} \cdot \nabla' + \beta - e\,V_A(|\boldsymbol{x}'|),$$

commutes with the spin-orbit operator,[1] [2]

$$K' = -\beta(\boldsymbol{L}' \cdot \boldsymbol{S}' + 1), \tag{5.5}$$

and at the same time with the total angular momentum operator $\boldsymbol{J}' = \boldsymbol{L}' + \boldsymbol{S}'$. Here, $\boldsymbol{L}'$ denotes the orbital angular momentum operator,

$$\boldsymbol{L}' = \boldsymbol{x}' \wedge (-i\nabla'),$$

and $\boldsymbol{S}'$ the spin angular-momentum operator,

$$\boldsymbol{S}' = -\frac{i}{4}\,\boldsymbol{\alpha} \wedge \boldsymbol{\alpha}.$$

The spin-orbit operator K' commutes not only with H_A', but also with the total angular momentum operator $\boldsymbol{J}'$. Moreover, the set of its eigenvalues $\sigma(K')$ is the set of all nonzero integers:

$$\sigma(K') = \{\pm 1, \pm 2, \pm 3, \dots\}\,.$$

Due to the relation,

$$\boldsymbol{J}'^2 = K'^2 - \frac{1}{4},$$

any eigenfunction of K' with eigenvalue κ is automatically an eigenfunction of $\boldsymbol{J}'^2$ with eigenvalue $j(j+1)$, where κ and j are related by:

$$j = |\kappa| - \frac{1}{2}.$$

Since H_A', K', and the third component J'^3 of the total angular momentum operator $\boldsymbol{J}'$ form a set of commuting, self-adjoint operators, it is clear that bound states of the electrostatic potential $V_A(|\boldsymbol{x}'|)$ are orthogonal, if they correspond to different eigenvalues. Any energy eigenvalue of a simultaneous eigenstate of H_A' and K', with the eigenvalues ϵ and κ respectively is at least $2|\kappa|$-fold degenerate, known as the angular momentum degeneracy of bound state energies for a spherical potential.

---

[1]Here the sign convention agrees with [SFVW95b].

[2]In principle, it is appropriate to give the operator K' (and the other operators defined in this section) an additional subscript A, in order to indicate that it is defined with respect to the primed spatial coordinates 5.1 of a rest frame of centre A. But for brevity K_A' is written simply as K'.

The energy eigenvalues, within an eigenspace of K' with eigenvalue κ, are commonly numbered in ascending order by an integer n, with

$$n = |\kappa|, |\kappa| + 1, |\kappa| + 2, \ldots \quad \text{if } \kappa < 0 \text{ and}$$
$$n = \kappa + 1, \kappa + 2, \kappa + 3, \ldots \quad \text{if } \kappa > 0.$$

If degeneracies within an eigenspace of K', that are not angular momentum degeneracies, are counted by separate indices n, then any bound state of the radially symmetric potential V_A, which is a simultaneous eigenstate of the operators H'_A, K' and J'^3, is uniquely characterised by a triple index (n, κ, m). Here m denotes the eigenvalue of J'^3. However, such degeneracies do not occur for the Coulomb potential. For some potentials, like the Coulomb potential, the number of orthogonal bound states with the same eigenvalue κ is infinite. This number may be finite or even zero, depending on κ, for other attractive potentials, including the Yukawa potential and the class of potentials of equation (2.10)

Therefore, in the important case where $V_A(|\boldsymbol{x}'|)$ is the Coulomb potential, *every* triple (n, κ, m) satisfying $n \in \mathbb{N}$,

$$-n \leq \kappa < n \quad \text{with } \kappa \in \mathbb{Z}, \kappa \neq 0, \text{ and}$$
$$|m| \leq |\kappa| - \frac{1}{2} \quad \text{with } m \in \frac{2\mathbb{Z} + 1}{2},$$

corresponds to a Coulomb–Dirac bound state, which is simultaneously an eigenstate of the operators H'_A, K' and J'^3, and vice versa. These mutually orthogonal Coulomb–Dirac bound states are consecutively numbered by the single non-negative integer,

$$i = \frac{(2n-1)(n-1)n}{3} + 2\kappa^2 + \kappa + m - \frac{1}{2} = 0, 1, 2, \ldots. \tag{5.6}$$

This integer i constitutes the linear index for bound states, employed in numerical calculations presented in this work (see e.g. figure 5.1 on page 55). The linear ordering of Coulomb–Dirac bound states by their index i includes their partial ordering due to the energy eigenvalues. This means that $i(n, \kappa, m) \leq i(\hat{n}, \hat{\kappa}, \hat{m})$ implies $\epsilon_{n\kappa m} \leq \epsilon_{\hat{n}\hat{\kappa}\hat{m}}$.

The integer n represents the principal quantum number of an eigenstate in the nonrelativistic limit of the Dirac equation and the orbital angular momentum quantum number l with respect to that limit, is given by:

$$l = \begin{cases} |\kappa| - 1 & \text{if } \kappa < 0, \\ \kappa & \text{if } \kappa > 0, \end{cases}$$

Table 5.1 lists the 28 lowest Coulomb–Dirac bound states, including their conventional spectroscopic labels. Clearly, everything described in this section applies similarly to bound states of the spherically symmetric electrostatic potential $V_B(|\boldsymbol{x}''|)$ in the doubly primed Lorentz frame.

5.3 Basis functions

5.3.1 Undistorted basis functions. All basis sets of coupled channel calculations presented in this work comprise a certain number of *bound-electron* wave functions of both centre A and centre B. These basis functions are first constructed in their

TABLE 5.1. Single and triple indices of the 28 lowest Coulomb–Dirac bound states and their designations in spectroscopic notation. The integer i is defined in equation (5.6).

i	n	κ	m	spectrosc.
0	1	-1	$-\frac{1}{2}$	$1\mathrm{s}_{1/2}(-\frac{1}{2})$
1	1	-1	$+\frac{1}{2}$	$1\mathrm{s}_{1/2}(+\frac{1}{2})$
2	2	-1	$-\frac{1}{2}$	$2\mathrm{s}_{1/2}(-\frac{1}{2})$
3	2	-1	$+\frac{1}{2}$	$2\mathrm{s}_{1/2}(+\frac{1}{2})$
4	2	1	$-\frac{1}{2}$	$2\mathrm{p}_{1/2}(-\frac{1}{2})$
5	2	1	$+\frac{1}{2}$	$2\mathrm{p}_{1/2}(+\frac{1}{2})$
6	2	-2	$-\frac{3}{2}$	$2\mathrm{p}_{3/2}(-\frac{3}{2})$
7	2	-2	$-\frac{1}{2}$	$2\mathrm{p}_{3/2}(-\frac{1}{2})$
8	2	-2	$+\frac{1}{2}$	$2\mathrm{p}_{3/2}(+\frac{1}{2})$
9	2	-2	$+\frac{3}{2}$	$2\mathrm{p}_{3/2}(+\frac{3}{2})$
10	3	-1	$-\frac{1}{2}$	$3\mathrm{s}_{1/2}(-\frac{1}{2})$
11	3	-1	$+\frac{1}{2}$	$3\mathrm{s}_{1/2}(+\frac{1}{2})$
12	3	1	$-\frac{1}{2}$	$3\mathrm{p}_{1/2}(-\frac{1}{2})$
13	3	1	$+\frac{1}{2}$	$3\mathrm{p}_{1/2}(+\frac{1}{2})$

i	n	κ	m	spectrosc.
14	3	-2	$-\frac{3}{2}$	$3\mathrm{p}_{3/2}(-\frac{3}{2})$
15	3	-2	$-\frac{1}{2}$	$3\mathrm{p}_{3/2}(-\frac{1}{2})$
16	3	-2	$+\frac{1}{2}$	$3\mathrm{p}_{3/2}(+\frac{1}{2})$
17	3	-2	$+\frac{3}{2}$	$3\mathrm{p}_{3/2}(+\frac{3}{2})$
18	3	2	$-\frac{3}{2}$	$3\mathrm{d}_{3/2}(-\frac{3}{2})$
19	3	2	$-\frac{1}{2}$	$3\mathrm{d}_{3/2}(-\frac{1}{2})$
20	3	2	$+\frac{1}{2}$	$3\mathrm{d}_{3/2}(+\frac{1}{2})$
21	3	2	$+\frac{3}{2}$	$3\mathrm{d}_{3/2}(+\frac{3}{2})$
22	3	-3	$-\frac{5}{2}$	$3\mathrm{d}_{5/2}(-\frac{5}{2})$
23	3	-3	$-\frac{3}{2}$	$3\mathrm{d}_{5/2}(-\frac{3}{2})$
24	3	-3	$-\frac{1}{2}$	$3\mathrm{d}_{5/2}(-\frac{1}{2})$
25	3	-3	$+\frac{1}{2}$	$3\mathrm{d}_{5/2}(+\frac{1}{2})$
26	3	-3	$+\frac{3}{2}$	$3\mathrm{d}_{5/2}(+\frac{3}{2})$
27	3	-3	$+\frac{5}{2}$	$3\mathrm{d}_{5/2}(+\frac{5}{2})$

respective primed and doubly primed rest frames and then Lorentz-transformed into the unprimed frame of reference, where the coupled channel ansatz is made. In their rest frames the bound states are taken to be eigenfunctions of their corresponding time-independent Hamiltonians, spin-orbit operators and third component of their total angular momentum operators, as described in the previous section. Hence, these basis functions are of the form:

$$
\begin{aligned}
\Phi_{\mathrm{A},i}(t,\boldsymbol{x}) &= S(-\chi_{\mathrm{A}})\,\exp(-\mathrm{i}t'\epsilon_{\mathrm{A},i})\phi_{\mathrm{A},i}(\boldsymbol{x}'), \\
\Phi_{\mathrm{B},j}(t,\boldsymbol{x}) &= S(-\chi_{\mathrm{B}})\,\exp(-\mathrm{i}t''\epsilon_{\mathrm{B},j})\phi_{\mathrm{B},j}(\boldsymbol{x}'').
\end{aligned}
\tag{5.7}
$$

Here, the indices i and j refer to the linear index (5.6) of orthonormal bound state eigenfunctions of fixed energy and angular momentum. By construction, the wave functions $\phi_{\mathrm{A},i}$ and $\phi_{\mathrm{B},j}$ solve the following energy eigenvalue equations in their respective rest frames:

$$
\begin{aligned}
\left[-\mathrm{i}\boldsymbol{\alpha}\cdot\nabla' + \beta - e\,V_{\mathrm{A}}(|\boldsymbol{x}'|)\right]\phi_{\mathrm{A},i}(\boldsymbol{x}') &= \epsilon_{\mathrm{A},i}\,\phi_{\mathrm{A},i}(\boldsymbol{x}'), \\
\left[-\mathrm{i}\boldsymbol{\alpha}\cdot\nabla'' + \beta - e\,V_{\mathrm{B}}(|\boldsymbol{x}''|)\right]\phi_{\mathrm{B},j}(\boldsymbol{x}'') &= \epsilon_{\mathrm{B},j}\,\phi_{\mathrm{B},j}(\boldsymbol{x}').
\end{aligned}
$$

Their precise form is not important here and given in appendix A. Although they refer to the primed and doubly primed frames respectively, the energy eigenvalues $\epsilon_{\mathrm{A},i}$ and $\epsilon_{\mathrm{B},j}$, and the eigenfunctions $\phi_{\mathrm{A},i}(\boldsymbol{x}')$ and $\phi_{\mathrm{B},j}(\boldsymbol{x}'')$ are not primed, because eigenvalues and time-independent eigenfunctions cannot be transformed to moving frames

meaningfully, unless the external field vanishes (cf. section B.3). The boosted wave functions $\Phi_{\Gamma,i}(t, \boldsymbol{x})$ of equation (5.7) solve the scattering-channel Dirac equations,

$$[H_0 + W_\Gamma(t, \boldsymbol{x}) - \mathrm{i}\partial_t]\, \Phi_{\Gamma,i}(t, \boldsymbol{x}) = 0, \qquad (5.8)$$

and will be referred to as *undistorted* basis functions, as opposed to phase-distorted basis functions introduced in the following subsection.

The specific expressions for overlap and interaction matrix elements (cf. equations (4.6) and (4.7) respectively) in the case of undistorted basis functions are presented in the following. Due to the invariance of the scalar product (discussed in section B.2), and since by construction the eigenfunctions $\phi_{\mathrm{A},i}(\boldsymbol{x}')$ are orthonormal in the primed reference frame, the basis functions $\Phi_{\mathrm{A},i}(t, \boldsymbol{x})$ in the unprimed reference frame are orthonormal as well for all times t. The same is true for the bound-state wave functions $\Phi_{\mathrm{B},j}(t, \boldsymbol{x})$ of centre B. Therefore we have:

$$
\begin{aligned}
N_{\mathrm{A}j,\mathrm{A}i}(t) &= \delta_{ij}, \\
N_{\mathrm{B}j,\mathrm{B}i}(t) &= \delta_{ij}.
\end{aligned}
\qquad (5.9)
$$

The overlap matrix elements (4.6) between basis functions of different centres become:

$$
\begin{aligned}
N_{\mathrm{A}j,\mathrm{B}i}(t) &= \int \exp(\mathrm{i}t'\epsilon_{\mathrm{A},j} - \mathrm{i}t''\epsilon_{\mathrm{B},i})\, \phi^\dagger_{\mathrm{A},j}(\boldsymbol{x}')\, S(-\chi_{\mathrm{A}} - \chi_{\mathrm{B}})\, \phi_{\mathrm{B},i}(\boldsymbol{x}'')\, \mathrm{d}^3x, \\
N_{\mathrm{B}j,\mathrm{A}i}(t) &= \int \exp(\mathrm{i}t''\epsilon_{\mathrm{B},j} - \mathrm{i}t'\epsilon_{\mathrm{A},i})\, \phi^\dagger_{\mathrm{B},j}(\boldsymbol{x}'')\, S(-\chi_{\mathrm{A}} - \chi_{\mathrm{B}})\, \phi_{\mathrm{A},i}(\boldsymbol{x}')\, \mathrm{d}^3x.
\end{aligned}
\qquad (5.10)
$$

Certainly, the overlap matrix is hermitian, such that $N_{\Delta j,\Gamma i}(t) = N_{\Gamma i,\Delta j}(t)^*$ holds, which is evident already from definition (4.6). The overlap matrix elements (5.10) are vanishing only as t approaches $\pm\infty$ and are nonzero otherwise (cf. section 3.4).

As verified by using equation (5.8), the interaction matrix elements (4.7) between undistorted basis functions are given in the present context by the following expressions:

$$
\begin{aligned}
V_{\mathrm{A}j,\mathrm{A}i}(t) &= \int \Big\{ -eV_{\mathrm{B}}(r_{\mathrm{B}}(t, \boldsymbol{x})) \Big\} \times \\
&\qquad \times \exp(\mathrm{i}t'\epsilon_{\mathrm{A},j} - \mathrm{i}t'\epsilon_{\mathrm{A},i})\, \phi_{\mathrm{A},j}(\boldsymbol{x}')^\dagger\, S(-2\chi_{\mathrm{A}} + 2\chi_{\mathrm{B}})\, \phi_{\mathrm{A},i}(\boldsymbol{x}')\, \mathrm{d}^3x \\
V_{\mathrm{A}j,\mathrm{B}i}(t) &= \int \Big\{ -eV_{\mathrm{A}}(r_{\mathrm{A}}(t, \boldsymbol{x})) \Big\} \times \\
&\qquad \times \exp(\mathrm{i}t'\epsilon_{\mathrm{A},j} - \mathrm{i}t''\epsilon_{\mathrm{B},i})\, \phi_{\mathrm{A},j}(\boldsymbol{x}')^\dagger\, S(\chi_{\mathrm{A}} - \chi_{\mathrm{B}})\, \phi_{\mathrm{B},i}(\boldsymbol{x}'')\, \mathrm{d}^3x \\
V_{\mathrm{B}j,\mathrm{A}i}(t) &= \int \Big\{ -eV_{\mathrm{B}}(r_{\mathrm{B}}(t, \boldsymbol{x})) \Big\} \times \\
&\qquad \times \exp(\mathrm{i}t''\epsilon_{\mathrm{B},j} - \mathrm{i}t'\epsilon_{\mathrm{A},i})\, \phi_{\mathrm{B},j}(\boldsymbol{x}'')^\dagger\, S(-\chi_{\mathrm{A}} + \chi_{\mathrm{B}})\, \phi_{\mathrm{A},i}(\boldsymbol{x}')\, \mathrm{d}^3x \\
V_{\mathrm{B}j,\mathrm{B}i}(t) &= \int \Big\{ -eV_{\mathrm{A}}(r_{\mathrm{A}}(t, \boldsymbol{x})) \Big\} \times \\
&\qquad \times \exp(\mathrm{i}t''\epsilon_{\mathrm{B},j} - \mathrm{i}t''\epsilon_{\mathrm{B},i})\, \phi_{\mathrm{B},j}(\boldsymbol{x}'')^\dagger\, S(2\chi_{\mathrm{A}} - 2\chi_{\mathrm{B}})\, \phi_{\mathrm{B},i}(\boldsymbol{x}'')\, \mathrm{d}^3x
\end{aligned}
\qquad (5.11)
$$

Numerically the matrix elements (5.10) and (5.11) have to be evaluated by three-dimensional quadrature formulas (see appendix A). Although the interaction matrix is not hermitian, the partial symmetry $V_{\Gamma j,\Gamma i} = V^*_{\Gamma i,\Gamma j}$ is useful to reduce the effort of the computationally very demanding numerical evaluation. The fundamental solution $F(t, t_\mathrm{i})$ is then computed by integrating the differential equation (4.8) between

some suitable initial and final times, t_i and t_f, chosen in a symmetrical fashion as $t_\mathrm{i} = -t_\mathrm{f}$.

5.3.2 Phase-distorted basis functions. Compared to the definition (5.7) of the undistorted basis functions, the *phase-distorted* basis functions have an additional phase factor, in order to satisfy Coulomb boundary conditions. They are defined as:

$$\begin{aligned}
\Phi_{\mathrm{A},i}(t, \boldsymbol{x}) &= \exp(\mathrm{i}g_\mathrm{B}(t, \boldsymbol{x}))\, S(-\chi_\mathrm{A})\, \exp(-\mathrm{i}t'\epsilon_{\mathrm{A},i})\phi_{\mathrm{A},i}(\boldsymbol{x}'), \\
\Phi_{\mathrm{B},j}(t, \boldsymbol{x}) &= \exp(\mathrm{i}g_\mathrm{A}(t, \boldsymbol{x}))\, S(-\chi_\mathrm{B})\, \exp(-\mathrm{i}t''\epsilon_{\mathrm{B},j})\phi_{\mathrm{B},j}(\boldsymbol{x}'').
\end{aligned} \tag{5.12}$$

We do not use different symbols for phase-distorted and undistorted basis functions, because they will not both occur in the same equation. In equations (5.12) the energy eigenvalues $\epsilon_{\mathrm{A},i}$ and $\epsilon_{\mathrm{B},j}$, and the eigenfunctions $\phi_{\mathrm{A},i}(\boldsymbol{x}')$ and $\phi_{\mathrm{B},j}(\boldsymbol{x}'')$ are identical to those of the previous section. Although the phase-distorted basis functions are not energy or angular momentum eigenfunctions in the primed and doubly primed reference frames respectively (cf. section B.3 of the appendix), they are denoted by analogy to the undistorted functions according to table 5.1.

For the present numerical work the following gauge functions $g_\Gamma(t, \boldsymbol{x})$ have been used,

$$g_\Gamma(t, \boldsymbol{x}) = \frac{e^2 \tilde{Z}_\Gamma}{v}\, \log \frac{d_\Gamma(t, \boldsymbol{x}) + v\gamma_\Gamma(t - v_\Gamma x^3)}{|b_\mathrm{A} - b_\mathrm{B}|}, \tag{5.13}$$

with $d_\Gamma(t, \boldsymbol{x})$ as in equation (5.3) and $v = \tanh|\chi_\mathrm{A} - \chi_\mathrm{B}|$. Remember that $Z_\Gamma = \tilde{Z}_\Gamma$ for the Coulomb potential. The phase-distorted basis functions (5.12) then solve the following Coulomb-distorted scattering-channel Dirac equations (cf. section 3.7):

$$\begin{aligned}
\left[H_0 + W_\mathrm{A}(t, \boldsymbol{x}) + W_\mathrm{B}^\infty(t, \boldsymbol{x}) - \mathrm{i}\partial_t\right] \Phi_{\mathrm{A},i}(t, \boldsymbol{x}) &= 0, \\
\left[H_0 + W_\mathrm{B}(t, \boldsymbol{x}) + W_\mathrm{A}^\infty(t, \boldsymbol{x}) - \mathrm{i}\partial_t\right] \Phi_{\mathrm{B},j}(t, \boldsymbol{x}) &= 0.
\end{aligned}$$

We turn to the specific expressions for overlap and interaction matrix elements in the case of phase-distorted basis functions. Since the additional phase factor cancels in scalar products between basis functions of the same centre, phase-distorted basis functions belonging to the same scattering channel are orthonormal for the same reason as above:

$$\begin{aligned}
N_{\mathrm{A}j,\mathrm{A}i}(t) &= \delta_{ij}, \\
N_{\mathrm{B}j,\mathrm{B}i}(t) &= \delta_{ij}.
\end{aligned} \tag{5.14}$$

The overlap between basis functions of different channels is different for undistorted and phase-distorted basis functions. The remaining elements of the hermitian overlap matrix $N(t)$ are given by:

$$\begin{aligned}
N_{\mathrm{A}j,\mathrm{B}i}(t) &= \int \exp(\mathrm{i}g_\mathrm{A}(t, \boldsymbol{x}) - \mathrm{i}g_\mathrm{B}(t, \boldsymbol{x})) \times \\
&\qquad \times \exp(\mathrm{i}t'\epsilon_{\mathrm{A},j} - \mathrm{i}t''\epsilon_{\mathrm{B},i})\, \phi_{\mathrm{A},j}(\boldsymbol{x}')^\dagger\, S(-\chi_\mathrm{A} - \chi_\mathrm{B})\, \phi_{\mathrm{B},i}(\boldsymbol{x}'')\, \mathrm{d}^3 x \\
N_{\mathrm{B}j,\mathrm{A}i}(t) &= \int \exp(\mathrm{i}g_\mathrm{B}(t, \boldsymbol{x}) - \mathrm{i}g_\mathrm{A}(t, \boldsymbol{x})) \times \\
&\qquad \times \exp(\mathrm{i}t''\epsilon_{\mathrm{B},j} - \mathrm{i}t'\epsilon_{\mathrm{A},i})\, \phi_{\mathrm{B},j}(\boldsymbol{x}'')^\dagger\, S(-\chi_\mathrm{A} - \chi_\mathrm{B})\, \phi_{\mathrm{A},i}(\boldsymbol{x}')\, \mathrm{d}^3 x
\end{aligned} \tag{5.15}$$

Finally, in the case of phase-distorted basis functions the elements of the interaction matrix $V(t)$ are explicitly:

$$
\begin{aligned}
V_{\mathrm{A}j,\mathrm{A}i}(t) &= \int \left\{ eV_{\mathrm{B}}(d_{\mathrm{B}}(t,\boldsymbol{x})) - eV_{\mathrm{B}}(r_{\mathrm{B}}(t,\boldsymbol{x})) \right\} \times \\
&\quad \times \exp(\mathrm{i}t'\epsilon_{\mathrm{A},j} - \mathrm{i}t'\epsilon_{\mathrm{A},i})\, \phi_{\mathrm{A},j}(\boldsymbol{x}')^{\dagger}\, S(-2\chi_{\mathrm{A}} + 2\chi_{\mathrm{B}})\, \phi_{\mathrm{A},i}(\boldsymbol{x}')\, \mathrm{d}^3 x \\
V_{\mathrm{A}j,\mathrm{B}i}(t) &= \int \exp(\mathrm{i}g_{\mathrm{A}}(t,\boldsymbol{x}) - \mathrm{i}g_{\mathrm{B}}(t,\boldsymbol{x})) \left\{ eV_{\mathrm{A}}(d_{\mathrm{A}}(t,\boldsymbol{x})) - eV_{\mathrm{A}}(r_{\mathrm{A}}(t,\boldsymbol{x})) \right\} \times \\
&\quad \times \exp(\mathrm{i}t'\epsilon_{\mathrm{A},j} - \mathrm{i}t''\epsilon_{\mathrm{B},i})\, \phi_{\mathrm{A},j}(\boldsymbol{x}')^{\dagger}\, S(\chi_{\mathrm{A}} - \chi_{\mathrm{B}})\, \phi_{\mathrm{B},i}(\boldsymbol{x}'')\, \mathrm{d}^3 x \\
V_{\mathrm{B}j,\mathrm{A}i}(t) &= \int \exp(\mathrm{i}g_{\mathrm{B}}(t,\boldsymbol{x}) - \mathrm{i}g_{\mathrm{A}}(t,\boldsymbol{x})) \left\{ eV_{\mathrm{B}}(d_{\mathrm{B}}(t,\boldsymbol{x})) - eV_{\mathrm{B}}(r_{\mathrm{B}}(t,\boldsymbol{x})) \right\} \times \\
&\quad \times \exp(\mathrm{i}t''\epsilon_{\mathrm{B},j} - \mathrm{i}t'\epsilon_{\mathrm{A},i})\, \phi_{\mathrm{B},j}(\boldsymbol{x}'')^{\dagger}\, S(-\chi_{\mathrm{A}} + \chi_{\mathrm{B}})\, \phi_{\mathrm{A},i}(\boldsymbol{x}')\, \mathrm{d}^3 x \\
V_{\mathrm{B}j,\mathrm{B}i}(t) &= \int \left\{ eV_{\mathrm{A}}(d_{\mathrm{A}}(t,\boldsymbol{x})) - eV_{\mathrm{A}}(r_{\mathrm{A}}(t,\boldsymbol{x})) \right\} \times \\
&\quad \times \exp(\mathrm{i}t''\epsilon_{\mathrm{B},j} - \mathrm{i}t''\epsilon_{\mathrm{B},i})\, \phi_{\mathrm{B},j}(\boldsymbol{x}'')^{\dagger}\, S(2\chi_{\mathrm{A}} - 2\chi_{\mathrm{B}})\, \phi_{\mathrm{B},i}(\boldsymbol{x}'')\, \mathrm{d}^3 x.
\end{aligned}
\tag{5.16}
$$

Only the difference of the gauge functions g_{A} and g_{B} appears in the integrands. Note that the partial symmetry of the interaction matrix, $V_{\Gamma j,\Gamma i} = V_{\Gamma i,\Gamma j}^{*}$, holds for undistorted as well as phase-distorted basis functions.

5.4 Numerical tests

Before we describe in section 5.5 the inclusion of basis functions representing the scattering channel C of asymptotically free particles, some numerical calculations will be presented in this section. These results are based on a coupled channel expansion exclusively making use of bound state basis functions. Accordingly, only transition probabilities of excitation and charge transfer may be obtained by such calculations.

Numerical investigations of this kind have been carried out, and published in series of papers, by Toshima and Eichler (see the original articles [TE88B, TE88A, TE90] and also [EIC90, EM95]). The work of these authors represents the only fully relativistic two-centre coupled channel calculations available in the literature. Therefore, reproducing some of their results is an important check of the new computer program. At the same time the present work is the first independent verification of the numerical results of Toshima and Eichler.

The relativistic two-centre coupled channel calculations reported by Toshima and Eichler have been performed for a particular frame of reference, namely the *target frame*, where the initial configuration is at rest [TE88B, TE88A, TE90]. This corresponds in the present program (e.g.) to a calculation in a frame of reference, where the velocity of centre A is zero, $v_{\mathrm{A}} = 0$, and where the initial electronic configuration is a bound state of centre A.

In figure 5.1 such a calculation is presented for a symmetrical collision of two point-like uranium nuclei, where the charge numbers are $Z_{\mathrm{A}} = Z_{\mathrm{B}} = 92$. It has been performed in a rest frame of nucleus A, with a coupled channel basis comprised of the ten lowest Coulomb–Dirac bound states of each point charge. The time-evolution of the squared moduli of the expansion coefficients $c_{\Gamma,i}(t)$ is shown for undistorted basis functions, for an initial electronic configuration $(\mathrm{A}, 1\mathrm{s}_{1/2})$. The collision energy and
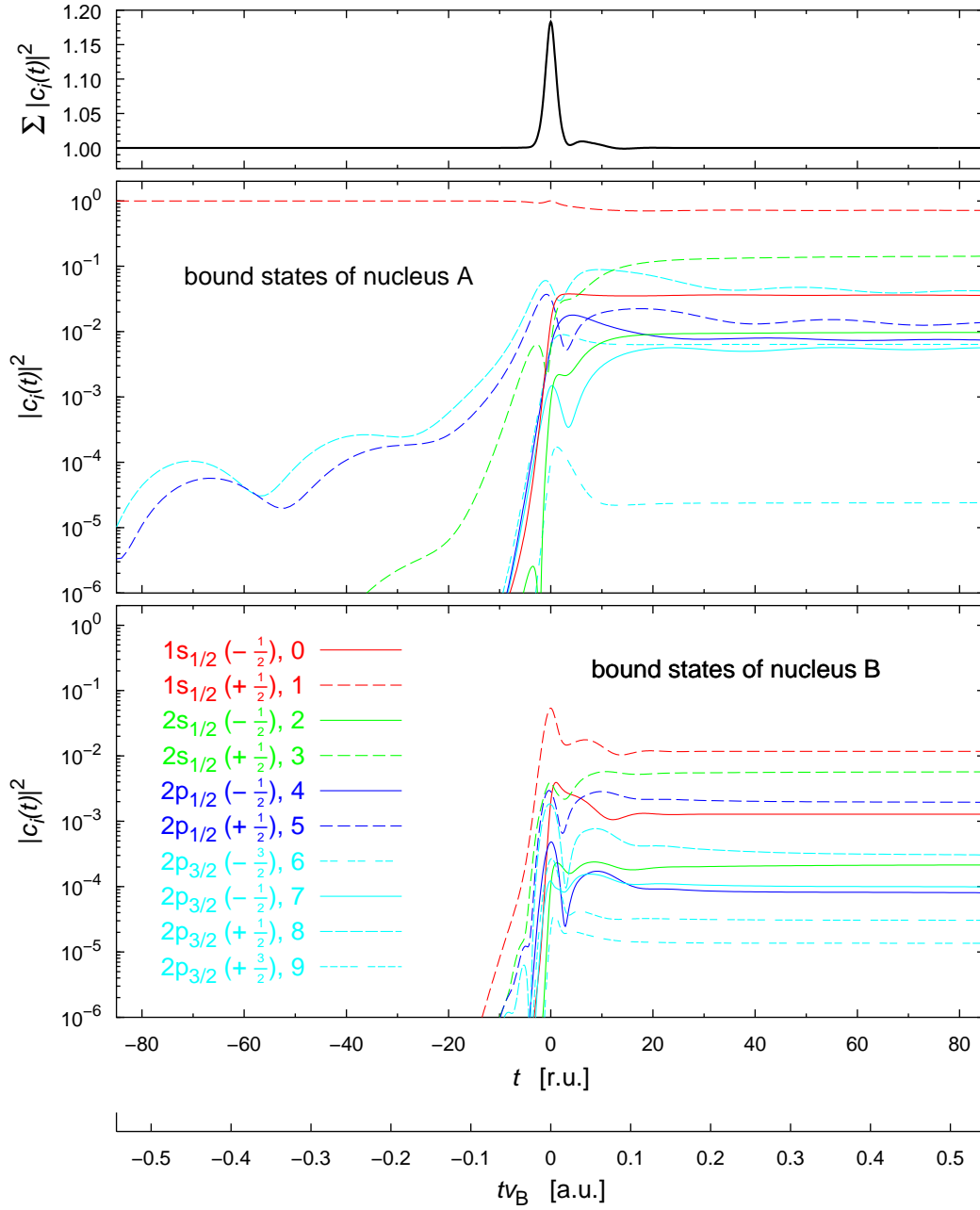
FIGURE 5.1.   Time evolution of the squared moduli of the coefficients $c_i(t)$, as obtained from a numerical coupled channel calculation in the rest frame of nucleus A. The initial configuration presented here is $(A, 1s_{1/2}(+\frac{1}{2}))$. The collision energy $T = 1\,\text{GeV/u}$ corresponds to a velocity $v_B = 0.876\,\text{r.u.}$. The impact parameter is $b = 1.37\,\text{r.u.}$ or 0.01 atomic units. The charge numbers are $Z_A = Z_B = 92$ and the ten lowest undistorted bound states have been used as basis functions. A second abscissa axis, employing atomic units, is provided to facilitate the comparison with [TE88B, figure 1]. Moreover, this second axis represents a length scale, giving the distance between the centres along the e_3-axis. Note, that the K-shell radius of nucleus A (which is not Lorentz-contracted) is approximately $1.5\,\text{r.u.}$ or $0.011\,\text{a.u.}$ (cf. figure 1.2 on page 9). Hence, the time interval where the K-shell radii of both centres are overlapping is small, compared to the total time axis shown here. The top plot demonstrates that the fundamental solution of the coupled channel equations is only asymptotically unitary, which implies that the sum $\sum_i |c_i(t)|^2$ over all states of the expansion is not a constant (cf. section 4.2 and figure 5.3).
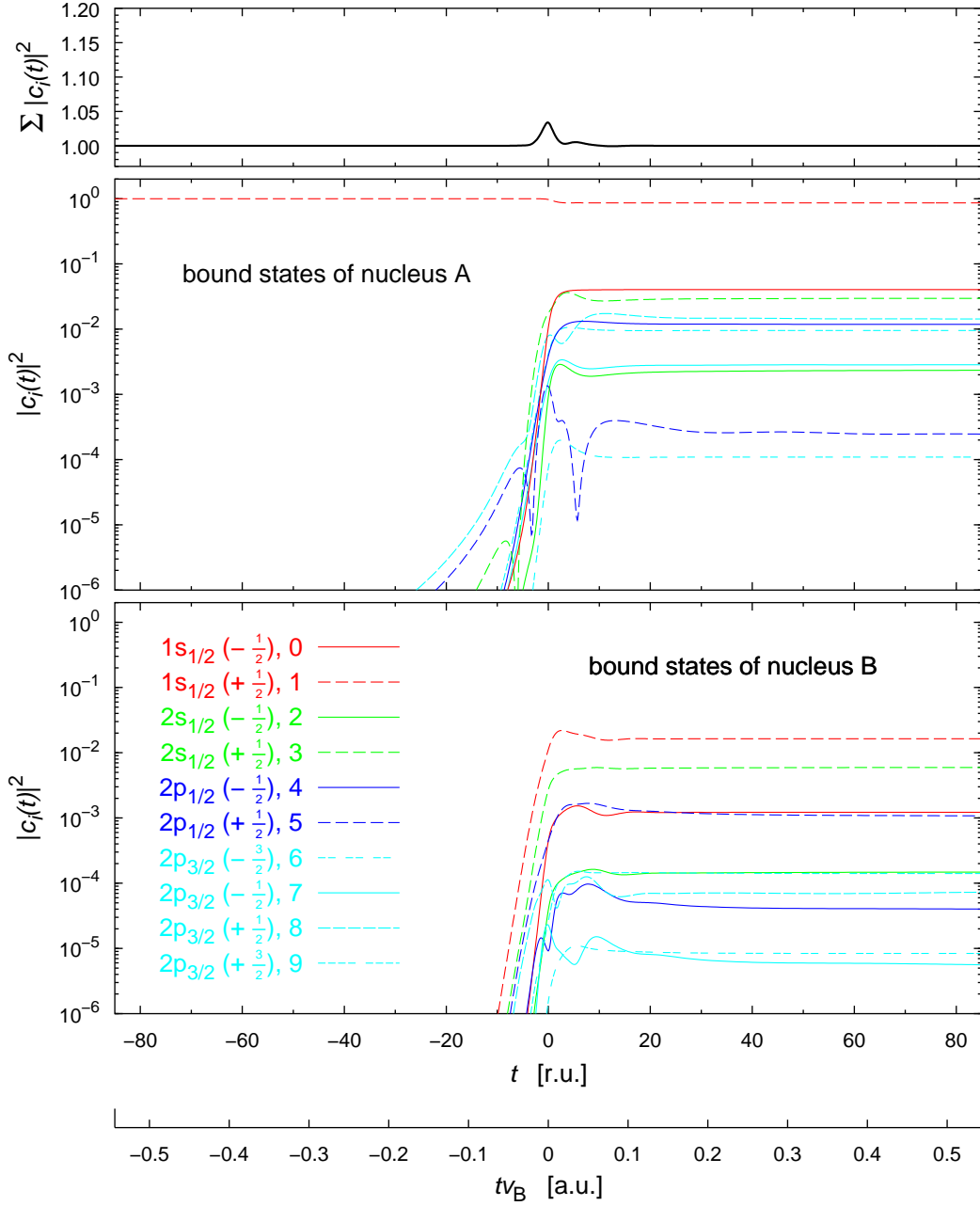
FIGURE 5.2. Time evolution of the squared moduli of the expansion coefficients $c_i(t)$, obtained from a coupled channel calculation with the same parameters and initial configuration as in figure 5.1, but making use of phase-distorted basis functions.

impact parameter are exactly the same as those of an analogous calculation published in [TE88B].

A comparison of the two plots at the bottom of figure 5.1 with [TE88B, figure 1] yields that their match is almost perfect. This confirms that the present numerical code is functioning properly. The numerical results published by Toshima and Eichler more than ten years ago represent an enormous achievement, in a time, when computing facilities have been much less powerful than today. The marginal difference
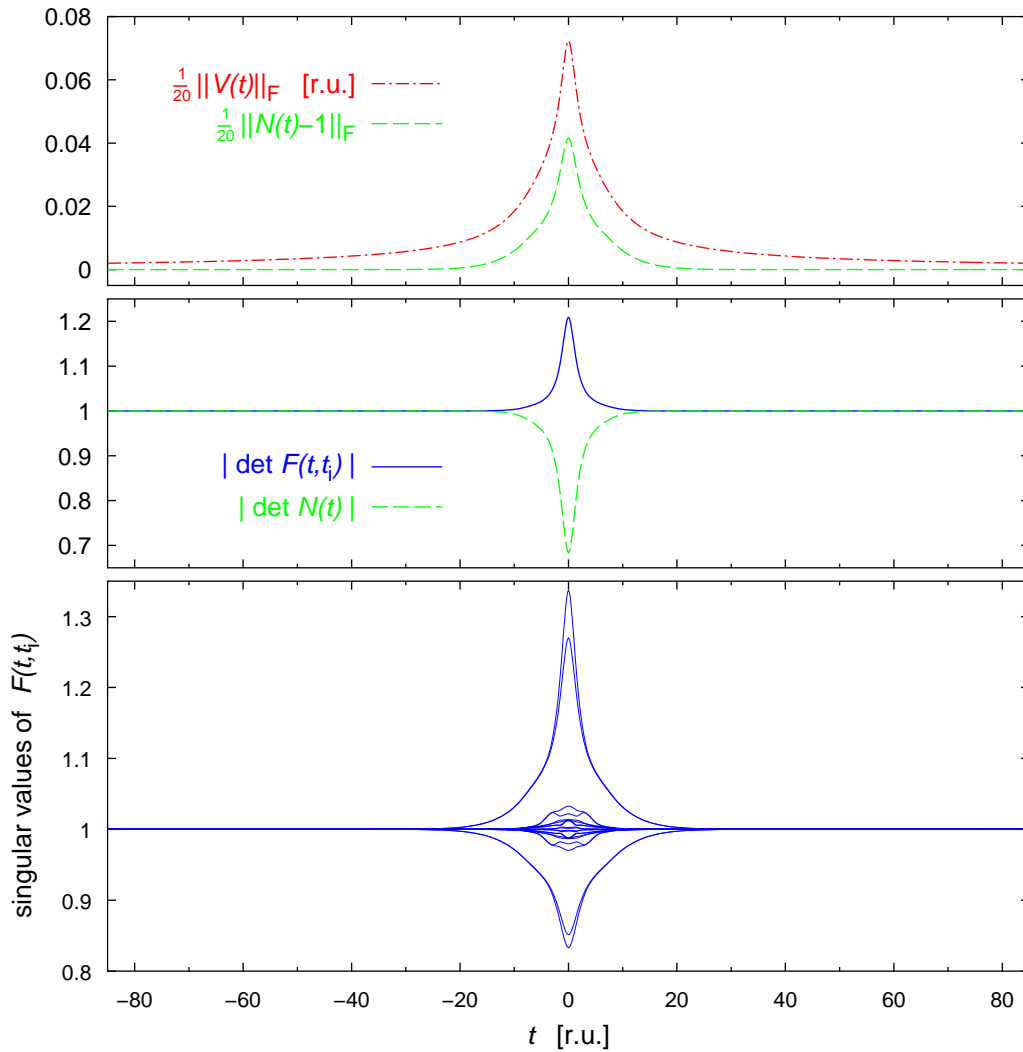
FIGURE 5.3. Properties of the overlap matrix $N(t)$, the interaction matrix $V(t)$ and the fundamental solution matrix $F(t, t_i)$ for the same calculation as shown in figure 5.1.

between the two figures is, therefore, attributed to the greater numerical accuracy of the present numerical results, due to the availability of more powerful computing facilities for the present work.

The two corresponding plots of figure 5.2 show the time-evolution of the squared moduli of the expansion coefficients, for the same collision system and parameters as in figure 5.1, with the only difference that phase-distorted basis functions have been used. In fact, the data of both figures originates from the same run of the program, which integrates the coupled channel equations for undistorted and phase-distorted basis functions simultaneously. The plot in the middle of figure 5.2 may be compared with [TE90, figure 2] or [EM95, p. 178]. The qualitative resemblance is clearly seen, although [TE90, figure 2] represents a calculation using the 18 lowest phase-distorted bound states of each centre.

A principal difference, between the plots in the middle of figures 5.1 and 5.2 respectively, is the missing excitation of target bound states in the calculation with
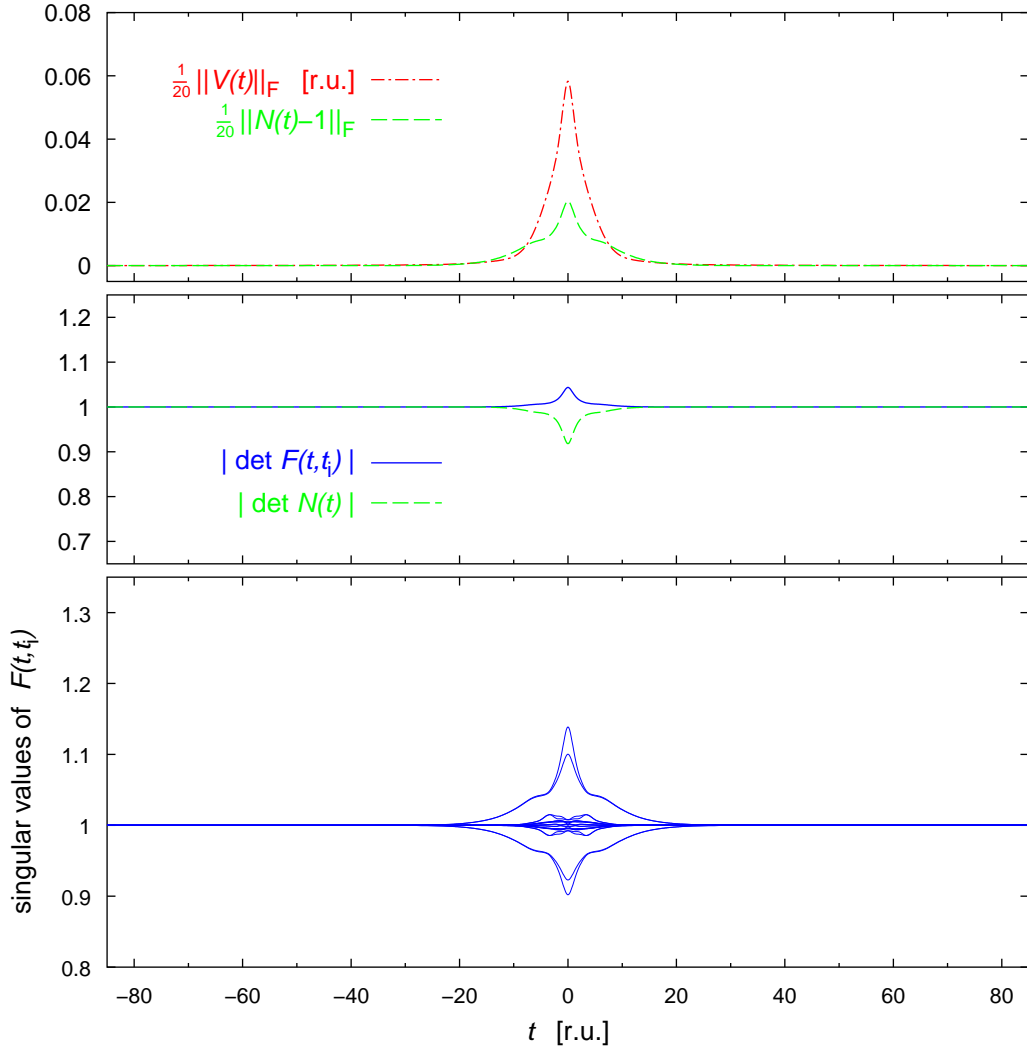
FIGURE 5.4. Properties of the matrices $N(t), V(t)$ and $F(t, t_{\mathrm{i}})$ for the numerical calculation with phase-distorted basis functions presented in figure 5.2.

phase-distorted basis functions, much before the closest approach of the centres at $t = 0$. It demonstrates the effect of the phase distortion, making the interaction short-ranged. In figure 5.1 the long-range character of the Liénard-Wiechert potential leads to target excitations long before the time of closest approach of the nuclei. In detail this has been described first in [TE90].

Finally, let us turn to figures 5.3 and 5.4 which illustrate typical features of the overlap and interaction matrices, $N(t)$ and $V(t)$, and of the fundamental solution $F(t, t_{\mathrm{i}})$ of the coupled channel equations, as explained in the previous section. Since these properties are known due to analytical considerations, their numerical verification constitutes another test for the numerical code. Such plots are not yet available, apparently in the quoted works the full fundamental solution has not been determined.

The green line of the top plot of figure 5.3 shows the root mean squared deviation of the overlap matrix $N(t)$ from the unit matrix for undistorted basis functions. Up to a constant factor this root mean squared deviation is equal to the Frobenius norm

$\|N(t) - 1\|_{\mathrm{F}}$ of the square matrix $N(t) - 1$ [GV96]:

$$\|N(t) - 1\|_{\mathrm{F}} = \left(\sum_{\Delta,\Gamma,j,i} |N_{\Delta j, \Gamma i}(t) - \delta_{\Delta\Gamma}\delta_{ji}|^2 \right)^{1/2}. \qquad (5.17)$$

The non-orthogonality of the basis functions during the collision and their asymptotic orthonormality is properly obtained by the numerical calculation. For the existence of the inverse matrix $N^{-1}(t)$ only the linear independence of the basis functions at any time t is necessary, which is equivalent to the regularity of the overlap matrix $N(t)$. This regularity of $N(t)$ is observably provided, since the determinant $\det N(t)$ is clearly seen to be nonzero for all times t.

In the red line of figure 5.3 shows the root mean squared modulus of the interaction matrix elements, which are vanishing for large times, and are increasing towards $t = 0$, the time of closest approach of the centres.

In the bottom diagram of figure 5.3 the singular values of the fundamental solution $F(t, t_{\mathrm{i}})$ are plotted as a function of time. As explained in subsection 4.2.1, the unitarity of the fundamental solution is equivalent to the property, that all singular values of $F(t, t_{\mathrm{i}})$ are equal to one. Analytically this has been proved to hold asymptotically, and it is also obtained from the present numerical calculation for large times t. A measure of the accuracy of a numerical computation is the difference between the singular values and unity at the final time t_{f}.

In figure 5.4 the same quantities are presented for the calculation with phase-distorted basis functions. There are two striking differences between calculations with undistorted and phase-distorted basis functions. First, it is seen that the overlap of phase-distorted basis functions is smaller. Secondly, as t tends to $\pm\infty$, the interaction matrix elements decrease much faster to zero in figure 5.4 compared to figure 5.3. Again, this reflects the short-range character of the scattering theory with Coulomb-corrected, or phase-distorted, basis functions.

5.5 Free-particle basis functions

In order to describe ionisation and pair creation with the coupled channel method, the coupled channel basis needs to be extended by basis functions representing free particles. This section describes the basis functions chosen for the present numerical approach. Alternative basis functions, which have been used in other numerical coupled channel treatments of the two-centre Dirac equation, are discussed briefly, in order to motivate of the present choice.

5.5.1 Free Dirac wave packets. Free particle solutions of the two-centre Dirac equation, at least for short range forces, asymptotically approach solutions of the free Dirac equation. The time-dependent free wave packet (cf. appendix B),

$$\Phi(t, \boldsymbol{x}) = (2\pi)^{-\frac{3}{2}} \int e^{i\boldsymbol{x}\cdot\boldsymbol{p}} \left\{ e^{it\mu(\boldsymbol{p})}\, \hat{\phi}_+(\boldsymbol{p}) + e^{-it\mu(\boldsymbol{p})}\, \hat{\phi}_-(\boldsymbol{p}) \right\} \mathrm{d}^3p,$$

solves the time-dependent free Dirac equation. Here $\mu(\boldsymbol{p}) = \sqrt{1 + \boldsymbol{p}^2}$ is the free energy corresponding to the three-momentum $\boldsymbol{p}$. Therefore, in a coupled channel calculation, the free-particle scattering channel C might be represented by a finite set of free
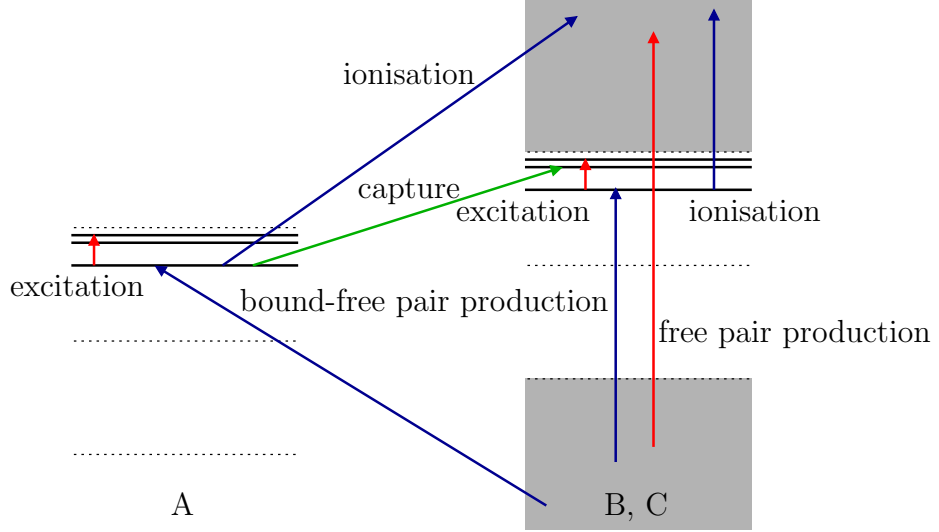
FIGURE 5.5.   Asymmetrical description of the free-particle scattering channel C in a coupled channel calculation, by using wave packets of continuum eigenfunctions of centre B.

Dirac wave packets. In principle, this has been done in [THGS95, GMS⁺97], where the time-dependent free Dirac wave packets have been approximated by stationary wave packets, in a centre of charge frame. In these calculations the bound-state scattering channels have been omitted, such that only transition amplitudes between asymptotically free particles, in particular the free pair production amplitudes, have been obtained.

5.5.2 Weyl eigendifferentials. The basis functions of the coupled channel expansion (4.1) do not necessarily have to be solutions of the scattering-channel Dirac equations. In order to determine transition amplitudes it is sufficient, that the basis functions are asymptotically approaching asymptotic conditions, i.e. solutions of the scattering-channel wave equations. Such basis functions are, e.g., time-dependent wave packets constructed by means of continuum eigenfunctions of the electrostatic potential of one of the two centres. Consider for example continuum eigenfunctions $\phi_{B,\epsilon}(\boldsymbol{x}'')$ of the potential $V_B(|\boldsymbol{x}''|)$ in the doubly primed rest frame of centre B,

$$[-i\boldsymbol{\alpha}\cdot\nabla'' - eV_B(|\boldsymbol{x}''|)]\,\phi_{B,\epsilon}(\boldsymbol{x}'') = \epsilon\,\phi_{B,\epsilon}(\boldsymbol{x}''). \tag{5.18}$$

Here, the energy eigenvalue ϵ is in the continuous spectrum $|\epsilon| > 1$. These continuum eigenvalues are infinitely degenerate, which is, however, not important for the moment. Time-dependent, or Weyl, wave packets of these eigenfunctions, which are Lorentz transformed into the unprimed frame, exactly solve the Dirac equation of scattering channel B:

$$\left[H_0 + W_B(t, \boldsymbol{x}) - i\partial_t\right] S(-\chi_B)\left\{\frac{1}{\sqrt{\Delta_\epsilon}}\int_{\bar{\epsilon}-\Delta_\epsilon/2}^{\bar{\epsilon}+\Delta_\epsilon/2}\exp(-it''\epsilon)\,\phi_{B,\epsilon}(\boldsymbol{x}'')\,d\epsilon\right\} = 0$$

These wave packets asymptotically approach free wave packets as t goes to $\pm\infty$, provided that V_B is short-ranged, which is a standard result from quantum mechanical two-particle scattering theory [RS79, Tha92]. Therefore, they represent asymptotically free particles. Such Weyl wave packets are clearly orthogonal to the bound
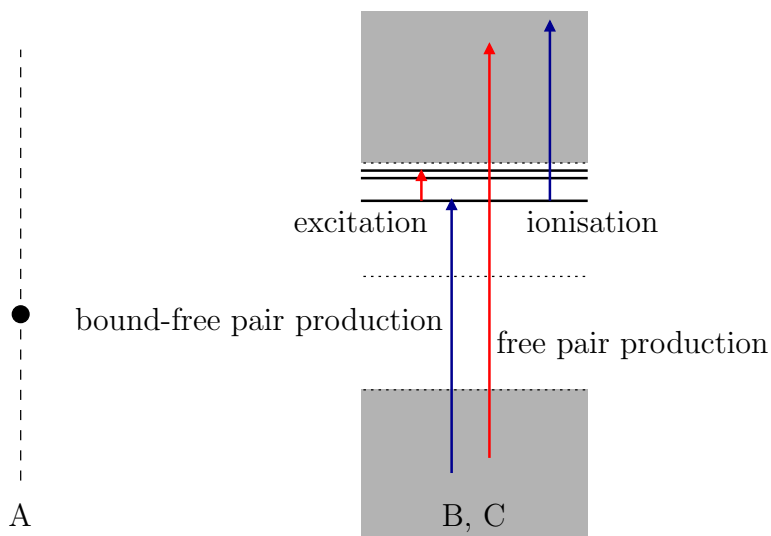
FIGURE 5.6.   Asymmetrical description of the free-particle scattering channel C
in a coupled channel calculation, as in figure 5.5, but here the charge transfer
channel is omitted as well. Hence, centre A only acts as a perturbation.

states of centre B. The Weyl wave packets are also asymptotically orthogonal to the
bound states of centre A, since they are spreading asymptotically in the same way
as the wave packets of the free Dirac equation (see section 3.4). In principle, Weyl
wave packets of one of the two centres may, therefore, be used as basis functions, rep-
resenting the free-particle scattering channel in a coupled channel calculation. This
approach is schematically depicted in figure 5.5.

The main argument, against the use of Weyl wave packets in numerical calcula-
tions, is the additional energy integration, necessary for a numerical determination
of overlap and interaction matrix elements. This presents a considerable numerical
complexity in practical calculations, well-known already from less demanding nonrela-
tivistic coupled channel calculations [BM92]. Nevertheless, relativistic *single*-centre
coupled channel calculations in the target frame have been done and presented in
[MGS91]. There, a coupled channel basis comprising bound states of one particular
centre (the target) and Weyl wave packets packets of the same centre have been used
(cf. figure 5.6).

Clearly, the choice of centre B for the construction of the wave packets is asym-
metrical. Weyl wave packets of centre A are equally suitable for the representation of
the free-particle channel, at least in a symmetrical collision system. Hence, a coupled
channel basis comprising a (necessarily) finite number of Weyl wave packets, of both
centre A and centre B, at first glance, seems to be a more appropriate choice. But it
is not clear, how to construct these wave packets such that they are asymptotically
orthogonal and, moreover, the approach towards the asymptotic orthogonality is fast
enough for numerical calculations. Numerical calculations using a two-centre basis
comprising free-particle states of this kind have not been attempted yet.

5.5.3 Stationary wave packets. Weyl wave packets are obtained from continuum
eigenstates of the respective electrostatic potentials of the centres A and B. Their
principal advantage over free Dirac wave packets, described in the first subsection, is

that they should be more suitable for the description of a solution of the two-centre Dirac equation. This holds in particular for strong external forces, i.e. large charge numbers, or equivalently for free electrons and positrons of low kinetic energy.

As an approximation to time-dependent wave packets, stationary wave packets have been used in the literature and also for the present work. Again, as an example, consider centre B and its continuum eigenfunctions $\phi_{\mathrm{B},\epsilon}(\boldsymbol{x}'')$ in the doubly primed rest frame as in equation (5.18). In the doubly primed frame a stationary wave packet is defined as:

$$\Phi''_{\mathrm{B},\bar{\epsilon}}(t'',\boldsymbol{x}'') = \frac{1}{\sqrt{\Delta_\epsilon}} \exp(-\mathrm{i}t''\bar{\epsilon}) \int_{\bar{\epsilon}-\Delta_\epsilon/2}^{\bar{\epsilon}+\Delta_\epsilon/2} \phi_{\mathrm{B},\epsilon}(\boldsymbol{x}'') \, \mathrm{d}\epsilon.$$

It solves the time-dependent Dirac equation in the doubly primed frame approximately:

$$\left[H''_0 - eV_{\mathrm{B}}(|\boldsymbol{x}''|) - \mathrm{i}\partial_{t''} \right] \Phi''_{\mathrm{B},\bar{\epsilon}}(t'',\boldsymbol{x}'') \approx 0.$$

By construction a stationary wave packet is localised around the spatial origin of the doubly primed coordinates for all times. Although stationary wave packets do not spread, they are usually considered as a helpful substitutes for Weyl wave packets. The use of stationary wave packets is sometimes referred to as the 'discretisation of the continuum'.

For a spherically symmetric external field the continuum eigenvalues ϵ are infinitely degenerate, since an eigenfunction $\phi_{\mathrm{B},\epsilon}(\boldsymbol{x}'')$ may be a simultaneous eigenfunction of the spin-orbit operator K'', with any of the eigenvalues $\kappa = \pm 1, \pm 2, \pm 3, \ldots$. Stationary wave packets are usually constructed from eigenfunctions with definite values of the angular momentum quantum numbers κ and m. Such wave packets, denoted by $\Phi''_{\mathrm{B};\bar{\epsilon},\Delta_\epsilon,\kappa,m}(t'',\boldsymbol{x}'')$ are orthogonal in the doubly primed reference frame, if their energy intervals are non-overlapping or if they have different angular momenta.

The advantage of stationary wave packets over Weyl wave packets is, that the energy integration needs to be carried out only once, yielding radial wave functions, which can be tabulated for later reference. The energy integration does not need be included in every single evaluation of an overlap or an interaction matrix element. Consequently numerical computations become less demanding.

Another advantage is that the stationary wave packets of *different* centres are asymptotically orthogonal, due to their localisation at different centres. This makes a *two-centre* description of the free-particle scattering channel feasible. As a consequence of the splitting of the free-particle basis functions into two subsets, attributed to centre A and centre B respectively, ionisation and pair creation processes both can be subdivided into 'excitation'- and 'transfer'-type processes. This is depicted in figure 5.7.

Single-centre relativistic coupled channel calculations, using stationary wave packets, have been reported in [RMS+91, RSG93, BRBW93, BRBW94]. These single-centre approaches can only describe excitation-like processes, as depicted in figure 5.6, and, therefore, they even exclude the description of the charge transfer process. A relativistic two-centre coupled channel calculation, including wave packets of *both* centres, has been implemented for the first time in this work.
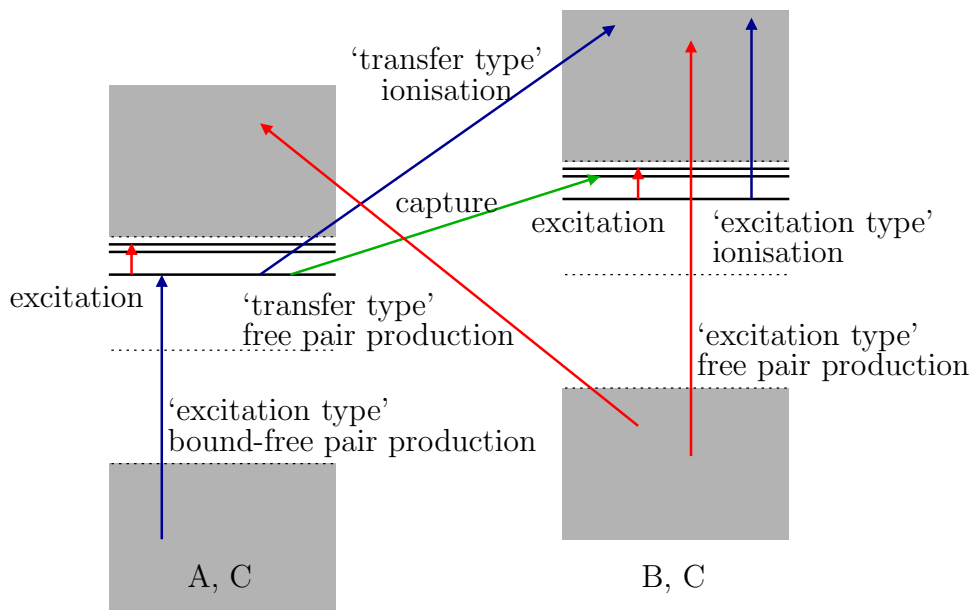
FIGURE 5.7. The two-centre approximation of the free-particle scattering channel C. Ionisation and pair creation processes may be of 'excitation'- or 'transfer'-type. A similar schematic picture has previously appeared in [EIC95].

5.5.4 Details of the present approach. Similar to bound-state basis functions, stationary wave packets for the coupled channel basis are constructed as eigenfunctions of the spin-orbit operators and the third components of the total angular momentum in the primed and doubly primed frames respectively. These wave functions have to be Lorentz-boosted into the unprimed reference frame. The parameters of such wave packets, namely the mean energy $\bar{\epsilon}$, the width of the energy interval Δ_ϵ, the spin-orbit quantum number κ and the third component of the total angular momentum m, are again abbreviated by single indices i or j. Using this notation, the additional undistorted basis functions, which have been employed in numerical calculations of the present work, have the following form in the unprimed reference frame:

$$
\begin{aligned}
\Phi_{A,i}(t,\boldsymbol{x}) &= S(-\chi_A)\frac{\exp(-\mathrm{i}t'\bar{\epsilon}_i)}{\sqrt{\Delta_{\epsilon i}}}\int_{\bar{\epsilon}_i-\Delta_{\epsilon i}/2}^{\bar{\epsilon}_i+\Delta_{\epsilon i}/2}\phi_{A,\epsilon,\kappa_i,m_i}(\boldsymbol{x}')\,\mathrm{d}\epsilon, \\
\Phi_{B,j}(t,\boldsymbol{x}) &= S(-\chi_B)\frac{\exp(-\mathrm{i}t''\bar{\epsilon}_j)}{\sqrt{\Delta_{\epsilon j}}}\int_{\bar{\epsilon}_j-\Delta_{\epsilon j}/2}^{\bar{\epsilon}_j+\Delta_{\epsilon j}/2}\phi_{B,\epsilon,\kappa_j,m_j}(\boldsymbol{x}'')\,\mathrm{d}\epsilon.
\end{aligned}
\tag{5.19}
$$

The precise forms of the normalised continuum eigenfunctions $\phi_{A,\epsilon,\kappa,m}(\boldsymbol{x}')$ and $\phi_{B,\epsilon,\kappa,m}(\boldsymbol{x}'')$ are given in appendix A. In (5.19) the energy integrals obviously take the roles of the time-independent bound state eigenfunctions, appearing in the corresponding equations (5.7).

However, the basis functions (5.19) solve the Dirac equations of the scattering channels A and B respectively only approximately,

$$
\begin{aligned}
\left[H_0 + W_A(t,\boldsymbol{x}) - \mathrm{i}\partial_t\right]\Phi_{A,i}(t,\boldsymbol{x}) &\approx 0, \\
\left[H_0 + W_B(t,\boldsymbol{x}) - \mathrm{i}\partial_t\right]\Phi_{B,j}(t,\boldsymbol{x}) &\approx 0,
\end{aligned}
$$

as pointed out earlier. For the determination of the elements of the interaction matrix this fact is neglected, and the matrix elements are calculated according to equations (5.11), even if the basis function on the right hand side of the scalar product corresponds to a wave packet. This procedure is customary also for single-centre coupled channel calculations.

Unfortunately, a further drawback exists for coupled channel calculations in which the centre, a stationary wave packet is attributed to, is moving. Due to the approximation of the time-evolution of stationary wave packets in their rest frame, Lorentz-transformed wave packets of the same centre are no longer orthonormal in the unprimed frame, even if they are mutually orthogonal and normalised in their rest frame. The reason is that the Lorentz-boost invariance of the scalar product requires, that both wave functions *exactly* solve the same Dirac equation (see section B.2). Note, that such a difficulty does not exist for Weyl wave packets, because they are proper solutions of the wave equations of the respective scattering channel.

This problem has not appeared in the single-centre calculations with stationary wave packets [RMS⁺91, RSG93, BRBW93, BRBW94]. There, the frame of reference of the coupled channel calculation has *always* been identical to the rest frame of the centre the coupled channel basis referred to. Obviously, in a two-centre approach, at least one of the centres is moving. In practical calculations of this work the overlap matrix elements involving wave packets are evaluated numerically, using the expressions (5.10).

Also phase-distorted wave packets have been used, which are defined in the same way as the phase-distorted basis functions that represent bound states. The matrix elements with phase-distorted wave packets are also evaluated according to the equations (5.15) and (5.16). Numerical results obtained from calculations with coupled channel bases, comprising both bound-state and free-particle functions, are presented in sections 6.6 and 6.7 of the next chapter.

Numerical Results and Discussion

In this chapter, the new numerical results of this thesis are presented. In section 6.1 we start with numerical investigations of the relativistic electron capture process by calculations performed in various frames of reference. The influence of the number of bound-state basis functions on the total capture cross section is studied. In sections 6.2 and 6.3 parametric dependencies of electron capture on the collision energy and the charge numbers of the colliding nuclei are investigated. In sections 6.4 and 6.5 the effect of different reference frames and of Coulomb boundary conditions is elucidated systematically by numerical examples. In section 6.6 we turn to the process of bound-free pair creation in heavy-ion collisions and investigate two-centre effects. The last section 6.7 briefly describes the influence of free-particle basis functions on electron capture cross sections.

Many of the results exclusively consider electron capture. The reason is that the corresponding numerical calculations are computationally much less demanding, compared to calculations employing free-particle basis functions. Furthermore, the results presented here concerning electron capture have not been reported previously in the literature. Many computations required considerable computing time and have been performed on clusters of workstations and personal computers, and on massively parallel processor systems.

6.1 Charge transfer

In this section, charge transfer calculations are presented, which have been done with a set of basis functions only comprising bound-state wave functions. The emphasis is on the total charge-transfer cross section $\sigma_{\text{capture}}(1s_{1/2})$ for an initial electronic configuration $1s_{1/2}$. This cross section is obtained by a weighted integral over the impact-parameter-dependent transfer probability $P(b)$, where b denotes the impact parameter [EM95]:

$$\sigma_{\text{capture}}(1s_{1/2}) = 2\pi \int_0^\infty P(b) b \, \mathrm{d}b.$$

Here $P(b)$ is the sum over the approximate transition probabilities for all transitions from an initial $1s_{1/2}$-configuration of the target nucleus, to an *arbitrary* final configuration that corresponds to a bound state of the projectile nucleus. Note that the role of the target nucleus may be taken by either nucleus A or nucleus B, depending on which nucleus the initial configuration is associated with. Therefore, $P(b)$ is the sum over the probabilities of transitions to the bound states of either nucleus B or nucleus A.

Coupled channel calculations, presented in this section, have been done for three different basis sets, which respectively comprise the two, ten and 28 lowest bound states of each centre. The charge numbers of both centres are throughout $Z_A, Z_B =$
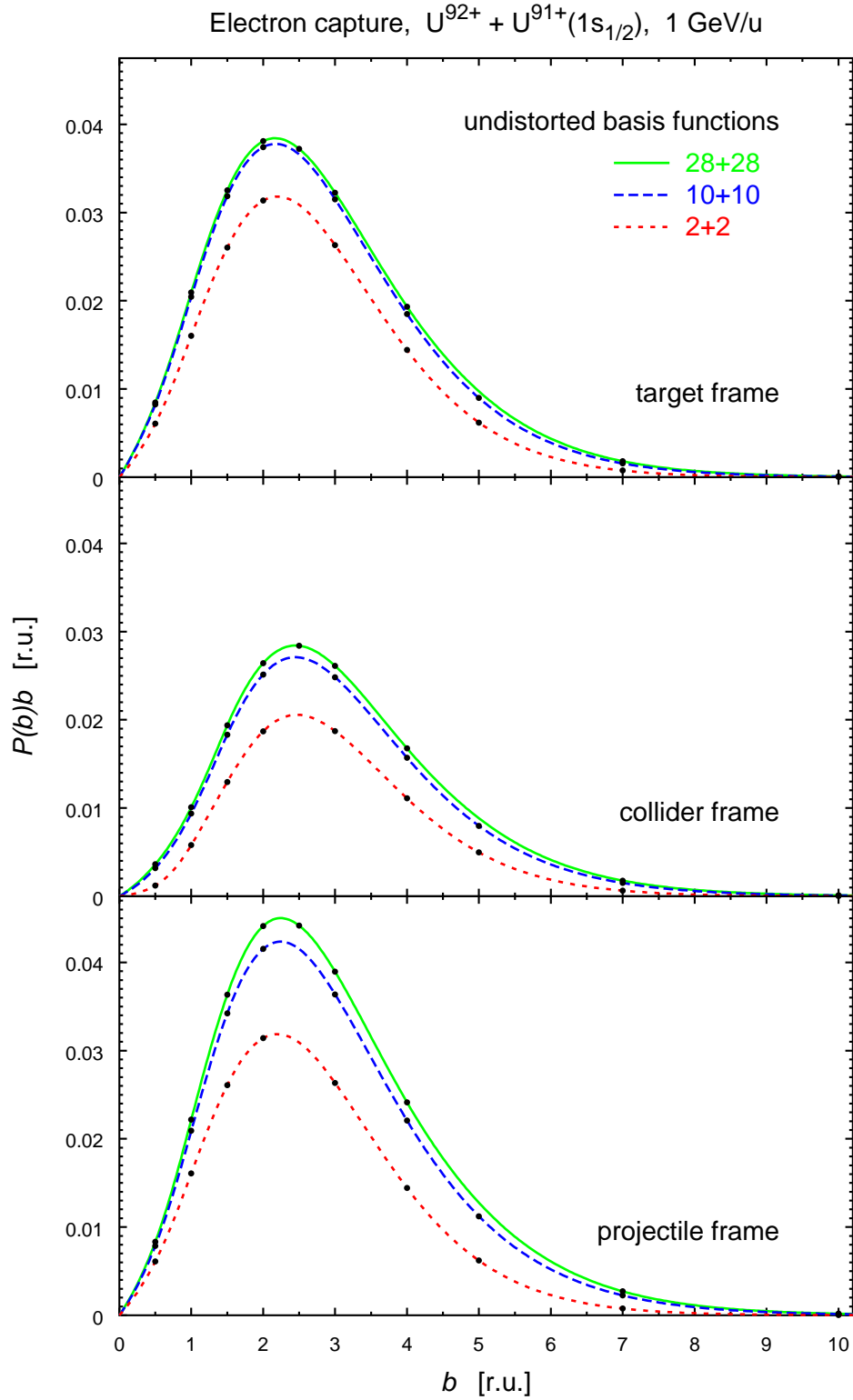
FIGURE 6.1.   Weighted total capture probabilities $P(b)b$ from coupled channel calculations with *undistorted* basis functions. The initial configuration is $1s_{1/2}$ and the basis' comprise either the two, ten or 28 lowest bound states of each nucleus.
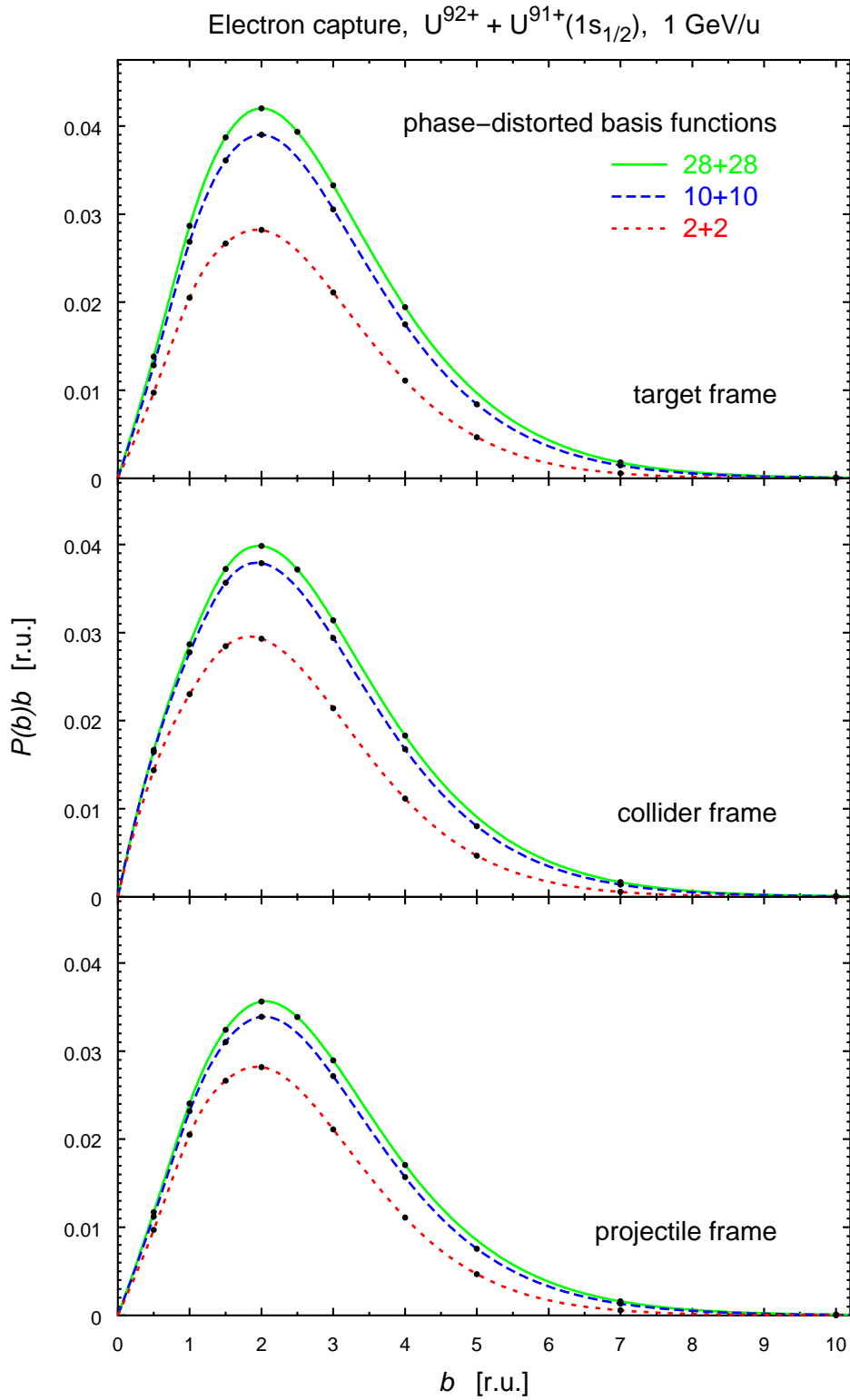
FIGURE 6.2. Weighted total capture probabilities $P(b)b$ as in figure 6.1, but obtained from coupled channel calculations with *phase-distorted* basis functions (see equation (5.12)).

TABLE 6.1. Total capture cross sections $\sigma_{\text{capture}}(1s_{1/2})$ in kbarn for the collision system $U^{91+}(1s_{1/2}) + U^{92+}$ at a collision energy of $T = 1\,\text{GeV/u}$. The first row and column of the table describe the coupled channel basis. The second row gives the frame of reference in which the coupled channel equations have been solved.

no. states	undistorted basis			phase-distorted basis		
	target	collider	projectile	target	collider	projectile
$2 + 2$	0.922	0.582	0.923	0.837	0.892	0.836
$10 + 10$	1.164	0.838	1.330	1.219	1.208	1.072
$28 + 28$	1.206	0.898	1.441	1.333	1.288	1.146

92, corresponding to uranium nuclei, and the collision energy is $T = 1\,\text{GeV/u}$, or equivalently $\gamma = 2.0735$. Calculations have been carried out, on one hand in the rest frame of nucleus A, and on the other hand in the collider frame, where both centres move with equal, but opposite, velocities. The calculations in the rest frame of nucleus A provide capture probabilities both for the target frame and the projectile frame, since the fundamental solution of the coupled channel equations has always been determined (cf. chapters 4 and 5). Hence, capture cross sections are obtained by a numerical solution of the coupled channel equations in the target, collider and projectile frames. These frames are illustrated in figure 1.2 on page 9.

Figure 6.1 shows the weighted capture probabilities $P(b)b$ for the calculations with undistorted basis functions. Analogous calculations, with a phase-distorted basis, are presented in the subsequent figure 6.2. The total capture cross sections are listed in table 6.1.

Discussion. Charge transfer cross sections, calculated in different Lorentz frames by means of relativistic coupled channel calculations, are presented here for the first time. The differences between charge transfer probabilities, which are obtained in different frames of reference, clearly show the violation of the Lorentz boost invariance, as a consequence of the coupled channel approximation. The cross sections computed in the *target* frame are in good agreement with similar existing data [TE90, table I][EM95, p. 241].

The simple 4-state calculations yield cross sections, which are remarkably close to the values obtained with more basis functions. This demonstrates the importance of the $1s_{1/2}$-states of the projectile for the charge transfer process [EM95]. Moreover, the differences between the cross sections, obtained with 10+10 and 28+28 basis functions, are generally smaller than the differences between the cross sections computed in different reference frames, using the same number of basis functions. Therefore, it must be expected that a further increase of the number of *bound* states, used in the coupled channel expansion, will not modify the numerical results significantly. By contrast, the difference between the results obtained in relatively moving reference frames is expected to remain, if only the number of *bound* states is increased.

The increase of the total cross section with the number of basis functions has a simple explanation: the total capture probability $P(b)$, which is plotted here, comprises the transition probabilities to an increased number of final configurations. The

small difference between the total capture cross sections obtained from calculations with 10+10 and 28+28 bound states reflects the fact that the higher bound states of the projectile are less important for the capture process. In fact, the individual transition probabilities from an initial 1s-configuration to some particular final configuration are slightly changing as well, if different sets of basis functions are used. But this represents a minor effect.

There are two conclusions from the above observations. First, a coupled channel expansion using only bound states is not a sufficient approximation to the exact solution of the two-centre Dirac equation. This fact is only revealed by the frame dependence of the results. An assessment, e.g., of the top plot of figure 6.1 alone might suggest that the coupled channel calculation has converged, in the sense that an increased number of basis functions will not modify the results. The extension of the coupled channel basis by free-particle wave functions seems to be necessary, in order to construct a better approximation to the exact solution of the two-centre Dirac equation. A more accurate approximation to this solution is then expected to provide Lorentz-frame invariance of the numerical calculations. This reflects the importance of the ionisation process for the collision system and collision energy, which have been considered. This is known from perturbation theories and is also observed in experiments [BGF+97].

Second, for a theoretical study of the capture process, using a pure bound-state basis, it is helpful to determine the cross sections in various frames of reference and thereby to obtain an estimate of the systematic error, due to the frame dependence of the calculations.

Finally, the difference between calculations with undistorted and phase-distorted basis functions should be noted: The difference between the results obtained in different Lorentz frames is smaller for calculations with phase-distorted basis functions. This suggests that the frame dependence of the capture calculations is reduced by using phase-distorted basis functions (for a more detailed discussion see section 6.4 below).

6.2 Collision-energy dependence of capture

In spite of the difficulties, regarding the frame dependence of capture calculations, it is tempting to study, by means of the coupled channel method, the parametric dependencies of the capture cross sections on the collision energy and the charge numbers of the colliding nuclei. Such a nonperturbative investigation has not been done previously. In this section results for the collision-energy dependence are presented.

Capture cross sections have been determined for different collision energies ranging from $0.4\,\mathrm{GeV/u}$ up to $1.3\,\mathrm{GeV/u}$. Two different collision systems, $\mathrm{U}^{91+}(1\mathrm{s}_{1/2}) + \mathrm{U}^{92+}$ and $\mathrm{Au}^{78+}(1\mathrm{s}_{1/2}) + \mathrm{Au}^{79+}$, have been considered in three different reference frames, namely the target, collider and projectile frames (as in the previous section). Coupled channel calculations have been done, which employ the ten lowest bound states of each nucleus. The results for the total capture cross sections obtained from these

TABLE 6.2. Total capture cross sections $\sigma_{\text{capture}}(1s_{1/2})$ in units of kbarn as a function of the collision energy T for the collision system $\text{U}^{91+}(1s_{1/2}) + \text{U}^{92+}$. The cross sections have been obtained by means of coupled channel calculations using the ten lowest bound states of each nucleus.

$Z_{\text{A}}, Z_{\text{B}} = 92$	undistorted basis			phase-distorted basis		
T [GeV/u]	target	collider	projectile	target	collider	projectile
0.4	9.50	8.84	10.1	10.3	10.2	9.89
0.7	2.77	2.28	3.07	3.00	2.98	2.75
1.0	1.16	0.838	1.33	1.22	1.21	1.07
1.4	0.618	0.384	0.711	0.606	0.599	0.516
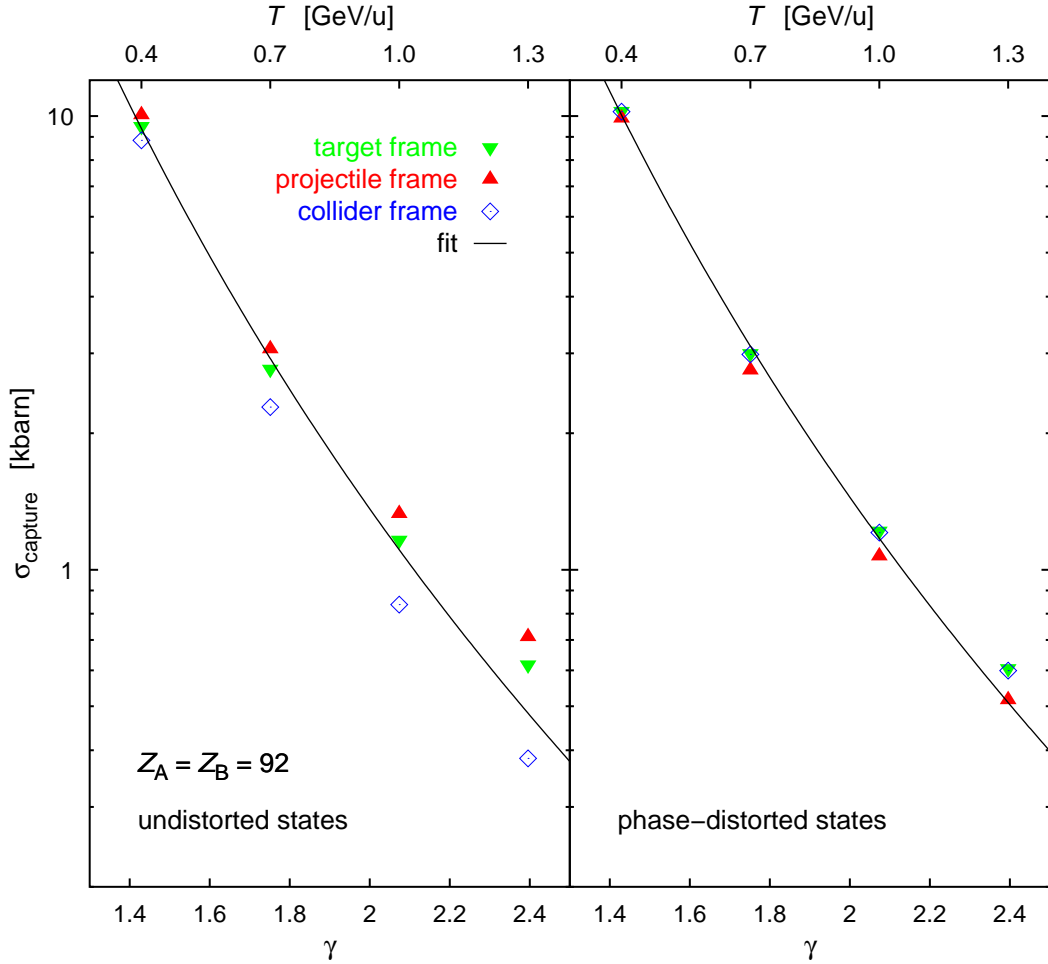
FIGURE 6.3. Collision-energy dependence of electron capture by a bare uranium projectile from hydrogen-like uranium with an initial 1s-configuration. The cross sections plotted here correspond to the numerical values given in table 6.2.

TABLE 6.3. Total capture cross sections in units of kbarn as in table 6.2, but for the collision system $Au^{78+}(1s_{1/2}) + Au^{79+}$.

$Z_A, Z_B = 79$	undistorted basis			phase-distorted basis		
T [GeV/u]	target	collider	projectile	target	collider	projectile
0.4	7.35	6.96	7.73	7.47	7.51	7.11
0.7	1.84	1.55	1.98	1.75	1.76	1.58
0.96	0.812	0.606	0.868	0.703	0.707	0.610
1.4	0.376	0.237	0.393	0.281	0.287	0.237
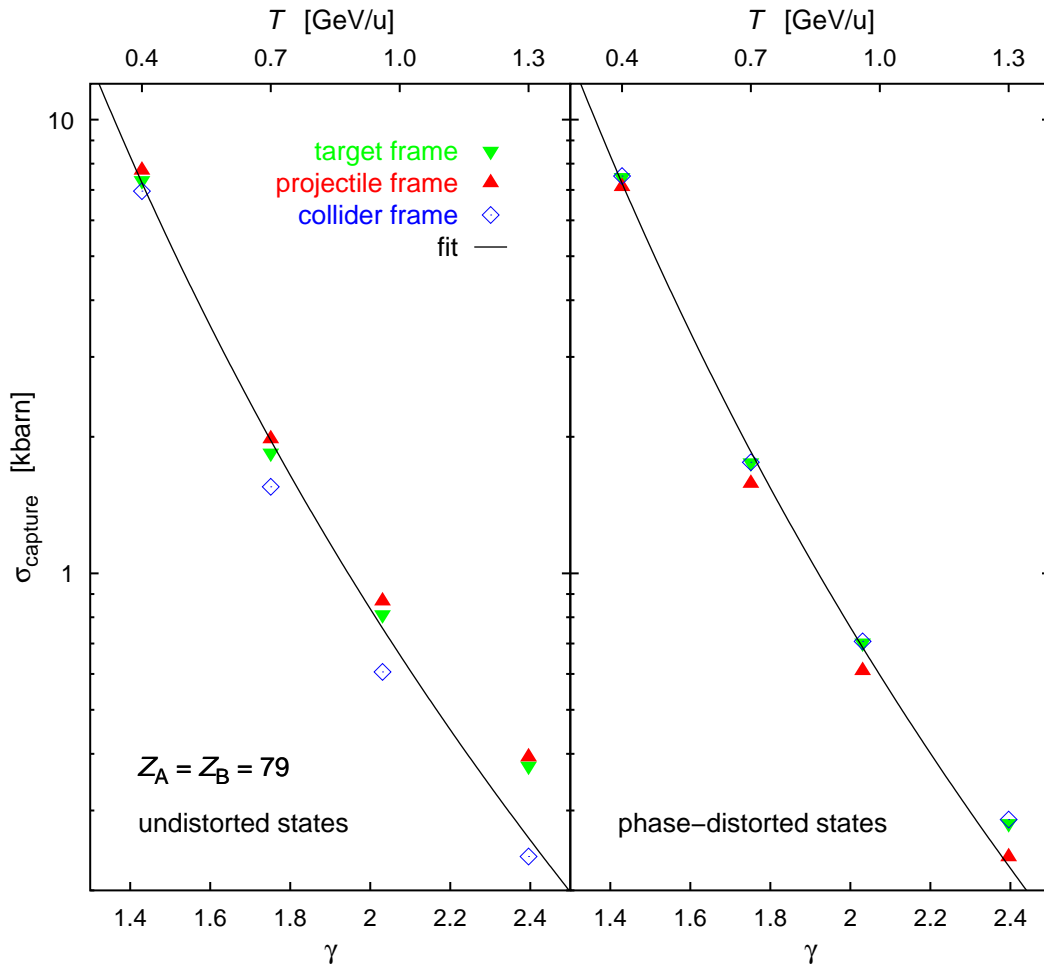
FIGURE 6.4. As figure 6.3, but for hydrogen-like gold colliding with a bare gold projectile. The cross sections plotted here correspond to the numerical values given in table 6.3.
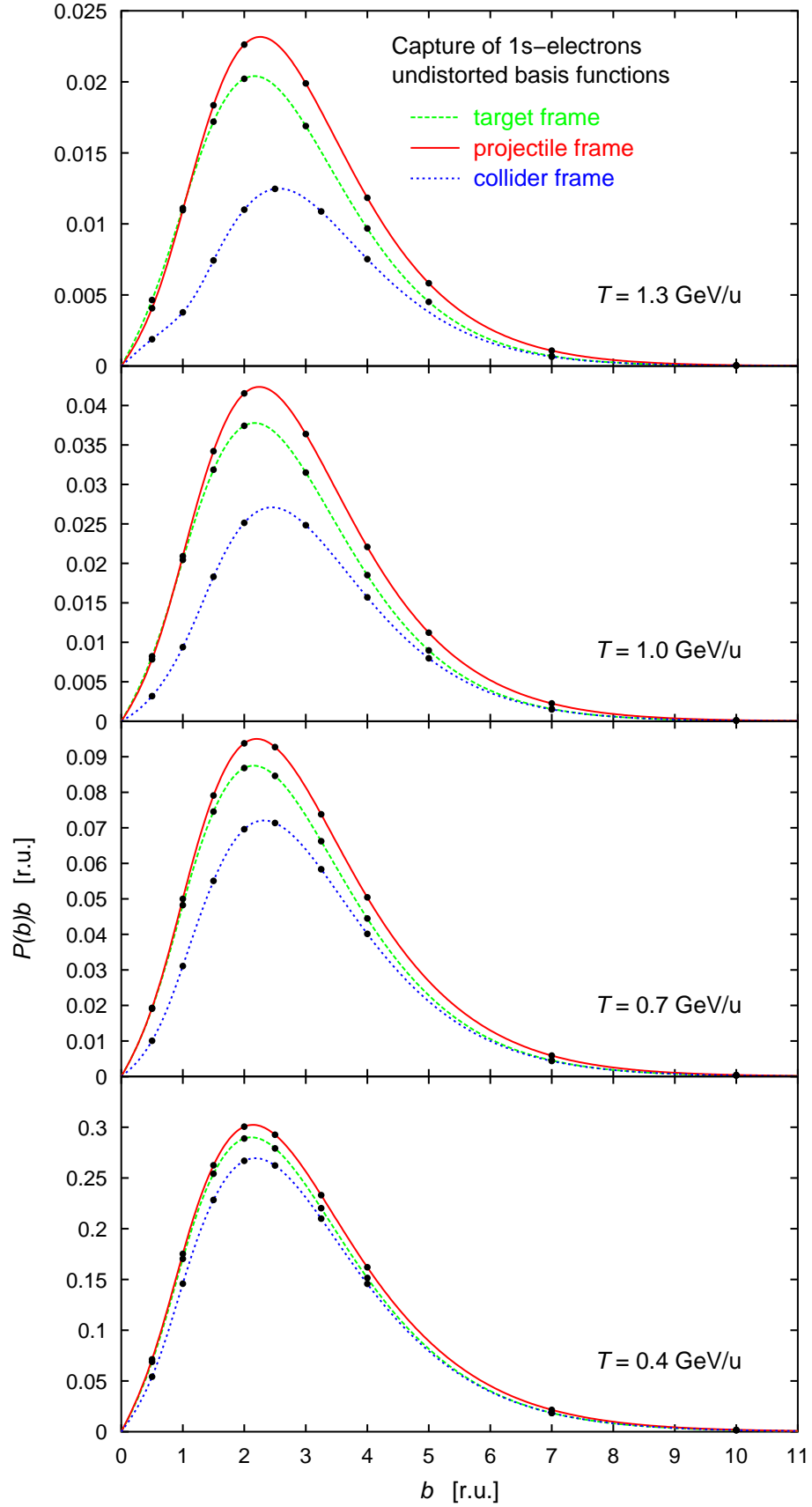
FIGURE 6.5.   Weighted total capture probabilities $P(b)b$ as a function of the impact parameter b for the collision system $U^{91+}(1s_{1/2})+U^{92+}$. The results shown here have been obtained by calculations with an undistorted basis. Regarding the length scale, note that the K-shell radius of uranium is $1.5\,\mathrm{r.u.}$.
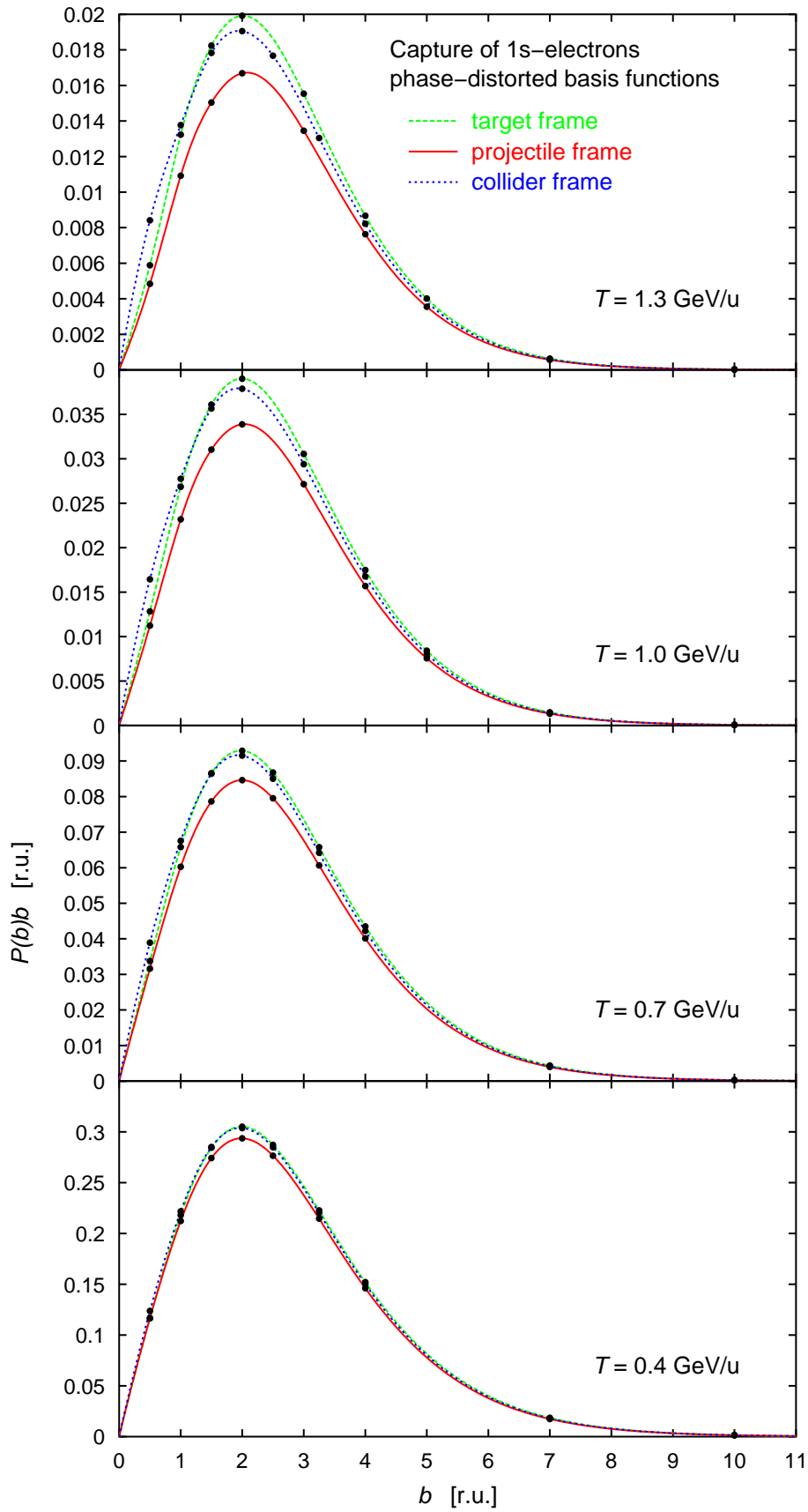
FIGURE 6.6. The same as in figure 6.5, but corresponding to calculations with a phase-distorted basis functions.

calculations are given in the tables 6.2 and 6.3. The same data is presented in the figures 6.3 and 6.4.

In both figures, a fit to the energy dependence of the total capture cross section is shown as well. For the determination of the fit functions, the mean values of the capture cross sections obtained in different reference frames have been fitted to the function,

$$\sigma_{\text{capture}}(1s_{1/2}) = a\gamma^{-b}, \qquad (6.1)$$

by a numerical least-squares algorithm. Here again, γ denotes the Lorentz factor describing the collision energy (cf. section 2.1). The values for the fit parameters a and b are given in table 6.4, for both collision systems and calculations with undistorted as well as phase-distorted basis functions. In this table also alternative fit functions are presented, which are of the form $\sigma_{\text{capture}}(1s_{1/2}) = aT^{-b}$, where T is the kinetic energy of the collision given in GeV/u.

Finally, the figures 6.5 and 6.6 show the weighted total capture probabilities $P(b)b$ as a function of the impact parameter b, but for the symmetrical uranium collision system only.

Discussion. A principal feature, exhibited by the figures 6.3 and 6.4, is the remarkably similar energy dependence obtained from calculations with undistorted and phase-distorted basis functions. Furthermore, the absolute values of the total cross sections are comparable for both methods of calculation. This relationship is very different compared to the corresponding perturbative capture theories. Note that the coupled channel calculations with undistorted basis functions as well as the perturbative Oppenheimer–Brinkmann–Kramers (OBK) approximation [EM95] correspond to a scattering theory not taking into account the long-range character of the Coulomb interaction. On the other hand calculations with phase-distorted basis functions as well as the boundary-corrected Born approximation (B1B) [EM95] are approximations to the exact scattering theory with Coulomb boundary conditions. In the literature, it has been found that generally the simple OBK cross sections are significantly larger than the B1B cross sections and that the latter provide a better description of experimentally measured cross sections of (nonradiative) electron capture [EM95]. Such a difference is not observable for the presumably more accurate coupled channel approaches presented here.

As observed already in the previous section, the difference of the cross sections from calculations in different reference frames is clearly smaller, if a phase-distorted basis is used. As demonstrated in particular by the figures 6.5 and 6.6, the frame dependence of the cross sections increases for growing collision energy. This reflects the fact that a Lorentz boost between the rest frames of both centres mixes time and spatial coordinates more weakly as the collision energy decreases (leading to the Galilean transform in the limit of very small collision energies).

For the range of collision energies chosen here, various perturbation theories are available for a comparison with the present results [EM95]. Almost all of these perturbative approximations predict a dependence of the capture cross section which is proportional to γ^{-1} for large collision energies. More precisely, the relativistic unsymmetrical eikonal theory of electron capture [Eic85, ISE93, EM95], which provides

TABLE 6.4. Fit parameters for the collision-energy dependence of the capture cross sections, given in table 6.2 and 6.3. The arithmetic mean values of cross sections obtained in different reference frame have been fitted to the respective functions given in the first row, using a least-squares fit. Here, γ denotes the Lorentz factor giving the collision energy and T denotes the kinetic energy in GeV/u.

	fit function	$\sigma[\text{kbarn}] = a\gamma^{-b}$		$\sigma[\text{kbarn}] = aT^{-b}$	
$Z_{\mathrm{A}}, Z_{\mathrm{B}}$		a	b	a	b
92 (U)	undist. basis	73	5.7	1.1	2.3
	ph.-dist. basis	79	5.8	1.2	2.4
79 (Au)	undist. basis	72	6.4	0.69	2.6
	ph.-dist. basis	80	6.7	0.60	2.8

satisfactory agreement with many experiments, shows such a decrease of the cross section for collision energies above $10\,\text{GeV/u}$. The collision energy dependence, as predicted by nonrelativistic capture theories for high collision velocities, is T^{-6} in first-order and $T^{-5.5}$ in second order perturbation theory [BM92]. Therefore, the fits to the present relativistic coupled channel results, given in table 6.4, show that the range of collision energies around $1\,\text{GeV/u}$ constitutes an intermediate region, between the high energy regimes of nonrelativistic and relativistic perturbative capture theories. The presently found much faster decrease of the capture cross section, as compared to the relativistic high energy behaviour, is also predicted by the unsymmetrical relativistic eikonal approximation for collision energies below $10\,\text{GeV/u}$ [ISE93]. It must be noted, however, that the eikonal theory is a high-energy approximation.

Experimentally the energy dependence of capture has been measured in particular for La^{57+} bare nuclei impinging on a target foil of Au, at collision energies of 0.405, 0.96 and $1.3\,\text{GeV/u}$ [BGF$^+$97]. It has been found that the capture cross section falls off approximately as γ^{-3}, similarly indicating that the collision energies considered here belong to an intermediate range, between the high-energy regimes of relativistic and nonrelativistic collisions respectively. The quantitative difference of the exponent of decrease is difficult to account for.

6.3 Charge-number dependence of capture

The dependence of the electron-capture cross section on the charge number of the target and projectile nuclei has been investigated here, for the first time, using the coupled channel method. Numerical calculations have been carried out for a collision energy of $0.96\,\text{GeV/u}$ and various symmetrical and unsymmetrical collision systems of heavy nuclei, with charge numbers ranging from $Z_{\mathrm{A}}, Z_{\mathrm{B}} = 66$ up to $Z_{\mathrm{A}}, Z_{\mathrm{B}} = 92$. As in the previous section, a coupled channel basis comprising the ten lowest bound

states of each centre has been used. For the numerical calculations, the rest frame of
nucleus A has been chosen such that cross sections for the target and projectile frames
have been obtained. Table 6.5 lists the results for the total cross sections for capture
from an initial $1s_{1/2}$-configuration to one of the bound states of the projectile nucleus.
The data of this table is plotted in figure 6.7. The corresponding weighted impact-
parameter-dependent total capture probabilities $P(b)b$ are shown in the figures 6.8,
6.9 and 6.10 for nine different collision systems.

Discussion. In spite of the manifest differences between the cross sections corre-
sponding to different bases and reference frames, figure 6.5 demonstrates a general
tendency of the charge-number dependence of electron capture in heavy ion collisions
at $0.96\,\mathrm{GeV/u}$ collision energy. For the range of charge numbers consider here, it is
observed that the electron-capture cross section grows more strongly with the pro-
jectile charge-number, compared to the target charge-number. The increase is not
even linear for the target charge-number dependence, and it is slightly stronger than
linear for the projectile charge-number dependence.

This result should be compared to the Z_T-Z_P-dependence of other relativistic
capture theories that are based on perturbation theory. Roughly, most capture theo-
ries predict, for large collision energies, a charge-number dependence of nonradiative
electron-capture according to, $\sigma_\mathrm{capture} \propto Z_\mathrm{T}^5 Z_\mathrm{P}^5$ [EM95]. For a collision energy of
$10\,\mathrm{GeV/u}$ this behaviour is confirmed by numerical evaluations of cross sections based
on the unsymmetrical eikonal approximation [ISE93]. Clearly the present results
show a much weaker increase of the cross section with growing target and projectile
charge-numbers. In experiments, however, capture from higher atomic shells, which

TABLE 6.5. Total capture cross sections $\sigma_\mathrm{capture}(1s_{1/2})$ as a function of the
projectile and target charge numbers, Z_T and Z_P, for a collision energy of
$0.96\,\mathrm{GeV/u}$. The cross sections are given in kbarn. The columns are subdivided
to distinguish between results obtained in the target (tar.) and projectile (proj.)
frames respectively. Similarly the rows are subdivided in order to present the
data obtained from calculations with undistorted and phase-distorted basis func-
tions. The cross sections have been obtained from coupled channel calculations
with the ten lowest bound states of each nucleus and are plotted in figure 6.7.

| Z_T	Z_P	92 (U)		86 (Rn)		79 (Au)		66 (Dy)	
		tar.	proj.	tar.	proj.	tar.	proj.	tar.	proj.
92 (U)	undist.	1.295	1.465	1.115	1.230	0.908	0.961	0.555	0.533
	ph.-dist.	1.355	1.198	1.128	0.995	0.873	0.767	0.475	0.412
86 (Rn)	undist.	1.235	1.402	1.080	1.187	0.890	0.939	0.553	0.535
	ph.-dist.	1.231	1.080	1.035	0.906	0.811	0.708	0.452	0.390
79 (Au)	undist.	1.102	1.266	0.975	1.083	0.812	0.868	0.513	0.507
	ph.-dist.	1.043	0.908	0.885	0.770	0.703	0.610	0.401	0.344
66 (Dy)	undist.	0.792	0.907	0.710	0.788	0.597	0.643	0.387	0.390
	ph.-dist.	0.652	0.563	0.562	0.486	0.455	0.394	0.270	0.232
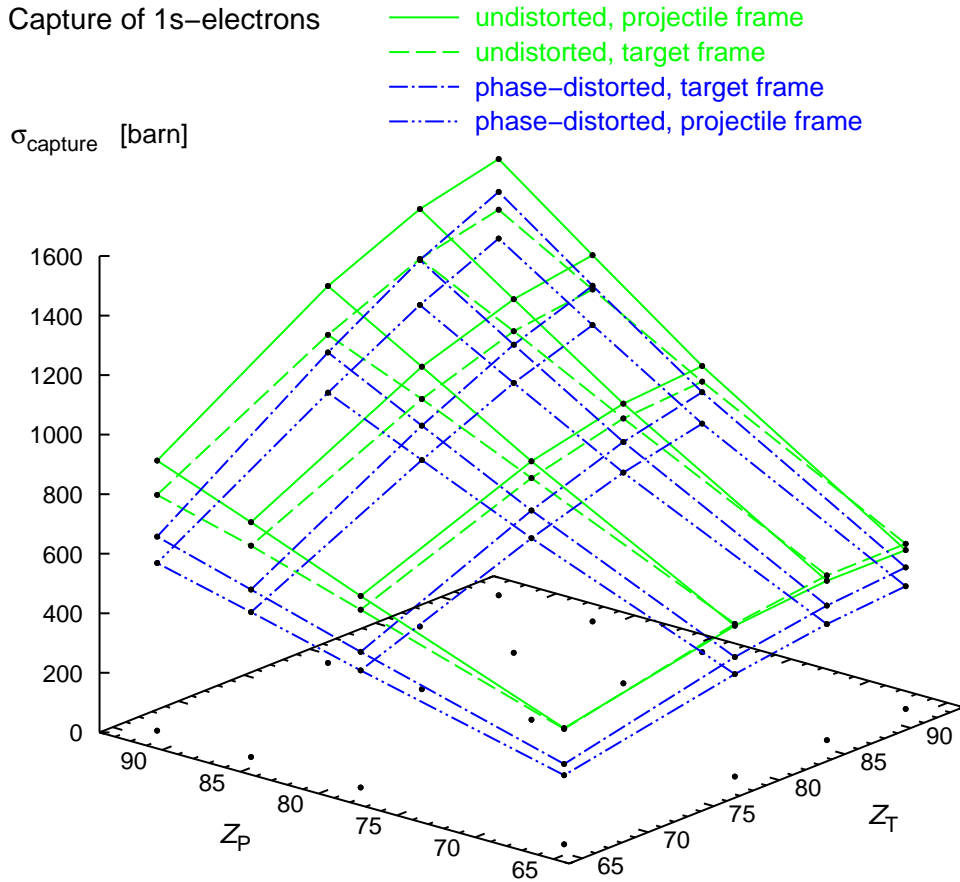
FIGURE 6.7. The dependence of the total cross section of 1s-electron-capture on the charge numbers Z_T and Z_P of the target and projectile nuclei respectively is presented here. The data has been obtained by integrating the interpolating functions of the figures 6.8, 6.9 and 6.10, and additional data for the remaining collision systems involving $Z_T = 86$ or $Z_P = 86$. It is clearly discernible that the capture cross section grows more strongly for growing Z_P compared with the dependence on Z_T.

is not considered here, becomes more important for larger charge numbers. Therefore, the presently found slow increase of the capture cross section, as a function of the charge numbers Z_T and Z_P, presumably underestimates the charge-number dependence of experimentally determined total cross sections of (nonradiative) electron capture slightly.

In [BGF$^+$97] measurements of electron capture by U^{92+}-ions impinging on solid target foils of Cu, Ag and Au have been reported. The collision energy was 0.96 GeV/u and is, therefore, identical to the collision energy of the present numerical calculations. It has been found that the existing perturbation theory of electron capture was able to account for the measured cross sections for the targets Cu and Ag. But for the Au target the total cross section obtained from perturbation theory overestimated the experimental value of 3.4 kbarn by about 20% (see figure 5
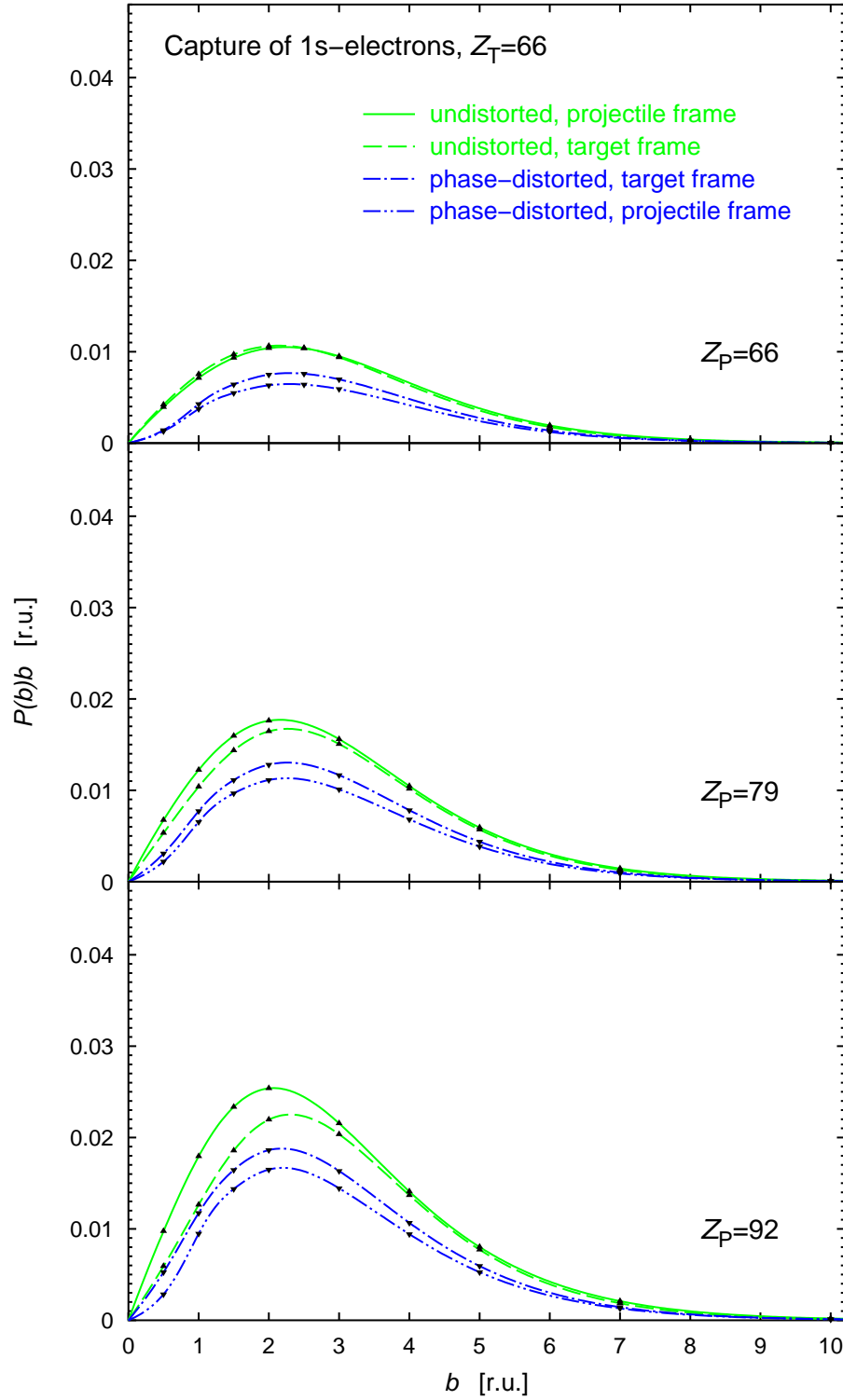
FIGURE 6.8.   The impact parameter dependence of electron capture for a colli-
sion energy of $0.96\,\mathrm{GeV/u}$ is presented here for nine different heavy-ion collision
systems. The data has been computed by relativistic coupled channel calculations
employing the 10 lowest bound states of each nucleus. The initial configuration is
a 1s-state of the target nucleus with charge number Z_T. Four different series' of
calculations, performed in the rest frames of the target and the projectile respec-
tively, using either undistorted or phase-distorted asymptotic states, are shown
(see the text for explanations).
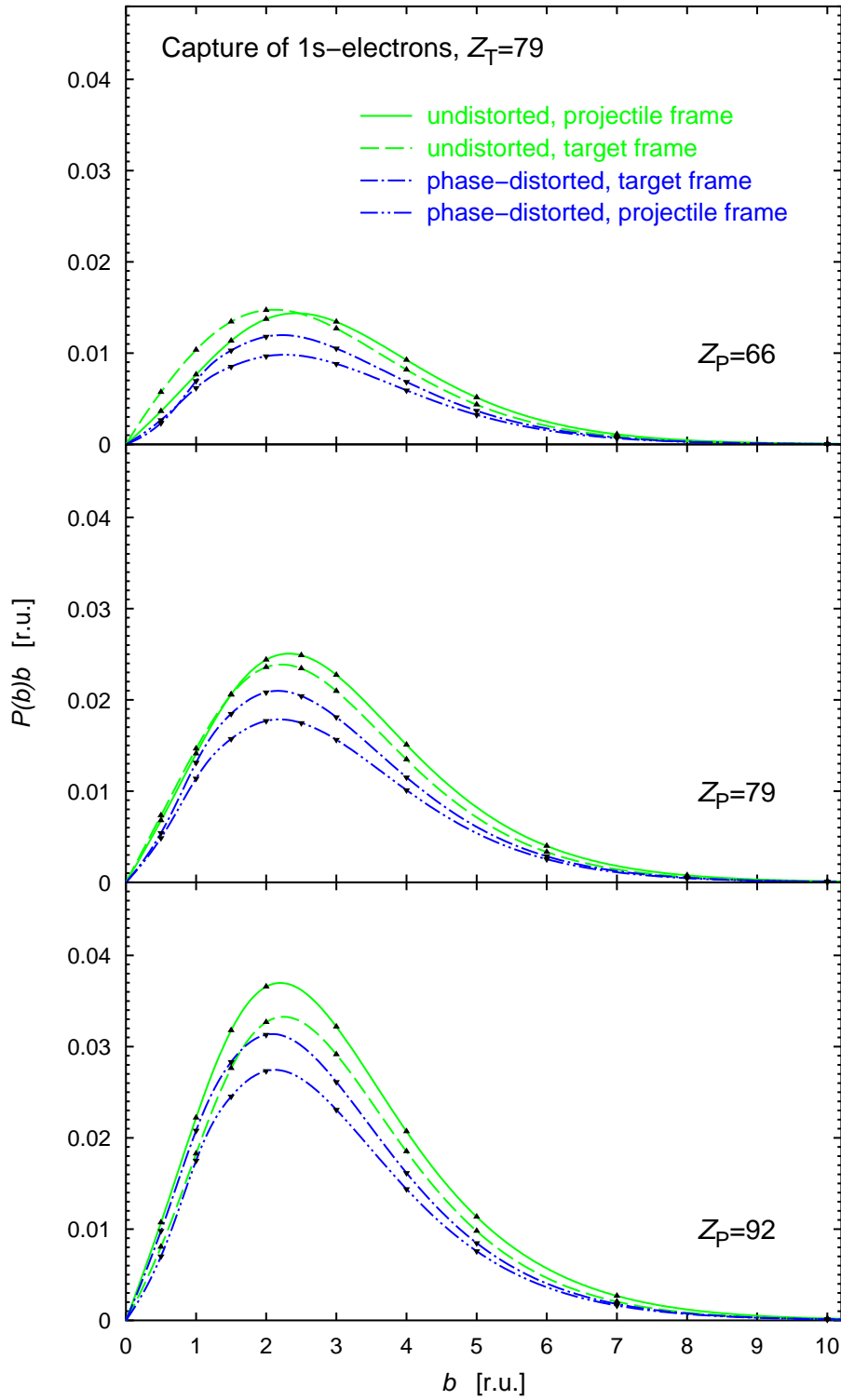
FIGURE 6.9. (See figure 6.8)

in [BGF⁺97]). The present calculations roughly support these experimental find-
ings, namely that the charge-number dependence of the nonradiative capture cross
section is overestimated by the perturbative theories, if collisions of *heavy* ions at
intermediate relativistic energies are considered.
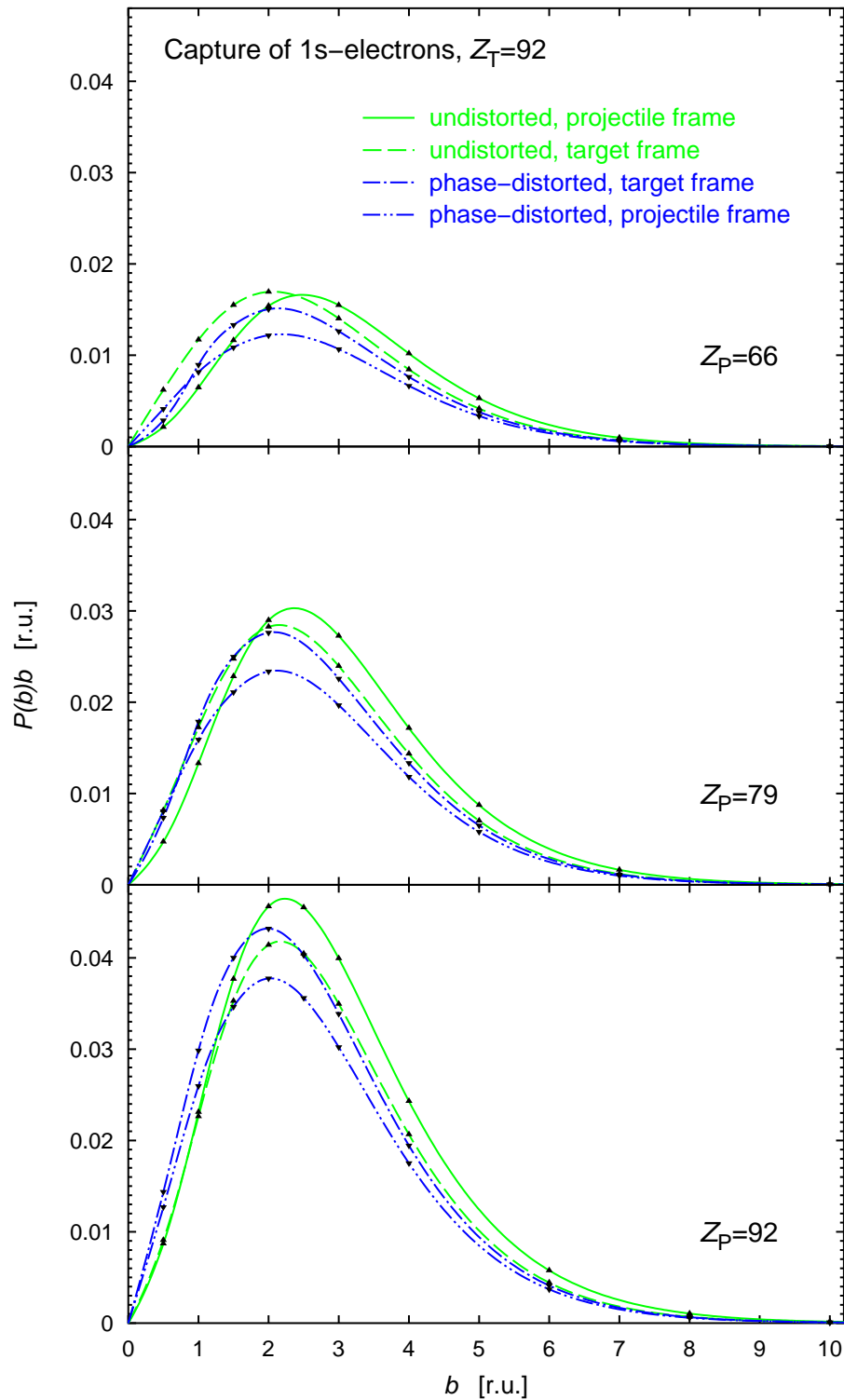
FIGURE 6.10. (See figure 6.8)

A direct comparison of the measured cross section with the present numerical results is not straightforward, since the coupled channel method allows for target excitations, which are not possible in solid targets. Moreover the measured cross section of 3.4 kbarn, for the collision $U^{92+} + Au$, comprises the process of radiative electron

capture, contributing approximately 1.0 kbarn (according to [BGF+97]). Nevertheless, the presently determined value for electron capture from a filled target-K-shell is roughly 2 kbarn (cf. table 6.5) and the remaining difference to the experimental value may convincingly be ascribed to nonradiative capture from higher target-shells.

Regarding the systematic difference between calculations with an undistorted and with a phase-distorted basis in figures 6.7–6.10, note, however, that cross sections obtained from calculations with undistorted basis functions in the *collider* frame are expected to be smaller than those of the target and projectile frames. This fact has been established in the preceding sections.

6.4 Frame dependence

The aim of this section is to elucidate further the influence of the choice of the reference frame on two-centre coupled channel calculations.

6.4.1 Continuum of reference frames. For a sequence of different reference frames, the total capture probability is shown in figure 6.11, for transitions from initial 1s- or 2s-configurations to an arbitrary bound state of the projectile nucleus. Again, the calculations have been done using a basis comprising the ten lowest bound states of each nucleus. The parameter used to characterise the different reference frames, employed for the coupled channel calculations, is the following fraction of the target and projectile rapidities, χ_{T} and χ_{P}, in $\boldsymbol{e}_3$-direction (cf. section 5.1):

$$\xi = \frac{\chi_{\mathrm{T}} + \chi_{\mathrm{P}}}{\chi_{\mathrm{T}} - \chi_{\mathrm{P}}}. \tag{6.2}$$

Clearly, $\xi = 0$ corresponds to the collider frame, and $\xi = -1$ and $\xi = 1$ to the target and projectile frames respectively. If the modulus of ξ is greater than one, then both centres are moving in the same direction with different absolute velocities. The value for the impact parameter $b = 2$ r.u. chosen for the calculations shown in figure 6.11, approximately coincides with the maximum of the $P(b)b$-plots presented in the previous sections. Note as well that the K-shell radius of uranium is approximately 1.5 r.u., representing a typical length scale of the collision system considered in figure 6.11.

Figure 6.11 exhibits the strong frame dependence of capture probabilities obtained from coupled channel calculations using exclusively undistorted bound-state basis functions. The uncertainty of the results for the initial 1s-configuration is nearly of the same order of magnitude as the probability itself. This has not been noted before in the literature. The solid green line, corresponding to calculations with phase-distorted bound-state basis functions, shows a much weaker dependence on the reference frame of the calculation. This fact, anticipated already in section 6.1, suggests that a coupled channel expansion with phase-distorted basis functions yields a better approximation to the exact solution of the two-centre Dirac equation, than an expansion using the same number of undistorted states.

6.4.2 Time axes in relatively moving frames. For three different frames of reference, the green dashed lines in figure 6.12 show the deviation of the overlap matrix $N(t)$ from the unit matrix, as measured by the Frobenius norm $\|N(t) - 1\|_{\mathrm{F}}$
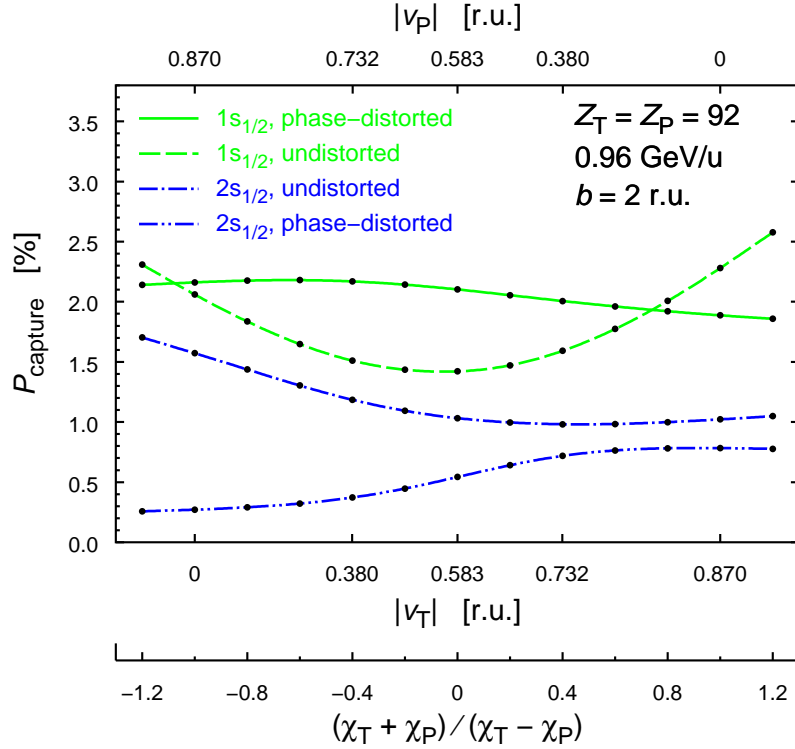
FIGURE 6.11. Total capture probabilities $P(b)$ in thirteen different reference frames and for two different initial configurations are shown. The data was obtained by coupled channel calculations employing the 10 lowest bound states of each centre, either with undistorted or phase-distorted basis functions. The charge numbers are $Z_T = Z_P = 92$, the impact parameter is $b = 2$ r.u. and the kinetic energy 0.96 GeV/u in all calculations. Apart from the axis for the ratio of rapidities $(\chi_T + \chi_P)/(\chi_T - \chi_P)$, which is used to characterise the various reference frames, two further abscissa axes are provided for the velocities of the centres. The values -1, 0 and 1 of the ratio $(\chi_T + \chi_P)/(\chi_T - \chi_P)$ correspond to the target, collider and projectile frames respectively.

(see section 5.4). The time interval of a non-vanishing Frobenius norm represents the time interval during which the basis functions of different centres overlap and, thereby, relates the time axes of different coordinate systems. It is seen that the reference frame with the shortest overlap time (the 'fastest collision') is the collider frame. In other frames the overlap time is longer. A short calculation, taking into account the Lorentz contraction of bound-state basis functions and the relative speed of the centres, yields that the overlap time is 'dilated' with respect to the collider frame approximately by the following factor:

$$\cosh\left(\frac{\chi_A + \chi_B}{2}\right). \tag{6.3}$$

This relationship among the time axes of relatively moving frames is qualitatively exhibited by figure 6.12.
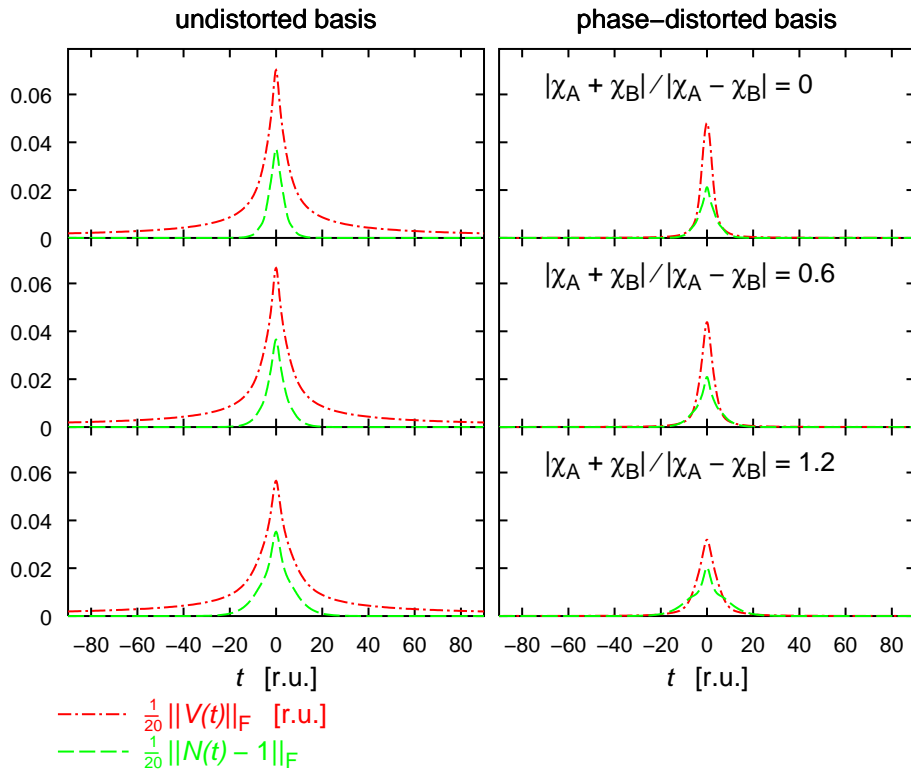
FIGURE 6.12. This figure illustrates the relation of the time axes of different relatively moving reference frames. The parameters for the coupled channel calculations, presented here, are same as in figure 6.11. The width of the green curve, representing the Frobenius norm of the matrix $N(t) - 1$, characterises the time interval in which the basis functions of different centres significantly overlap. It is seen that in calculations with phase-distorted basis functions the interaction matrix $V(t)$ is essentially vanishing outside this time interval. Contrary, the interaction matrix elements with undistorted basis functions are only slowly decreasing as $\pm t$ increases.

6.5 Coulomb boundary conditions

In this section we show that Coulomb boundary conditions take effect in arbitrary reference frames.

From figure 6.12 it is inferred as well that Coulomb boundary conditions, i.e. the use of phase-distorted basis functions, lead to a short-range interaction in any reference frame considered in numerical calculations (cf. section 3.7). More precisely, in calculations with phase-distorted basis functions the matrix elements of the interaction matrix $V(t)$ decrease much faster to zero as time increases (or decreases), compared to calculations using undistorted bases. This verifies the efficacy of the Coulomb boundary conditions in arbitrary reference frames.

Finally, turn to the figures 6.13 and 6.14. The time-evolution of the squared moduli of the coefficients $c_i(t)$ is shown for the target and projectile frames, and two other frames of reference, in which the centres are moving with different velocities and in opposite directions. The initial configuration is a $1s_{1/2}$-state of centre A, the latter taking, therefore, the role of the target. Again, the collision system considered
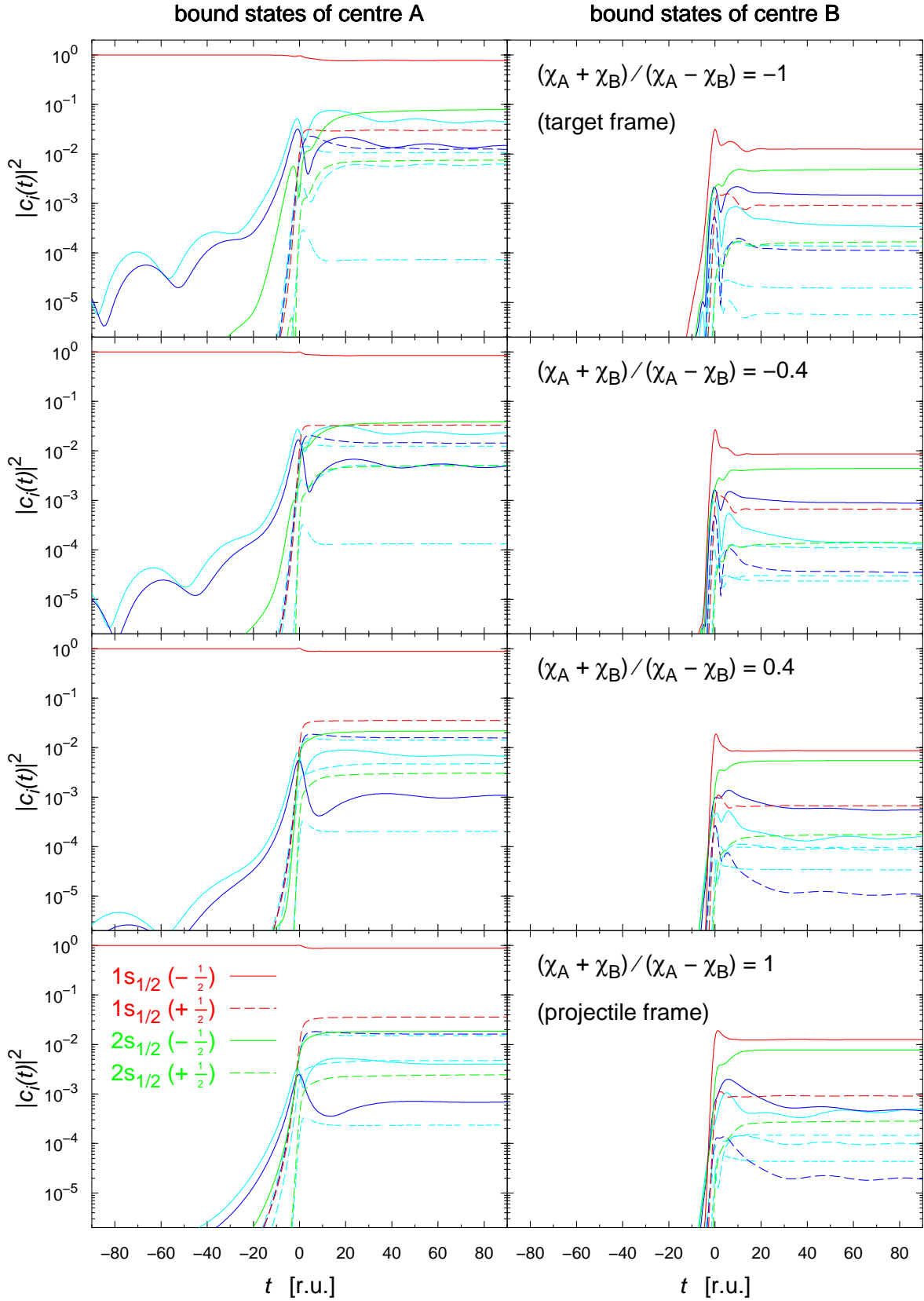
FIGURE 6.13. The time evolution of the squared moduli of the expansion co-efficients $c_i(t)$ obtained from coupled channel calculations with *undistorted* basis functions, in four different reference frames. The initial configuration is a $1s_{1/2}$-state of nucleus A. The allocation of line styles to basis functions is the same as in figure 5.1 on page 55. Parameters which are common to all four calculations are: $T = 0.96\,\text{GeV/u}$, $b = 2\,\text{r.u.}$ and $Z_\text{T} = Z_\text{P} = 92$. They are, therefore, identical to those of figure 6.11.
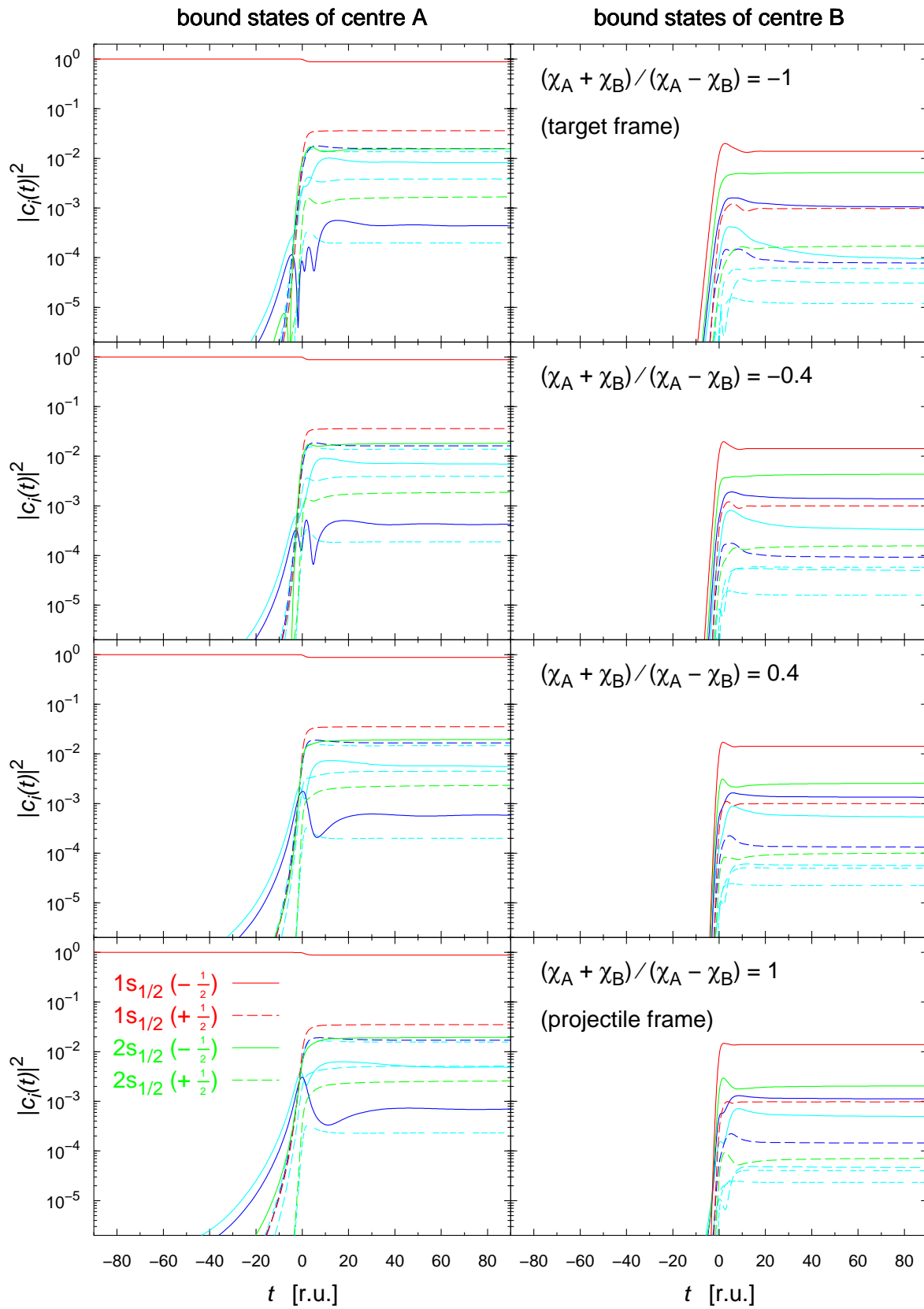
FIGURE 6.14.   As figure 6.13, but for calculations with *phase-distorted* basis functions.

is $Z_A, Z_B = 92$ at a collision energy of $T = 0.96\,\text{GeV/u}$, with an impact parameter of $b = 2\,\text{r.u.}$. In fact, the plots take another view on the same calculations, also presented in the figures 6.11 and 6.12.

A distinctive feature of figure 6.13, showing results obtained with an undistorted basis, is the existence of long-range target excitations for the target-frame calculation. Gradually passing over to the projectile frame, the extent of the target excitations decreases. Correspondingly, oscillations between the projectile states, after the collision, become increasingly visible, and they are greatest in the projectile frame. Qualitatively this can be understood as follows: since the excitation of target states is mainly caused by the magnetic field of the projectile [TE90, EM95], these excitations are, hence, vanishing in the projectile frame. Similarly, in the projectile frame, the target nucleus causes long-range interactions between projectile bound-states.

A detailed analysis of state-differential cross sections of electron excitation and transfer is not presented in this thesis. The reason is the extraordinary frame dependence of the transition probabilities, clearly exhibited in figure 6.13. For this series of calculations, using undistorted basis functions in various reference frames, some transition probabilities vary over more than one order of magnitude. It has been checked that this is not a spurious effect, due to the finite time interval $[t_i, t_f]$ of numerical calculations, but is a clear signature of the violation of the Lorentz invariance as a consequence of the coupled channel ansatz. In particular, it was found that the initial and final times t_i and t_f of a numerical calculation may be chosen shorter than reported in [TE88a], thereby reducing computational effort without loss of accuracy.

This frame dependence of single transition-amplitudes is less vigorous for the calculations with phase-distorted basis functions, reflecting the similar behaviour of the total capture probabilities, which was discussed already. At first glance, it might seem surprising that the excitation of target bound-states, in calculations performed with undistorted and phase-distorted bases in the *projectile* frame, is nearly identical. This fact is observed by comparison of the bottom plots of the figures 6.13 and 6.14. But, as stated above, the use of Coulomb boundary conditions mainly removes the long-range part of the projectile magnetic-field, the bound states of the target nucleus are exposed to. Clearly, the latter does not exist in the projectile frame.

6.6 Bound-free pair creation

In this section, results from coupled channel calculations with free-particle basis functions are presented. These calculations required much computing time and have been feasible only as distributed multiple-processor computations.

The main motivation for the present choice of free-particle basis functions has been explained in section 5.5. In the literature relativistic coupled channel calculations of bound-free pair creation have been reported by several authors [RMS+91, MGS91, RSG93, BRBW93, BRBW94]. All of these use a *single*-centre basis of bound states and wave packets. Therefore, these calculations can only describe excitation-like processes (cf. figure 5.6). In the present approach we make an attempt to allow for the description of excitation- and transfer-like processes at the same time by using a two-centre basis (cf. figure 5.7).

Bound-free pair production has been observed first in heavy-ion collisions with collision energies in the $1\,\mathrm{GeV/u}$ energy range [BGF+93, BGF+94]. The experimentally found cross sections for this process could not be explained reliably by existing theoretical descriptions [BGF+97], namely perturbation theories, single-centre coupled channel calculations or nonperturbative numerical solutions of the two-centre Dirac equation in momentum space [MBS95, MBS96]. Discrepancies have been reported for the absolute value of the total cross section and its dependencies on nuclear charge numbers and the collision energy. The agreement between observation and perturbative calculations is more satisfactory at higher collision energies of about $10\,\mathrm{GeV/u}$ [BCD+98]. It has been proposed that the discrepancy at intermediate energies is due to two-centre effects, not accounted for in usual perturbative calculations or single-centre coupled channel approaches.

The aim of the present calculations is not to determine cross sections, in better agreement with experiment than cross sections obtained by the previous theoretical approaches. This cannot be expected because of our very limited basis size due to numerical constraints. Instead, we attempt to assess the relative importance of the transfer-like pair creation process, neglected in single-centre approaches, compared to the excitation-like mechanism. In other words, the aim is to get a qualitative insight into two-centre effects in bound-electron free-positron pair creation at intermediate relativistic collision energies.

It has been proposed in [Eic95, ED96, IE96] that apart from familiar excitation-like processes also transfer-like processes contribute to the cross section of bound-free pair creation. In these articles, perturbative calculations are reported treating bound-free pair creation as a charge-transfer process. Note that perturbative treatments must take either point of view and cannot combine both mechanism. In the calculations a different asymptotic energy dependence of the total cross section, compared to the usual perturbative treatment of bound-free pair production as an excitation-like process, was obtained. However, a unified treatment of excitation- and transfer-like pair creation processes, as depicted in figure 5.7, is not feasible in the framework of perturbation theory. It has been attempted in the present work by means of a coupled channel approach.

In the following, results from coupled channel calculations for the collision system $Z_A, Z_B = 92$ at a collision energy of $0.96\,\mathrm{GeV/u}$ and $1\,\mathrm{GeV/u}$ respectively are presented. Most coupled channel bases comprise the ten lowest bound states of each nucleus. Furthermore, Lorentz-transformed stationary wave-packets of the form (5.19) are included, either for one centre or for both centres. For the reason of computational feasibility the parameters, defining the free-particle basis functions (5.19), have been chosen according to:

$$
\begin{aligned}
\kappa &= \pm 1, \\
\Delta_\epsilon &= 0.3\,\mathrm{r.u.}, \\
\bar{\epsilon} &= \pm 1.15, \pm 1.45, \pm 1.75\,\mathrm{r.u.}.
\end{aligned}
$$

For each centre, these parameters yield 24 free-particle basis functions, half of them with positive energy and the other half with negative energy. The radial wave functions of these wave packets are approximately localised within a sphere of $200\,\mathrm{r.u.}$
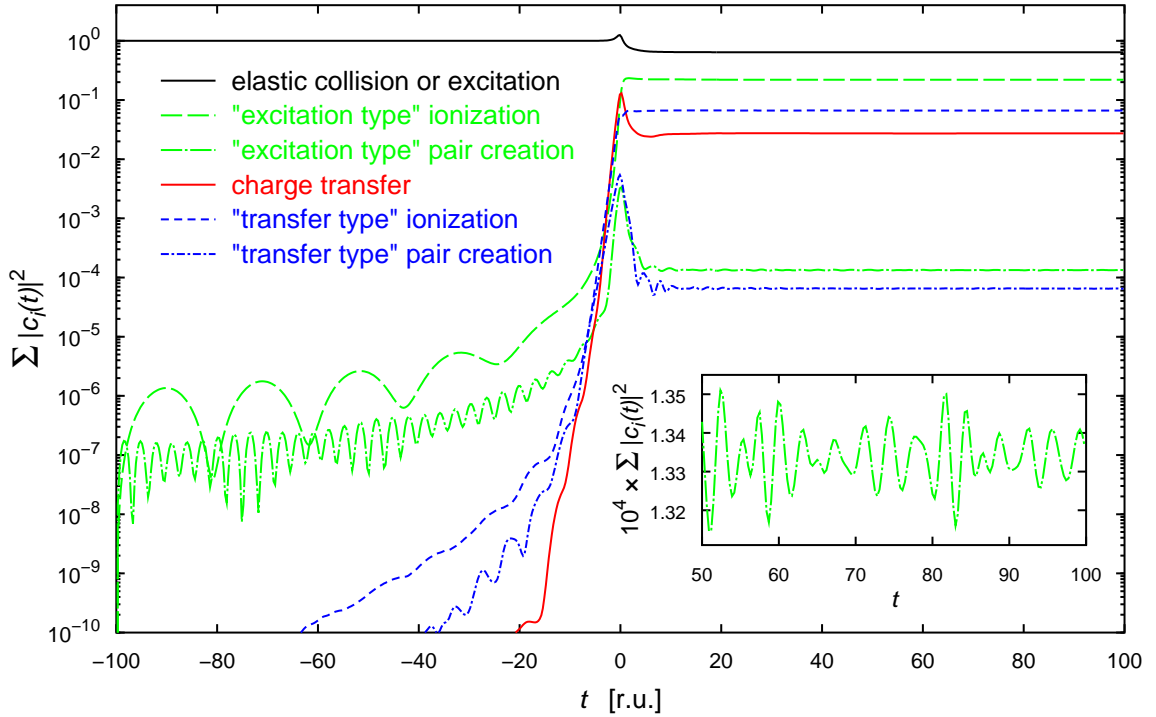
FIGURE 6.15. Time evolution of the sums over squared moduli of the expansion
coefficients $c_i(t)$. The sums are taken over those coefficients which correspond to
the same atomic process. For large times t these sums yield the probabilities of
the respective processes, as indicated in the legend (see figure 5.7 as well). The
charge numbers are $Z_A, Z_B = 92$ and the collision is taking place at a collision
energy of $T = 1\,\text{GeV/u}$ with an impact parameter of $b = 0.5\,\text{r.u.}$. The data
shown here has been computed by a coupled channel calculation in the collider
frame using 68 basis functions. The initial configuration is a $1\text{s}_{1/2}$ bound state.
Due to the long-range character of the Coulomb interaction, oscillations of the
coefficients are present, for large negative as well as positive times. The inset
shows these oscillations for the probability of the excitation-like bound-free pair
creation process.

(with respect to their respective rest frames) and have been cut off outside this vol-
ume. They are oscillating functions and, therefore, the numerical evaluation of ma-
trix elements, in particular of the two-centre interaction and overlap matrix elements,
becomes computationally more demanding in comparison with matrix elements in-
volving only bound-state basis functions.

It should be noted that the mean energies $\bar{\epsilon}$ of these wave packets are too small
to account for the experimentally observed electron and positron energy spectra
[BGF+97]. Therefore, results of the present coupled channel calculations are gener-
ally not expected to yield cross sections of bound-free pair creation in quantitative
agreement with experiment. The present emphasis is on a qualitative understand-
ing of two-centre effects in pair creation. In addition, the frame dependence of the
coupled channel calculations is studied.
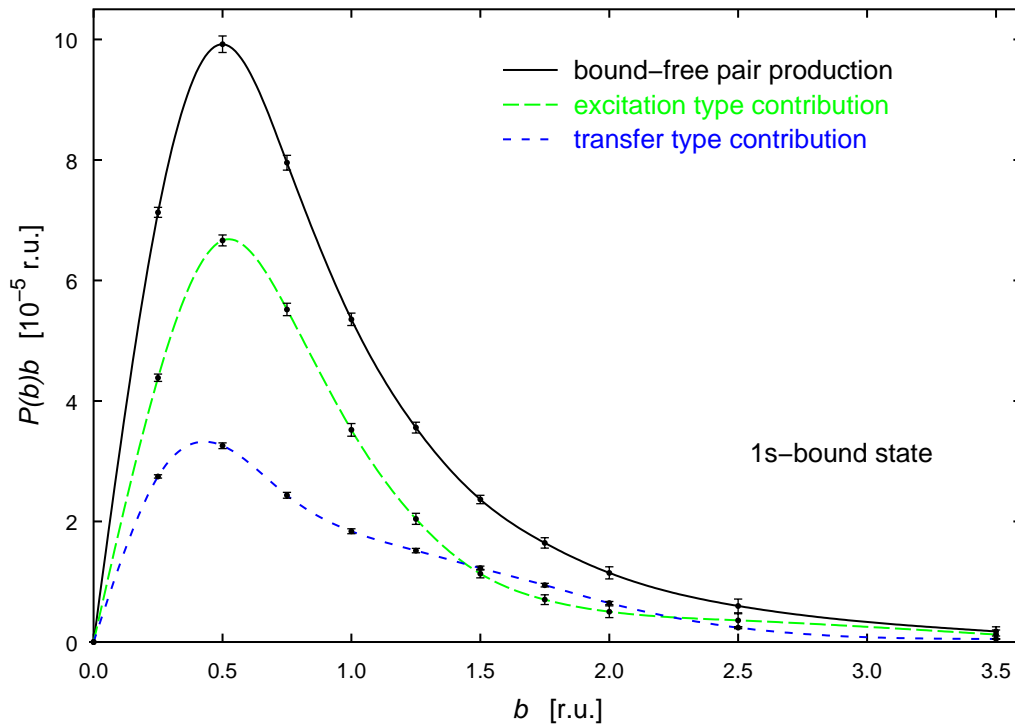
FIGURE 6.16. Weighted probabilities for bound-electron free-positron pair creation as a function of the impact parameter, obtained from coupled channel calculations in the collider frame using a two-centre basis of 68 basis functions. The collision energy is $1\,\mathrm{GeV/u}$ and the results shown refer to a collision of two bare uranium nuclei. The electron is created in a $1\mathrm{s}_{1/2}$ state of one of the nuclei.

6.6.1 Collider frame calculation. Coupled channel calculations with a symmetrical basis, comprising the ten lowest bound states and 24 wave packets at each centre, have been performed for a series of impact parameters in the collider frame. A collision energy of $1\,\mathrm{GeV/u}$ was chosen and the calculations have been done using an undistorted basis. Figure 6.15 shows the time evolution of the sum of the squared moduli of expansion coefficients $c_i(t)$, which belong to the same scattering channel. It is distinguished between excitation-like and transfer-like processes for the free-particle scattering channels, in accordance with figure 5.7. The initial configuration is a $1\mathrm{s}_{1/2}$ bound state of centre A. Transition amplitudes to bound states of centre B are interpreted as charge-transfer amplitudes (red line). Transitions to wave packets of positive energy are attributed to either excitation-like or transfer-like ionisation (green and blue dashed lines). Finally, transition amplitudes to wave packets of negative energy are interpreted as bound-free pair creation amplitudes (green and blue dashed-dotted lines) (cf. section 3.6).

Figure 6.15 clearly exhibits the long-range character of the Coulomb potential leading to a coupling of the initial state to wave packets of negative and positive energy of centre A, much before the closest approach of the centres at time $t = 0$. These couplings are present also for the outgoing channels, leading to oscillations of the probabilities at large times t. These oscillations are shown, as an example, for the excitation-like pair creation probability and the time interval $t = 50 \ldots 100\,\mathrm{r.u.}$
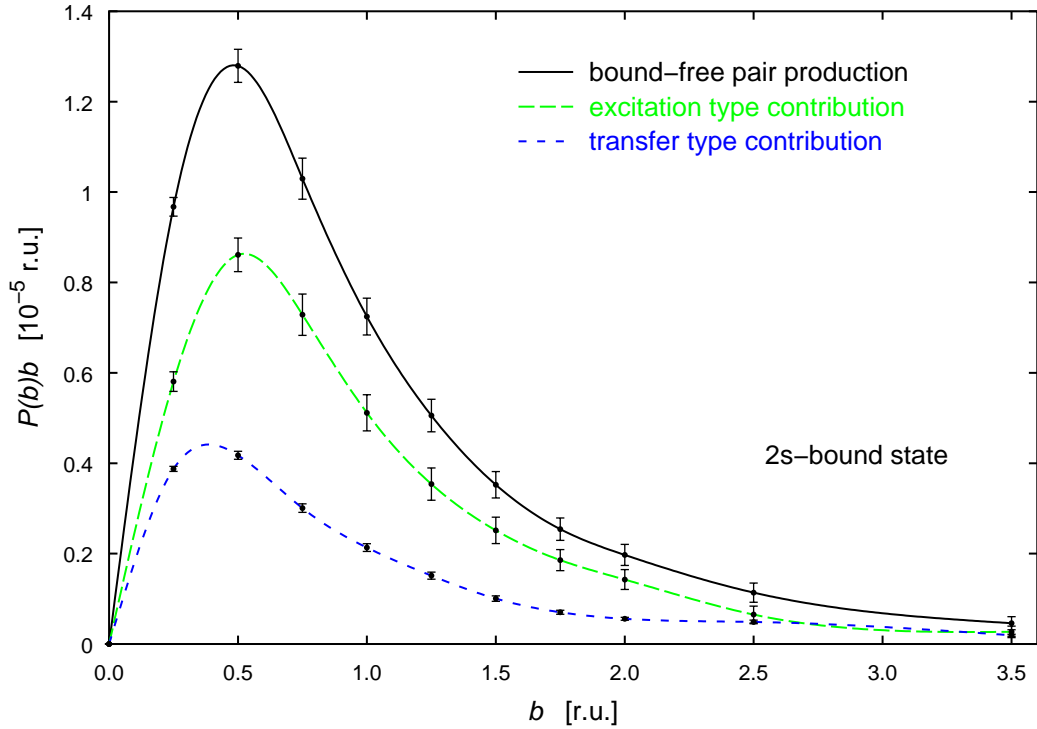
FIGURE 6.17. As figure 6.16, but the electron is created in a $2s_{1/2}$ bound state of one of the colliding nuclei.

by the inset of figure 6.15. It is seen that the amplitude of these oscillations is small and that there is no shift of the mean value as time increases.

The presence of these oscillations demonstrates another numerical complexity: The time steps for the numerical integration of the coupled channel equations (4.8) have to be chosen much smaller, compared to the computationally less demanding pure capture calculations, discussed in the previous sections. If wave packets of higher energy $\bar{\epsilon}$, than considered here, were used, not only the evaluation of matrix elements becomes more involved, but also the time-integration of the coupled equations becomes even more demanding.

Figure 6.16 shows the weighted probabilities for bound-free pair creation, in which the electron is created in a $1s_{1/2}$ bound state. The different contributions from excitation- and transfer-like pair creation probabilities are given, the total probability of bound-free pair creation just being the sum of these two contributions. It is discernible that excitation- and transfer-like processes are of similar relative importance, the excitation-type process being favoured. Note that the maximum of the weighted pair creation probability $P(b)b$ is at an impact parameter $b = 0.5$ r.u.. Compared to the charge transfer process, the the main contribution to the pair-creation cross section comes from smaller impact parameters, due to the great field strength necessary for pair production.

Figure 6.17 shows the analogous plot for bound-free pair production, in which the electron is created in a $2s_{1/2}$ bound state. The corresponding weighted probabilities are approximately one order of magnitude smaller than in figure 6.16. Again it is observed that excitation- and transfer-like processes are of equal importance. The
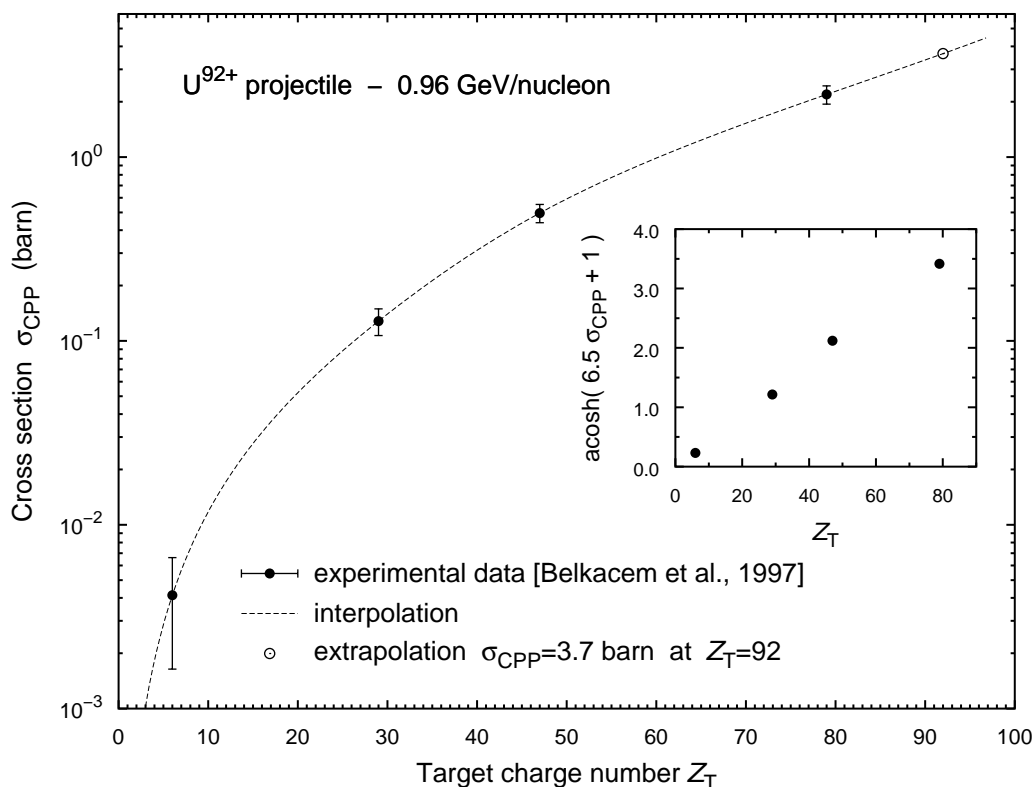
FIGURE 6.18. Linearisation and interpolation of experimental data for bound-free pair creation, as reported in [BGF$^+$97, figure 16]. In the experiment a bare U^{92+} projectile impinged with a kinetic energy of 0.96 GeV/u on solid targets of mylar, Cu, Ag and Au ($Z_T = 6, 29, 47$ and 79). The cross sections are extrapolated to obtain an estimate for a hypothetical solid uranium target.

error bars in both figures, 6.16 and 6.17, represent the amplitude of the oscillations of the final probabilities in the time interval $t = 50 \ldots 100$ r.u. due to the long-range Coulomb interaction, as discussed above.

By integrating the weighted total probabilities of bound-free pair production, shown in the figures 6.16 and 6.17, estimates for the total cross sections of this process are obtained. According to the present rough calculations, for the creation of a $1s_{1/2}$-electron the cross section is 0.95 barn. The corresponding cross section for the creation of a $2s_{1/2}$-electron is 0.13 barn. In fixed target experiments bound electrons can be created only as bound states of the projectile, i.e. of a nucleus of the particle beam in the experiment. Experiments that distinguish specific final states of the created electron are not available yet. The experimentally measured total cross section, therefore, always comprise contributions from all bound states of the projectile. According to the present calculations the contribution of $1s_{1/2}$ states amounts to 2 barn, whereas $2s_{1/2}$ states only contribute 0.2 barn. This reflects a major fraction of the total cross section is due to the creation of $1s_{1/2}$-bound electrons.

6.6.2 Experimental cross section. At this point, we shall compare these calculations briefly with experimental results. In [BGF$^+$97] total bound-free pair creation cross sections for U^{92+} impinging on target foils of mylar, Cu, Ag and Au, at a

collision energy of $0.96\,\mathrm{GeV/u}$, have been reported. These experimental results are plotted in figure 6.18, which partially reproduces [BGF$^+$97, figure 16]. The inset of figure 6.18 shows a linearisation of the experimental data, not noted before. This corresponds to a Z_T^2-dependence of the pair creation cross section for small target charge numbers Z_T, as expected by perturbation theory [EM95, BGF$^+$97].[1] According to this linearisation, the cross section grows exponentially as a function of Z_T for large target charge-numbers Z_T, where perturbation theory is expected to fail. It has been noted already in [BGF$^+$97] that the experimental data is not in agreement with the Z_T^2-dependence predicted by perturbation theory.

This linearisation is presented here, mainly because it is used to extrapolate the experimental data to the collision system $\mathrm{U}^{92+} + \mathrm{U}$. The interpolation function shown in the main plot of figure 6.18 represents a cubic spline interpolation of the linearised data. The extrapolation of this interpolation function to $Z_\mathrm{T} = 92$ yields a cross section of $3.7\,\mathrm{barn}$. Other extrapolation methods give similar values, ranging between 3.5 and $4\,\mathrm{barn}$. It is surprising how close experimental data and the calculation presented in the previous subsection are, taking into account the rather insufficient coupled channel basis. However, a critical judgement might as well regard this coincidence as accidental.

6.6.3 Frame dependence. The calculations in the collider frame using 68 basis functions, presented in subsection 6.6.1, clearly demonstrate that the transfer-like process contributes significantly to the total cross section of bound-free pair creation.

In view of the Lorentz-frame dependence of coupled channel calculations, observed in the capture calculations, it is natural to study the relation between excitation- and transfer-like pair creation also in other computational frames of reference. Coupled channel calculations using the same 68 undistorted basis functions as in subsection 6.6.1 have been carried out in a rest frame of centre A. In this Lorentz frame it must be distinguished, whether the electron is created in a bound state of centre A or centre B. This distinction is not necessary for the collider frame calculation in which the probabilities are the same due to parity conservation.

In this subsection we discuss the plots (1), (2), (6) and (7) of figure 6.19.

In figure 6.19 the plots (1) and (2) show weighted bound-electron free-positron pair creation probabilities, similar to figure 6.16. In plot (1) the electron is created in a $1\mathrm{s}_{1/2}$-state of nucleus A, whereas in plot (2) it is created in a $1\mathrm{s}_{1/2}$-state of nucleus B. The difference of the results by more than one order of magnitude is striking. The excitation-like pair creation is dominant for the creation of a bound-electron at centre A and the transfer-like process is nearly negligible. By contrast, the transfer-like pair creation mechanism is relatively more important if the electron is created in a bound state of centre B.[2] While passing over from plot (1) of figure 6.19, to figure 6.16, and then to plot (2) of figure 6.19 the excitation-like contribution is

---

[1] Here Z_T is the charge number of the *experimental target*. In the experiments measuring bound-free pair creation the electron is created in a bound state of the *experimental projectile*.

[2] Remember the following. If the electron is created in a bound state of nucleus B, then the laboratory frame in a fixed-target experiment is identical to the presently considered rest frame of A.
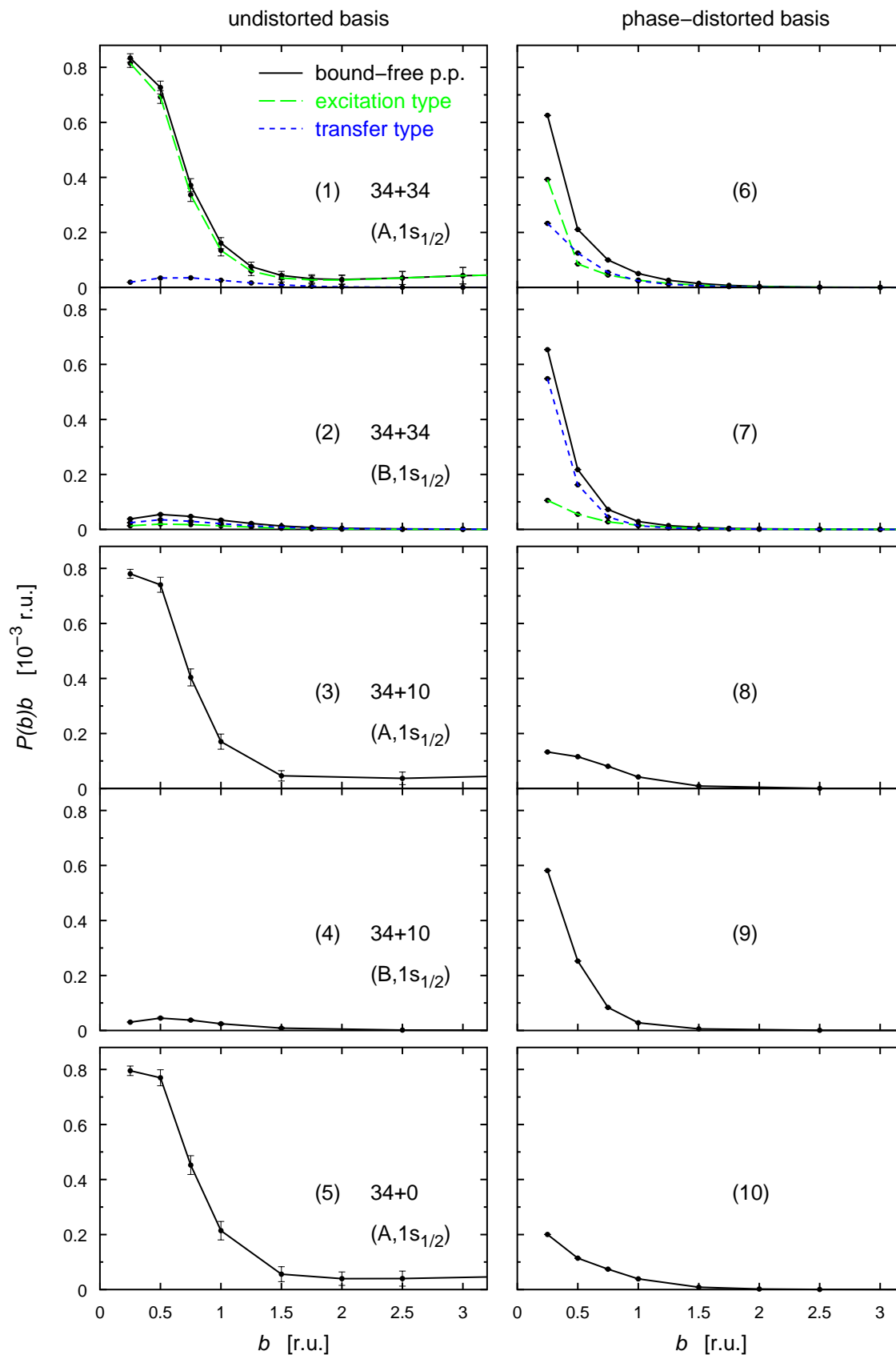
FIGURE 6.19. Weighted probabilities $P(b)b$ for bound-free pair creation, obtained from calculations with free-particle basis functions in the rest frame of centre A, using three different basis sets. All bases comprise the ten lowest bound states and 24 free-particle states of of centre A. The number of basis functions at centre B is varying. The electron is created in a $1s_{1/2}$ bound state of either centre A or centre B, as indicated.

dramatically reducing, showing a similar reduction of excitations as exhibited already by figure 6.13.[3]

The difference of the pair creation probabilities is a numerical artifact, because in a symmetrical collision system the exact probabilities for the creation of a 1s-electron at nucleus A and nucleus B are the same. The reason for this artifact is the very small basis size, which had to be used for numerical reasons. Larger bases might not show such a big frame dependence.

The symmetry mentioned is preserved only by coupled channel calculations in the collider frame, which has been verified. This might suggest that coupled channel calculations performed in the collider frame yield the best results for symmetrical collision systems. Also, experimental data is matched best, by numerical results obtained in the collider frame. On the other hand it is not a priori clear, whether the exact solution of the two-centre Dirac equation is approximated best by a coupled channel ansatz in the collider frame.[4]

The plots (6) and (7) show weighted probabilities obtained from calculations with the corresponding 68 phase-distorted basis functions. The frame dependence of the total pair creation probabilities is much reduced by phase-distorting the basis functions. This resembles the behaviour of the capture calculations. On the other hand the excitation-like process is dominating for the creation of a bound electron at centre A, whereas the transfer-like process is clearly dominating for the creation of a bound electron at centre B. Calculations with phase-distorted basis functions do not exhibit oscillations of the final pair creation probabilities, which are shown in figure 6.15, and which have been observed for the calculations in rest frame of centre A as well, when using an undistorted basis. Note that results obtained with the present, small phase-distorted basis significantly overestimate the experimental cross section of bound-free pair creation.

6.6.4 Two-centre effects. In this subsection, we discuss all plots shown in figure 6.19 and their mutual relation, with an emphasis on two-centre effects.

Single-centre coupled channel calculations and 'semi-two-centre' calculations have been carried out, in order to compare directly the previously discussed results with unsymmetrical representations of the free-particle scattering channel, also reported in the literature [RMS+91, MGS91, RSG93, BRBW93, BRBW94]. Accordingly, these calculations have been performed also in the rest frame of centre A. For the single-centre calculations a basis comprised of the ten lowest bound states and 24 wave packets of centre A has been employed. Semi-two-centre calculations refer to a basis which includes, in addition, the ten lowest bound states of centre B. Clearly, in both cases the free-particle states are always localised at centre A. But as opposed to single-centre calculations, the semi-two-centre calculations allow for the creation of a bound electron at both centre A and centre B. These bases are schematically depicted by figures 5.5 and 5.6.

---

[3]Note the different scale of the ordinate axes in the figures 6.16 and 6.19.

[4]This reasoning is applicable to the capture calculations of the preceding sections in an analogous way.

It should be mentioned that the single-centre and semi-two-centre bases, used here, only include wave packets, which are at rest in the reference frame of the calculation. Therefore, interpretive difficulties, arising from the slight non-orthogonality of Lorentz-boosted stationary wave packets attributed to the same centre, do not occur (see section 5.5).

First the plots (1), (3) and (5) of figure 6.19 may be compared. It is seen that bound-free pair production, with the creation of an electron in a bound state of centre A, is neither influenced significantly by the presence of the bound states of centre B, nor by the presence the wave packets attributed to centre B. Hence, the effect of the extension of an undistorted single-centre basis by bound states and scattering states of the second centre is not important, in coupled channel calculations in which the created electron is at rest.

By contrast, regarding the fully symmetrical *phase-distorted* basis, the transfer-like pair creation process is relatively more important, as exhibited by plot (6) of figure 6.19. It may be conjectured that this fact is due to a reduced frame dependence of such calculations, as observed already for the pure capture calculations. Omitting the free-particle basis functions of centre B in plot (8) not only removes the possibility for this contribution, but also reduces the magnitude of excitation-like pair creation probability. This is observed also, but less significantly, in plot (10) of figure 6.19, for which the bound states of centre B have been excluded from the basis, too. Hence, the the extension of a *phase-distorted* single-centre basis clearly affects the pair creation probabilities.

The plots (2) and (4), both represent the creation of an electron in a $1s_{1/2}$ bound state of centre B. Their comparison shows that the transfer-like pair creation, already dominant for the fully symmetric calculation with 68 basis functions (cf. plot (2)), is enhanced slightly by the omission of the wave packets of centre B (cf. plot (4)). The qualitatively similar behaviour is observed for the calculations with phase-distorted bases (cf. plots (7) and (9)), which unfortunately yield very different probabilities of bound-free pair creation.

6.6.5 Conclusion. The various calculations do not provide a coherent picture of the importance of two-centre effects in the process of bound-electron free-positron pair creation. The probabilities obtained from calculations in the collider frame are most convincing, because they do not suffer from obvious numerical artifacts, as the violation of the symmetry of electron creation at centre A or B. The collider frame calculations demonstrate the importance of a symmetrical description of the free-particle scattering channel for collisions in the $1\,\mathrm{GeV/u}$ collision-energy range. Due to the computational difficulty of the calculations presented, larger coupled channel bases have not been feasible, but they are necessary to avoid the numerical artifacts, like the strong frame-dependence exhibited by figure 6.19.

6.7 Free-particle channels and charge transfer

The coupled channel calculations including free-particle basis functions, as presented in the previous section, also provide probabilities for electron capture. Since this atomic process has been studied extensively in sections 6.1 to 6.4 of this chapter,
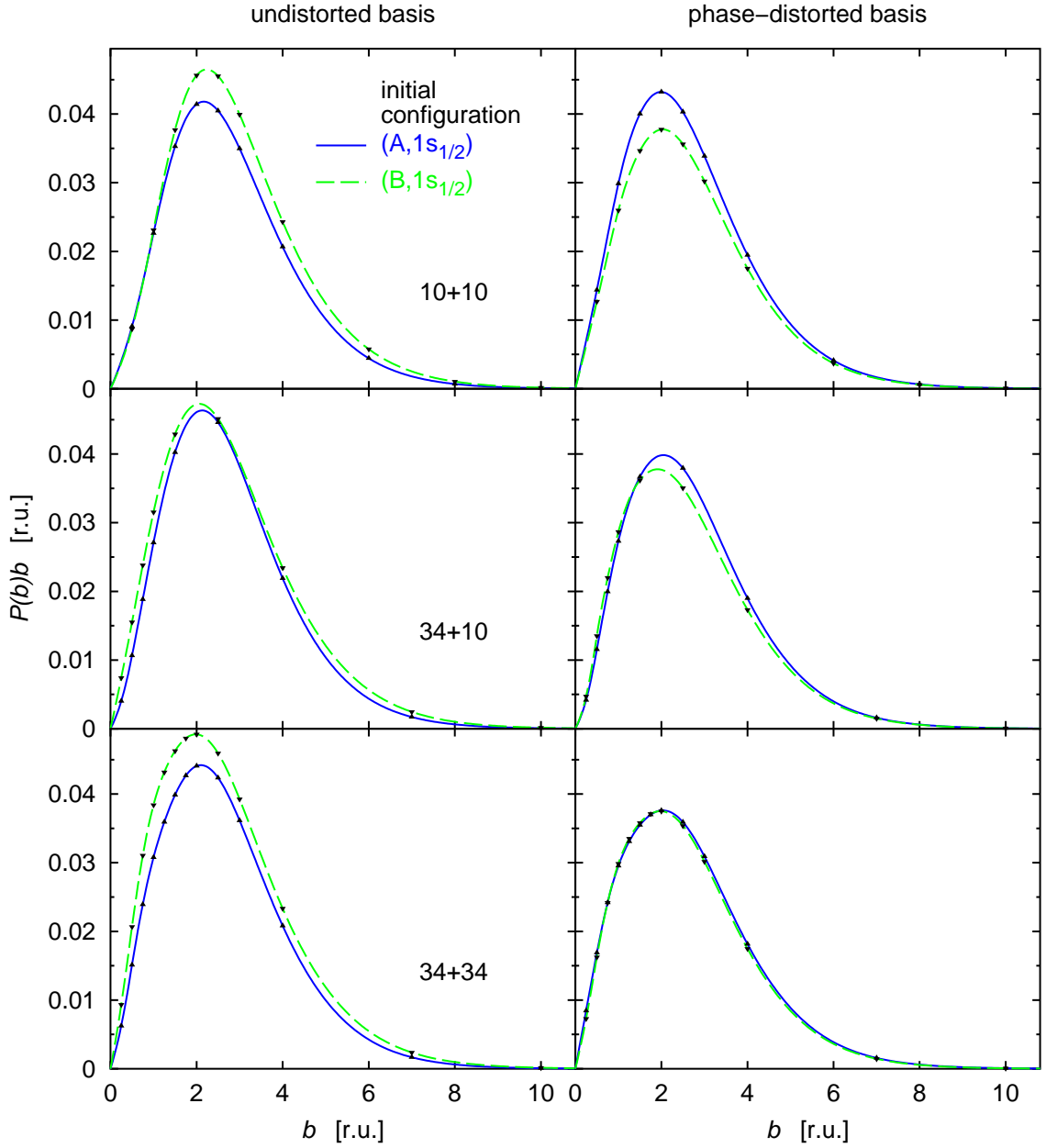
FIGURE 6.20. Weighted total probabilities $P(b)b$ of electron capture for the collision $U^{91+}(1s_{1/2}) + U^{92+}$ as a function of the impact parameter b. The collision energy is $0.96\,\mathrm{GeV/u}$. Results obtained from coupled channel calculations, performed in the rest frame of centre A with six different sets of basis functions, are shown. All bases contain the ten lowest bound states of each centre. The calculations with 68 basis functions, denoted by the label '34+34', comprise stationary wave packets at both centres, as described in section 6.6. The label '34+10' denotes semi-two-centre calculations, in which only stationary wave packets of centre A are included into the coupled channel basis. The addition of free-particle basis functions to the coupled channel basis only comprising bound states (upper two plots) does not have a significant effect on the charge transfer cross section. In calculations with phase-distorted basis functions the inclusion of wave packets clearly reduces the frame dependence.
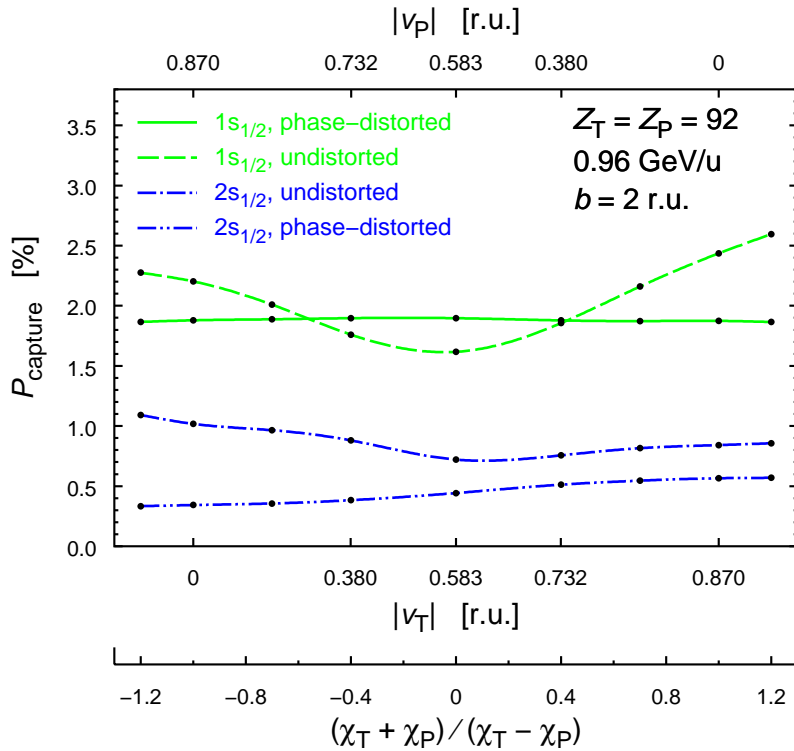
FIGURE 6.21. The frame dependence of the capture probability for the same collision parameters as in figure 6.11. The only difference to figure 6.11 is that the probabilities shown here have been computed with a basis of 68 basis functions, which comprises the 48 wave packets described in section 6.6.

using bases comprising bound states only, the results obtained with free-particle bases should be compared with the pure capture calculations. No such investigation exists in the literature.

Two different questions may be addressed. First, the influence of the free-particle basis functions on the calculated total cross section of electron capture may be investigated. Since ionisation probabilities are expected and, indeed, found to be much larger than capture probabilities, at least for the collision energies considered here, it could be that the omission of free-particle basis functions introduces a significant systematic error in the calculated capture cross sections. Second, it is interesting to ask, whether the addition of free-particle states to the coupled channel basis reduces the frame dependence of the capture probabilities. This has been conjectured in section 6.1.

In comparison to the pair creation process, the main contributions to electron capture cross sections come from larger impact parameters. The physical reason is that pair creation requires much stronger electromagnetic fields; in peripheral collisions, the peak energy density of the electromagnetic field of the nuclei increases as the impact parameter decreases [Tel87]. The calculations presented in the previous section had to be extended to impact parameters up to $b = 10$ r.u. in order to obtain the full impact-parameter dependence of electron capture in calculations also employing free-particle states. For the results of this section, the basis described in

the previous section has been used and the same collision system and energy have been considered, namely $Z_A, Z_B = 92$ and $T = 0.96\,\text{GeV/u}$.

6.7.1 Total capture cross section. In figure 6.7 weighted capture-probabilities are presented that have been obtained by coupled channel calculations in the rest frame of nucleus A. Two different initial conditions are shown in each plot. Several different bases have been used. The two diagrams at the top of figure 6.7 represent calculations using a pure bound-state basis. This data has appeared already in figure 6.10 and is replotted to allow for a convenient comparison. The other four plots show results from calculations with bases comprising free-particle states.

It has been found that ionisation probabilities in numerical calculations of this work, which make use of free-particle states, are approximately one order of magnitude *larger* than the capture probabilities shown here. Since ionisation is not accounted for in coupled channel calculations with bases comprised of bound states only, it is remarkable that the omission of free particle states does *not* have major effect on the capture cross section. It is seen that the addition of free-particle states slightly enhances the capture cross section in calculations with undistorted bases. The opposite behaviour is exhibited by the capture probabilities corresponding to phase-distorted bases. Note that the frame dependence of the capture probabilities has nearly vanished in the calculation with phase-distorted states which employs wave packets at both centres (plot at the bottom right of figure 6.10).

6.7.2 Frame dependence. For the impact parameter $b = 2\,\text{r.u.}$ the total capture probability has been evaluated in various frames of reference, using the fully symmetrical basis described in the previous section, comprised of the ten lowest bound states and 24 stationary wave packets of each centre. The results are shown in figure 6.21. Analogous calculations using a pure bound-state basis have been presented in figure 6.11 on page 82. Comparing these two figures the reduced frame dependence due to the addition of free-particle states is clearly noticed in figure 6.21. The reduction of the frame dependence is very convincing for the calculation with phase-distorted basis functions, in particular if the $1s_{1/2}$ initial configuration is considered. Although a diminished frame dependence is present also for calculations with undistorted bases, it is less satisfactory, presumably reflecting that the coupled channel basis is still too small. Nevertheless, the present results demonstrate that the frame dependence of the numerically determined capture cross section is diminished by the adding of stationary wave packets to the coupled channel basis.

Numerical and Algorithmic Details

In this appendix, the computer code is described which was used to produce the numerical results presented in this thesis. It also comprises the details of the computational methods and explicitly some formulas which have been omitted in the main part of this work. Furthermore, improvements of the code, which have not been implemented yet, are proposed. The main aim of such changes must be the reduction of the compute time, thereby making larger bases feasible.

The present program is the first of its kind which is capable of performing numerical computations in various different relativistic frames of reference. In *any* previously existing computer code that numerically solves the relativistic coupled channel equations a particular frame of reference was chosen, namely the reference frame where the initial electronic state was at rest. Moving initial configurations have not been considered. Not only coupled channel codes, but also other numerical approaches to solve the two-centre Dirac equation (like the momentum space approach, finite element and finite difference calculations) have only considered initial configurations at rest in the frame of the computation.

For coding the C/C++ programming languages have been used predominantly [STR97, CSC+97]. For the convenience of readers who are interested in reading the source code (although not reproduced here), we quote identifiers occasionally.

A.1 General definitions

At the time of writing, the program is capable of solving the coupled channel equations in those frames of reference where both nuclei, A and B, move along straight line trajectories parallel to the $\boldsymbol{e}_3$-axis of the coordinate system. The impact parameter plane is chosen to be the $\boldsymbol{e}_1$-$\boldsymbol{e}_3$-plane and the time of closest approach of the nuclei is $t = 0$. In the subsequent discussion the trajectories are assumed to be of the form,

$$\boldsymbol{R}_\mathrm{A}(t) = -\frac{b}{2}\,\boldsymbol{e}_1 + tv_\mathrm{A}\,\boldsymbol{e}_3, \qquad \boldsymbol{R}_\mathrm{B}(t) = \frac{b}{2}\,\boldsymbol{e}_1 + tv_\mathrm{B}\,\boldsymbol{e}_3, \tag{A.1}$$

with

$$-\infty < b < \infty, \qquad -1 < v_\Gamma < 1, \ \text{with } \Gamma = \mathrm{A,B}, \qquad \text{and} \qquad -\infty < t < \infty.$$

However, recall that any translation of the origin of the spatial coordinate system in the $\boldsymbol{e}_1$-$\boldsymbol{e}_2$-plane will yield an identical set of coupled equations (cf. section 5.1). The input parameters of the computer program that determine these trajectories are listed in table A.1. In terms of the rapidities $\chi_\mathrm{B}^\mathrm{c}$ and $\chi_\mathrm{frame}^\mathrm{c}$ the velocities v_A and v_B are determined according to:

$$\begin{aligned} v_\mathrm{A} &= \tanh(-\chi_\mathrm{B}^\mathrm{c} - \chi_\mathrm{frame}^\mathrm{c}), \\ v_\mathrm{B} &= \tanh(\chi_\mathrm{B}^\mathrm{c} - \chi_\mathrm{frame}^\mathrm{c}). \end{aligned}$$

TABLE A.1. Command line parameters of the main program.

`chi`	Rapidity χ_B^c of nucleus B in the collider frame.
`chiframe`	Rapidity χ_{frame}^c of the frame of reference with respect to the collider frame.
`b`	Impact parameter b in relativistic units.
`zA zB`	Charge number of projectiles A and B respectively.
`nmaxA nmaxB`	Maximum principal quantum numbers of bound-state basis functions of centre A and B respectively.
`kappaA kappaB`	Maximum absolute values of the spin-orbit quantum numbers κ of free-particle basis functions.
`ti tf dt tinnr dtinnr`	Variables $t_f, t_i, \Delta_t, t_{inner}$ and $\Delta_{t,inner}$ that determine the time grid (cf. section A.4), in relativistic units.
`infile`	Name of a checkpoint file. Necessary for the continuation of a previously interrupted computation.
`id`	Identification string of a coupled channel calculation.

The Lorentz factor γ specifying the collision energy (i.e. the kinetic energy of one of the projectiles measured in the rest frame of the other projectile) is then given in terms of the rapidity χ_B^c by:

$$\gamma = \cosh(2\chi_B^c).$$

Half the distance between the centres A and B at time t in the unprimed frame, denoted by f in the following, is equal to:

$$f = \frac{1}{2}\sqrt{b^2 + t^2(v_B - v_A)^2} \tag{A.2}$$

In the present context, primed rest-frame coordinates (t', x', y', z') of centre A and doubly primed rest-frame coordinates (t'', x'', y'', z'') of centre B are defined as,

$$t' = \gamma_A(t - v_A z), \qquad x' = x + \frac{b}{2}, \qquad y' = y, \qquad z' = \gamma_A(z - v_A t) \tag{A.3}$$

$$t'' = \gamma_B(t - v_B z), \qquad x'' = x - \frac{b}{2}, \qquad y'' = y, \qquad z'' = \gamma_B(z - v_B t). \tag{A.4}$$

These definitions are emphasised, because the definitions of the basis functions below explicitly refer to the direction of the z'- and z''-axis. Note that the directions have been chosen to be equal to the direction of the z-axis of the computational frame of reference. In the program radial coordinates $(r_A, \vartheta_A, \varphi_A)$ for the rest frame of A are

defined in terms of these Cartesian coordinates according to, [1]

$$r_A = \sqrt{x'^2 + y'^2 + z'^2}, \qquad \cos\vartheta_A = \frac{z'}{r_A}, \qquad \varphi_A = \arg\left(x' + \mathrm{i}y'\right), \tag{A.5}$$

The spatial radial coordinates $(r_B, \vartheta_B, \varphi_B)$ in the rest frame of B are given similarly in terms of the doubly primed Cartesian coordinates (x'', y'', z'').

A.2 Basis functions

As described in sections 5.2 and 5.3, in the present impementation of the coupled channel method the basis functions $\Phi_{\Gamma,i}(t, \boldsymbol{x})$ are eigenfunctions of the spin-orbit operator and the third component of angular momentum in their respective rest frames. In this section we give the precise forms of the eigenfunctions $\phi_{A,i}(\boldsymbol{x}')$ and $\phi_{B,i}(\boldsymbol{x}'')$, referred to in sections 5.3 and 5.5. The following presentation covers the eigenfunctions $\phi_{A,i}(\boldsymbol{x}')$ referring to the rest frame of centre A. Everything stated in the following applies in an analogous way to eigenfunctions $\phi_{B,i}(\boldsymbol{x}'')$ in the rest frame of centre B.

A.2.1 Spin-angular functions. Numerical calculations make use of the standard Dirac-Pauli representation of the Dirac matrices (see equation (C.2) of appendix C). For this representation, the spin-orbit operator K' defined in equation (5.5) is block-diagonal:

$$K' = \begin{pmatrix} -\frac{1}{2}\boldsymbol{\sigma}\cdot\boldsymbol{L}' - 1 & 0 \\ 0 & \frac{1}{2}\boldsymbol{\sigma}\cdot\boldsymbol{L}' + 1 \end{pmatrix}.$$

In this case, the third component J'^3 of the angular momentum operator $\boldsymbol{J}'$ is a diagonal block-matrix as well:

$$J'^3 = -\mathrm{i}\frac{\partial}{\partial\varphi_A} + \frac{1}{2}\begin{pmatrix} \sigma_3 & 0 \\ 0 & -\sigma_3 \end{pmatrix}.$$

Both K' and J'^3 only contain differentiation operators with respect to the angular variables ϑ_A and φ_A. Therefore, a simultaneous eigenstate $\phi_A(\boldsymbol{x}')$ of K' and J'^3, with eigenvalues κ and m respectively, is of the form:

$$\phi_A(\boldsymbol{x}') = \frac{1}{r_A}\begin{pmatrix} \mathrm{i}P(r_A)\,\chi_\kappa^m(\vartheta_A, \varphi_A) \\ Q(r_A)\,\chi_{-\kappa}^m(\vartheta_A, \varphi_A) \end{pmatrix}, \tag{A.6}$$

with complex-valued radial functions $P(r_A)$ and $Q(r_A)$. The imaginary constant has been added for later convenience. The two-spinors $\chi_\kappa^m(\vartheta, \varphi)$ must satisfy the following eigenvalue equations:

$$\begin{aligned} \left[\tfrac{1}{2}\boldsymbol{\sigma}\cdot\boldsymbol{L}' + 1\right]\chi_\kappa^m(\vartheta, \varphi) &= -\kappa\,\chi_\kappa^m(\vartheta, \varphi), \\ \left[-\mathrm{i}\partial_{\varphi_A} + \tfrac{1}{2}\sigma_3\right]\chi_\kappa^m(\vartheta, \varphi) &= m\,\chi_\kappa^m(\vartheta, \varphi). \end{aligned}$$

---

[1]This notation represents a minor inconsistency with previous notation: In this appendix r_A is not primed, although it is identical to the Lorentz scalar $r_A'(t', \boldsymbol{x}')$ as defined in section 2.1.

A suitable choice for these spin-angular functions $\chi_\kappa^m(\vartheta, \varphi)$ is given by the following definition: [2]

$$\chi_\kappa^m(\vartheta, \varphi) = \frac{1}{\sqrt{2l+1}} \begin{pmatrix} -\sqrt{l-m+\frac{1}{2}}\, Y_l^{m-\frac{1}{2}}(\vartheta, \varphi) \\ \sqrt{l+m+\frac{1}{2}}\, Y_l^{m+\frac{1}{2}}(\vartheta, \varphi) \end{pmatrix} \qquad \text{for } \kappa > 0, \text{with } l = \kappa,$$

$$\chi_\kappa^m(\vartheta, \varphi) = \frac{1}{\sqrt{2l+1}} \begin{pmatrix} \sqrt{l+m+\frac{1}{2}}\, Y_l^{m-\frac{1}{2}}(\vartheta, \varphi) \\ \sqrt{l-m+\frac{1}{2}}\, Y_l^{m+\frac{1}{2}}(\vartheta, \varphi) \end{pmatrix} \qquad \text{for } \kappa < 0, \text{with } l = |\kappa| - 1.$$

In this work we refer to the following phase convention for spherical harmonic functions $Y_l^p(\vartheta, \varphi)$ and associated Legendre polynomials $P_l^p(\cos\vartheta)$:

$$Y_l^p(\vartheta, \varphi) = e^{ip\varphi} \sqrt{\frac{2l+1}{4\pi} \frac{(l-p)!}{(l+p)!}} \underbrace{\frac{(-1)^{l+p}}{2^l\, l!} (\sin\vartheta)^p \left[\frac{d}{d(\cos\vartheta)} \right]^{l+p} (\sin\vartheta)^{2l}}$$

$$= e^{ip\varphi} \sqrt{\frac{2l+1}{4\pi} \frac{(l-p)!}{(l+p)!}} \qquad P_l^p(\cos\vartheta)$$

The spin-angular functions $\chi_\kappa^m(\vartheta, \varphi)$ constitute a complete set of orthonormal functions on the unit sphere. For the numerical evaluation of the spherical harmonics the formula,

$$Y_l^p(\vartheta, \varphi) = e^{ip\varphi} \sqrt{\frac{2l+1}{4\pi} \frac{(l-|p|)!}{(l+|p|)!}} P_l^{|p|}(\cos\vartheta) \times \begin{cases} (-1)^p & \text{if } p < 0, \\ 1 & \text{if } p > 0, \end{cases}$$

is most suitable, because numerically stable recursion relations exist, which allow for the determination of associated Legendre polynomials P_l^p of positive order p [PTVF92]. Owing to the presently adopted phase conventions, the spin-angular functions $\chi_\kappa^m(\vartheta, \varphi)$ also satisfy the relation [Ros61, eq. (1.65')],

$$\boldsymbol{e}_r \cdot \boldsymbol{\sigma}\, \chi_\kappa^m(\vartheta, \varphi) = -\chi_{-\kappa}^m(\vartheta, \varphi), \tag{A.7}$$

with $\boldsymbol{e}_r = (\cos\varphi \sin\vartheta, \sin\varphi \sin\vartheta, \cos\vartheta)$.

A.2.2 Radial Dirac equation. As explained in chapter 5, basis functions attributed to centre A are constructed either from eigenstates of the channel Hamiltonian $H_A' = -i\boldsymbol{\alpha} \cdot \nabla' + \beta - eV_A(r_A)$ (for bound states) or as superpositions of continuum eigenfunctions of H_A' (in the case of wave packets). A simultaneous eigenfunction

---

[2]Spin-angular functions $\chi_\kappa^m(\vartheta, \varphi)$ are also known as central field spinors [Ros61], spinor spherical harmonics [Sch95], or spherical spinors [SFVW95B]. In the literature *many* different phase conventions for spin-angular functions, spherical harmonics, and associated Legendre polynomials can be found. For example, the present choice is in agreement with [AS65, PTVF92, Jac99] regarding associated Legendre polynomials (but disagreeing with [Edm57]), in agreement with [Edm57, Ros61, Dav65, PTVF92, Jac99] regarding spherical harmonics (but disagreeing with [Sch55], [BS77], as well as [LL86, BLP82]), and finally in agreement with [Ros61] regarding the Clebsch-Gordon coefficients which determine the spherical spinors. In consequence of different phase conventions, equation (A.7) does not hold for spin-angular functions as defined, e.g., in [BD66] or [BLP82]. However, similar equations are given by the latter authors. In the present work, the numerical algorithm of [PTVF92, sec. 6.8] is used to compute associated Legendre functions, in combination with the definition of spherical spinors $\chi_\kappa^m(\vartheta, \varphi)$ as in [Ros61, eq. (1.60')].

$\phi_A(\boldsymbol{x}')$ of the operators H_A', K' and J'^3, with eigenvalues ϵ, κ and m respectively, is of the form (A.6). Owing to equation (A.7) it can be verified that the eigenvalue equation,

$$[H_A' - \epsilon]\,\phi_A(\boldsymbol{x}') = 0,$$

is equivalent to the following radial Dirac equation for the radial wave functions $P(r_A)$ and $Q(r_A)$:

$$\frac{\mathrm{d}}{\mathrm{d}r_A}\begin{pmatrix} P(r_A) \\ Q(r_A) \end{pmatrix} = \begin{pmatrix} -\dfrac{\kappa}{r_A} & -\epsilon - eV_A(r_A) - 1 \\ \epsilon + eV_A(r_A) - 1 & \dfrac{\kappa}{r_A} \end{pmatrix}\begin{pmatrix} P(r_A) \\ Q(r_A) \end{pmatrix}. \qquad (A.8)$$

Note that the imaginary factor in equation (A.6) leads to the present form (A.8) of the radial Dirac equation, which allows for real-valued solutions $P(r_A)$ and $Q(r_A)$.

An algorithm for an accurate numerical solution of the radial differential equation (A.8) has been published by Salvat et al. [SM91, SFVW95A, SFVW95B]. It assumes that a singularity of the radial potential $V_A(r)$ at $r = 0$ is at most Coulomb-like, more precisely,

$$\lim_{r \to 0} V_A(r) r < \infty,$$

is assumed. Furthermore, it is assumed that the potential $V_A(r)$ vanishes as r tends to infinity and that the limit

$$\lim_{r \to \infty} V_A(r) r = \tilde{Z}_A$$

exists. The algorithm of Salvat et al. allows for the computation of the radial wave functions of normalised bound states and determines their eigenvalues at the same time. Furthermore, radial wave functions corresponding to continuum eigenfunctions with positive energy $\epsilon > 1$ can be determined. The latter radial functions are normalised by the code of Savat et al. such that the upper component $P(r)$ is oscillating with unit amplitude as $r \to \infty$. Only *regular* solutions of the radial Dirac equation are computed, which are distinguished by their property of square integrability at the boundary $r = 0$. For this work the code of Salvat et al. has been ported to the C programming language and extended to allow for the computation of radial wave functions of negative energy $\epsilon < -1$.

The normalisation of continuum eigenfunctions $\phi_{A,\epsilon}(\boldsymbol{x}')$ on the energy scale is obtained by a multiplication of their radial wave functions $P(r_A)$ and $Q(r_A)$ by the factor,

$$\frac{1}{\sqrt{\pi}}\left(\frac{\epsilon + 1}{\epsilon - 1}\right)^{1/4}.$$

That normalisation of continuum wave functions provides that radial wave packets of the form,

$$\frac{1}{\sqrt{\Delta_\epsilon}}\int_{\epsilon - \Delta_\epsilon/2}^{\epsilon + \Delta_\epsilon/2}\phi_{A,\epsilon}(\boldsymbol{x}')\,\mathrm{d}\epsilon,$$

are normalised in the primed frame.

For the numerical calculations presented in this work the Coulomb potential $V_\Gamma(r_\Gamma) = eZ_\Gamma/r_\Gamma$ has been considered for both centres $\Gamma = A, B$. However, due

to the fact that the radial wave functions of the basis functions are determined by
a numerical integration of the radial Dirac equation (A.8), it is straightforward to
extend the existing code to allow for a numerical coupled channel solution of a two-
centre Dirac equation with more general moving charge distributions. This possibility
has motivated the preference of the present determination of the radial wave func-
tions over other numerical methods to compute Coulomb-Dirac wave functions or the
related Whittaker functions [AS65, MRG73, GMR85, CEL].

A.2.3 Implementation details. For bound states, the radial wave functions are
computed at the beginning of a coupled channel calculation and tabulated for a few
thousand radii for later linear interpolation. The size of the radial grid in relativistic
units was chosen according to $r_{\max} = (2n^2 + Cn^{1.2})/(e^2 Z)$, with a constant C taking
a value between 15 and 20. Here Z is the charge number of the respective centre and
n the principal quantum number of the bound state. Wave functions of wave packets
are integrated using a Gaussian quadrature formula for the energy integration and
tabulated in the same way as bound state radial wave functions, to allow for the
later evaluation of the radial functions by linear interpolation. For the wave packets
as described in section 6.6 a radial grid of size 200 r.u. was used. To check the
code, radial wave functions obtained by the present program have been compared to
corresponding plots published in [BS85].

For numerical calculations, a finite coupled channel basis has to be specified. In
the present program this can be done partly by command line parameters, denoted
by `nmaxA`, `nmaxB`, `kappaA` and `kappaB` (cf. table A.1). The first two parameters
determine the maximum principal quantum number of bound-state basis functions of
centres A and B respectively. The second two parameters fix the maximum absolute
values of the spin-orbit quantum numbers κ of free-particle basis functions. The
mean energies $\bar{\epsilon}$ and the widths Δ_ϵ of the energy interval of wave packets cannot be
chosen on the command line presently. In the source code tabulated radial Dirac
wave functions attributed to the same centre are subsumed by an object of the class
`DiracRadialBasis`. It is the constructor of this class that evaluates radial wave
functions according to the algorithm of Salvat et al..

A.3 Quadrature formulas

The three-dimensional integrals presented in section 5.3 have to be evaluated fully
numerically. This evaluation takes the major part of the computing time and is,
hence, the reason for the numerical complexity of the computational task of solving
the relativistic coupled channel equations (4.8). Efficient quadrature formulas for
these integrals will take into account the distance between the centres as well as the
fact whether the two states occurring in the integrand are located at the same or
a at different centres. Therefore, two different quadrature schemes are used in the
program. Both procedures introduce some curved spatial coordinates in the com-
putational, unprimed frame of reference. The three-volume integrals (5.10), (5.11),
(5.15) and (5.16) are then rewritten as a sequence of three nested one-dimensional in-
tegrals over these curved coordinates. The latter are evaluated successively by means
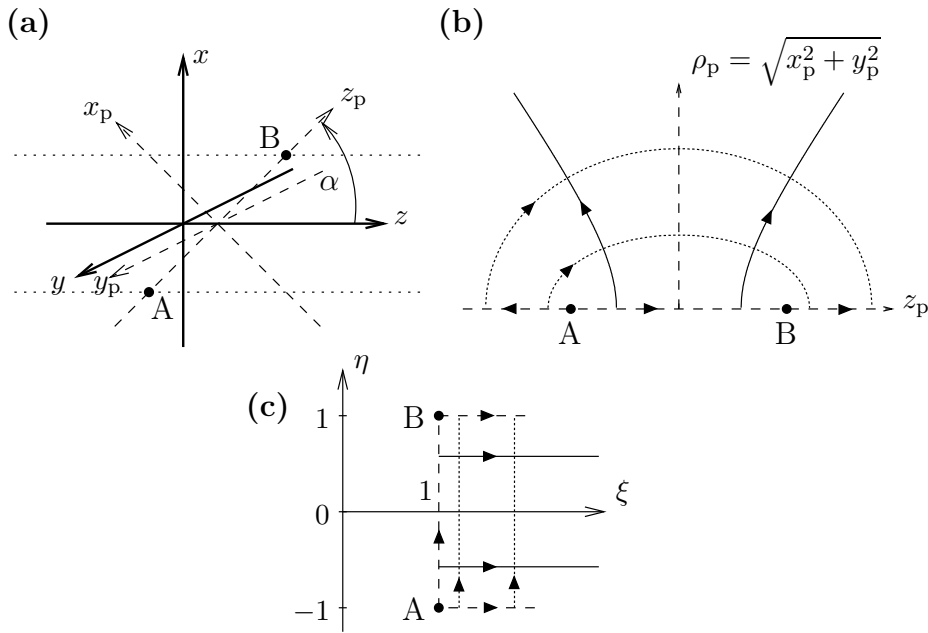
FIGURE A.1. Prolate spheroidal coordinates. (a) The centres A and B are moving in the x-z-plane. The straight line going through the centres, from A to B, defines the z_p-coordinate axis. (b) A half-plane is rotated around the z_p-axis. (c) The half-plane is parameterised by elliptical coordinates.

of one-dimensional quadrature formulas. The first quadrature method described below is based on prolate spheroidal coordinates, the second on contracted spherical coordinates around one of the centres.

A.3.1 Quadrature using prolate spheroidal coordinates. If the distance of the centres A and B is small compared to the extension of the integrand and in the case of scalar products between states located at different centres, a quadrature method based on prolate spheroidal coordinates is employed. These coordinates are elliptical coordinates of the half-plane which are rotated into the third spatial dimension in order to obtain coordinates of the whole three-dimensional space [AS65, MS88]. Their definition in the present context is depicted in figure A.1.

Elliptical coordinates are rotated around the z_p-axis which is defined as the coordinate axis passing through the centres from A to B at some fixed time t. Let $\rho_p = \sqrt{x_p^2 + y_p^2}$ denote the distance of some point (x, y, z) from the z_p-axis. Elliptical coordinates (ξ, η) of the (z_p, ρ_p)-half-plane can be defined in terms of a conformal mapping, namely the principal branch of the complex arcsin-function [AS65, FL92], as follows:

$$\xi = \cosh\left(\Im \arcsin \frac{z_p + i\rho_p}{f}\right),$$

$$\eta = \sin\left(\Re \arcsin \frac{z_p + i\rho_p}{f}\right).$$

By this mapping the (z_p, ρ_p)-half-plane is mapped one to one and onto the strip,

$$1 \leq \xi < \infty \qquad \text{and} \qquad -1 \leq \eta \leq 1.$$

The inverse mapping is simply given by:

$$z_{\mathrm{p}} = f\xi\eta, \qquad \rho_{\mathrm{p}} = f\sqrt{(\xi^2 - 1)(1 - \eta^2)}. \tag{A.9}$$

Therefore, while passing over from Cartesian coordinates (x, y, z) to prolate spheroidal coordinates (ξ, η, φ), where φ is the angle of rotation around the z_{p}-axis, the volume element transforms like:

$$\mathrm{d}x\,\mathrm{d}y\,\mathrm{d}z = \mathrm{d}\varphi\,\rho_{\mathrm{p}}\,\mathrm{d}\rho_{\mathrm{p}}\,\mathrm{d}z_{\mathrm{p}} = f^3(\xi^2 - \eta^2)\,\mathrm{d}\varphi\,\mathrm{d}\eta\,\mathrm{d}\xi.$$

For large ξ the quantity $f\xi$ is approximately equal to the spatial distance of some point with the coordinates (ξ, η, φ) from the origin of the $(x_{\mathrm{p}}, y_{\mathrm{p}}, z_{\mathrm{p}})$-coordinate system.

For their numerical evaluation the infinite-volume integrals (5.10), (5.11), (5.15) and (5.16) are approximated by nested one-dimensional integrals over finite intervals,

$$\int_1^{\xi_{\max}} \mathrm{d}\xi \int_{-1}^1 \mathrm{d}\eta \int_0^{2\pi} \mathrm{d}\varphi\, f^3(\xi^2 - \eta^2)\, \dots\,,$$

since the relevant integrands are expected to give negligible contributions to the infinite integral outside some sufficiently large ellipsoid characterised by $\xi < \xi_{\max}$. The ξ- and η-integrals are then computed by Gauß-Legendre quadrature formulas which corresponds to a polynomial interpolation of the integrand as a function of ξ and η respectively, see e.g. [AS65, PTVF92, DH93]. The φ-integration is carried out using the extended trapezoidal rule which is more simple than the Gauß-Legendre quadrature. Nonetheless, it is appropriate because the integrand is periodic in φ and the n-point extended trapezoidal rule is an exact quadrature formula for all trigonometric polynomials up to the order $n - 1$. The n-point extended trapezoidal rule for the φ-integral corresponds to an integral over the interpolation of the integrand using a trigonometric polynomial of the order $n-1$. Contrary to the Gauß-Legendre quadrature formula the trapezoidal rule takes into account the periodicity of the integrand in φ [HH89, DR75, DH93].

In order to evaluate the integrand for some space-time point with coordinates (t, ξ, η, φ) the space-time coordinates $(t', r_{\mathrm{A}}, \vartheta_{\mathrm{A}}, \varphi_{\mathrm{A}})$ and $(t'', r_{\mathrm{B}}, \vartheta_{\mathrm{B}}, \varphi_{\mathrm{B}})$ of this event have to be computed. For the sake of completeness the transformations performed by the program will be described here. Starting from prolate spheroidal coordinates (ξ, η, φ) the spatial Cartesian coordinates $(x_{\mathrm{p}}, y_{\mathrm{p}}, z_{\mathrm{p}})$ are determined according to equation (A.9) and the following relations:

$$x_{\mathrm{p}} = \rho_{\mathrm{p}}\cos\varphi, \qquad y_{\mathrm{p}} = \rho_{\mathrm{p}}\sin\varphi.$$

The Cartesian coordinates (x, y, z) are then obtained by a rotation around the y_{p}-axis followed by a translation in z-direction:

$$x = x_{\mathrm{p}}\cos\alpha + z_{\mathrm{p}}\sin\alpha, \qquad y = y_{\mathrm{p}}, \qquad z = -x_{\mathrm{p}}\sin\alpha + z_{\mathrm{p}}\cos\alpha + \frac{t(v_{\mathrm{B}} + v_{\mathrm{A}})}{2}.$$

Here the coefficients of the rotation matrix are given by:

$$\sin\alpha = \frac{b}{2f}, \qquad \cos\alpha = \frac{t(v_{\mathrm{B}} - v_{\mathrm{A}})}{2f}.$$

Finally the space-time coordinates $(t', r_{\mathrm{A}}, \vartheta_{\mathrm{A}}, \varphi_{\mathrm{A}})$ and $(t'', r_{\mathrm{B}}, \vartheta_{\mathrm{B}}, \varphi_{\mathrm{B}})$ are computed from (t, x, y, z) by Lorentz boosts according to equations (A.3), (A.4) and (A.5).

It is important to note that the times t' and t'' in the rest frames of the respective centres, are functions of both t and z. For some particular time t they, therefore, have to be evaluated for each spatial coordinate (ξ, η, φ) separately. For the purpose of computational efficiency there are different functions implementing the coordinate transformation for computations in the collider frame, where $\chi_A = -\chi_B$, for computations in the rest frame of centre A, where $\chi_A = 0$, and for arbitrary frames of reference.

Quadrature methods based on prolate spheroidal coordinates have also been used in nonrelativistic coupled channel calculations [FRI] and by Toshima and Eichler for their relativistic calculations of excitation and charge transfer in the target frame [TE88A].

A.3.2 Quadrature using contracted and translated spherical coordinates.

For scalar products at large times t, between states which are located at the same projectile Γ (single centre integrals), a quadrature method is used that is based on the radial coordinates $(r_\Gamma, \vartheta_\Gamma, \varphi_\Gamma)$ defined in equation (A.5). A short calculation shows that the volume element $\mathrm{d}x\,\mathrm{d}y\,\mathrm{d}z$ in the unprimed frame is given in terms of the radial coordinates of the boosted frame at time t by:

$$\mathrm{d}x\,\mathrm{d}y\,\mathrm{d}z = \frac{r_\Gamma^2}{\gamma_\Gamma}\,\mathrm{d}r_\Gamma\,\mathrm{d}\cos\vartheta_\Gamma\,\mathrm{d}\varphi_\Gamma.$$

In order to verify this relation, it must be remembered that the Cartesian coordinate z at time t in the unprimed frame may be written as,

$$z = \frac{r_\Gamma \cos\vartheta_\Gamma}{\gamma_\Gamma} + v_\Gamma t, \tag{A.10}$$

due to the uniform motion of centre Γ. For a numerical evaluation, the matrix elements (5.11) and (5.16) are approximated by nested one-dimensional integrals of the form,

$$\int_0^{r_{\max}}\mathrm{d}r_\Gamma \int_{-1}^{1}\mathrm{d}\cos\vartheta_\Gamma \int_0^{2\pi}\mathrm{d}\varphi_\Gamma\,\frac{r_\Gamma^2}{\gamma_\Gamma}\ldots,$$

similarly to the previous subsection. Gauß-Legendre quadrature formulas are used for the computation of the r_Γ- and $\cos\vartheta_\Gamma$-integrals and the extended trapezoidal rule for the φ_Γ-integral for the same reasons as described above.

In order to evaluate the integrand of an interaction matrix element between two basis functions located both, e.g., at centre A (cf. equations (5.11) and (5.16)) it is necessary to calculate times t' and t'', the distance d_B, and the radius r_B. Here the radius r_B must correspond to a space-time point with spatial coordinates $(r_A, \cos\vartheta_A, \varphi_A)$ in rest frame A, but with time t in the unprimed coordinate system.

The times t' and t'', of the rest frames of centre A and B respectively, are obtained by first determining z, as in equation (A.10), and then using the relations $t' = \gamma_A(t - v_A z)$ and $t'' = \gamma_B(t - v_B z)$. The radius r_B must be computed according to,

$$r_B = \left[(r_A \sin\vartheta_A)^2 + b^2 + z''^2 - 2b\,r_A \sin\vartheta_A \cos\varphi_A\right]^{\frac{1}{2}},$$

where $z'' = \gamma_B(z - v_B t)$, as already defined above, and $\sin \vartheta_A = \sqrt{1 - (\cos \vartheta_A)^2}$. The distance d_B, as given in equation (5.3), can be expressed simply in terms of t''.

An analogous procedure has been implemented for the numerical determination of matrix elements between two basis functions that are both located at centre B.

A.3.3 Discussion and improvements. The evaluation of the elements of the interaction and overlap matrices, $N(t)$ and $V(t)$, is the main reason for the computational complexity of relativistic coupled-channel calculations as presented in this thesis. In [RSG93, BRBW94] *single*-centre coupled channel calculations of heavy-ion collisions using much larger bases have been reported. As the coupled channel basis in that approach is comprised of eigenstates (and wave packets) of one centre only, there are no two-centre matrix elements. However, in the present two-centre calculations the number of two-centre integrals that have to be evaluated is nearly twice as large as the number of single-centre integrals, showing that the major effort is to compute the former.

In [RSG93, BRBW94] Coulomb boundary conditions have not been used and calculations have been carried out in the rest frame of the basis functions (target frame). As described in [RSG93] the external field of a point-like projectile can be decomposed into a multipole series (see also [EM95]). Although, compared to the nonrelativistic case, this expansion is complicated slightly by the Lorentz contraction of the projectile potential, angular momentum algebra can be used to reduce the computational effort of determination of the matrix elements. Three-dimensional integrals for the interaction matrix elements $V_{ij}(t)$ can be reduced to infinite sums over two one-dimensional integrals, one of which does not need to be evaluated for every pair of indices (i, j) separately, because it mainly depends on the spin-angular quantum numbers of the corresponding basis functions [RSG93]. This integration method is not applicable if coupled channel calculations with phase-distorted basis functions are considered, as done in this work. If coupled channel calculations not satisfying Coulomb boundary conditions are an option, the program can be optimised by evaluating the single-centre integrals according to the method described in [RSG93].

We conclude this section with a few remarks about further ideas to optimise the numerical quadrature. Two-dimensional quadrature formulas for the integration on the unit sphere have been developed for numerical calculations of quantum chemistry [DEL96]. These might turn out to be more efficient than the present integration method for the unit sphere using nested one-dimensional quadrature formulas. Another feature of the presently adopted quadrature formulas is the use of a fixed number of points, independent of, e.g., the distance between the centres. One should expect, however, that the convergence of the quadrature formulas with respect to the number of points at which the integrands must be evaluated does depend on the distance of the centres and the different types of wave functions. Therefore, adaptive quadrature methods based on extrapolation techniques (Romberg quadrature) might be more powerful [PTVF92, DH93]. On the other hand, the Romberg quadrature method requires sufficient smoothness of the integrand, which is not provided by the present evaluation of radial wave functions by linear interpolation of tabulated data. Finally, there are alternatives to the use of prolate spheroidal coordinates for the

quadrature of two-centre integrals. Different multi-centre integration schemes have been developed for calculations in quantum chemistry. E.g., the decomposition of multi-centre integrals into a sum of weighted single-centre integrals, as described in [Bec88, PJB94], is applicable in principal also in the present context. In conclusion, we have proposed improvements of the present quadrature schemes. It must be remembered, however, that all these proposals require careful and time-consuming implementation, testing and evaluation before they can replace the present methods. They should be object of future work.

A.4 Integration of the coupled channel equations

A.4.1 Matrix computations. The program integrates the coupled differential equations (4.8) for undistorted and phase-distorted bases simultaneously. For the integration of these differential equations the coefficient matrices,

$$-iN(t)^{-1}V(t),$$

must be determined for both choices of the basis functions. This is achieved by means of an LU-decomposition [PTVF92, DH93] of the respective overlap matrix $N(t)$. For matrix computations the 'Template Numerical Toolkit' (TNT) [Poz00] has been used and slightly extended to allow for the LU-decomposition of complex-valued matrices.

Singular value decompositions of the fundamental solution matrices $F(t, t_i)$, as described in subsection 4.2.1 and presented in figures 5.3 and 5.4, have been performed by interfacing the TNT package to the Fortran library for linear algebra LAPACK [ABB$^+$99]. The latter is optimised and available in binary format for many computing architectures. It provides the Fortran routines `ZGESVD` and `CGESVD`, which implement the singular value decomposition for complex-valued matrices.

A.4.2 Time integration. The overlap and interaction matrices $N(t)$ and $V(t)$ are numerically evaluated only for the times of a time grid. This time grid has upper and lower boundaries t_f and t_i, usually chosen in a symmetrical manner as $t_i = -t_f$. The spacing of the time grid is chosen to be equidistant, with a time step Δ_t, except for an inner time-interval. In this inner time-interval, ranging from $-t_{inner}$ to t_{inner}, the equidistant spacing can be made smaller, using the time step $\Delta_{t,inner}$. These five parameters defining the time grid are controlled by command line parameters of the program, which are summarised in table A.1.

For times t not part of the time grid, the matrix $-iN(t)^{-1}V(t)$ of coefficients of the linear differential equation (4.8) is linearly interpolated. In the program this is achieved by means of the class `MatrixInterpolationTNT`. The integration of the coupled channel equations is, therefore, based on this linear interpolation function of the coefficient matrices.

For the integration of the differential equation over time intervals of the time grid, a sophisticated algorithm described in [PTVF92, ch. 16] is used. The powerful Burlisch–Stoer extrapolation technique is combined with a stepsize-control algorithm proposed by Deuflhard. In the present numerical code this integration method has

been implemented for differential equations with complex-valued coefficients as a class called `GBSDIntegrationTNT`.

The integration method works as follows: For a given stepsize H the so-called modified midpoint method is used to integrate the fundamental solution $F(t, t_i)$ from some time t to the time $t + H$. This method subdivides the stepsize H into n substeps each of size $h = H/n$. The modified midpoint rule is applied several times with increasing n, yielding several results for the same integration step from t to $t+H$. These different results are then extrapolated to the limit of vanishing substep-size, $h = 0$, using a polynomial interpolation (Richardson's deferred approach to the limit). If the (estimated) numerical error of this extrapolation is larger than a given error bound the stepsize H may be reduced. The stepsize adjustment strategy proposed by Deuflhard, described in [PTVF92, sec. 16.4], has been used with minor modifications for the present program.

A time grid has been used for the integration of the coupled channel equations also in [TE88A]. The effect of the Burlisch–Stoer–Deuflhard integration method in the present context is that the accuracy of the numerically evaluated fundamental solution $F(t, t_i)$ is practically determined by the choice of the time grid only. In order to control this accuracy the asymptotic unitarity of the fundamental solution can be verified. As described in section 4.2 asymptotic unitarity is provided, if the singular values of the fundamental solution are all equal to one at large times t. The smaller grid spacings in the inner time-interval $[-t_{\text{inner}}, t_{\text{inner}}]$ of the time grid allows for a rough adaption: At small times t the coefficients of the differential equations grow strongly as t tends to zero, due to maximum interaction at the closest approach of the centres (see e.g. figures 5.1 to 5.4).

A.4.3 Improvements. It may be attempted to apply the Burlisch–Stoer–Deuflhard integration method directly, without using a time grid and interpolating the coefficient matrices. However, it must be remembered that the numerical calculation of the overlap and interaction matrices by three-dimensional quadrature is very time-consuming and the use of directly evaluated coefficient matrices may actually increase the computing time. Furthermore extrapolation techniques, as the integration method described, require sufficient smoothness of the numerically evaluated coefficients as a function of time [PTVF92]. This may not be provided due to numerical inaccuracies of the quadrature formulas described above, but it is clearly true for the linear interpolation used for numerical calculations of this work. Finally note that using cubic splines for the interpolation of the coefficient matrices is presumably a valuable improvement of the present code, allowing for a larger spacing of the time grid and providing the necessary smoothness of the coefficients necessary for the Burlisch–Stoer–Deuflhard method.

A.5 Distributed computations

The numerical code has to perform two different tasks: On one hand, the numerical evaluation of the matrix elements, on the other hand the time integration of the coupled channel equations. In principle these two tasks can be separated from each other. They may be implemented in different programs, provided the matrix elements

can be passed from one program to the other. The latter could be achieved by storing the matrix elements, or the coefficient matrices of the differential equation, on mass storage devices. Another possibility is to write software that is able to exchange data using communication links.

The latter approach has been implemented. In this approach the process integrating the differential equations (master process) sends requests for matrix elements to a process only evaluating matrix elements (server process). A single master process is able to communicate with several different server processes. In the present program, a request of the master process sent to a server process contains the values of the following parameters:

$$\chi_{\mathrm{B}}^{\mathrm{c}}, \chi_{\mathrm{frame}}^{\mathrm{c}}, b, t, i \text{ and } j. \tag{A.11}$$

Here i and j are the row and column indices of the requested matrix elements. After the computation, of overlap and matrix elements for undistorted as well as phase-distorted bases, the server process returns four complex numbers to the master, namely the values of the matrix elements:

$$N_{ij}^{\mathrm{u}}(t), V_{ij}^{\mathrm{u}}(t), N_{ij}^{\mathrm{p}}(t) \text{ and } V_{ij}^{\mathrm{p}}(t).$$

Here the superscripts u and p refer to undistorted and phase-distorted bases respectively. As soon as the master process receives these results from a particular server process the former sends a new request to the server. The master process communicates with all server processes simultaneously, assembles the overlap and interaction matrices, determines the matrix of coefficients $-\mathrm{i}N(t)^{-1}V(t)$, integrates the differential equations and writes the results to several output files.

The program is constructed such that it can either take the role of a master or a server process. Typically, several processes are started simultaneously on different processors or networked computers. These processes are numbered and the first process automatically takes the role of the master process, establishing communication links to the other processes, which automatically start their operation in the server mode. If only a single process is started, it carries out both tasks, evaluating matrix elements and integrating the differential equations.

The principal advantage of the multiple-processor over single-processor computations is the much increased computing speed. E.g., a computation taking several days on a single-processor workstation could be executed on a network of workstations and personal computers during several hours. In many numerical calculations of this work multiple-processor computations have been necessary in order to get acceptable compute times. In addition, the parallelisation of the code allowed for the use of massively parallel processor systems, providing access to such powerful computing machinery.

A.5.1 Implementation details. Two different kinds of computing facilities have been used for the present work. On one hand, a heterogeneous network of workstations and personal computers connected via standard ethernet hardware, on the other hand, massively parallel processor systems of type Cray T3E. The communication between processes was realised by means of the massage passing interface [MPI96, GLS99]. Due to the fact that an implementation of the message passing interface is available both for TCP/IP-connected workstations [MPI00] and for the

proprietary hardware of the Cray T3E, it was technically feasible to write a *portable* code that could be used on both types of hardware.

We would like to close this appendix with a few remarks about technical aspects. The network of workstations and personal computers, connected via ethernet, included several different computing architectures, namely: Compaq True64 Unix running on workstations with Alpha processors, Sun Solaris for Sun Sparc computers, Hewlett-Packard Ultrix on HP-RISC computers, and Linux for personal computers with Intel processors. For all these systems (and additionally the Cray T3E architecture) the program sources had to be compiled and linked using different, partially incompatible compilers and linkers. This fact required adapting of sources to the various environments, selectable by preprocessor directives [REG96] and compiler options. Having made available binaries of the program for the different computing architectures, the latter have been used simultaneously for a single, distributed coupled channel calculation. Typical distributed computations lasted several hours.

Finally, it should be emphasised that priority has always been given to numerical accuracy leading to long compute times. The optimisation of both accuracy and computing speed at the same time must be an object of future work. The potential for such improvements has been partly described in this appendix.

Mathematical Supplement

This appendix provides some mathematical results not found in the literature in the specific form necessary for this work. Their proofs are either outlined or given in detail.

B.1 Spreading of regular wave packets

In this section, a mathematical theorem regarding the spreading of free Dirac wave packets is formulated. It is applied in the existence and orthogonality proofs for the wave operators in sections 3.3 and 3.4.

A free Dirac wave packet $\phi(\boldsymbol{x})$ is a linear superposition of plane waves:

$$\phi(\boldsymbol{x}) = (2\pi)^{-\frac{3}{2}} \int \mathrm{e}^{\mathrm{i}\boldsymbol{x}\cdot\boldsymbol{p}}\, \hat{\phi}(\boldsymbol{p})\, \mathrm{d}^3 p. \tag{B.1}$$

Here $\hat{\phi}(\boldsymbol{p})$ denotes the Fourier transform of $\phi(\boldsymbol{x})$, which obviously must be four-spinors. The time-evolution of $\phi(\boldsymbol{x})$ is most easily written in terms of the Fourier transform $\hat{\phi}(\boldsymbol{p})$. It is necessary for that purpose to make a spectral decomposition of the state space with respect to the free Dirac Hamiltonian $H_0 = -\mathrm{i}\boldsymbol{\alpha}\cdot\nabla + \beta$. Orthogonal projectors $P_{\mathrm{C}\pm}$ onto the spectral subspaces of H_0 of positive and negative energy respectively,

$$P_{\mathrm{C}\pm} = \frac{1}{2}\left(1 \pm \frac{H_0}{|H_0|}\right),$$

are given in momentum space by a simple multiplication operator:

$$P_{\mathrm{C}\pm} = \frac{\mu(\boldsymbol{p}) \pm \boldsymbol{p}\cdot\boldsymbol{\alpha} \pm \beta}{2\mu(\boldsymbol{p})}$$

(see e.g. [THA92, SCH95]). Here,

$$\mu(\boldsymbol{p}) = \sqrt{1 + \boldsymbol{p}^2},$$

denotes the relativistic energy of a free electron with momentum $\boldsymbol{p}$. Due to the property,

$$P_{\mathrm{C}+} + P_{\mathrm{C}-} = 1,$$

the Fourier transform $\hat{\phi}(\boldsymbol{p})$ may be decomposed by means of these projectors $P_{\mathrm{C}\pm}$ into a sum of two functions,

$$\hat{\phi}(\boldsymbol{p}) = \hat{\phi}_+(\boldsymbol{p}) + \hat{\phi}_-(\boldsymbol{p}),$$

where

$$\hat{\phi}_\pm(\boldsymbol{p}) = P_{\mathrm{C}\pm}\hat{\phi}(\boldsymbol{p}).$$

113

The free time-evolution $\Phi(t, \boldsymbol{x}) = \mathrm{e}^{-\mathrm{i}tH_0}\,\phi(\boldsymbol{x})$ of the initial wave packet $\phi(\boldsymbol{x})$ is then given by,

$$\Phi(t, \boldsymbol{x}) = (2\pi)^{-\frac{3}{2}} \int \mathrm{e}^{\mathrm{i}\boldsymbol{x}\cdot\boldsymbol{p}} \left\{ \mathrm{e}^{\mathrm{i}t\mu(\boldsymbol{p})}\,\hat{\phi}_+(\boldsymbol{p}) + \mathrm{e}^{-\mathrm{i}t\mu(\boldsymbol{p})}\,\hat{\phi}_-(\boldsymbol{p}) \right\} \mathrm{d}^3p,$$

because in the momentum representation and on the spectral subspaces of H_0, which have been introduced above, the free unitary time-evolution $\mathrm{e}^{-\mathrm{i}tH_0}$ is simply a multiplication operator (see e.g. [THA92, SCH95]).

B.1.1 Regular wave packets. In this work, a regular wave packet is defined as a wave packet $\Phi(t, \boldsymbol{x}) = \mathrm{e}^{-\mathrm{i}tH_0}\,\phi(\boldsymbol{x})$ where each component of the Fourier transform $\hat{\phi}(\boldsymbol{x})$ has compact support and is infinitely differentiable. Making use of the notation common in the mathematical physics literature [RUD74, RS80, KAT80], a regular wave packet, therefore, satisfies by definition:

$$\hat{\phi}(\boldsymbol{x}) \in C_0^\infty(\mathbb{R}^3)^4.$$

The term 'regular wave packet' is taken from the corresponding definition in the case of the Klein-Gordon field in [RS79, p. 42], where the term smooth solution is used synonymously.

The importance of regular wave packets of the free Dirac equation in this work is manifested in following property, which is useful in scattering theory. A regular free Dirac wave packet (in three spatial dimensions) satisfies for any time t and coordinate $\boldsymbol{x}$ the following inequality:

$$\|\Phi(t, \boldsymbol{x})\|_2 \leq \frac{\text{const.}}{(1 + |t|)^{3/2}}. \tag{B.2}$$

Since the L^2-norm $\|\Phi(t)\|$ is time-independent this inequality describes the spatial spreading of the wave packet for large times t.

A mathematical proof of this statement is possible with the aid of the method of stationary phase [HÖR76, RS79]. Noting that $\hat{\phi}_+(\boldsymbol{x}), \hat{\phi}_-(\boldsymbol{x}) \in C_0^\infty(\mathbb{R}^3)^4$ for regular wave packets, mainly the Corollary to Theorem XI.15 in [RS79] has to be be applied. Although the explicit proof in the case of the Dirac equation was not found in the literature, its details will not be presented here. A similar result for regular wave packets of the Klein-Gordon equation constitutes Theorem XI.17(b) in [RS79].

B.2 Lorentz invariance of the scalar product

In this section, it is proved that the scalar product $(\Psi_1(t), \Psi_2(t))$ between two wave functions $\Psi_1(t, \boldsymbol{x})$ and $\Psi_2(t, \boldsymbol{x})$ is invariant under Lorentz-boosts, if they are both solutions of the same Dirac equation. Lorentz-invariance means that the scalar product $(\Psi_1'(t'), \Psi_2'(t'))'$ in a Lorentz-transformed frame between the Lorentz-transformed wave functions $\Psi_1'(t', \boldsymbol{x}')$ and $\Psi_2'(t', \boldsymbol{x}')$ satisfies,

$$\left(\Psi_1'(t'), \Psi_2'(t')\right)' = \left(\Psi_1(t), \Psi_2(t)\right), \tag{B.3}$$

for arbitrary t and t'. The assumptions necessary to prove this result will be stated in the subsequent presentation. Only Lorentz boosts will be considered since rotations and translations do not transform the time axis and the time-independence of the

scalar product is equivalent to the unitarity of the time evolution. The existence of such a unitary time evolution will be assumed here.

Consider two Dirac wave functions $\Psi_1(t, \boldsymbol{x})$ and $\Psi_2(t, \boldsymbol{x})$ which are solutions of the same Dirac equation,

$$[H_0 + W(t, \boldsymbol{x}) - \mathrm{i}\partial_t]\,\Psi_i(t, \boldsymbol{x}) = 0, \qquad i = 1, 2.$$

The external field $W(t, \boldsymbol{x})$ is required to be a hermitian matrix, i.e.

$$W(t, \boldsymbol{x})^\dagger = W(t, \boldsymbol{x}),$$

which is true in particular for external electromagnetic fields $(A^0, \boldsymbol{A})$, where $W(t, \boldsymbol{x}) = q(A^0 - \boldsymbol{\alpha} \cdot \boldsymbol{A})$. The hermitian conjugate Dirac spinors $\Psi_i^\dagger(t, \boldsymbol{x})$ then solve the following hermitian conjugate equation,

$$\mathrm{i}\nabla \cdot (\Psi_i^\dagger \boldsymbol{\alpha}) + \Psi_i^\dagger \gamma^0 + \mathrm{i}\partial_t \Psi_i^\dagger + \Psi_i^\dagger W = 0.$$

By taking the difference between the hermitian conjugate equation for Ψ_1 multiplied from the right by Ψ_2 and the Dirac equation for Ψ_2 multiplied from the left by $\Psi_1^\dagger$ one obtains:

$$\nabla \cdot (\Psi_1^\dagger \boldsymbol{\alpha} \Psi_2) + \partial_t(\Psi_1^\dagger \Psi_2) = 0.$$

Recalling the definition of the adjoint spinor, $\overline{\Psi} = \Psi^\dagger \gamma^0$, this equation may be rewritten as the four-divergence of a complex Lorentz four-vector,

$$\partial_\mu(\overline{\Psi}_1 \gamma^\mu \Psi_2) = 0. \tag{B.4}$$

The familiar continuity equation of the four-current density $j^\mu = q\overline{\Psi}\gamma^\mu\Psi$ is an implication of this result.

In the following $\Lambda = \Lambda(\boldsymbol{v})$ shall denote a pure Lorentz boost from an unprimed Lorentz frame to a primed frame moving with velocity $\boldsymbol{v}$ with respect to the unprimed frame:

$$(\Lambda^\mu{}_\nu) = \begin{pmatrix} \gamma & -\gamma \boldsymbol{v}^{\mathrm{T}} \\ -\gamma \boldsymbol{v} & \left(1 + (\gamma - 1)\hat{\boldsymbol{v}}\hat{\boldsymbol{v}}^T\right) \end{pmatrix},$$
$$x'^\mu = \Lambda^\mu{}_\nu x^\nu. \tag{B.5}$$

Again, γ is the Lorentz factor corresponding to the velocity $\boldsymbol{v}$. In order to show the invariance of the scalar product of Dirac spinors under Lorentz boosts we note that the scalar product at time $t = a$ in the unprimed frame is an integral over a three-dimensional flat hypersurface of Minkowski space,

$$\int_{t=a} \Psi_1^\dagger(t, \boldsymbol{x})\Psi_2(t, \boldsymbol{x})\,\mathrm{d}^3x. \tag{B.6}$$

The same comment applies to the scalar product computed at time $t' = b$ in the primed frame,

$$\int_{t'=b} \Psi_1'^\dagger(t', \boldsymbol{x}')\Psi_2'(t', \boldsymbol{x}')\,\mathrm{d}^3x'. \tag{B.7}$$

The hyperplanes $t = a$ and $t' = b$ may be characterised using the unit timelike normal vectors n^μ and m^μ pointing forward in time:

$$\begin{aligned} \partial D^{\mathrm{a}} &= \{x : n_\mu x^\mu - a = 0, n^\mu = (1, \boldsymbol{0})\} \\ \partial D^{\mathrm{b}} &= \{x : m_\mu x^\mu - b = 0, m^\mu = \gamma(1, \boldsymbol{v})\}\,. \end{aligned}$$
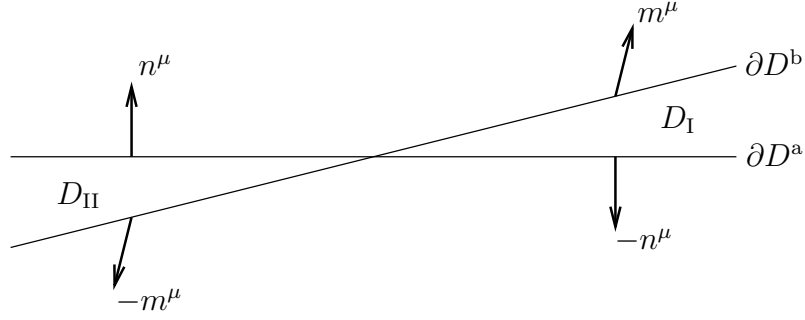
FIGURE B.1. Sketch of four-wedges.

The hyperplanes ∂D^{a} and ∂D^{b} are depicted in figure B.1. The Minkowski space is cut into four subsets by these hyperplanes. Two of them, necessary in the subsequent calculation, are given by the following definitions:

$$D_{\mathrm{I}} = \left\{ x : \ n_\mu x^\mu \geq a \ \text{and} \ m_\mu x^\mu \leq b \right\} = \left\{ x : \ a \leq x^0 \leq \gamma^{-1} b + \boldsymbol{v} \cdot \boldsymbol{x} \right\},$$

$$D_{\mathrm{II}} = \left\{ x : \ n_\mu x^\mu \leq a \ \text{and} \ m_\mu x^\mu \geq b \right\} = \left\{ x : \ \gamma^{-1} b + \boldsymbol{v} \cdot \boldsymbol{x} \leq x^0 \leq a \right\}.$$

Their distinctive feature is that the intersections of D_{I} and D_{II} respectively with the four-dimensional cylinder of radius R, defined through $\boldsymbol{x}^2 \leq R^2$, have finite volume in Minkowski space. The boundaries ∂D_{I} and ∂D_{II} of D_{I} and D_{II} respectively may be decomposed uniquely into flat bounded hypersurfaces,

$$\partial D_{\mathrm{I}} = \partial D_{\mathrm{I}}^{\mathrm{a}} \cup \partial D_{\mathrm{I}}^{\mathrm{b}} \quad \text{and} \quad \partial D_{\mathrm{II}} = \partial D_{\mathrm{II}}^{\mathrm{a}} \cup \partial D_{\mathrm{II}}^{\mathrm{b}},$$

such that the following decomposition is valid at the same time:

$$\partial D^{\mathrm{a}} = \partial D_{\mathrm{I}}^{\mathrm{a}} \cup \partial D_{\mathrm{II}}^{\mathrm{a}} \quad \text{and} \quad \partial D^{\mathrm{b}} = \partial D_{\mathrm{I}}^{\mathrm{b}} \cup \partial D_{\mathrm{II}}^{\mathrm{b}}.$$

See figure B.1 in order to understand this quite formal definitions easily.

To complete the proof, the scalar product (B.7) in the primed frame is rewritten as follows:

$$\int_{t'=b} \Psi_1'^\dagger(t', \boldsymbol{x}') \Psi_2'(t', \boldsymbol{x}') \, \mathrm{d}^3 x'$$

$$= \int_{t'=b} \overline{\Psi}_1(\Lambda^{-1}(t', \boldsymbol{x}')) \, \gamma(\gamma^0 - \boldsymbol{v} \cdot \boldsymbol{\gamma}) \, \Psi_2(\Lambda^{-1}(t', \boldsymbol{x}')) \, \mathrm{d}^3 x'$$

$$= \int_{\partial D^{\mathrm{b}}} \overline{\Psi}_1(t, \boldsymbol{x}) \gamma^\mu \Psi_2(t, \boldsymbol{x}) \, g_{\mu\nu} \, m^\nu \, \mathrm{d}S(x)$$

$$= \int_{\partial D_{\mathrm{I}}^{\mathrm{b}}} \overline{\Psi}_1(x) \gamma^\mu \Psi_2(x) \, m_\nu \, \mathrm{d}S(x) \ - \int_{\partial D_{\mathrm{II}}^{\mathrm{b}}} \overline{\Psi}_1(x) \gamma^\mu \Psi_2(x) \, (-m_\nu) \, \mathrm{d}S(x)$$

Here $\mathrm{d}S(x)$ denotes the hypersurface element at the space-time point x (following the notation of [FOR84]). The scalar product in the unprimed frame may be written in a similar form:

$$\int_{t=a} \Psi_1^\dagger(t, \boldsymbol{x}) \Psi_2(t, \boldsymbol{x}) \, \mathrm{d}^3 x$$

$$= \ -\int_{\partial D_{\mathrm{I}}^{\mathrm{a}}} \overline{\Psi}_1(x) \gamma^\mu \Psi_2(x) \, (-n_\nu) \, \mathrm{d}S(x) \ + \int_{\partial D_{\mathrm{II}}^{\mathrm{a}}} \overline{\Psi}_1(x) \gamma^\mu \Psi_2(x) \, n_\nu \, \mathrm{d}S(x)$$

The unit four-vectors appearing in the integrands above are the outer normal vectors on the boundaries of the four-volumes D_{I} and D_{II} respectively. If the solutions $\Psi_1(x)$

and $\Psi_2(x)$ decay sufficiently rapidly at *spatial* infinity for all t then the integral theorem of Gauß in four dimensions [FOR84, DAS93] may be used to conclude that the difference between the scalar products (B.6) and (B.7) is given in terms of four-dimensional volume integrals over the 'wedges' D_{I} and D_{II}:

$$\int_{t'=b} \Psi_1'^{\dagger}(t', \boldsymbol{x}')\Psi_2'(t', \boldsymbol{x}')\,\mathrm{d}^3 x' - \int_{t=a} \Psi_1^{\dagger}(t, \boldsymbol{x})\Psi_2(t, \boldsymbol{x})\,\mathrm{d}^3 x$$
$$= \int_{D_{\mathrm{I}}} \partial_\mu(\overline{\Psi}_1\gamma^\mu\Psi_2)\,\mathrm{d}^4 x - \int_{D_{\mathrm{II}}} \partial_\mu(\overline{\Psi}_1\gamma^\mu\Psi_2)\,\mathrm{d}^4 x$$

In order to understand the reasoning, remember that the finite volume integral over the intersection of D_{I} with the four-dimensional cylinder of radius R converges to the integral over D_{I} itself as the radius R goes to infinity. The Gaussian theorem may be used to rewrite this finite volume integral as a sum over hypersurface integrals over the boundary of the volume of the intersection. It is then noted that the hypersurface integral over that part of the four-dimensional cylinder which appears in this sum vanishes as $R \to \infty$. We conclude that both four-volume integrals vanish as a result of equation (B.4) and hence the scalar products (B.6) and (B.7) are equal and equation (B.3) is verified.

Obviously, the invariance property proved here implies the orthonormality of orthonormal stationary Dirac eigenstates after their Lorentz transformation to a moving frame.

The idea of using the integral theorem of Gauß was taken from the discussion of the free Dirac equation in [SCH95]. Thirring gives a similar proof for the Lorentz boost invariance of the total charge in classical electrodynamics [THI90, (1.3.18,2)]. Note also that for vanishing external field $W(t, \boldsymbol{x})$ the Lorentz invariance (B.3) proved in this section is a consequence of the fact that Lorentz boosts, only in this particular situation, are represented by a time-independent unitary operator $\exp(-\mathrm{i}\boldsymbol{v} \cdot \boldsymbol{N})$. The self-adjoint generator of this unitary transform is given by $\boldsymbol{N} = \frac{1}{2}(H_0\boldsymbol{x} + \boldsymbol{x}H_0)$ where H_0 is the free Dirac-Hamiltonian [THA92]. Such a generator does not exist if the Dirac field is subject to a time-dependent external field.

B.3 Transformations of eigenstates

Consider an eigenfunction $\psi(\boldsymbol{x})$ of a time-independent Dirac-Hamiltonian $H_0 + W(\boldsymbol{x})$ with eigenvalue ϵ,

$$[H_0 + W(\boldsymbol{x})]\,\psi(\boldsymbol{x}) = \epsilon\,\psi(\boldsymbol{x}). \tag{B.8}$$

Indeed, the external field $W(\boldsymbol{x})$ does not necessarily need to originate in a minimally coupled external electromagnetic field. Other kinds of covariant external fields, like scalar potentials or non-minimally coupled electromagnetic fields (Pauli term, etc.), are not explicitly excluded in this section. (See, for example, [THA92] for a complete classification of covariant external fields.) The time-dependent wave function,

$$\Psi(t, \boldsymbol{x}) = \exp(-\mathrm{i}t\epsilon)\,\psi(\boldsymbol{x}),$$

solves the corresponding time-dependent Dirac equation,

$$[H_0 + W(\boldsymbol{x}) - \mathrm{i}\partial_t]\,\Psi(t, \boldsymbol{x}) = 0. \tag{B.9}$$

Clearly, $\Psi(t, \boldsymbol{x})$ is also an eigenfunction of $H_0 + W(\boldsymbol{x})$ for any time t.

B.3.1 Lorentz boosts. In the unprimed coordinate system of equations (B.9) and (B.8) the hermitian matrix $W(\boldsymbol{x})$ shall not have an explicit time-dependence, as emphasised above. Now consider primed coordinates $(t', \boldsymbol{x}')$ obtained by a Lorentz boost with velocity $\boldsymbol{v}$ from the unprimed coordinates $(t, \boldsymbol{x})$, as in equation (B.5). As usual, let $S(\Lambda)$ denote the four-spinor representation matrix of the Lorentz boost $\Lambda^{\mu}{}_{\nu}$, corresponding to the representation of the γ-matrices employed in the definition of the free Dirac Hamiltonian H_0. The Lorentz transform of the time-dependent Dirac equation (B.9) in the primed frame is given by,

$$[H'_0 + W'(t', \boldsymbol{x}') - \mathrm{i}\partial_{t'}]\,\Psi'(t', \boldsymbol{x}') = 0, \qquad (B.10)$$

with $\Psi'(t', \boldsymbol{x}') = S(\Lambda)\Psi(t, \boldsymbol{x})$ and $(t, \boldsymbol{x}) = \Lambda^{-1}(t', \boldsymbol{x}')$. Due to the Lorentz boost to the unprimed frame, the transformed external field $W'(t', \boldsymbol{x}')$, generally given by [THA92],

$$W'(t', \boldsymbol{x}') = S(\Lambda)^{-1\dagger}\, W\!\left(\Lambda^{-1}(t', \boldsymbol{x}')\right) S(\Lambda)^{-1}, \qquad (B.11)$$

picks up an explicit (though trivial) time-dependence. Here $W(t, \boldsymbol{x}) = W(\boldsymbol{x})$ has been introduced only to simplify the notation. Since, by construction, $\Psi'(t', \boldsymbol{x}')$ solves equation (B.10), the following holds:

$$
\begin{aligned}
H'(t')\,\Psi'(t', x') &= \mathrm{i}\partial_{t'}\,\Psi'(t', x') \\
&= S(\Lambda)\,\mathrm{i}\partial_{t'}\left\{\exp(-\mathrm{i}t\epsilon)\psi(\boldsymbol{x})\right\} \\
&= \epsilon\, S(\Lambda)\exp(-\mathrm{i}t\epsilon)\psi(\boldsymbol{x})\frac{\partial t}{\partial t'} + S(\Lambda)\exp(-\mathrm{i}t\epsilon)\,(\mathrm{i}\partial_i\psi(\boldsymbol{x}))\frac{\partial x^i}{\partial t'} \\
&= \gamma\epsilon\,\Psi'(t', x') - \gamma\, S(\Lambda)\exp(-\mathrm{i}t\epsilon)\,\boldsymbol{v}\cdot(-\mathrm{i}\nabla\psi(\boldsymbol{x})),
\end{aligned}
$$

with $\gamma = (1 - \boldsymbol{v}^2)^{-1/2}$. This means that $\Psi'(t', x')$ is an eigenstate of $H'_0 + W'(t', \boldsymbol{x}')$, if and only if the eigenfunction $\psi(\boldsymbol{x})$ of $H_0 + W(\boldsymbol{x})$ in the unprimed reference frame, is also an eigenfunction of the momentum operator $\boldsymbol{P} = -\mathrm{i}\nabla$. In fact the latter condition is equivalent to the property, that the external potential $W(\boldsymbol{x})$ of equation (B.8) is a constant, i.e. does not depend on the unprimed spatial coordinate $\boldsymbol{x}$. Clearly, this is precisely the case of free motion, and furthermore the only case, where the Lorentz-boosted Hamilton operator $H'(t')$ is time-independent.

Hence, it is meaningful only in that circumstance to Lorentz-transform the energy eigenvalue ϵ to a moving frame. The usual transformation law of the energy-momentum four-vector is then retained from the preceding calculation:

$$
\begin{aligned}
H'(t')\,\Psi'_{p'}(t', x') &= \gamma\epsilon\,\Psi'_{p'}(t', x') - \gamma S(\Lambda)\exp(-\mathrm{i}t\epsilon)\,\boldsymbol{v}\cdot(\boldsymbol{p}\Psi_p(\boldsymbol{x})) \\
&= \gamma(\epsilon - \boldsymbol{v}\cdot\boldsymbol{p})\Psi'_{p'}(t', x') = \epsilon'\Psi'_{p'}(t', x').
\end{aligned}
$$

Here the usual notation for energy-momentum four-vectors p and p' is employed, with $p = (\epsilon, \boldsymbol{p})$ and $p' = \Lambda p = (\epsilon', \boldsymbol{p}')$.

B.3.2 Galilean boosts in nonrelativistic quantum theory. The same problem may be addressed in nonrelativistic quantum mechanics. In order to discuss

this similarity briefly, consider a solution $\Phi(t, \boldsymbol{x})$ of the time-dependent Schrödinger equation,

$$\left[-\frac{1}{2}\nabla^2 + V(\boldsymbol{x}) - \mathrm{i}\partial_t\right]\Phi(t, \boldsymbol{x}) = 0,$$

which is of the form $\Phi(t, \boldsymbol{x}) = \exp(-\mathrm{i}t\epsilon)\,\phi(\boldsymbol{x})$ and, therefore, an eigenstate of the time-independent Hamiltonian $H = -\frac{1}{2}\nabla^2 + V(\boldsymbol{x})$. The Galilean-boosted Schrödinger wave function,

$$\Phi'(t, \boldsymbol{x}') = \exp\left(-\frac{\mathrm{i}}{2}t\boldsymbol{v}^2\right)\exp(\mathrm{i}\boldsymbol{v}\cdot\boldsymbol{x}')\,\exp(-\mathrm{i}t\epsilon)\,\phi(\boldsymbol{x}' + t\boldsymbol{v}),$$

corresponding to the passive Galilean boost, $\boldsymbol{x}' = \boldsymbol{x} - t\boldsymbol{v}$, with boost velocity $\boldsymbol{v}$, solves the Galilean-transformed Schrödinger equation,

$$\left[-\frac{1}{2}\nabla'^2 + V(\boldsymbol{x}' + t\boldsymbol{v}) - \mathrm{i}\partial_t\right]\Phi'(t, \boldsymbol{x}') = 0.$$

In the nonrelativistic Schrödinger theory, the Galilean-boosted wave function $\Phi'(t, \boldsymbol{x}')$ is likewise *not* an eigenfunction of the Galilean-boosted time-dependent Hamiltonian,

$$H'(t) = -\frac{1}{2}\nabla'^2 + V(\boldsymbol{x}' + t\boldsymbol{v}),$$

at any time t, except the external potential $V(\boldsymbol{x})$ is a constant. This is easily verified as in the previous subsection. However, contrary to the relativistic case, supposing that $\phi(\boldsymbol{x})$ is a bound state, the energy expectation value $\bar{\epsilon}'$ in the primed Galilean frame is given by a simple expression:

$$\bar{\epsilon}' = \left(\Phi'(t), H'(t)\,\Phi'(t)\right) = \epsilon + \frac{\boldsymbol{v}^2}{2}.$$

Moreover, the energy uncertainty is time-independent and grows at most linearly with the modulus of the boost velocity $\boldsymbol{v}$, since the following estimate holds:

$$0 \le \left(\Phi'(t), H'(t)^2\,\Phi'(t)\right) - \left(\Phi'(t), H'(t)\,\Phi'(t)\right)^2 \le \boldsymbol{v}^2 \int \phi(\boldsymbol{x})^*(-\nabla^2\phi)(\boldsymbol{x})\,\mathrm{d}^3x.$$

Therefore, $\Phi'(t, \boldsymbol{x})$ is an approximate eigenstate of the Galilean-boosted Schrödinger operator $H'(t)$ for small boost velocities $\boldsymbol{v}$.

B.3.3 Local gauge transformations. The discussion of local gauge transformations can be carried out along the lines of the discussion of Lorentz boosts. We sketch it briefly. It is well-known already in nonrelativistic and relativistic classical mechanics that the Hamiltonian is not a gauge-invariant observable [THI88]. The same is true in (non-)relativistic quantum theory. The locally gauge-transformed Dirac spinor,

$$\breve{\Psi}(t, \boldsymbol{x}) = \exp(-\mathrm{i}g(t, \boldsymbol{x}))\,\exp(-\mathrm{i}t\epsilon)\,\psi(\boldsymbol{x}),$$

solves the gauge-transformed Dirac equation, $\left[H_0 + \breve{W}(t, \boldsymbol{x}) - \mathrm{i}\partial_t\right]\breve{\Psi}(t, \boldsymbol{x}) = 0$, with the transformed external field,

$$\breve{W}(t, \boldsymbol{x}) = W(\boldsymbol{x}) + \{(\partial_t + \boldsymbol{\alpha}\cdot\nabla)g(t, \boldsymbol{x})\}.$$

The gauge-transformed wave function $\breve{\Psi}(t, \boldsymbol{x})$ is an eigenfunction of the transformed Dirac operator $\breve{H}(t) = H_0 + \breve{W}(t, \boldsymbol{x})$, if and only if the gauge function $g(t, \boldsymbol{x})$ is time-independent. Then, of course, $\breve{W}$ is time-independent as well.

Units, Notation, and Other Conventions

In this work, the notation and most conventions of Bjørken and Drell [BD66] are used whenever possible. Some important definitions and conventions are given in this chapter for the convenience of the reader.

C.1 System of units and physical constants

If not stated otherwise, relativistic natural units are used for which the vacuum velocity of light c, the reduced Planck constant $\hbar$ and the electron mass m_e all take the numerical value 1. Then the unit of length is the reduced Compton wave length $\lambda_c = \frac{\hbar}{m_e c}$ of the electron, the unit of time is $\lambda_c/c = \frac{\hbar}{m_e c^2}$, and the unit of energy is equal to $m_e c^2$. Therefore, the relativistic natural units of length and time have the following values in in MKSA units [MT00]:

quantity	numerical value	unit
$\frac{\hbar}{m_e c}$	3.86×10^{-13}	m
$\frac{\hbar}{m_e c^2}$	1.29×10^{-21}	s

For the electrical charge Gaussian units are used, which are commonly preferred in atomic physics. This means that the unit of electrical charge is chosen such that the potential energy of two charges Q and q at a distance r is equal to,

$$\frac{Qq}{r}.$$

In the Gaussian system the elementary charge e is related to the fine-structure constant α by:

$$\alpha = \frac{e^2}{\hbar c}.$$

The fine-structure constant α is the only *physical constant* which directly enters the numerical calculations. The numerical value which has been used to obtain the results of this thesis is [EM95],

$$\alpha^{-1} = 137.0359895,$$

deviating insignificantly from the recently recommended value of $\alpha^{-1} = 137.0359998$ [MT00]. In the system of units adopted here, we have $\alpha = e^2$. Cross sections are conventionally given in barn. Regarding the conversion from relativistic natural units to barn, note that the area of 1 barn corresponds to the $10^{-28} \, \text{m}^2$ in MKSA units and to the area,

$$0.670605 \times 10^{-3} \, \text{r.u.},$$

in relativistic natural units. The Lorentz factor γ associated with the kinetic energy T of a heavy-ion collision given in GeV/u in a fixed target frame is defined as:

$$\gamma = \frac{T}{m_{\mathrm{a.m.u.}}c^2} + 1. \tag{C.1}$$

For the purpose of conversion between these two quantities the value

$$m_{\mathrm{a.m.u}} = 0.931494 \,\mathrm{GeV}/c^2.$$

has been used for the the atomic mass unit $m_{\mathrm{a.m.u}}$ [MT00].

C.2 Dirac matrices and discrete symmetry transformations

In terms of the Pauli matrices $\boldsymbol{\sigma} = (\sigma_1, \sigma_2, \sigma_3)$ the standard Pauli–Dirac representation of the Dirac-matrices $\boldsymbol{\alpha} = (\alpha_1, \alpha_2, \alpha_3)$ and β is given by the following 4×4-matrices [BD66, THA92]:

$$\beta = \begin{pmatrix} 1 & 0 \\ 0 & -1 \end{pmatrix}, \qquad \alpha_i = \begin{pmatrix} 0 & \sigma_i \\ \sigma_i & 0 \end{pmatrix}. \tag{C.2}$$

For numerical calculations the standard representation has been used. However, analytical considerations of the present work do not refer to some particular representation, if not noted otherwise.

We use the convention,

$$g_{\mu\nu} = \mathrm{diag}(1, -1 - 1 - 1),$$

for the signature of the Minkowski metric, following [BD66, BLP82, EM95, SCH95, JAC99] and others. Since the Dirac-matrices are mutually anti-commuting and the γ-matrices are required to satisfy,

$$\gamma^\mu \gamma^\nu + \gamma^\nu \gamma^\mu = 2g^{\mu\nu}, \qquad \text{for } \mu, \nu = 0, \dots, 3,$$

the two sets of matrices are related by:

$$\gamma^0 = \beta, \qquad \gamma^i = \beta\alpha_i, \qquad \text{for } i = 1, 2, 3.$$

This relation is independent of the particular representation. However, it depends on the signature of the Minkowski metric, which is sometimes chosen differently [WEI95]. The definition of the matrix $\gamma^5 = \gamma_5$ adopted in this work is:

$$\gamma^5 = \mathrm{i}\gamma^0 \gamma^1 \gamma^2 \gamma^3 = -\mathrm{i}\alpha_1 \alpha_2 \alpha_3.$$

We refer to the following definitions of the operators of charge conjugation $\mathcal{C}$, time-reversal $\mathcal{T}$ and parity $\mathcal{P}$ acting on a classical Dirac field $\Psi(t, \boldsymbol{x})$ [SCH95]:

$$(\mathcal{C}\Psi)(t, \boldsymbol{x}) = \gamma^0 C \, \Psi^*(t, \boldsymbol{x}), \tag{C.3}$$

$$(\mathcal{T}\Psi)(t, \boldsymbol{x}) = \gamma_5 C \, \Psi^*(-t, \boldsymbol{x}), \tag{C.4}$$

$$(\mathcal{P}\Psi)(t, \boldsymbol{x}) = \gamma^0 \, \Psi(t, -\boldsymbol{x}). \tag{C.5}$$

These definitions are valid for any representation of the γ-matrices that is unitarily equivalent to the chiral representation or the standard representation. The matrix C

occurring in equations (C.3) and (C.4) is always unitary but depends on the representation. It satisfies

$$C^{-1}\gamma^\mu C = -\gamma^{\mu T}, \qquad C^T = -C \qquad \text{and} \qquad C^* C = -1, \qquad (C.6)$$

and exits for any representation which is unitarily equivalent to the chiral representation as a consequence of Pauli's fundamental theorem on the representation of the γ-matrices. Furthermore, C is uniquely defined up to a complex phase, which may be proved by means of Schur's lemma [Goo55, Tha92, Sch95]. The commutation properties of the discrete symmetry operators are summarised by the equation:

$$\{\mathcal{C}, \mathcal{P}\} = [\mathcal{P}, \mathcal{T}] = [\mathcal{T}, \mathcal{C}] = 0 \qquad (C.7)$$

The operators $\mathcal{C}$ and $\mathcal{P}$ are involutions,

$$\mathcal{C}^2 = \mathcal{P}^2 = 1,$$

whereas the double application of the time reversal operation changes the sign of a wave function,

$$\mathcal{T}^2 = -1.$$

Note that the operators defined in equations (C.3–C.5) belong to a particular representation of the covering group of the Poincaré group and that non-isomorphic representations of this group exist. Nevertheless, all different possibilities yield the same projective representation of the Poincaré group [Tha92, pp. 76, 104–105].

Due to the hermitian properties of the γ-matrices, namely $\gamma^{0\dagger} = \gamma^0$ and $\gamma^{i\dagger} = -\gamma^i$, the following useful 'commutation relations' are easily obtained:

$$-C\gamma^{0*} = \gamma^0 C, \qquad (C.8)$$
$$C\gamma^{i*} = \gamma^i C, \qquad i = 1, 2, 3, \qquad (C.9)$$
$$C\gamma_5^* = \gamma_5 C. \qquad (C.10)$$

For the standard representation (C.2) a common choice for C is [BD66, (5.6)],

$$C = i\gamma^2\gamma^0,$$

where the phase of C has been chosen such that C becomes a real-valued matrix.

C.3 Symbols and Notation

Table C.1: Table of symbols

$a_{\Delta l, \Gamma k}$	Transition amplitude from an initial configuration (Γ, k) to a final configuration (Δ, l).
$c_{\Gamma, k}(t)$ and $c_i(t)$	Coefficients of a coupled channel expansion.
$d_A(t, \boldsymbol{x})$	Distance between the centres A and B as measured in a rest frame of centre A (section 2.1).
$d_B(t, \boldsymbol{x})$	The same as $d_A(t, \boldsymbol{x})$, but with respect to a rest frame of centre B.

e	The physical unit charge $e > 0$. For natural relativistic and Gaussian units related to the fine structure constant by $e^2 = \alpha$.
$g(t, \boldsymbol{x})$	Gauge function.
$r_\text{A}(t, \boldsymbol{x}), r_\text{B}(t, \boldsymbol{x})$	Distance from a the centres A and B respectively in their respective rest frames (section 2.1).
$\boldsymbol{v}_\text{A}, \boldsymbol{v}_\text{B}$	Velocities of the centres A and B respectively.
v_A, v_B	Scalar three-velocities, which may be either positive or negative, in a frame where the centres move in the same direction. Hence, *not* the moduli of $\boldsymbol{v}_\text{A}$ and $\boldsymbol{v}_\text{B}$.
$\boldsymbol{x} = (x^1, x^2, x^3)$	Three-vectors. (In appendix A describing the numerical code $\boldsymbol{x} = (x, y, z)$ is used.)
x^μ, x^i	When using Einstein's summation convention, Greek indices $\mu, \nu, \sigma, \rho, \ldots$ are running from 0 to 3 and Latin indices $i, j, k, l, \ldots$ running from 1 to 3 only.
$(t, \boldsymbol{x})$ and $(A^0, \boldsymbol{A})$	Four-vectors.
$\mathbb{C}, \mathbb{R}$	The complex and real numbers respectively.
$D_0, D_i, \boldsymbol{D}$	A notation for partial differential operators, useful in calculations using the chain rule of differentiation: Partial differentiation with respect to the i-th argument of some function.
$H_0 = -\mathrm{i}\boldsymbol{\alpha} \cdot \boldsymbol{\nabla} + \beta$	Free Dirac-Hamiltonian in relativistic units and in general for an arbitrary representation of the γ-matrices.
$P(b)$	Impact parameter dependent probability.
$P_\text{A}(t)$ and $P_\text{B}(t)$	Projectors onto the subspace spanned by the bound states of centre A and B respectively (section 3.1).
$\Re$ and $\Im$	Real and imaginary parts respectively of some complex number.
T	Collision energy in GeV/u.
$\mathcal{T}_i, \mathcal{P}_i$	Discrete symmetry operators (section 2.4).
$V(t)$	Interaction matrix in the matrix notation of the coupled channel equation (section 4.2).
$V_\Gamma(r)$	Spherically symmetric electrostatic potential in a rest frame of centre Γ (sec. 2.2).
$W(t, \boldsymbol{x})$	A hermitian 4×4-matrix-valued function, acting as an external potential matrix of a Dirac equation. (Not necessarily an external electromagnetic field minimally coupled to the Dirac field [THA92].)

$W_\Gamma(t, \boldsymbol{x})$	External potential of the two-centre Dirac equation due to a static charge distribution in a rest frame of centre Γ (section 2.2).
$W_\Gamma^\infty(t, \boldsymbol{x})$	Residual external field caused by a long range force of centre Γ that remains for bound states at the other centre, even at large times (section 3.7).
$\partial_t, \partial_1, \partial_2, \partial_3$	Partial derivatives with respect to the variables t, x^1, x^2, x^3 respectively.
$\gamma^i = \beta\alpha_i$ and $\gamma^0 = \beta$	Dirac matrices. If not indicated otherwise the equations are stated without reference to a particular representation.
$\gamma_5 = \gamma^5 = \mathrm{i}\gamma^0\gamma^1\gamma^2\gamma^3$	Definition of the matrix γ_5.
γ_A and γ_B	Lorentz factors, $\gamma_\Gamma = [1 - \boldsymbol{v}_\Gamma^2]^{-1/2}$ for $\Gamma = \mathrm{A, B}$.
μ_A and μ_B	Inverse screening length of the model potential in section 2.2.
ϱ_A and ϱ_B	Nuclear radius in the model potential in section 2.2.
$\sigma_1, \sigma_2, \sigma_3$	Pauli matrices.
χ_A and χ_B	Rapidities of the respective centres in a frame of reference where the centres move along parallel trajectories.
Γ, Δ	Indices for the scattering channels, which may principally take the values A, B and C.
$\Phi_{\Gamma,k}(t, \boldsymbol{x})$	If not indicated otherwise, it denotes either a solution of a scattering-channel Dirac equation (an asymptotic configuration), or a basis function of the coupled-channel ansatz.
$\Psi(t, \boldsymbol{x})$	Usually denotes a solution of the two-centre Dirac equation.
$\Psi_{\Gamma,k}^\pm(t, \boldsymbol{x})$	Incoming $(+)$ and outgoing $(-)$ scattering states, which correspond to the asymptotic configuration $\Phi_{\Gamma,k}(t, \boldsymbol{x})$ (section 3.1).
$\Omega_\mathrm{A}(t, s), \Omega_\mathrm{B}(t, s), \Omega_\mathrm{C}(t, s)$	Product of time-evolution operators (section 3.1).
$\Omega_\mathrm{A}^\pm(s), \Omega_\mathrm{B}^\pm(s), \Omega_\mathrm{C}^\pm(s)$	Møller operators of the three scattering channels (section 3.1).
$\{\cdot, \cdot\}, [\cdot, \cdot]$	Anticommutator and commutator brackets.
$(\Psi_1(t), \Psi_2(t))$	Scalar product of wave functions.
$|\boldsymbol{x}|$	Modulus of a three-vector.
$\|\Psi(t)\| = \sqrt{(\Psi(t), \Psi(t))}$	Norm of the wave function $\Psi(t, \boldsymbol{x})$ at time t.
$\|v\|_2 = \sqrt{\sum_{i=1}^n v_i^* v_i}$	Norm of a finite vector $v \in \mathbb{C}^n$, as in [KAT80, DH93, GV96].
$\|M\|_2 = \sup_{v \in \mathbb{C}^n} \frac{\|Mv\|_2}{\|v\|_2}$	Matrix norm corresponding to the finite-vector norm $\|v\|_2$ [GV96].

$\|\Psi(t, \boldsymbol{x})\|_{L^2(\mathbb{R}^3, \mathrm{d}^3 x)^4}$	The same as the Hilbert space norm $\|\Psi(t)\|$, i.e. the square root of the spatial integral over $\|\Psi(t, \boldsymbol{x})\|_2^2$. This alternative notation is helpful, if the variable over which is integrated, must appear for some reason.
$\|f\|_{L^p(\mathbb{R}^3)}$ and $\|f(\boldsymbol{x})\|_{L^p(\mathbb{R}^3, \mathrm{d}^3 x)}$	L^p-norm of a function f, which is defined as, $\|f\|_{L^p(\mathbb{R}^3)} = (\int |f(\boldsymbol{x})|^p)^{1/p}$ [FOR84, RS80].
$\|f\|_{L^\infty(\mathbb{R}^n)}$	Suprenum norm of the function f [RS80].
$N^{\mathrm{T}}, \Psi^{\mathrm{T}}, \ldots$	Transposed of matrices, spinors, vectors etc.
$v^\dagger, \Psi^\dagger, N^\dagger$	Hermitian conjugates (i.e. the transposed and complex conjugated objects) of finite vectors, spinors, and finite matrices.
z^*, Ψ^*, N^*	Complex conjugate of a number z, Dirac spinor Ψ, matrix N.
$H^*, U(t, s)^*$	Adjoint of an operator acting on an infinite dimensional Hilbert space [RS80].

Bibliography

[ABB⁺99]   E. Anderson, Z. Bai, C. Bischof, S. Blackford, J. Demmel, J. Dongarra, J. Du Croz, A. Greenbaum, S. Hammarling, A. McKenney, and D. Sorensen, *LAPACK Users' Guide*, third ed., Society for Industrial and Applied Mathematics, Philadelphia, PA, 1999, http://www.netlib.org/lapack/.

[AMX⁺87]   R. Anholt, W. E. Meyerhof, X.-Y. Xu, H. Gould, B. Feinberg, R. J. McDonald, H. E. Wegner, and P. Thieberger, *Atomic collisions with relativistic heavy ions. VIII. Charge-state studies of relativistic uranium ions*, Phys. Rev. A (1987), 1586–1600.

[AS65]   M. Abramowitz and I. A. Stegun (eds.), *Handbook of Mathematical Functions*, Dover Publications, New York, 1965.

[BB88]   C. A. Bertulani and G. Baur, *Electromagnetic processes in relativistic heavy ion collisions*, Phys. Rep. **163** (1988), 299–408.

[BCD⁺98]   A. Belkacem, N. Claytor, T. Dinneen, B. Feinberg, and H. Gould, *Electron capture from pair production by Au^{79+} at 10.8 GeV/nucleon*, Phys. Rev. A **58** (1998), 1253–1255.

[BD66]   J. D. Bjorken and S. D. Drell, *Relativistische Quantenmechanik*, BI Wissenschaftsverlag, Mannheim, 1966.

[Bec88]   A. D. Becke, *A multicenter numerical integration scheme for polyatomic molecules*, J. Chem. Phys. **88** (1988), 2547–2553.

[BGF⁺93]   A. Belkacem, H. Gould, B. Feinberg, R. Bossingham, and W. E. Meyerhof, *Measurement of electron capture from electron-positron pair production in heavy ion collisions*, Phys. Rev. Lett. **71** (1993), 1514–1517.

[BGF⁺94]   A. Belkacem, H. Gould, B. Feinberg, R. Bossingham, and W. E. Meyerhof, *Projectile energy and atomic number dependence of electron capture from pair production in relativistic atomic collisions*, Phys. Rev. Lett. **73** (1994), 2432–2435.

[BGF⁺97]   A. Belkacem, H. Gould, B. Feinberg, R. Bossingham, and W. E. Meyerhof, *Capture, ionization, and pair-production processes in relativistic heavy-ion collisions in the 1-GeV/nucleon range*, Phys. Rev. A **56** (1997), 2806–2818.

[BH63]   W. Brenig and R. Haag, *General quantum theory of collision processes*, Quantum Scattering Theory (M. Ross, ed.), Indiana University Press, Bloomington, 1963, (first published in German in: Fortschr. Physik **7**, 183–242 (1959), pp. 13–108.

[BLP82]   V. B. Berestetskii, E. M. Lifshitz, and L. P. Pitaevskii, *Quantum Electrodynamics*, 2nd ed., Landau and Lifshitz, Course of Theoretical Physics, Vol. 4, Pergamon Press, Oxford, 1982.

[BM92]   B. H. Bransden and M. R. C. McDowell, *Charge Exchange and the Theory of Ion–Atom Collisions*, International Series of Monographs on Physics, no. 82, Clarendon Press, Oxford, 1992.

[BRBW93]   A. J. Baltz, M. R. Rhodes-Brown, and J. Weneser, *Bound-electron–positron pair production in relativistic heavy-ion collisions*, Phys. Rev. A **47** (1993), 3444–3447.

[BRBW94]   A. J. Baltz, M. R. Rhodes-Brown, and J. Weneser, *Convergence of bound-electron–positron pair production calculations for relativistic heavy-ion collisions*, Phys. Rev. A **50** (1994), 4842–4853.

[BRBW96]   A. J. Baltz, M. J. Rhoades-Brown, and J. Weneser, *Heavy-ion partial beam lifetimes due to Coulomb induced processes*, Phys. Rev. E **54** (1996), 4233–4239.

[BS77]   H. A. Bethe and E. E. Salpeter (eds.), *Quantum Mechanics of One- and Two-Electron Atoms*, Plenum Publishing Coorporation, New York, 1977.

[BS85]   H.-J. Bär and G. Soff, *Relativistic wave packets and delta-electron emission*, Physica **128C** (1985), 225–242.

[BS89]   C. Bottcher and M. R. Strayer, *Electron pair production from pulsed electromagnetic fields in relativistic heavy-ion collisions*, Phys. Rev. A **39** (1989), 1330–1341.

[Cap69]   A. Z. Capri, *Electron in a given time-dependent electromagnetic field*, J. Math. Phys. **10** (1969), 575–580.

[CBD$^+$97] N. Claytor, A. Belkacem, T. Dinneen, B. Feinberg, and H. Gould, *Ionization of Au^{78+} and electron capture by Au^{79+} at 10.8 GeV/nucleon*, Phys. Rev. A **55** (1997), R842–R845.

[CEL]   *Cern program library cernlib*, CERN: European Laboratory for Particle Physics, Information Technology Division, Geneva, http://cern.ch/cernlib/.

[CL55]   E. A. Coddington and N. Levinson, *Theory of Ordinary Differential Equations*, McGraw-Hill, New York, 1955.

[Coo57]   J. M. Cook, *Convergence to the Møller wave-matrix*, Journ. Math. and Phys. **26** (1957), 82–87.

[CSC$^+$97] J. R. Carey, S. G. Shasharina, J. C. Cummings, J. V. W. Reynders, and P. J. Hinker, *Comparison of C++ and Fortran 90 for object-oriented scientific programming*, Comput. Phys. Commun. **105** (1997), 20–36.

[Das93]   A. Das, *The Special Theory of Relativity: A Mathematical Exposition*, Universitext, Springer, New York, 1993.

[Dav65]   A. S. Davydov, *Quantum Mechanics*, Pergamon Press, Oxford, 1965.

[Del96]   B. Delley, *High order integration schemes on the unit sphere*, J. Comput. Chem. **17** (1996), 1152–1155.

[DH93]   P. Deuflhard and A. Hohmann, *Numerische Mathematik I*, Walter de Gruyter, Berlin, 1993.

[Dol64]   J. D. Dollard, *Asymptotic convergence and the Coulomb interaction*, J. Math. Phys. **5** (1964), 729–738.

[DR75]   P. J. Davis and P. Rabinowitz, *Methods of Numerical Integration*, Computer Science and Applied Mathematics, Academic Press, New York, 1975.

[DV66]   J. D. Dollard and G. Velo, *Asymptotic behaviour of a Dirac particle in a Coulomb field*, Nuov. Cim. **A 45** (1966), 801–812.

[ED96]   J. Eichler and D. P. Dewangan, *Asymptotic cross section for pair production in relativistic atomic collisions*, Unpublished (Hahn-Meitner-Institut Berlin), January 1996.

[Edm57]   A. R. Edmonds (ed.), *Angular Momentum in Quantum Mechanics*, Princeton University Press, Princeton, 1957.

[Eic85]   J. Eichler, *Relativistic eikonal theory of electron capture*, Phys. Rev. A **32** (1985), 112–121.

[Eic87]   J. Eichler, *Theory of relativistic charge exchange with Coulomb boundary conditions*, Phys. Rev. A **35** (1987), 3248–3255, (Erratum: PR A 37, 287 (1988)).

[Eic90]   J. Eichler, *Theory of relativistic ion-atom collisions*, Phys. Rep. **193** (1990), 165–277.

[Eic95]   J. Eichler, *Charge transfer from the negative-energy continuum: Alternative mechanism for pair production in relativistic atomic collisions*, Phys. Rev. Lett. **75** (1995), 3653–3656.

[EM95]   J. Eichler and W. E. Meyerhof, *Relativistic Atomic Collisions*, Academic Press, San Diego, 1995.

[FGS91]   E. S. Fradkin, D. M. Gitman, and S. M. Shvartsman, *Quantum Electrodynamics with Unstable Vacuum*, Springer Series in Nuclear and Particle Physics, Springer, New York, 1991.

[FL92]   W. Fischer and I. Lieb, *Funktionentheorie*, Vieweg, Braunschweig, 1992.

[For84]   O. Forster, *Analysis 3: Integralrechnung im $\mathbb{R}^n$ mit Anwendungen*, 3rd ed., Vieweg Verlag, Braunschweig, 1984.

[Fri]   W. Fritsch, private communication.

[Fri90]   H. Friedrich, *Theoretische Atomphysik*, Springer-Verlag, Berlin, 1990.

[GLS99]   W. Gropp, E. Lusk, and A. Skjellum, *Using MPI: Portable Parallel Programming with the Message-Passing Interface*, second edition ed., Scientific and Engineering Computation, MIT Press, Cambridge, Massachusetts, 1999.

[GMR85]   W. Greiner, B. Müller, and J. Rafelski, *Quantum Electrodynamics of Strong Fields*, Texts and Monographs in Physics, Springer-Verlag, Berlin, 1985.

[GMS⁺97]   N. Grün, C. Müller, W. Scheid, T. Steih, and R. Tenzer, *Electron-positron pair production in atomic relativistic heavy ion collisions*, Nuclear Physics at the Turn of the Millenium: Structure of Vacuum and Elementary Matter (Singapore), World Scientific, 1997, pp. 117–124.

[Goo55]   R. H. Good, Jr., *Properties of Dirac matrices*, Rev. Mod. Phys. **27** (1955), 187–211.

[Gra90]   G. M. Graf, *Phase space analysis of the charge transfer model*, Helv. Phys. Acta **63** (1990), 107–138.

[GV96]   G. H. Golub and C. F. Van Loan, *Matrix Computations*, 3rd ed., The John Hopkins University Press, Baltimore, 1996.

[Hag82]   G. A. Hagedorn, *Asymptotic completeness for the impact parameter approximation to three particle scattering*, Ann. Inst. H. Poincaré, Phys. Théor. **36** (1982), 19–40.

[HH89]   G. Hämmerlin and K.-H. Hoffmann, *Numerische Mathematik*, Grundwissen Mathematik, vol. 7, Springer-Verlag, 1989.

[Hör76]   L. Hörmander, *The existence of wave operators in scattering theory*, Math. Z. **146** (1976), 69–91.

[IB99]   D. C. Ionescu and A. Belkacem, *Dynamics of ionization mechanisms in relativistic collisions involving heavy and highly charged ions*, Preprint, September 30, 1999, Lawrence Berkeley National Laboratory, California 94720, 1999.

[IE96]   D. C. Ionescu and J. Eichler, *Bound-free electron-positron pair creation in relativistic heavy-ion collisions as a charge transfer process*, Phys. Rev. A **54** (1996), 4960–4967.

[Ion97]   D. C. Ionescu, *Elektromagnetische Elektron-Positron-Paarerzeugung in relativistischen Schwerionstößen*, Habilitationsschrift, Fachbereich Physik, Freie Universität Berlin, 1997.

[ISE93]   A. Ichihara, T. Shirai, and J. Eichler, *Cross sections for electron capture in relativistic atomic collisions*, At. Data Nucl. Data Tables **55** (1993), 63–79.

[Ito95]   H. T. Ito, *Charge transfer model and three-body scattering*, J. Math. Phys. **36** (1995), 115–132.

[Jac99]   J. D. Jackson, *Classical Electrodynamics*, 3rd ed., John Wiley & Sons, 1999.

[Kat80]   T. Kato, *Perturbation Theory for Linear Operators*, 2nd ed., Springer-Verlag, Berlin, 1980.

[KVD⁺98]   H. F. Krause, C. R. Vane, S. Datz, P. Grafström, H. Knudsen, C. Scheidenberger, and R. H. Schuch, *Electron capture and ionization of Pb ions at 33 TeV*, Phys. Rev. Lett. **80** (1998), 1190–1193.

[KVD⁺01]   H. F. Krause, C. R. Vane, S. Datz, P. Grafström, H. Knudsen, U. Mikkelsen, C. Scheidenberger, R. H. Schuch, and Z. Vilakazi, *Electron capture and ionization of 33-TeV Pb ions in gas targets*, Phys. Rev. A **63** (2001), 032711–1–5.

[KY91]   T. Kato and K. Yajima, *Dirac equation with moving nuclei*, Ann. Inst. H. Poincaré, Phys. Théor. **54** (1991), 209–221.

[LL86]   L. D. Landau and E. M. Lifschitz, *Quantenmechanik*, 9 ed., Lehrbuch der Theoretischen Physik, vol. 3, Akademie-Verlag Berlin, Berlin, 1986.

[MAE⁺85]   W. E. Meyerhof, R. Anholt, J. Eichler, H. Gould, C. Munger, J. Alonso, P. Thieberger, and H. E. Wegner, *Atomic collisions with relativistic heavy ions. III. Electron capture*, Phys. Rev. A **32** (1985), 3291–3301.

[MBS95]   K. Momberger, A. Belkacem, and A. H. Sørensen, *Non-pertubative momentum space approach to relativistic heavy-ion collisions*, Europhys. Lett. **32** (1995), 401–406.

[MBS96]   K. Momberger, A. Belkacem, and A. H. Sørensen, *Numerical treatment of the time-dependent Dirac equation in momentum space for atomic processes in heavy-ion collisions*, Phys. Rev. A **53** (1996), 1605–1622.

[MGS91]   K. Momberger, N. Grün, and W. Scheid, *Coupled channel analysis of electron-positron pair production in relativistic heavy ion collisions*, Z. Phys. D **18** (1991), 133–137.

[MGS98]   C. Müller, N. Grün, and W. Scheid, *Finite element formulation of the Dirac equation and the problem of fermion doubling*, Phys. Lett. A **242** (1998), 245–250.

[Mok94]   P. H. Mokler, *Reiche Ernte für die Atomphysik, Klare Sicht auf die Struktur höchstgeladener, schwerer Ionen — Ergebnisse vom Schwerionenspeicherring ESR*, Phys. Bl. **50** (1994), 145–147.

[MPI96]   *Message passing interface (MPI)*, http://www.mpi-forum.org/, 1995–1996.

[MPI00]   *MPICH: A portable implementation of MPI*, http://www.mcs.anl.gov/mpi/mpich/, Argonne National Laboratory, Mathematics and Computer Science Division, Argonne, 2000.

[MPS98]   P. J. Mohr, G. Plunien, and G. Soff, *QED corrections in heavy atoms*, Phys. Rep. **293** (1998), 228–369.

[MRG73]   B. Müller, J. Rafelski, and W. Greiner, *Electron wave functions in over-critical electrostatic potentials*, Nuov. Cim. **18A** (1973), 551–573.

[MS88]   P. Moon and D. E. Spencer, *Field theory handbook*, corrected 3rd printing, 2nd ed., Springer, Berlin, 1988.

[MT00]   P. J. Mohr and B. N. Taylor, *CODATA recommended values of the fundamental physical constants: 1998*, Rev. Mod. Phys. **72** (2000), 351–495.

[New82]   R. G. Newton, *Scattering Theory of Waves and Particles*, 2nd ed., Texts and Monographs in Physics, Springer-Verlag, New York, 1982.

[NW98]   J. W. Norbury and M. L. Waldsmith, *Heavy ion beam lifetimes at relativistic and ultrarelativistic colliders*, Phys. Rev. C **57** (1998), 1525–1527.

[PJB94]   J. M. Pérez-Jordá and A. D. Becke, *Automatic numerical integration techniques for polyatomic molecules*, J. Chem. Phys. **100** (1994), 6520–6534.

[Poz00]   R. Pozo, *Template numerical toolkit: A numeric library for scientific computing in C++*, http://math.nist.gov/tnt/, National Institute of Standards and Technology, Gaithersburg, 1996–2000.

[PTVF92] W. H. Press, S. A. Teukolsky, W. T. Vetterling, and B. P. Flannery, *Numerical Recipes: The Art of Scientific Computing*, 2nd ed., Cambridge University Press, Cambridge, 1992.

[Reg96]   Regionales Rechenzentrum für Niedersachsen/Universität Hannover, Hannover, *Die Programmiersprache C. Ein Nachschlagewerk*, 8th ed., 1996.

[RMS⁺91] K. Rumrich, K. Momberger, G. Soff, W. Greiner, N. Grün, and W. Scheid, *Nonperturbative character of electron-positron pair production in relativistic heavy-ion collisions*, Phys. Rev. Lett. **20** (1991), 2613–2616.

[Ros61]   M. E. Rose, *Relativistic Electron Theory*, Wiley, New York, 1961.

[RS75]   M. Reed and B. Simon, *Fourier Analysis, Self-Adjointness*, Methods of Modern Mathematical Physics, vol. 2, Academic Press, San Diego, 1975.

[RS79]   M. Reed and B. Simon, *Scattering Theory*, Methods of Modern Mathematical Physics, vol. 3, Academic Press, San Diego, 1979.

[RS80]   M. Reed and B. Simon, *Functional Analysis*, 2nd ed., Methods of Modern Mathematical Physics, vol. 1, Academic Press, San Diego, 1980.

[RSG93]   K. Rumrich, G. Soff, and W. Greiner, *Ionization and pair creation in relativistic heavy-ion collisions*, Phys. Rev. A **47** (1993), 215–228.

[Rud74]   W. Rudin, *Functional Analysis*, Tata McGraw-Hill, New Delhi, 1974.

[Rui77a] S. N. M. Ruijsenaars, *Charged particles in external fields. I. Classical theory*, J. Math. Phys. **18** (1977), 720–737.

[Rui77b]   S. N. M. Ruijsenaars, *Charged particles in external fields. II. The quantized Dirac and Klein-Gordon theories*, Commun. Math. Phys. **52** (1977), 267–294.

[Rui77c]   S. N. M. Ruijsenaars, *On Bogoliubov transformations for systems of relativistic charged particles*, J. Math. Phys. **18** (1977), 517–526.

[Sak67]   J. J. Sakurai, *Advanced Quantum Mechanics*, Addison-Wesley, Reading (Massachusetts), 1967.

[San72]   W. Sandhas, *The three-body problem*, Elementary Particle Physics, Multiparticle Aspects (Wien) (P. Urban, ed.), Acta Physica Austriaca, vol. Suppl. IX, Springer-Verlag, 1972, Proceedings of the XI. Internationale Universitätswochen für Kernphysik, Schladming, pp. 57–138.

[San74]   W. Sandhas, *The n-body problem*, Progress in Particle Physics (Wien) (P. Urban, ed.), Acta Physica Austriaca, vol. Suppl. XIII, Springer-Verlag, 1974, Proceedings of the XIII. Internationale Universitätswochen für Kernphysik, Schladming, pp. 679–710.

[Sch55]   L. I. Schiff, *Quantum Mechanics*, 2 ed., McGraw-Hill, New York, 1955.

[Sch58]   J. Schwinger (ed.), *Quantum Electrodynamics*, Dover, New York, 1958.

[Sch95]   G. Scharf, *Finite Quantum Electrodynamics*, 2nd ed., Texts and Monographs in Physics, Springer-Verlag, Berlin, 1995.

[Sei72]   R. Seiler, *Quantum theory of particles with spin zero and one half in external fields*, Commun. Math. Phys. **25** (1972), 127–151.

[SFVW95a]   F. Salvat, J. M. Fernández-Varea, and W. Williamson Jr., *Accurate numerical solution of the radial Schrödinger and Dirac wave equations*, Comput. Phys. Commun. **90** (1995), 151–168.

[SFVW95b]   F. Salvat, J. M. Fernández-Varea, and W. Williamson Jr., *Radial: A Fortran subroutine package for the solution of the radial Schrödinger and Dirac wave equations*, CPC Program Library, Belfast, http://www.cpc.cs.qub.ac.uk/, catalogue number ADBP, 1995, (see also [SFVW95a]).

[SM53]   A. Salam and P. T. Mathews, *Fredholm theory of scattering in a given time-dependent field*, Phys. Rev. **90** (1953), 690–695.

[SM91]   F. Salvat and R. Mayol, *Accurate numerical solution of the Schrödinger and Dirac wave equations for central fields*, Comput. Phys. Commun. **62** (1991), 65–79.

[Stö]   T. Stöhlker, private communication.

[Str97]   B. Stroustrup, *The C++ Programming Language*, 3rd ed., Addison-Wesley, Reading, Massachusetts, 1997.

[TBM$^+$92]   J. Thiel, A. Bunker, K. Momberger, N. Grün, and W. Scheid, *Electron-positron pair creation with capture and ionisation in relativistic heavy-ion collisons by the finite-difference method*, Phys. Rev. A **46** (1992), 2607–2612.

[TE88a]   N. Toshima and J. Eichler, *Coupled-channel theory of excitation and charge transfer in relativistic atomic collisions*, Phys. Rev. A **38** (1988), 2305–2316.

[TE88b]   N. Toshima and J. Eichler, *Coupled-channels treatment of excitation and charge transfer in $U^{92+} + U^{91+}$ collisions at 1 and 0.5 GeV/u*, Phys. Rev. Lett. **60** (1988), 573–576.

[TE89]   N. Toshima and J. Eichler, *Relativistic coupled-channel calculations including pseudostates*, Phys. Rev. A **40** (1989), 125–132.

[TE90]   N. Toshima and J. Eichler, *Direct reactions in relativistic atomic collisions and the influence of the Coulomb boundary conditions*, Phys. Rev. A **42** (1990), 3896–3900.

[Tel87]   E. Teller, *Remarks about fields of high intensity*, Nucl. Inst. Meth. **B24/25** (1987), 1–2.

[Tha92]   B. Thaller, *The Dirac Equation*, Texts and Monographs in Physics, Springer-Verlag, Berlin, 1992.

[THGS95]   J. Thiel, J. Hoffstadt, N. Grün, and W. Scheid, *Fermionic and bosonic coupled channel calculations in momentum space for electron-positron pair creation in relativistic heavy-ion collisions*, Z. Phys. D **34** (1995), 21–28.

[Thi88]   W. Thirring, *Klassische Dynamische Systeme*, 2nd ed., Lehrbuch der Mathematischen Physik, vol. 1, Springer-Verlag, Wien, 1988.

[Thi90]   W. Thirring, *Klassische Feldtheorie*, 2nd ed., Lehrbuch der Mathematischen Physik, vol. 2, Springer-Verlag, Wien, 1990.

[Thi94]   W. Thirring, *Quantenmechanik von Atomen und Molekülen*, 2nd ed., Lehrbuch der Mathematischen Physik, vol. 3, Springer-Verlag, Wien, 1994.

[VGS93]   M. Vidović, M. Greiner, and G. Soff, *Electromagnetic dissociation of Pb nuclei in peripheral ultrarelativistic heavy-ion collisions*, Phys. Rev. C **48** (1993), 2011–2015.

[VKD⁺00] C. R. Vane, H. F. Krause, S. Datz, P. Grafström, H. Knudsen, C. Scheidenberger, and R. H. Schuch, *Radiative electron capture at ultrarelativistic energies: 33-TeV Pb^{82+} ions*, Phys. Rev. A **62** (2000), 010701–1–4.

[Wal93]   W. Walter, *Gewöhnliche Differentialgleichungen*, 5th ed., Springer-Verlag, 1993.

[WBS90]   J. S. Wu, C. Bottcher, and M. R. Strayer, *Coherent particle production in a classical field approximation*, Phys. Lett. B **252** (1990), 37–42.

[Wei95]   S. Weinberg, *The Quantum Theory of Fields*, vol. 1, Cambridge University Press, Cambridge, 1995.

[Wil65]   J. H. Wilkinson, *The Algebraic Eigenvalue Problem*, Clarendon Press, Oxford, 1965.

[WOU⁺92] J. C. Wells, V. E. Oberacker, A. S. Umar, C. Bottcher, M. R. Strayer, J.-S. Wu, and G. Plunien, *Nonperturbative electromagnetic lepton-pair production in peripheral relativistic heavy-ion collisions*, Phys. Rev. A **45** (1992), 6296–6312.

[WSE99]   J. C. Wells, B. Segev, and J. Eichler, *Asymptotic channels and gauge transformations of the time-dependent Dirac equation for extremely relativistic heavy-ion collisions*, Phys. Rev. A **59** (1999), 346–357.

[Wül88]   U. Wüller, *Asymptotische Vollständigkeit beim Charge-Transfer-Modell*, Dissertation, Fachbereich Mathematik der Freien Universität Berlin, Berlin, 1988.

[Yaj80]   K. Yajima, *A multi-channel scattering theory for some time dependent Hamiltonians, charge transfer problem*, Commun. Math. Phys. **75** (1980), 153–178.

ACKNOWLEDGEMENTS

Scientific Contributions

Talks

1. T. Brunne, *Relativistische Zwei-Zentren Rechnungen mit gekoppelten Kanälen*, 21. Arbeitstagung Energiereiche Atomare Stöße in Riezlern (Austria), 2 February 2000.

2. T. Brunne, *Two-center coupled-channel calculations of relativistic ion-ion collisions*, seminar "Atomic Systems in Extreme Fields", Max-Planck-Institut für Physik komplexer Systeme in Dresden, 18 April 2000.

Posters

3. T. Brunne and J. Eichler, *Towards a Two-Center Coupled Channel Calculation of Pair Creation in Relativistic Ion-Ion Collisions*, 63. Physikertagung in Heidelberg, 19 March 1999.

4. T. Brunne and J. Eichler, *Relativistic Peripheral Heavy-Ion Collisions: Reference Frames and Coupled-Channel Calculations*, workshop "Atomic Systems in Extreme Fields", Max-Planck-Institut für Physik komplexer Systeme in Dresden, 23 March 2000.

5. T. Brunne and J. Eichler, *Coupled-Channel Calculations and Relativistic Invariance*, Frühjahrstagung der Deutschen Physikalischen Gesellschaft in Bonn, 5 April 2000.

Printed contribution

6. T. Brunne und J. Eichler, *Frame dependence of capture in coupled-channel calculations*, 21. Arbeitsbericht der Arbeitsgruppe Energiereiche Atomare Stöße, editors: J. M. Rost and J. Ullrich, Dresden, May 2000, ISSN 0724-4975.

Curriculum Vitae

Tim Brunne
Hobrechtstraße 62
12047 Berlin

Familienstand	Unverheiratet
04. 10. 1968	Geboren in Unna, Nordrhein-Westfalen
08. 1979 bis 06. 1988	Schulbesuch des Pestalozzi-Gymnasiums in Unna
06. 1988	Abitur
10. 1988 bis 12. 1989	Grundwehrdienst
10. 1989 bis 09. 1991	Studium der Physik an der Albert-Ludwigs-Universität in Freiburg im Breisgau
07. 1991	Vordiplom in Physik
10. 1991 bis 08. 1992	Stipendiat am Imperial College of Science, Technology and Medicine in London, Großbritannien
10. 1992	Imperial College International Diploma in Physics
10. 1992 bis 07. 1996	Studium der Physik an der Freien Universität Berlin
10. 1993 bis 09. 1996	Tutor am Fachbereich Mathematik der Freien Universität Berlin
07. 1996	Diplom in Physik
05. 1997 bis 04. 2001	Wissenschaftlicher Mitarbeiter (Doktorand) in der Abteilung Theoretische Physik des Hahn-Meitner-Instituts Berlin